ARSENIC-FREE DRINKING WATER
POWERED BY BACTERIA

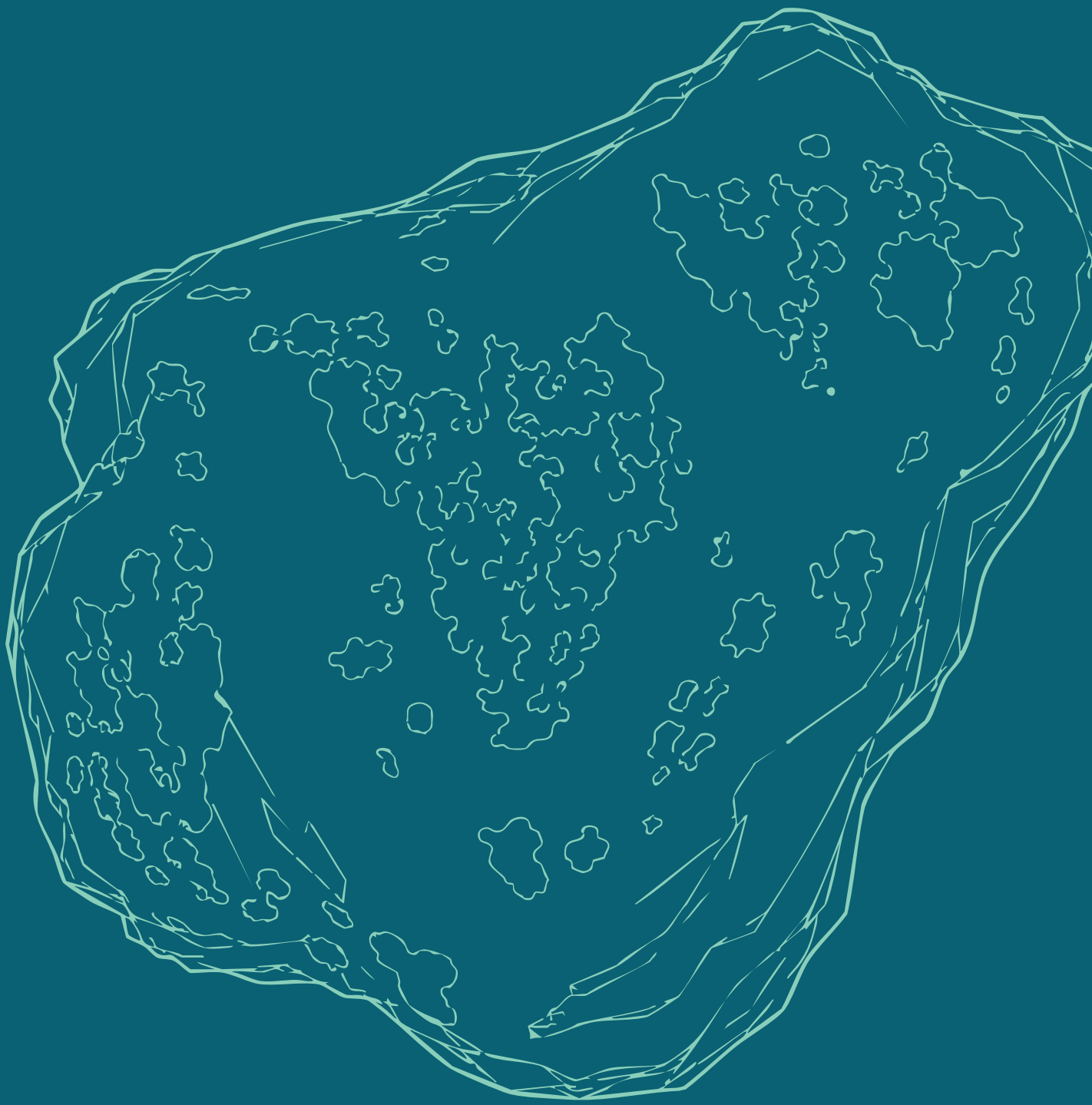

ROOS GOEDHART

Arsenic-Free Drinking Water Powered by Bacteria

Dissertation

for the purpose of obtaining the degree of doctor

at Delft University of Technology

by the authority of the Rector Magnificus,

Prof.dr.ir. H. Bijl,

chair of the Board for Doctorates

to be defended publicly on

Friday 25 September 2026 at 10:00

by

Rosa Christina GOEDHART

This dissertation has been approved by the promotors.

Composition of the doctoral committee:

Rector Magnificus	chairperson
Prof. dr. ir. D. van Halem	Delft University of Technology, promotor
Prof. dr. ir. M. K. de Kreuk	Delft University of Technology, promotor

Independent members:

Prof. dr. M. Kennedy	Delft University of Technology / IHE Delft Institute for Water Education
Prof. dr. H. Schmitt	Delft University of Technology / Rijksinstituut voor Volksgezondheid en Milieu
Prof. dr. L. Raskin	Yale University, USA
Dr. ing. M.A.H.J. van Kessel	Radboud University
Dr. C. Kirkland	Montana State University, USA
Prof. dr. N. Doorn	Delft University of Technology – *reserve member*

The research presented in this thesis was performed at the Sanitary Engineering Section, Water Management Department, Faculty of Civil Engineering, Delft University of Technology, the Netherlands. This work was funded by the Dutch Research Council (NWO), VIDI project 18369 'Anoxic-oxic arsenic removal by unravelling redox processes in drinking water filters'.

Key words:	Groundwater, Drinking water, Sand filtration, Biofilters, Arsenic, Iron, Manganese, Bacteria, Bangladesh
Printed by:	Ridderprint, www.ridderprint.nl
Cover:	Sand grain; inspired by Figure 2 Bii in Chapter 5 Vivianite mineral; inspired by Figure 7 in Chapter A3
Cover design by:	Lilly Deijmann
Copyright:	2026, Roos Goedhart
ISBN:	978-94-6518-407-4

An electronic version of this dissertation is available at: http://repository.tudelft.nl

If the journey of life resembles the march of rivers to the sea, at times meandering aimlessly, at others purposeful and unswerving, the bend in the flow is where the story takes a sudden turn, winding away from its predicted course into a fresh and unexpected direction

Elif Shafak – There are rivers in the sky

Table of Contents

Samenvatting

In Nederland hebben we extreem veel geluk met het veilige drinkwater dat op elk gewenst moment uit de kraan komt. Dit drinkwater wordt voor een groot deel geproduceerd uit grondwater: een betrouwbare bron van hoge kwaliteit die microbiologisch veilig is. Van nature voorkomende stoffen in grondwater, zoals ijzer (Fe), mangaan (Mn) en ammonium (NH_4), worden efficiënt verwijderd tijdens de zuivering, dankzij twee belangrijke stappen: beluchting en (zand)filtratie. Deze zuiveringstechnieken worden wereldwijd veel toegepast.

Een risico voor het produceren van veilig drinkwater is de aanwezigheid van arseen (As), een zeer giftige stof waarvan de concentratie in grondwater sterk kan variëren. De Wereldgezondheidsorganisatie (WHO) adviseert een maximale concentratie van 10 µg/l As in drinkwater. In Bangladesh komt As veel voor in het grondwater, en miljoenen mensen drinken water met concentraties boven de WHO-advieswaarde. In Nederland zijn de As-concentraties doorgaans veel lager. Desondanks hebben de Nederlandse drinkwaterbedrijven afgesproken de As concentratie in kraanwater te verlagen tot minder dan 1 µg/l, wat een technische uitdaging vormt voor drinkwatertechnologen.

Gebruikelijke methoden om de verwijdering van As te verbeteren zijn nu gebaseerd op het toevoegen van chemicaliën, waardoor de complexiteit van het proces en de operationele kosten toenemen. Zowel in Nederland als in landen zoals Bangladesh is daarom een sterke behoefte aan een robuuste, onderhoudsarme en natuurlijke oplossing. Om deze te kunnen ontwikkelen, is er eerst een beter begrip nodig van het gedrag van As tijdens beluchting en zandfiltratie in de huidige grondwaterzuivering.

Hoofdstuk 1 laat zien dat, hoewel zandfiltratie al eeuwenlang de dominante zuiveringstechnologie is, de complexe wisselwerking tussen de fysisch-chemische en biologische processen die na beluchting optreden nog steeds onvoldoende wordt begrepen. Een beter inzicht in deze processen is essentieel om de verwijdering van As verder te optimaliseren. Het doel van dit proefschrift is dan ook: **meer inzicht verkrijgen in de verwijderingsmechanismen van As tijdens de zuivering van grondwater, met een specifieke focus op de biologische oxidatie.**

Biologie zou namelijk een sleutelrol kunnen spelen bij het oplossen van de uitdaging om As-concentraties naar beneden te krijgen. Arseenoxiderende bacteriën (AsOB) kunnen ongeladen As(III) oxideren tot het negatief geladen As(V), een cruciale stap omdat As(V) veel sterker adsorbeert aan ijzer(hydr)oxiden, wat het belangrijkste verwijderingsmechanisme is van As in zandfilters. Ondanks hun mogelijke sleutelrol is de aanwezigheid en rol van deze bacteriën in grootschalige grondwaterzuiveringsinstallaties nog nauwelijks onderzocht.

In **Hoofdstuk 2** wordt de aanwezigheid van AsOB in grondwaterfilters in Bangladesh onderzocht. Daarbij bepaalden we bij zes zuiveringen de verwijderingsefficiëntie van As, Fe, Mn en NH_4. Bij alle zuiveringen bestond het risico op As-concentraties boven de WHO-advieswaarde van 10 µg/l in het gezuiverde water, ofwel door onvoldoende verwijdering,

ofwel door uitspoeling van ijzervlokken waaraan As was geadsorbeerd. In de filters trad oxidatie van As(III) op. Door middel van 'polymerase chain reaction' (PCR) werd in alle filters het *aio*-gen aangetoond, dat codeert voor het enzym dat As(III) kan oxideren. Dit bevestigt dat biologische processen bijdragen aan de oxidatie van As(III). De beperkte verwijdering van As was waarschijnlijk het gevolg van ongunstige omstandigheden voor adsorptie, waaronder competitie met fosfaat, lage Fe/As-verhoudingen en een stijging van de pH tijdens de zuivering.

Het vermogen van AsOB om As(III) te oxideren in zandfilters is in hoofdstukken 3 en 4 onderzocht d.m.v. een labstudie. Hiervoor zijn kolommen gevuld met Fe- of Mn- gecoat filterzand uit een bestaande zuivering. De kolommen ontvingen kraanwater waaraan As werd toegevoegd, waarna zich binnen twee weken een efficiënte As-oxiderende biofilm ontwikkelde. De oxidatiesnelheid werd gemeten over de hoogte van het filterbed. Inactivatie van de microbiële activiteit bevestigde dat de oxidatie biologisch van aard was.

De resultaten in **Hoofdstuk 3** tonen aan dat op Mn-gecoat filterzand de biologische oxidatie de bekende heterogene oxidatie van As(III) op Mn-oxides overtreft: de oxidatiesnelheid nam met een factor 14 toe. De samenstelling van de microbiële gemeenschap veranderde slechts beperkt na blootstelling aan As.

Hoofdstuk 4 behandelt de resultaten voor Fe-gecoat filterzand, het meest gebruikte adsorbens voor As in grondwaterzuivering. Naast oxidatie werd ook de verwijdering van As hier onderzocht. Door de transitie naar een biologisch oxiderend systeem, functioneert het filter als een As(V)-adsorberend in plaats van een As(III)-adsorberend filter. Dit verbeterde de filterprestaties, omdat As(V) doorgaans sterker adsorbeert aan ijzer(hydr)oxiden dan As(III). Gezien de overeenkomsten tussen de laboratorium kolommen en volwaardige zuiveringen, suggereren deze resultaten dat biologische As-oxidatie waarschijnlijk ook plaatsvindt in bestaande drinkwaterzuiveringen.

In **Hoofdstuk 5** wordt een karakterisatie van drinkwaterbiofilms beschreven op Mn-, Fe-, en gemengd Mn/Fe -gecoat filterzand met behulp van sequencing, bioorthogonal noncanonical amino acid tagging (BONCAT) en multimodale beeldvorming. Ondanks effectieve oxidatie van As(III) vertoonden de microbiële samenstelling en biologische activiteit van de biofilm na blootstelling aan As geen grote veranderingen. Dit suggereert dat de oxidatie van As(III) wordt uitgevoerd door een breed scala aan bacteriën die van nature aanwezig zijn op filterzand. De ontwikkeling van biofilms bleek sterker afhankelijk van de fysieke oppervlaktestructuur dan van de chemische samenstelling van de coating. Op het ruwere Mn-gecoate filterzand bleek een dichtere biofilm te groeien dan op het gladdere Fe-gecoate filterzand. De snelle aangroei van Fe-coatings en het frequent terugspoelen van filters beperken mogelijk de ontwikkeling van een biofilm.

Hoofdstuk 6 concludeert dat biologische As-oxidatie een belangrijk onderdeel is in grondwaterzuivering, en raadt aan om hier expliciet rekening mee te houden bij het ontwerpen van As-verwijderingsinstallaties. De oxidatie van As wordt uitgevoerd door een standaard biofilm, die zich van nature in drinkwaterfilters ontwikkelt. Daarom wordt

voorgesteld om vervolgonderzoek te richten op regulatie en stimulering van deze biologische oxidatie. Mogelijke strategieën om biologische oxidatie te stimuleren zijn minder intensieve beluchting, milder terugspoelen en het gebruik van filtermaterialen met een hoge porositeit. Om de verwijdering van As verder te stimuleren, zou oxidatie vóór of gelijktijdig met de verwijdering van Fe moeten plaatsvinden, en hiervoor worden verschillende ontwerpopties besproken. Daarnaast bleek de verwijdering van As in grootschalige biologische functionerende Fe-verwijderingsfilters ongeveer twee keer zo snel te verlopen als in overwegend chemisch gedomineerde Fe-verwijderingsfilters, wat aanleiding geeft tot verder onderzoek. Tot slot wordt de mogelijkheid toegelicht om As terug te winnen als kritieke grondstof uit Fe-gecoat filterzand, waarmee nieuwe perspectieven ontstaan voor een duurzamere grondwaterzuivering.

In de **Appendix** van dit proefschrift wordt een tweede onderzoek gepresenteerd naar een alternatieve, innovatieve methode voor de verwijdering van Fe uit grondwater. Hoofdstuk **A1** introduceert deze aanpak; in plaats van de traditionele combinatie van beluchting en filtratie wordt Fe onder zuurstofloze omstandigheden neergeslagen als Fe(II)-mineraal door toevoeging van een anion. Hiermee wordt de vorming van volumineus en waterig Fe(hydr)oxideslib deels voorkomen, terwijl er een waardevol mineraal gevormd kan worden.

Hoofdstuk A2 beschrijft verkennende experimenten naar de terugwinning van Fe uit anaeroob grondwater onder zuurstofloze omstandigheden. Door fosfaat te doseren werd het Fe(II)-fosfaatmineraal vivianiet ($Fe_3(PO_4)_2$•8 H_2O) gevormd, wat resulteerde in een efficiënte verwijdering van Fe en aanzienlijk minder slibvolume dan bij traditionele beluchting. De efficiëntie van de neerslag nam toe bij hogere verzadigingsindices, en die condities zijn kenmerkend voor concentraatstromen van membraanprocessen. Daarom is in **Hoofdstuk A3** de terugwinning van vivianiet uit dergelijke concentraatstromen onderzocht en de invloed van andere tweewaardige ionen. Daarbij werden mangaanionen en in beperkte mate magnesiumionen mee ingebouwd in het mineraal, zonder dat de Fe-verwijdering of de kristalmorfologie nadelig werden beïnvloed. Calciumionen daarentegen concurreerden met Fe, waardoor de Fe-verwijdering afnam. In **Hoofdstuk A4** wordt sulfide onderzocht als alternatief neerslag-anion. Dit leidde tot de vorming van compacte deeltjes en maakte tegelijkertijd een snelle verwijdering van Fe onder zuurstofloze omstandigheden mogelijk. **Hoofdstuk A5** beschrijft twee mogelijke ontwerpopties voor praktische toepassing van zuurstofloze Fe-verwijdering: directe dosering van het anion aan de waterstroom of toepassing van een pelletreactor waarin de kristallen gecontroleerd kunnen groeien.

Het terugwinnen van Fe als mineraal is een innovatieve zuiveringsmethode die de circulariteit van de drinkwatersector kan vergroten. Hierdoor wordt ijzerslib niet langer beschouwd als afval, maar als een waardevolle grondstof.

Summary

In the Netherlands, we are extremely lucky to have safe drinking water flowing out of our taps at any desired moment. This water is often produced from groundwater, a reliable, high-quality, and microbiologically safe resource. Natural groundwater constituents, such as iron (Fe), manganese (Mn), and ammonium (NH_4), are efficiently removed by aeration followed by sand filtration, a treatment strategy frequently applied worldwide. Yet, there is a risk: arsenic.

Arsenic (As) is a highly toxic substance, with concentrations in groundwater that vary depending on geological and geochemical conditions. The World Health Organization (WHO) has set a guideline value of 10 µg/L for As in drinking water. One of the worst affected countries is Bangladesh, where millions of people are exposed to As concentrations exceeding this limit. In the Netherlands, As concentrations are generally much lower. However, the association of Dutch drinking water companies agreed to reduce the As concentrations in tap water below 1 µg/L, creating a technical challenge for drinking water engineers.

Conventional approaches to enhance As removal rely on chemical additions, increasing process complexity and operation costs. Both in the Netherlands and in regions such as Bangladesh, there is a strong demand for robust, low-maintenance and natural treatment solutions. Achieving this requires a detailed understanding of As behavior during groundwater treatment.

Chapter 1 shows that although sand filtration has been the dominant treatment technology for centuries, the complex interplay between physicochemical and biological reactions initiated by aeration remains poorly understood. A better understanding of the reactions is essential for removal optimization. Therefore, the research aim of this thesis is: **unravel the removal pathways of arsenic in groundwater treatment, with a particular focus on the biological processes.**

Biology might play a key role in solving the challenge. Arsenic-oxidizing bacteria (AsOB) can oxidize As(III) to As(V), a crucial step since As(V) adsorbs more effectively to iron (hydr)oxides, which is the primary removal mechanism in sand filters. Despite their potential importance, the presence and role of AsOB in full-scale groundwater treatment systems have remained poorly understood.

Chapter 2 evaluates the presence of AsOB in groundwater filters in Bangladesh. Six household and community treatment filters were assessed for their removal performance of As, Fe, Mn and NH_4. All plants showed a risk of arsenic concentrations exceeding 10 µg/L in the treated water, either due to insufficient removal or due to iron floc carryover with adsorbed arsenic. As(III) oxidation was observed in the filters. The gene aio, encoding for the enzyme able to oxidize As(III), was detected in all filters using PCR, confirming a biological contribution. Complete As removal was likely limited due to unfavorable conditions for

adsorption, including competition with phosphate, low Fe/As ratios and pH increase during treatment.

The potential of AsOB for As(III) oxidation in filters was assessed in Chapters 3 and 4 using laboratory-scale column experiments. Columns packed with Fe- and Mn-coated filter sand from a full-scale treatment plant were fed with As-spiked tap water, resulting in the development of an efficient arsenic-oxidizing biofilm in around two weeks. Oxidation kinetics were quantified over the height of the filter bed, and microbial inactivation confirmed the biological nature of arsenic oxidation.

Chapter 3 demonstrates that on Mn-coated sand, biological oxidation outcompetes the acknowledged oxidizing power of surface-catalytic As(III) oxidation by Mn oxides, resulting in a 14-fold increase in oxidation kinetics. Only minor changes in microbial community composition were observed before and after As dosing.

Chapter 4 presents the results of the Fe-coated sand, which is the most used As adsorbent in groundwater treatment systems. In addition to oxidation, As removal was also studied. By the shift to a biological oxidizing system, the filter operated as an As(V)-adsorbing rather than an As(III)-adsorbing filter. This improves filter performance, since As(V) adsorption capacities tend to be higher than for As(III). Given the similarity between the column experiments and full-scale conditions, these results suggest that biological arsenic oxidation is likely already occurring in operational treatment plants.

Chapter 5 provides a detailed characterization of drinking water biofilms on Mn-, Fe- and mixed-coated filter sands using sequencing, bioorthogonal noncanonical amino acid tagging (BONCAT) activity measurements and multimodal imaging. No major shifts in community composition or overall activity were observed pre- and post-As exposure, while effective As(III) oxidation was measured. This suggests that biological As(III) oxidation is driven by a broad range of bacteria naturally present on filter sand. Biofilm development was found to depend more strongly on physical surface structure than on coating chemistry, with rougher Mn-coated sand supporting denser biofilms than smoother Fe-coated sand. Rapid Fe-coating growth and frequent backwashing are likely limiting biofilm development.

Chapter 6 concludes that biological arsenic oxidation is an important component of groundwater treatment and recommends explicitly considering this when designing arsenic removal plants. Oxidation of As is accommodated by a standard drinking water biofilm and it is suggested to focus on how oxidation is regulated and stimulated by exposure to As. Strategies to stimulate biological oxidation include reduced aeration, milder backwashing, and the use of a high-porosity filter media. To optimize arsenic removal, oxidation should occur before or simultaneously with iron removal and possible design options are given in this chapter. Additionally, arsenic removal was found to be twice as fast in full-scale biologically operated iron removal filters compared to chemically dominated filters, requiring further investigation. Finally, this chapter highlights the potential for recovering arsenic as a critical raw material from Fe-coated filter sand, opening new perspectives for sustainable groundwater treatment.

In the **Appendix** of this thesis, a second study is presented that explores an alternative, novel approach to iron removal from groundwater matrices. **Chapter A1** introduces this topic; instead of applying the conventional aeration-filtration method, iron is precipitated anoxically as Fe(II) minerals by dosing an anion, thereby avoiding the formation of voluminous and watery iron (hydr)oxide sludge.

Chapter A2 describes initial exploratory experiments on the anoxic precipitation of vivianite from anaerobic groundwater to recover iron. By dosing phosphate, the Fe(II)-phosphate mineral vivianite ($Fe_3(PO_4)_2$•8 H_2O) was successfully formed, resulting in efficient iron removal kinetics and a reduced solid volume compared to conventional aeration. Precipitation efficiency increases at higher saturation indices, conditions that are characteristic of membrane concentrate streams. Consequently, **Chapter A3** investigates vivianite recovery from such concentrate streams, and the effect of other divalent ions present in the stream. Co-removal of Mn^{2+} and limited co-removal of Mg^{2+} were found, without hindering Fe removal efficiencies or altering morphological changes of the vivianite crystal. In contrast, co-removal of Ca^{2+} occurred at the expense of iron removal. In **Chapter A4,** sulfide is evaluated as an alternative precipitating agent, forming compact particles while enabling rapid iron removal under anoxic conditions. **Chapter A5** describes two possible design options for practical application of anoxic iron removal; either dosing the anion directly to the stream, or installing a pellet reactor to grow the crystals.

Altogether, anoxic iron removal is an innovative treatment option, which could potentially increase the circularity of the industry. This approach no longer considers iron sludge a waste, but rather values it as a new resource.

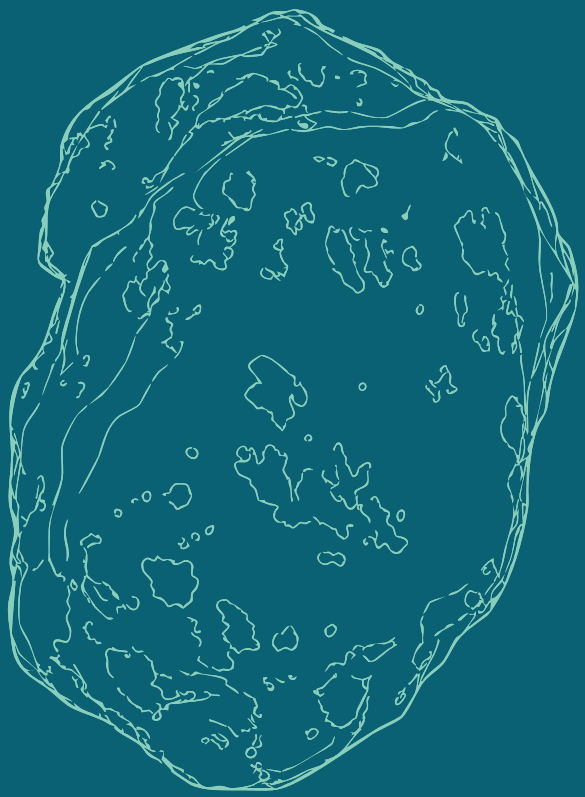

01

Introduction

Part of this chapter is published as:
Corbera Rubio, F., Goedhart, R., Laureni, M., van Loosdrecht, C. M. & van Halem, D. (2024) A biotechnological perspective on sand filtration for drinking water production. Current Opinion in Biotechnology, 90, 103221.

1.1 Access to safe drinking water is everything

A moment of appreciation

I would like to start this thesis by stating how lucky we are in the Netherlands that safe drinking water flows from our taps every single second of the day. This has become so extremely normal to us, that it is easily taken for granted. Yet, this is not the standard for everyone. Worldwide, one in four people still lack access to safely managed drinking water services. For hundreds of millions of people, obtaining drinking water is not a matter of turning a tap on, but a daily task that requires more than thirty minutes of collection time. Approximately four percent of the global population only has access to untreated wells or surface waters, exposing them to significant health risks [1].

Water is everything

The philosopher Thales of Miletus, around 600 years BC, said the origin of everything is water. I agree. Availability of clean drinking water forms the foundation upon which many other aspects of society depend. It directly supports human health by reducing the spread of water-borne diseases, both through drinking and the availability of water for basic hygiene such as handwashing. Beyond health, water availability supports food production and industrial activity, contributing to food security and employment. The importance of safe drinking water extends even further: safe water access is a catalyst for gender equity and women's empowerment. Globally, women and girls spend more than three times as much time fetching water when not available on premises than men and boys [1,2]. A burden that negatively impacts girls' school attendance and can pose direct threats to their safety [3]. Improved access to drinking water also contributes to poverty reduction and economic growth; the economic benefits of achieving safely managed drinking water services are estimated to be up to two times higher than the associated costs [4,5]. In practice, a country cannot sustainably develop without reliable access to safe drinking water, and it is its inhabitants who bear the consequences of this absence most directly.

My activism rant

"Given this knowledge, why do so many people still lack access to this fundamental resource? I believe this is a social challenge rather than a technical challenge. Engineering solutions for water abstraction, treatment and distribution are widely available. Instead, inequalities in water access often arise from social, political and infrastructural challenges, caused by misaligned priorities within governing systems. Investments in basic water infrastructure often compete with short-term economic or political interests, while at the same time insufficient regulations and enforcements allow water sources to become increasingly polluted by industrial and agricultural activities.

This might sound like a 'far from home' problem, but it is not. In the Netherlands in 2023 alone, 32 licenses were provided to discharge PFAS in our water bodies [6], nitrogen pollution from the excessive livestock industry in the Netherlands destroys aquatic systems and how

is it possible that glyphosate is still legally used?! The failure of governments to protect our waterbodies has direct consequences on the health of nature and its inhabitants, including us. Regulations from the European Union are basically being ignored. 26 years after the notice of the 'Kaderrichtlijn Water', not a single water body in the Netherlands complies with the directive, resulting in yearly fines from 2027 onwards."

The Netherlands is in a water crisis.

Engineers will fix it

I think we can all agree that source protection is more efficient than investing in more technologies to properly treat the water. But as long as that is not happening, the engineers will fix it. Because thankfully, we are really good at treating water.

To make drinking water, there are two main sources available: surface water and groundwater. Surface water is all the water visible above ground, such as rivers and lakes. Since it is 'at the surface', it is very susceptible to pollution. Animals live in and around it, cleaned or raw municipal and industrial wastewater can end up in the water bodies, (micro)plastics are present, transported via air or rainwater discharge, etc. However, even severely polluted surface water can technically be turned into clean and safe drinking water, and this happens in many areas around the world. This thesis, however, focuses on 'the better water source' [7]; groundwater.

Groundwater

Groundwater is the most widely used source of drinking water worldwide and is generally considered a reliable and high-quality resource. Formed through the slow infiltration of rainwater and surface water into the soil, groundwater undergoes a natural filtration process.

During this journey, harmful bacteria and viruses are effectively removed. Groundwater is therefore often microbiologically safe to drink. In addition, being stored underground, groundwater is relatively well protected from direct human-caused pollution compared to surface water. As a result, groundwater treatment is often remarkably simple. Only two steps are necessary to remove naturally containing contaminants: 1) expose the water to oxygen and 2) filter the water over a bed with sand, called sand filters. In most cases, the water leaving the filter meets drinking water standards without the need for further treatment. Its effectiveness, robustness and simplicity make it the most widely applied water treatment method in the world.

Yet, there is a risk. Arsenic.

Arsenic

Arsenic is widely recognized as a highly toxic substance. Notoriously known as an effective rat poison, but also often used in medieval stories (that are probably partly real) to poison anyone you want to get rid of; husbands, kings, mistresses... Arsenic's lack of color, taste and odor contributed to this reputation, making arsenic a silent and effective poison.

Arsenic is also a naturally occurring element and widely present in the Earth's crust. It can end up in the groundwater when it dissolves from arsenic-bearing sediments in the soil. As a result, arsenic contamination of groundwater occurs in many areas in the world [8]. When groundwater is used as a source for drinking, there is a risk that arsenic ends up in the drinking water. The World Health Organization (WHO) has set the guideline value for maximum allowed arsenic concentrations in drinking water to 10 µg/L [9]. Figure 1 illustrates the probability of finding higher concentrations in different areas in the world. It is estimated that worldwide, around 94-220 million people are potentially exposed to high concentrations of arsenic via their groundwater [8]. Prolonged consumption of arsenic containing water can result in severe health effects, including arsenicosis and increased cancer risks [10].

This research focuses specifically on two regions; the Netherlands and Bangladesh. Both have their challenges with arsenic, albeit on a completely different scale.

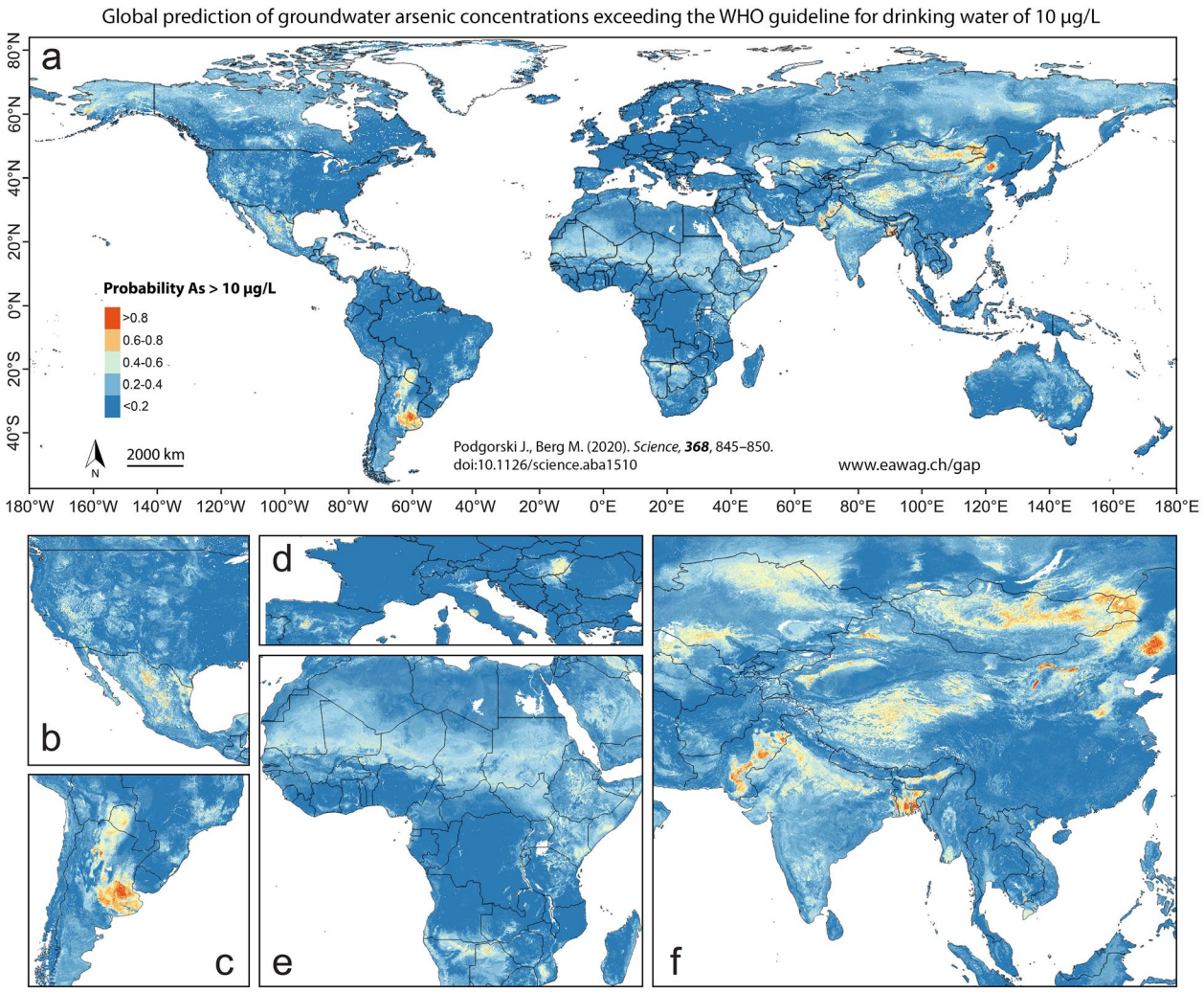

Figure 1: Image from Podgorski J, Berg M (2020) with permission of the authors. Global prediction of groundwater arsenic exceeding 10 µg/L (WHO guideline value) for A) the entire globe and B)-F) zoomed-in sections of the main more densely populated affected areas [8].

Challenge of arsenic in the Netherlands

In the Netherlands, low concentrations of arsenic are present in the groundwater. In total, there are only nine groundwater abstraction locations where arsenic concentrations exceed the WHO guideline value of 10 µg/L [11]. The produced tap water always complies with the WHO guideline.

The question therefore is not whether drinking water in the Netherlands is safe, but how safe it should be. In 2016, the Association of Dutch Drinking Water Companies (Vewin) voluntarily adopted a more stringent target than the WHO value, aiming to reduce arsenic concentrations in tap water below 1 µg/L. This ambition is supported by a cost-benefit analysis, which estimated that the cost associated for achieving the target level of <1 µg/L are lower than the health related costs associated with arsenic consumption, and can lead to an annual societal benefit of €7.2-14 million [12]. Achieving such low concentrations presents new challenges for existing treatment systems in the Netherlands.

Challenge of arsenic in Bangladesh

In Bangladesh, arsenic contamination of groundwater occurs on a much bigger scale. Historically, surface water was the primary source of drinking water. Increasing pollution of the surface waters led to a large-scale transition towards groundwater as a safer alternative, initiated by international organizations in the 1970s. This shift successfully reduced waterborne diseases. However, the water was not tested for arsenic.

It was only in 1993, that elevated arsenic concentrations in groundwater were discovered. Around two-thirds of the wells turned out to contain arsenic concentrations above the WHO guideline of 10 µg/L. By then, prolonged exposure had already occurred, resulting in severe health effects, including arsenicosis and increased cancer risks [10]. As a result, this unfortunate event is commonly referred to as 'the largest mass poisoning in history'.

These high arsenic concentrations (as high as 1660 µg/L has been reported [13]) is pure bad luck, caused by natural geochemical conditions. Bangladesh is formed by sediments deposited from the Himalayas and happen to contain lots of arsenic-bearing sediments. The reducing conditions present in the soil cause arsenic to mobilize from iron bearing minerals into the groundwater [14]. Hence, this largest mass poisoning in history is a result of an unfortunate combination of geology, geochemistry and well-intended interventions.

How to solve these challenges?

Conventional approaches to enhance arsenic removal currently rely on the addition of chemicals to the groundwater treatment process. These strategies share a common drawback: they depend on additional chemical dosing and thereby increase operational complexity. In Bangladesh, the infrastructure and monitoring necessary for chemical dosing is often simply not available. Therefore, there is a worldwide growing support to find simple and natural solutions.

Biology might be the key to solving the challenges. Arsenic-oxidizing bacteria (AsOB) are bacteria that are able to convert the form of arsenic present in groundwater, called arsenite (As(III)), into arsenate (As(V)), which promotes removal efficiencies in groundwater filters. Despite the widespread application of these filters, the role of AsOB remains poorly understood, limiting our ability to predict, optimize and control arsenic removal in groundwater treatment systems.

Research aim: Unravel the removal pathways of arsenic in groundwater treatment, with a particular focus on the biological processes.

1.2 Theoretical background

Black box of groundwater sand filters

Treating groundwater by aeration followed by sand filtration has been the dominant groundwater treatment technology for centuries. Relatively simple designs and operational conditions yield reliable and robust systems for the removal of the main groundwater contaminants, namely iron, manganese and ammonium. However, behind its seemingly trivial working principles, sand filters harbor a high degree of complexity. Groundwater has been stored deep in the ground and does not contain any oxygen anymore. Upon the first step, aeration, the introduction of oxygen onsets a sophisticated network of simultaneous, interconnected and uncontrolled physicochemical and biological reactions. Additionally, the continuous accumulation of iron and manganese particles within sand filters clogs the filters and forces practitioners to backwash the sand filter. During backwashing, the water flow is inverted and accelerated to fluidize the sand, which removes the particles. Backwashing disturbs the steady-state processes over the height of the filter and creates a dynamic system. This inherent complexity makes both research and process optimization challenging. As a result, sand filters have traditionally been considered as a *black box*: groundwater goes in, clean drinking water comes out – but we do not fully understand what happens in between.

It is precisely this complexity that makes the research to sand filtration both challenging and intriguing. Opening the black box is essential for improving treatment efficiency and robustness. Motivated by this challenge, my colleagues and I aim to deepen our understanding of the mechanisms that control the removal of contaminants within groundwater sand filtration systems.

Opening the black box

Figure 2 shows an overview of the chemical and biological reactions known to possibly take place within a sand filter, focusing on the four main ionic groundwater contaminants iron (Fe), manganese (Mn), ammonium (NH_4), and arsenic (As). Although this thesis focuses on arsenic removal, Figure 2 illustrates that all these processes are interconnected, and changes in one pathway will influence others. To place arsenic removal in context, the removal mechanisms of each constituent are briefly discussed below.

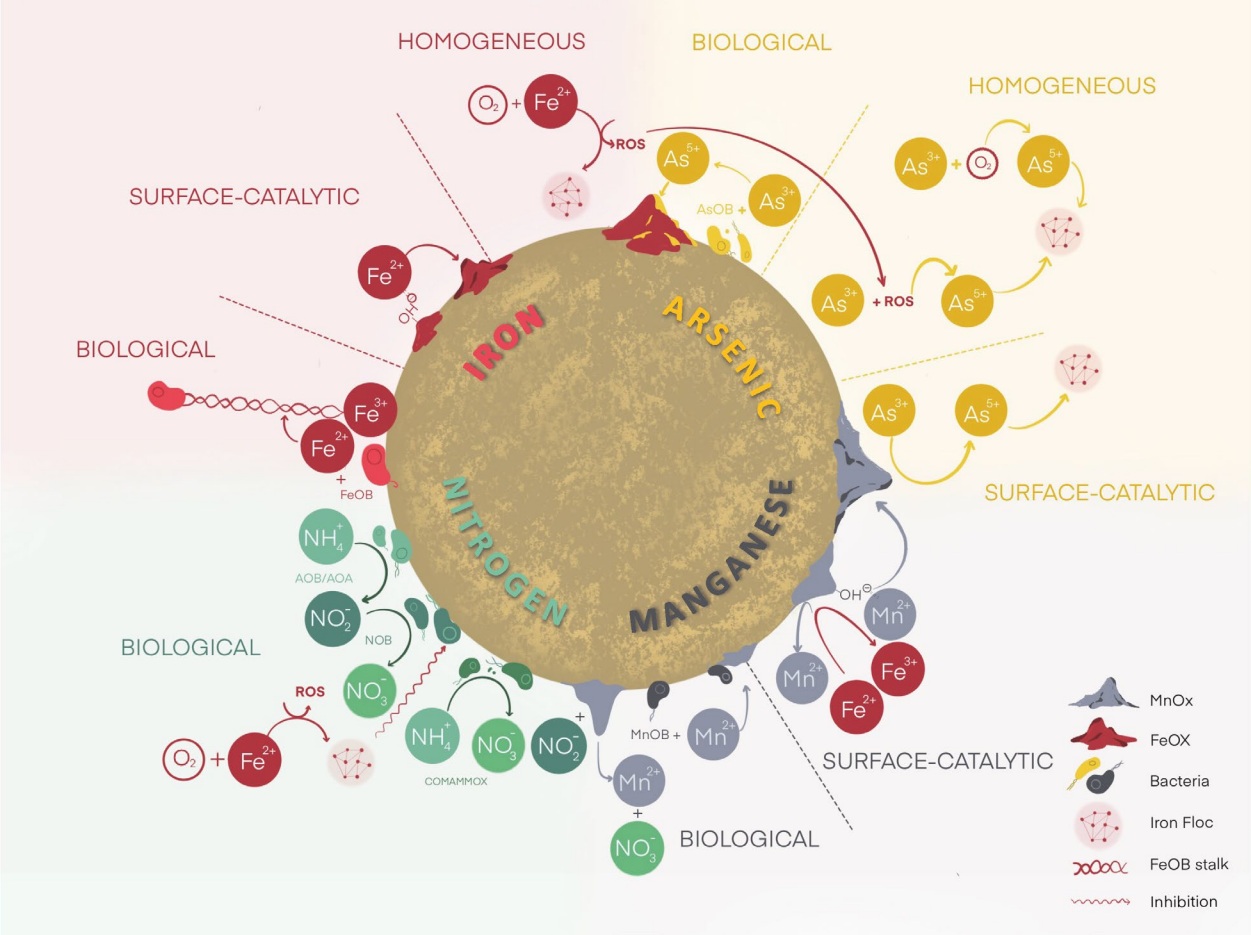

Figure 2: Biological and physicochemical reactions involved in the transformation of the main groundwater contaminants, namely, iron, arsenic, manganese, and nitrogen. Oxidation processes are divided into chemical (homogeneous, surface-catalytic) and biological. Homogeneous reactions take place when both reactants are in the same phase, in this case, the water phase, and are especially relevant for iron (with O2) and As (with ROS that are generated from iron oxidation and, to a lesser extent, with O2). Surface-catalytic reactions take place when the reactants are in two different phases, in this case, water and solid. Surface-catalytic oxidation is relevant for iron (catalyzed by Fe oxides), manganese (commonly known as autocatalytic, by Mn oxides), and arsenic (by Mn oxides). Biological reactions are driven by microorganisms. Nitrogen transformations are exclusively biological, either as the canonical two-step nitrification carried out by AOB and NOB or as the one-step comammox. The (by)products of all these simultaneous reactions interact with each other, and these interactions play a critical role in determining the fate of each contaminant. Our current understanding is that ROS produced during homogeneous iron oxidation oxidize As(III), while iron flocs and iron oxides adsorb As(V) and As(III). Iron flocs inhibit nitrifying bacteria, and Fe(II) oxidizes to Fe(III), while Mn oxides are reduced. Mn oxides are also reduced by nitrite, which is oxidized to nitrate. All the depicted reactions are feasible and proved to occur in sand filters. The inhibition of nitrifying bacteria by iron flocs and the chemical oxidation of nitrite couple of reduction of Mn oxides are the only exceptions still awaiting experimental confirmation in full-scale filters.. Abbreviations: MnOx, manganese oxides; FeOx, iron oxides; ROS, reactive oxygen species; AOB, ammonia-oxidizing bacteria; AOA, ammonia-oxidizing archaea; comammox, complete ammonia-oxidizing (bacteria); NOB, nitrite-oxidizing bacteria. Figure from Corbera-Rubio F et al. (2024) [15].

Iron in anaerobic groundwater is present as dissolved ferrous iron (Fe(II)). In the first treatment step, aeration, Fe(II) is oxidized to ferric iron (Fe(III)), which is poorly soluble and immediately precipitates. Iron flocs are formed and physically retained in the filter bed (homogeneous removal, Figure 2 red). Alternatively, iron can precipitate directly onto the sand grains, forming an iron oxide coating around the filter sand (surface-catalytic, Figure 2 red). A third pathway involved iron-oxidizing bacteria (FeOB), which catalyze the oxidation of Fe(II) and produce characteristic stalk-like Fe(III) structures (biological, Figure 2 red). Müller et al. (2024) demonstrated that shifting towards biological iron oxidation results in up to four times more treated water before backwashing is necessary, showing the potential of biological driven reactions in sand filters [16].

Manganese removal also proceeds via both chemical and biological pathways (Figure 2, grey). Chemically, Mn(II) can be removed through surface-catalytic oxidation: dissolved Mn(II) adsorbs onto pre-existing Mn-oxides, where it is oxidized to Mn(III) or Mn(IV) and incorporated into the Mn-oxide coating. This process is autocatalytic; in absence of Mn-oxides, manganese removal does not readily occur. Consequently, new filters often require extended start-up periods before effective manganese removal is achieved. To accelerate this process, filters are nowadays often inoculated with Mn-coated sand grains[17]. This also promotes biological manganese oxidation, as Mn-oxidizing bacteria (MnOB) will be transported as well.

Ammonium removal is exclusively biological (Figure 2, green). Ammonium is oxidized to nitrite by ammonium-oxidizing bacteria (AOB), after which nitrite is further oxidized to nitrate by nitrite-oxidizing bacteria (NOB). Microorganisms capable of performing both steps are referred to as complete ammonia oxidizers (comammox). Ammonium removal further illustrates the interconnected nature of filter processes: nitrification typically initiates only after iron has been fully removed, as the precipitation of iron flocs can inhibit the development of nitrifying biofilm on the sand grain surface [18].

Arsenic is the focus of this dissertation. Arsenic removal in sand filters primarily relies on adsorption to iron-oxides. In anaerobic groundwater, arsenic predominantly occurs as arsenite (As(III), H_3AsO_3). Iron-oxides, however, exhibit a higher adsorption affinity for the oxidized and negatively charged arsenate (As(V), $H_2AsO_4^-$, $HAsO_4^{2-}$). Efficient arsenic removal therefore depends critically on the oxidation of As(III) to As(V). Homogeneous oxidation of As(III) is slow, occurring on timescales of days. Consequently, surface-catalytic oxidation by Mn-oxides [19] and catalyzed oxidation by reactive oxygen species [20] have long been considered the dominant As(III) oxidation pathways in sand filters (Figure 2, yellow section). Increasingly, however, studies suggest that microorganisms can also mediate arsenic oxidation [21–23]. Experimental proof of biologically driven arsenic oxidation in full-scale rapid sand filters is still lacking. As a result, it remains unclear which of the processes depicted in Figure 2

(yellow) dominates in arsenic oxidation. The first two research questions are defined to fill this knowledge gap:

Research question 1: Can arsenic-oxidizing bacteria be found in full-scale groundwater treatment plants and how does the microbial community composition relate to arsenic oxidation and removal performance?

Research question 2: How does biological As(III) oxidation influence arsenic oxidation kinetics and removal efficiencies in groundwater sand filters compared to physicochemical oxidation pathways?

Design of sand filters

The design of sand filters is relatively easy and based on the aeration, filtration principle. The foundation is the same everywhere, but the actual design of the filter beds can vary. In the Netherlands, we have centralized water treatment plants: one treatment plant provides water to whole cities. In Bangladesh, decentralized treatment plants are much more common, where a plant provides water for a few households or one village. Naturally, the design parameters are completely different. The intensity of aeration and the type of filter beds can vary too, which influences where and how removal processes occur within the filter bed.

In most plants, filters are designed to remove iron first, followed by manganese and ammonium. Simply following thermodynamic laws, oxidation of Fe(II) is more favorable than Mn(II) [24], and this preference is further reinforced by the fact that iron concentrations in groundwater are usually much higher than manganese concentrations. Based on these principles, one would expect a vertically stratified filter bed as illustrated in Figure 3A [25]. Sand grains in the upper part of the filter are predominantly coated with Fe-oxides, grains in the lower part with Mn-oxides.

In practice, filter beds rarely behave in such sequential manner. Instead of distinct layers, mixed Fe/Mn-coatings are commonly observed throughout the filter bed (Figure 3B). This discrepancy is caused by backwashing. At each backwashing event, grains are fully mixed, disrupting any vertical stratification that may have developed during filtration [25]. Over time, this leads to the formation of mixed Fe/Mn-coatings on individual sand grains and enables simultaneous iron and manganese removal within a single filter bed.

To better separate these processes, alternative filter designs can be employed. One approach is the use of a dual-media filter bed, consisting of filter media with different grain sizes within a single filter (Figure 3C). Because grains of different sizes mix less during backwashing, a degree of stratification can be maintained. Another approach involves the use of two filter beds in series, where iron is removed in the first filter and manganese in the

second. In these filters, sand grains have a more homogeneous iron or manganese coating, compared to a single filter bed, as illustrated in Figure 3.

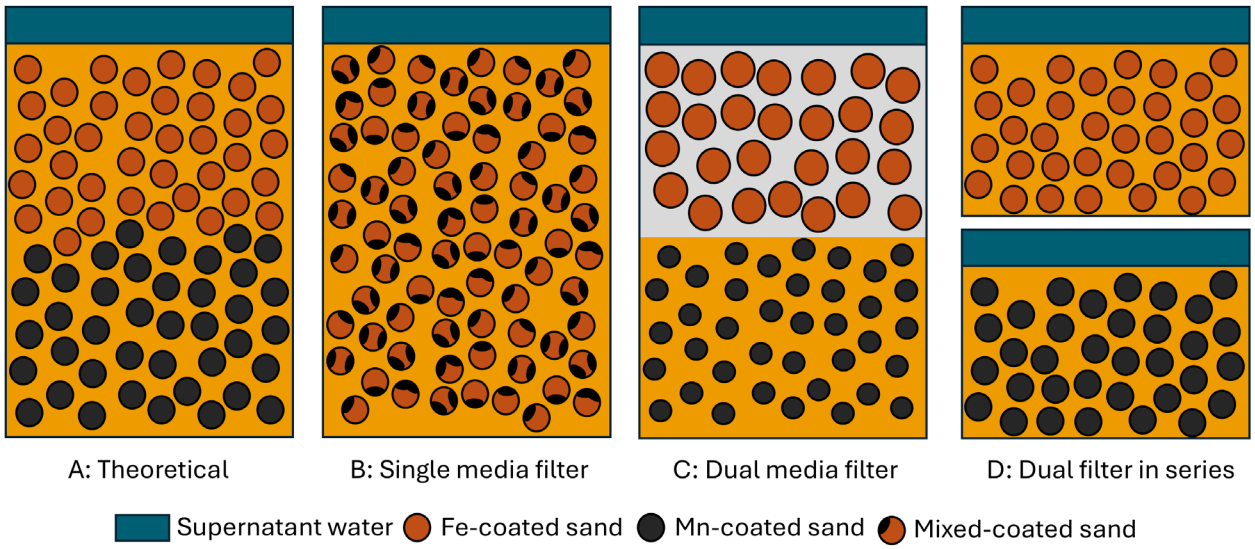

Figure 3: Adapted from Kruisdijk et al. (2024) with permission from the authors [25]. Sequence of oxidation and removal of iron (Fe) and manganese (Mn) in theory (A) and in practice (B-D). A: Sequential Fe oxidation followed by Mn Oxidation. B: Simultaneous Fe and Mn oxidation. C: Sequential Fe and Mn oxidation separated by using two different filter medias. D: Sequential Fe and Mn oxidation by using two separate filter beds.

The coating is important for surface-catalytic reactions, but also for the biological conversion in the filter bed. Bacteria colonize more efficiently in the filter bed when sand grains harbor a porous mineral coating [26]. However, it is unknown what the influence of the different mineral coatings is on the growth of bacteria in sand filters.

Research question 3: What is the role of the filter sand coating on the growth of biofilms in groundwater filters?

Influence of arsenic on biofilters

The central role of biology in sand filtration has become increasingly recognized, and sand filters are now commonly referred to as biofilters. Attention towards the role of arsenic-oxidizing bacteria is also growing and will be further explored in this thesis. But what about the inverse relationship: the impact of arsenic itself on drinking water biofilms? The toxic element arsenic can interfere with cellular metabolism and enzymatic activities. The presence of arsenic may impose a pressure on the biofilm, and whether the presence of arsenic affects the activity of co-occuring organisms essential for drinking water treatment, is currently unknown. This lack of understanding limits our ability to assess the performance and resilience of biofilters exposed to arsenic. Addressing this gap leads to the final research question of this thesis:

Research question 4: What influence does toxic arsenic has on the activity and composition of a standard drinking water biofilm on coated filter sand?

1.3 Outline

This thesis combines fieldwork and laboratory experiments to unravel the oxidation and removal pathways of arsenic in groundwater sand filters. Each chapter addresses a specific part of the puzzle and contributes to answering the research questions introduced earlier.

Chapter 2 evaluates the performance of decentralized groundwater treatment plants to remove arsenic. Fieldwork was conducted at six arsenic iron removal plants in two districts in Bangladesh. The contribution of each filter step to arsenic removal was assessed. Both physicochemical and biological indicators were analyzed, including microbial community composition and the presence of Fe- and As-oxidizing bacteria. This chapter addresses Research Question 1 by examining how arsenic is oxidized and removed in full-scale treatment systems.

Chapter 3 focuses on the kinetics of As(III) oxidation on Mn-coated filter sand. Column experiments were performed using mature reactive Mn-coated sand, known for its catalytic properties towards As(III) oxidation. By gradually shifting the system from physicochemical towards biological As(III) oxidation, this chapter investigates how the biology influences As(II) oxidation kinetics, addressing Research Question 2.

In **Chapter 4**, similar column experiments were conducted using Fe-coated sand, reflecting the most common conditions in full-scale groundwater treatment. The kinetics of As(III) oxidation were followed over time and the effect of biological As(III) oxidation on the removal via iron-oxide coated sand is discussed, thereby offering a complementary perspective on Research Question 2.

Chapter 5 explores the development and functioning of an arsenic-oxidizing biofilm on metal-coated filter sand in greater detail. Using multimodal imaging, the distribution of both the biofilm and the metals on Fe-, Mn- and mixed Fe/Mn-coated filter sand was visualized. In addition, the impact of arsenic exposure on the drinking water biofilm was investigated by assessing changes in microbial activity and community composition using bioorthogonal non-canonical amino acid tagging (BONAT) and sequencing. This chapter addresses Research Questions 3 and 4 and represents the first application of BONCAT to drinking water biofilms.

References

1. World Health Organization (WHO), United Nations Children's Fund (UNICEF). *Progress on Household Drinking-Water, Sanitation and Hygiene 2000-2024: Special Focus on Inequalities*. 2025.
2. UN-Women, DESA. *Progress on the Sustainable Development Goals: The Gender*. 2024.
3. Nauges C, Strand J. Water Hauling and Girls' School Attendance: Some New Evidence from Ghana. *Environmental and Resource Economics 2015 66:1*. 2015;66(1):65-88. doi:10.1007/S10640-015-9938-5
4. Hunter PR, MacDonald AM, Carter RC. Water Supply and Health. *PLoS Med*. 2010;7(11):e1000361. doi:10.1371/JOURNAL.PMED.1000361
5. WaterAid. *Mission-Critical: Invest in Water, Sanitation and Hygiene for a Healthy and Green Economic Recovery WaterAid*. 2021.
6. AT OSBORNE. *Inventarisatie Vergunde PFAS Emissies in Nederland*. 2023.
7. Corbera Rubio F. *A Biotechnological Perspective on Groundwater Sand Filtration*. 2024. doi:10.4233/UUID:43146D99-7AC2-43FE-8B93-5BFDB410C825
8. Podgorski J, Berg M. Global threat of arsenic in groundwater. *Science (1979)*. 2020;368(6493):845-850. doi:10.1126/science.aba1510
9. World Health Organization. *Guidelines for Drinking-Water Quality: Fourth Edition Incorporating the First and Second Addenda*. 2022.
10. Smith AH, Lingas EO, Rahman M. Contamination of drinking-water by arsenic in Bangladesh: a public health emergency. *Bull World Health Organ*. Published online 2000.
11. Stuijfzand PJ, Rossum P van, Mendizabal I. Does arsenic, in groundwaters of the compound Rhine-Meuse-Scheldt-Ems delta, menace drinking water supply in the Netherlands? Published online 2008:102-125.
12. Van Der Wens P, Baken K, Schriks M. Arsenic at low concentrations in Dutch drinking water: assessment of removal costs and health benefits. In: *Arsenic Research and Global Sustainability: Proceedings of the Sixth International Congress on Arsenic in the Environment (As2016)*. CRC press; 2016:563.
13. BGS and DPHE. *Arsenic Contamination of Groundwater in Bangladesh. 2, Final Report, BGS Technical Report*. 2001.
14. Smedley PL, Kinniburgh DG. A review of the source, behaviour and distribution of arsenic in natural waters. *Applied Geochemistry*. 2002;17(5):517-568. doi:10.1016/S0883-2927(02)00018-5
15. Corbera-Rubio F, Goedhart R, Laureni M, van Loosdrecht MC, van Halem D. A biotechnological perspective on sand filtration for drinking water production. *Curr Opin Biotechnol*. 2024;90:103221. doi:10.1016/J.COPBIO.2024.103221
16. Müller S, Corbera-Rubio F, Schoonenberg Kegel F, Laureni M, van Loosdrecht MCM, van Halem D. Shifting to biology promotes highly efficient iron removal in groundwater filters. *Water Res*. 2024;262(March):122135. doi:10.1016/j.watres.2024.122135
17. Haukelidsaeter S, Boersma AS, Behrends T, et al. Inoculation Improves Microbial Manganese Removal during the Start-Up of Rapid Sand Filters. *ACS ES&T Water*. 2025;5:2479-2489. doi:10.1021/ACSESTWATER.5C00050

18. Corbera-Rubio F, Kruisdijk E, Malheiro S, et al. A difficult coexistence: Resolving the iron-induced nitrification delay in groundwater filters. *Water Res*. 2024;260:121923. doi:10.1016/J.WATRES.2024.121923

19. Gude JCJ, Rietveld LC, van Halem D. As(III) oxidation by MnO2 during groundwater treatment. *Water Res*. 2017;111:41-51. doi:10.1016/J.WATRES.2016.12.041

20. Hug SJ, Leupin O. Iron-catalyzed oxidation of Arsenic(III) by oxygen and by hydrogen peroxide: pH-dependent formation of oxidants in the Fenton reaction. *Environ Sci Technol*. 2003;37(12):2734-2742. doi:10.1021/es026208x

21. Crognale S, Casentini B, Amalfitano S, Fazi S, Petruccioli M, Rossetti S. Biological As(III) oxidation in biofilters by using native groundwater microorganisms. *Science of the Total Environment*. 2019;651:93-102. doi:10.1016/j.scitotenv.2018.09.176

22. Gude JCJ, Rietveld LC, van Halem D. Biological As(III) oxidation in rapid sand filters. *Journal of Water Process Engineering*. 2018;21:107-115. doi:10.1016/J.JWPE.2017.12.003

23. Diba F, Hoque MN, Rahman MS, et al. Metagenomic and culture-dependent approaches unveil active microbial community and novel functional genes involved in arsenic mobilization and detoxification in groundwater. *BMC Microbiol*. 2023;23(1):241. doi:10.1186/s12866-023-02980-0

24. Appelo CAJ, Postma D. Geochemistry, groundwater and pollution, second edition. *Geochemistry, Groundwater and Pollution, Second Edition*. Published online 2004:1-649.

25. Kruisdijk E, van Breukelen BM, van Halem D. Simulation of rapid sand filters to understand and design sequential iron and manganese removal using reactive transport modelling. *Water Res*. 2024;267(September):122517. doi:10.1016/j.watres.2024.122517

26. Gülay A, Tatari K, Musovic S, Mateiu R V., Albrechtsen HJ, Smets BF. Internal Porosity of Mineral Coating Supports Microbial Activity in Rapid Sand Filters for Groundwater Treatment. *Appl Environ Microbiol*. 2014;80(22):7010. doi:10.1128/AEM.01959-14

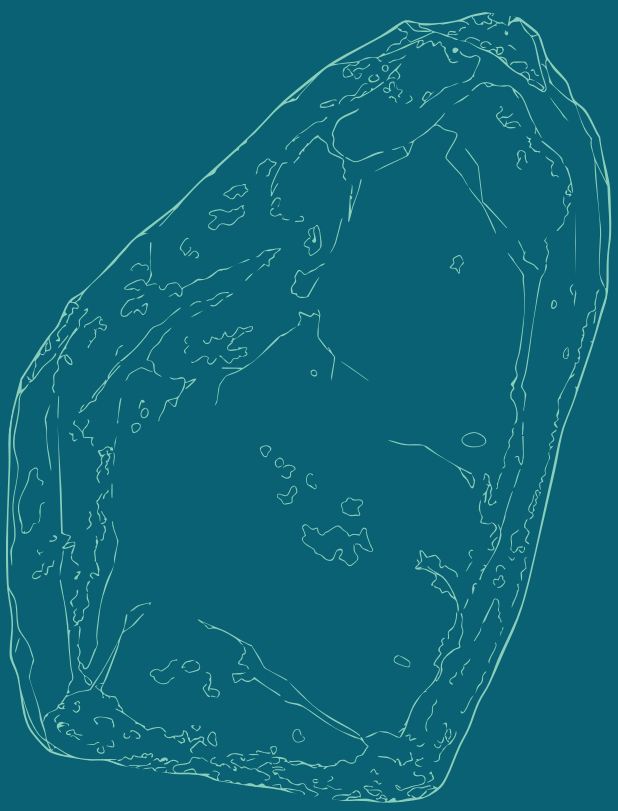

02

Biological Performance of Arsenic-Treating Decentralized Groundwater Plants in Bangladesh

In collaboration with:
Emiel Kruisdijk, Merle de Kreuk, Doris van Halem (TU Delft); Tanvir Ahmed, Mehedi Hasan, Belal Hossain (Bangladesh University of Engineering and Technology); Arefeen Haider and Fatema Tuz Zohra Khan (ICDDR,B, Bangladesh).

Abstract

Decentralized drinking water plants for iron (Fe) and arsenic (As) removal are widely applied in Bangladesh to treat groundwater. These systems rely on aeration followed by sand filtration. Removal of As relies on oxidation of As(III) to As(V) and subsequent adsorption onto Fe-(hydr)oxides formed during Fe(II) oxidation. Besides the well-known physicochemical pathways, microbial oxidation of As and Fe may contribute substantially to treatment performance. This study investigates the presence of As- and Fe-oxidizing bacteria in the plants, and the additional role of biology in the removal of NH_4 and Mn. All six treatment plants monitored produced drinking water exceeding the guideline value of 10 µg/L As. Community-scale plants achieved efficient Fe removal (>99%) and limited As removal (66-79%). Household-scale plants showed substantial variability in treatment performance due to inconsistent operation and showed a risk of Fe-floc breakthrough, potentially exposing users to elevated concentrations of Fe-bound As in the filtrate. Incomplete NH_4 and Mn removal was observed across multiple systems, partly attributed to insufficient dissolved oxygen (DO) availability. By using PCR, markers associated with As- and Fe-oxidizing bacteria were detected throughout the plants. 16S rRNA sequencing showed microbial communities associated with the oxidation of NH_4, CH_4, Fe, and the need of proper aeration to suppress undesirable pathogens. The results demonstrate that decentralized As-treating groundwater plants in Bangladesh are biologically active rather than solely physicochemical treatment systems. Optimization of oxygen supply, hydraulic retention time and biofilm-supporting surface area may enhance the removal contaminants, thereby improving the reliability of water treatment in Bangladesh.

2.1 Introduction

Arsenic (As) is a naturally occurring contaminant in groundwater and poses severe health risks upon prolonged exposure, even at ug/L concentrations [1,2]. Worldwide, an estimated 94 to 220 million people are potentially exposed to groundwater As concentrations exceeding the World Health Organization (WHO) guideline value of 10 µg/L, of whom approximately 94% live in Asia [3]. Within this region, Bangladesh is considered the most severely affected country [4,5], where groundwater As concentrations as high as 1670 µg/L have been reported [6]. The origin of As in Bangladeshi groundwater is primarily geogenic, associated with sediments eroded from the Himalayan orogenic belt and deposited across the Bengal delta. Reductive dissolution, partly mediated by microbes, and desorption drive As mobilization[7].

The widespread exposure of As in Bangladesh is linked to a national shift in the 1970s of the main drinking water source; from microbiologically unsafe surface water to groundwater. At the time, As measurements were not performed, and its contamination was only identified in 1993, after prolonged consumption had already occurred. Chronic exposure resulted in widespread health effects, including arsenicosis and cancer, and has been described as 'the largest mass poisoning in history' [8].

Following recognition of this problem, multiple strategies were developed to reduce As exposure from groundwater. One implemented solution is the use of groundwater treatment plants, which are considered robust, low-cost systems and are used worldwide, both in centralized and decentralized treatment. These systems require minimal maintenance, no chemical addition, and can be constructed from locally available materials. In Bangladesh, these systems are commonly referred to as Arsenic Iron Removal Plants (AIRPs). AIRPs are installed for communities or extended households by several different aid and development organizations across Bangladesh. Despite the extensive use of AIRPs, studies have shown that the removal efficiency varies from 50-98% [9–11]. With removal efficiencies in this range, many AIRPs remain unable to meet the WHO guideline of 10 µg/L.

The working principle of groundwater treatment plants is aeration followed by filtration. Anaerobic groundwater is pumped through a well to the surface and is aerated through cascade, spray or plate aeration. After aeration, the water flows through a (series of) filter media, in which both physicochemical and biological removal processes take place [12]. The most commonly used filter media is sand.

Besides As, the filters are primarily designed to remove iron (Fe), manganese (Mn) and ammonium (NH_4). Fe is mainly removed to improve aesthetic water quality. Mn can be neurotoxic, and the WHO set the guideline for Mn in drinking water to 0.08 mg/L [13]. NH_4 removal is mainly important to maintain microbial stability of the filtered water, to prevent pathogen growth. In groundwater filters, Fe is typically removed first through homogeneous oxidation during aeration, forming Fe-(hydr)oxides. Subsequently, heterogeneous oxidation of Fe(II) can take place on the formed Fe-(hydr)oxides s [14]. Under low pH and low dissolved oxygen (DO) conditions, biological Fe removal can also occur [15] After Fe removal, Mn and NH_4 removal typically takes place [16,17], either within the same filter bed or in sequential beds in

series [18]. Mn removal can happen both via surface-catalytic oxidation in the presence of Mn oxides and biologically by manganese-oxidizing bacteria [19]. Mn oxides are formed and retained in the filter bed. NH_4 removal, by oxidation to nitrate (NO_3), is exclusively biological and is mediated by ammonium-oxidizing bacteria (AOB) and/or comammox organisms [20,21]. Complete conversion to NO_3 is essential; the WHO guideline for NO_3 is around 17 times higher than for nitrite (NO_2), as NO_2 poses a greater health risk [13,22]. Effective biological removal requires porous filter media with a high surface area to support microbial colonization [23].

Removal of As in groundwater filters primarily occurs via adsorption to Fe-(hydr)oxides. In anaerobic groundwater, As is predominantly present as arsenite (As(III)), whereas under oxic conditions, arsenate (As(V)) dominates [24]. Oxidation of As(III) by air is slow (half-life of 4-9 days[25]) and plays a minor role in filters with a hydraulic residence time of minutes. In groundwater filters, As(III) oxidation is catalyzed through three mechanisms: i) by reactive oxygen species generated during Fe(II) oxidation [26], ii) surface-catalytic oxidation by Mn oxides present on filter coatings [27] and iii) biological oxidation by arsenic-oxidizing bacteria (AsOB) [28,29]. Since As(V) generally exhibits higher adsorption efficiencies for Fe-(hydr)oxides and As(III) oxidation is expected to occur via the three mentioned catalytic processes during treatment, groundwater filters should be ideally designed to promote As(V) removal.

The role of microbial processes in groundwater filters for the removal of As, Fe and Mn has gained increasing recognition [12], prompting a gradual shift from viewing these systems as purely physicochemical filters to conceptualizing them as biofilters. The objective of this study is to assess if As- and Fe-oxidizing bacteria are present in As-treating decentralized groundwater plants in Bangladesh, and the additional role of biology in the removal of co-contaminants such as NH_4 and Mn. Therefore, the biological and physicochemical performance of groundwater treatment plants was evaluated in two different districts in Bangladesh. In total, six plants were sampled, and the contribution of individual filter steps was assessed for the removal of Fe, As, Mn and NH_4. Microbial community composition was analyzed using 16S rRNA gene sequencing, and PCR analyses were performed to detect the markers for genes related to biological As- and Fe-oxidation.

2.2 Materials and Methods

2.2.1 Study area and design of treatment plants

Fieldwork was conducted in Bangladesh in March 2024, where two types of treatment plants were investigated: three household- and three community-scale treatment plants. A schematic overview of both systems is given in Figure 1. Pictures of the plants are given in Figures S1 and S2.

The household-scale treatment plants were located in the Manikganj district and served one to two households per plant. These household-scale treatment systems are hereafter referred to as H1-H3. The community-scale treatment plants were located in the Satkhira

district and served approximately 25-80 households per plant. These systems are hereafter referred to as C1-C3.

H1-H3 were installed by NGO 'The Society for People's Action in Change and Equity' (SPACE) since 2009 [30]. Anaerobic groundwater was extracted using an electric pump and entered the first tank. Originally, aeration occurred via an aeration tray. However, this tray was only present at H3 at the time of sampling (Figure S1). At H1 and H2, water entered the system without an aeration step. Next, the water flowed upwards through a filter bed consisting of brick chips (~10 cm at H1-3), followed by charcoal (~6 cm at H1 and H3, ~10 cm for H2) and sand (0-2 cm at H1, ~10 cm at H2 and ~20 cm at H3). Fine fishnets separated the different filter materials to prevent mixing. Treated water was collected from the supernatant of the second tank via a tap. The height of the aeration and filter tank was around 90 and 60 cm respectively with a diameter of 65 cm . The system can hold about 350 L of water, typical use is 150-200 L per day [10].

No user fee was charged for water consumption of the household-scale treatment plants. Operation and maintenance was initially carried out by trained technicians, but responsibility was transferred to the users in 2012. Subsequent maintenance difficulties may have contributed to reduced As removal performance or, in some cases, complete discontinuation of filter use [30]. Filters were typically drained and flushed upon clogging to remove accumulated Fe flocs. At H1-H3, the filters were still in use and the last cleaning had occurred several weeks prior to sampling.

C1-C3 were installed by the NGO WaterAid Bangladesh between 2013 and 2019. Anaerobic groundwater was abstracted using a hand pump and aerated using three perforated plates in series (Figure S2). Water then flowed upward through the first stone filter of approximately 50 cm (filter 1). Subsequently, water was aerated in an open gutter with air contact and then passed upward through a second stone filter of around 30 cm (filter 2). A third aeration step occurred via overflow onto an aeration tray above the final downflow sand filter of approximately 30 cm (filter 3). Treated water was stored in a closed storage chamber, from which users obtained water via a tap. The system can treat up to 1200 Liters per day [31]. The height of the filter tanks was around 105 cm. The tanks of the filters had a dimension of 70 x 70, 100 x 70 and 100 x 100 cm for the three subsequent filters respectively.

Users of the community-scale treatment plants pay a monthly fee per household of approximately BDT 50 (0.35 euro cents) [31]. A designated caretaker is responsible for fee collection, regular monitoring including basic water quality checks, and coordination of maintenance activities. Monthly cleaning is done by a trained and paid team. During cleaning, the system was drained to remove accumulated Fe sludge, then flushed and scrubbed with tap water mixed with bleach. The stones and the top of the sand layer were removed, washed with bleach-containing water, and returned to the filter. C1-C3 were cleaned around three weeks prior to sampling.

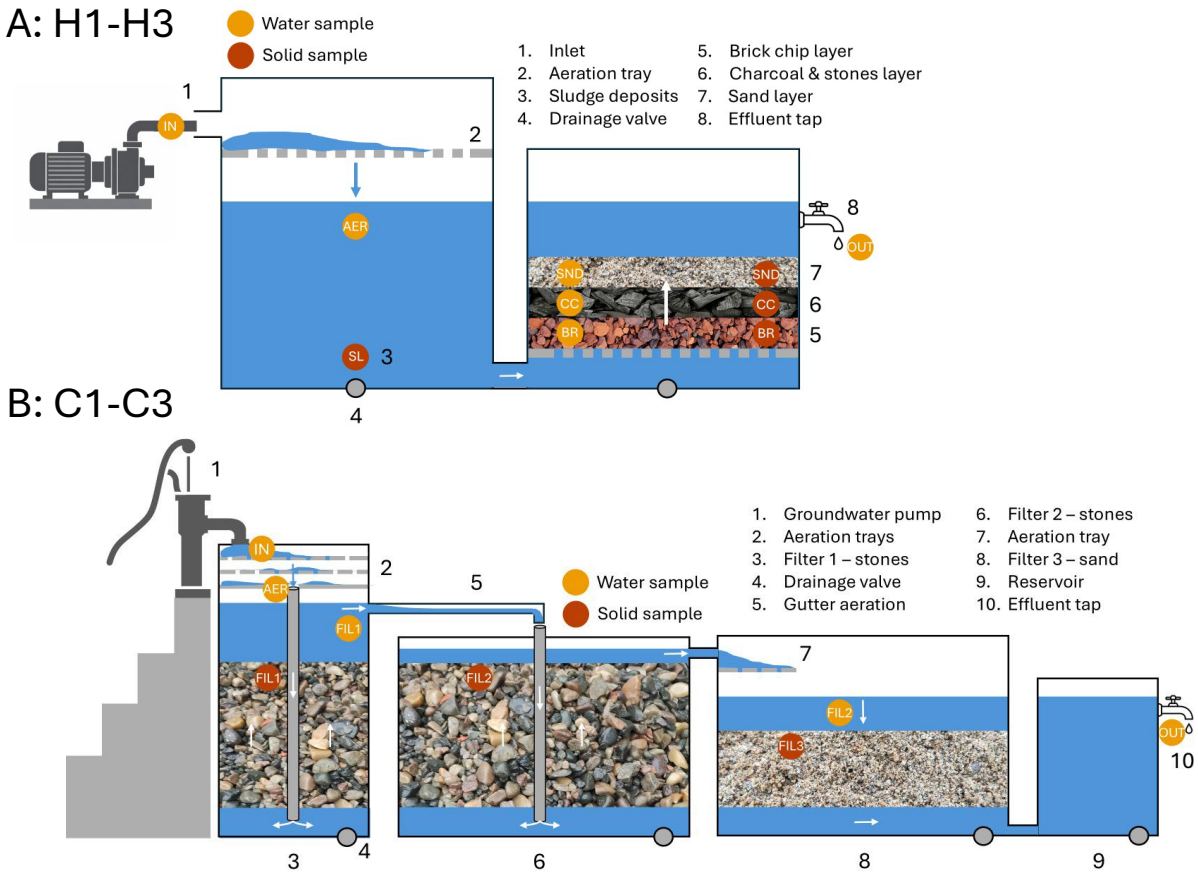

Figure 1: Schematic overview of the A) household-scale treatment plants H1-H3 in Manikganj and B) community-scale treatment plant C1-C3 in Satkhira. Yellow circles indicate samples points of water samples, red circles indicate samples points of solid samples. IN = Inlet, AER = Aeration, SL = Sludge, FIL = Filter, OUT = Outlet effluent

2.2.2 Water and solid samples collection

Figure 1 shows the sample collection points of the treatment systems. After collection, water samples for water quality analysis were stored in 15 mL Falcon tubes, and for microbial analysis in autoclaved glass bottles.

Water samples were taken from the influent raw groundwater and from the effluent drinking water upon first arrival at the plants, without disturbing the filters. Subsequently, water samples were taken after each distinct filter step, which allowed assessing the performance of the individual filters and identifying in which filters removal took place.

At C1-C3, water samples were collected of the distinct filter steps without disturbing the filters: after aeration, filter 1 and 2 (Figure 1B).

At H1-H3, the three filter layers are stacked within a single tank, preventing direct sampling of water after each separate filter step. To enable sampling at different depths, mini-filters with tubes attached were installed in the filter bed as follows. Prior to installation, the plants were drained. The mini-filters were made by filling syringes with cotton, fitted with filter socks and connected to 4 mm tubing were placed within each filter layer. The tanks were filled with

water again and left overnight. The next day, the system was continuously operated for 1 hour, replacing approximately 4 bed volumes. Subsequently, profiles were taken at two different time points for H1-H3: one during continuous operation with the groundwater pump on, and one after 2.5 hours of stagnation to determine the influence of retention time. Samples of the distinct filter steps were extracted by applying suction with a second syringe connected to the other end of the tubing. A picture of the sampling setup is provided in Figure S3. At C1-C3, a removal profile during continuous operation was not feasible due to the large dimensions of the plants and the use of a manual instead of electric pump.

Solid samples were taken for DNA extraction from the collection points as indicated in Figure 1. Filter media was collected from the top part of the filter bed. For C1-C3, media was simply scooped from the bed. For H1-H3, filter media as well as sludge samples were collected while installing the mini-filters. Samples were stored at 4 ºC before extraction in autoclaved glass bottles or sterile Falcon tubes.

2.2.3 Water quality analysis

Dissolved oxygen (DO) and pH were measured immediately after sampling using a WTW multimeter (3630 IDS), equipped with DO and pH probes. Aeration during sampling was minimized as much as possible. This was particularly challenging for effluent samples from the community-scale treatment plants, where water collection from taps inherently introduced DO.

At each sampling point, both filtered (0.2 µm) and unfiltered samples were collected. Fe in the filtered samples is hereafter referred to as Fe dissolved and Fe in the unfiltered samples as Fe(tot), as we expect that all formed Fe-(hydr)oxides are filtered [32,33]. Speciation analysis of As(III) and As(V) was performed on the filtered samples immediately after sampling. A 10 mL syringe was filled with Amberlite IRA-400 chloride anion ion-exchange resin. Prior to speciation analysis, the resin was washed twice with deionized water and conditioned with one volume of filtered sample by passing the sample through the resin. Afterwards, 10 mL of filtered sample was passed through the resin. The effluent contained As(III), while As(V) retained on the resin. As(V) concentrations were calculated as the difference between As(tot) and As(III). Each resin cartridge was used to process a maximum of four samples.

NH_4 concentrations were measured directly in the field using a Lovibond MD 610 photometer with the Ammonia T test. All remaining water quality parameters were analyzed after completion of the field work. Concentrations of As, Fe and Mn were measured by inductively coupled plasma mass spectrometry (ICP-MS, Analytikal Jena PlasmaQuant MS), total P was determined by inductively coupled plasma optical emission spectrometry (ICP-OES, Agilent 5800 VDV). It is assumed that phosphate is the only P species present, and therefore total P is referred to as phosphate (PO_4) hereafter.

Sludge samples were imaged using Environmental SEM (Quanta FEG 650: FEI at 0.5ºC and 6–8 mbar H2O atmosphere).

2.2.4 Oxygen demand calculations

The theoretical oxygen demand required for complete oxidation of Fe(II), Mn(II) and NH_4 was calculated based on the following stoichiometric reactions:

$$Fe(II) + 0.25\ O_2 + 2.5\ H_2O \rightarrow\ Fe(OH)_3(s) + 2H^+$$

$$Mn(II) + 0.5\ O_2 + H_2O \rightarrow\ MnO_2(s) + 2H^+$$

$$NH_4 + 2\ O_2 \rightarrow NO_3^- + 2H^+ + H_2O$$

Among these constituents, NH_4 has the highest molar oxygen demand, requiring 2 mol O_2 per mol of NH_4, compared to Fe(II) and Mn(II), which require 0.25 and 0.5 mol O_2 per mol, respectively.

2.2.5 DNA Extraction

DNA was extracted using the Qiagen DNeasy PowerSoil Pro Kit (Qiagen, Germany) following the manufacturer's protocol, with minor modifications depending on the sample type. For water samples, 500 mL of each sample was filtered through sterile membrane filters (0.22 µm), after which the filter membrane was transferred into 5 mL tubes. Solution CD1 (800 µL) and 0.5 mm glass beads were added, and samples were lysed using a bead beater (Mini-BeadBeater, Biospecproducts), at 3000 rpm, for 30 s. The lysate was centrifuged at 15,000 × g for 3 min, and the supernatant was transferred to a clean 2 mL microcentrifuge tube. Subsequent purification steps were performed according to the manufacturer's instructions, and DNA was eluted as recommended by the kit protocol.

For sand and sludge samples, 250 mg of material was processed directly following the standard kit protocol. For stone and brick samples, 10 g of material was washed thoroughly with 90 mL phosphate-buffered saline (PBS) to release the biomass from the surface of the samples. The wash solution was filtered, and DNA extraction was performed using the same procedure as described for water samples.

2.2.6 PCR for arsenic- and iron-oxidizing bacteria

PCR assays were performed to detect (i) bacterial DNA using universal 16S rRNA markers, (ii) arsenite oxidase (aio) functional gene markers associated with As(III)-oxidizing bacteria, and (iii) Fe-oxidizing bacteria based on probes developed for *Gallionella*-like bacteria (Ga-FeOB). '*Gallionella*-like' refers to Fe-oxidizing bacteria that are phylogenetically close to *Gallionella*, but from distinct clades and often represent uncultured novel lineages [34].

A two-round strategy was applied: first-round PCR for broad detection/enrichment, followed by second-round nested PCR for 16S- and Ga-FeOB–targeted assays and second-round re-amplification (two-round/semi-nested PCR) for aioA. Primer sets and optimized annealing temperatures are listed in Table 1.

All PCR reactions were carried out in 25 µL of total volume, containing 12.5 µL Hot-Start GoTaq® Ready-to-Use Master Mix (Promega, USA), 0.4 µL each of forward and reverse primers, 2 µL of template, and nuclease-free water to volume. Thermal cycling consisted of

an initial denaturation at 94 °C for 3 min, followed by 35 cycles of denaturation at 94 °C for 1 min 30 s, annealing at the primer-specific optimized temperature for 30 s, and extension at 72 °C for 1 min 30 s, with a final extension at 72 °C for 5 min.

In the first round, extracted DNA was used to amplify bacterial 16S rRNA with Fc27/RC1492 (annealing 60 °C) and arsenite oxidase gene markers with aioAF/aioAR (annealing 62 °C). In the second round, first-round products diluted 1:10–1:50 were used as templates. Universal 16S rRNA was amplified using Eub338F/Eub518R (annealing 60 °C) and Ga-FeOB was targeted using 628F/998R (annealing 57 °C), both using the diluted Fc27/RC1492 first-round amplicon as template. For arsenite oxidase detection, aoxBM1-2F/aoxBM2-1R (annealing 60 °C) was applied using the diluted aioAF/aioAR first-round product as template for second-round re-amplification (semi-nested PCR) targeting aioA markers associated with arsenite-oxidizing bacteria.

Table 1: The primers used in PCR experiments, with their corresponding sequence, target group and annealing temperature

Primer pair (F/R)	Sequence	Target gene/group	Annealing (°C)	Ref.
Fc27 / RC1492	5'–AGA GTT TGA TCC TGG CTC AG–3' 5'–TAC GGC TAC CTT GTT ACG ACT T–3'	Bacterial 16S rRNA	60	[35]
Eub338F / Eub518R	5'–ACT CCT ACG GGA GGC AGC AG–3' 5'–ATT ACC GCG GCT GCT GG–3'	Universal 16S rRNA	60	[36]
aioAF / aioAR	5'–CCA CTT CTG CAT CGT GGG–3' 5'–TGT CGT TGC CCC AGA TGA–3'	Arsenite oxidase gene, large subunit (aioA)	62	[37]
aoxBM1-2F / aoxBM2-1R	5'–CCA CTT CTG CAT CGT GGG NTG YGG NTA–3' 5'–GGA GTT GTA GGC GGG CCK RTT RTG DAT–3'	Arsenite oxidase gene, large subunit (aioA)	60	[38]
628F / 998R	5'–GBM AGG CTA GAG TGT AGC–3' 5'–CTC TGG AAA CTT CCT GAC–3'	Gallionella-like bacteria	57	[34]

2.2.7 16S rRNA gene amplicon sequencing

Selected DNA extracts were subjected to 16S rRNA gene amplicon sequencing following the Earth Microbiome Project (EMP) 16S Illumina Amplicon Protocol (v2) [35], targeting the V4 region using the updated degenerate 515F-Y/806R-B primer pair with Illumina adapter and barcode constructs [36]. DNA purity and concentration were assessed prior to library preparation using NanoDrop (A260/280 ratio 1.8–2.0) and Qubit fluorometric quantification. During library QC, fragment/library profiles were assessed using a LabChip GX Bioanalyzer.

Amplicon PCR was performed in triplicate per sample, and replicate reactions were pooled per sample before downstream processing, as recommended in the EMP protocol. Amplicons were checked for expected size, then normalized and pooled in equal amounts across samples to generate the final sequencing pool, followed by PCR clean-up according to the EMP workflow.

Sequencing was carried out on an Illumina MiSeq platform using a MiSeq v2 (500-cycle) cartridge, generating paired-end 2 × 250 bp reads. In line with EMP recommendations for low-diversity amplicon libraries, PhiX spike-in (15%) was included in the run.

Demultiplexed paired-end reads generated on the Illumina MiSeq platform were imported into QIIME 2 for quality control and downstream sequence processing [41]. Primer and adapter sequences were removed prior to analysis. Reads were quality filtered, denoised, merged, and screened for chimeras using DADA2 implemented in QIIME 2 [41,42]. High-quality representative sequences were retained as amplicon sequence variants, and an ASV feature table containing the abundance of each sequence variant per sample was generated for downstream taxonomic profiling [42]. Taxonomic classification was performed in QIIME 2 using the SILVA reference database [43]. The resulting taxonomy assignments were combined with the ASV feature table to generate sample-wise taxonomic abundance tables. ASV counts were collapsed to the class and family taxonomic ranks, and relative abundance (RA) was calculated for each sample by dividing the number of reads assigned to each taxon by the total number of reads in that sample and multiplying by 100. The final abundance tables were exported from QIIME 2 and further processed in R.

For visualization, the top 15 most abundant taxa across all samples, based on mean RA, at class and family levels were plotted individually. Remaining lower-abundance taxa were grouped as “Others.” Relative-abundance profiles were visualized as stacked bar plots to compare microbial community composition between influent and effluent samples for H3 and C1–C3. Duplicate samples were retained as separate observations to assess consistency between replicates and sample-level variation.

2.3 Results

2.3.1 Water quality performance of community-scale treatment plants

Figure 2 presents the removal efficiencies of Fe, As, Mn, NH_4, and PO_4 after the individual treatment steps of the community-scale treatment plants, together with the profiles of DO, pH and Fe/As Ratio. The three plants operated under relatively comparable conditions: influent groundwater concentrations were of similar magnitude, and all plants were cleaned and backwashed approximately three weeks prior to sampling.

Aeration was the first treatment step and increased DO concentrations to approximately 5 mg/L, accompanied by a pH increase due to CO_2 degassing. Fe(II) oxidation initiated upon aeration, while limited As(tot) was removed at this stage. In contrast, partial PO_4 removal already occurred during aeration, likely through adsorption onto freshly formed Fe-

(hydr)oxides. Partial oxidation of As(III) to As(V) was observed at C2 during aeration, which was not observed at C1 and C3.

In the first stone filter (filter 1), Fe(II) oxidation continued and the formed Fe-(hydr)oxides were partly retained within the filter bed. This resulted in approximately 94% PO_4 removal. Similarly, filter 1 was the main step responsible for As removal, with total As efficiencies ranging from 66-79%. The Fe/As ratio in filter 1 ranged between 25 and 38. Simultaneously, DO concentrations decreased in this step due to Fe(II) oxidation and partial NH_4 oxidation.

The second stone filter removed the remaining Fe flocs, resulting in total Fe removal efficiencies of >99%. Despite the effective Fe removal, no further As(tot) removal was observed. This demonstrates that efficient Fe removal does not necessarily result in adequate As removal. A possible explanation of the lack of As removal is the combination of decreasing Fe/As ratio (<10) and increasing pH values (~7.3 to ~7.8), both of which substantially reduce the adsorption of As(V) to Fe-(hydr)oxides [44–46]. Although Filter 2 did not contribute to further As(tot) removal, continued oxidation of As(III) to As(V) was observed, and As(III) represented only 4% of remaining As(tot) after this step. Mn and NH_4 removal also initiated in Filter 2, consistent with other groundwater treatment plants where Mn and NH_4 removal typically start only after Fe removal is completed [18,20].

An additional aeration step prior to the third sand filter further increased pH due to CO_2 degassing, and further stimulated Mn and NH_4 oxidation. Nevertheless, complete removal of Mn and NH_4 was not achieved within the sand filter bed. Effluent Mn concentrations ranged from 6.9 – 22 µg/L, which is below the WHO guideline value of 80 µg/L. Effluent NH_4 concentrations ranged from 0.3-2.0 mg/L. Although NH_4 does not have a set guideline by the WHO, complete nitrification is important to ensure biological stability of the produces water and to prevent the formation of undesired nitrite (Lytle et al., 2007). Notably higher NH_4 concentrations were observed in the groundwater of C2, despite the proximity of C1-C3. Possibly, the groundwater was locally contaminated with manure, sewage or other (animal) waste pollution.

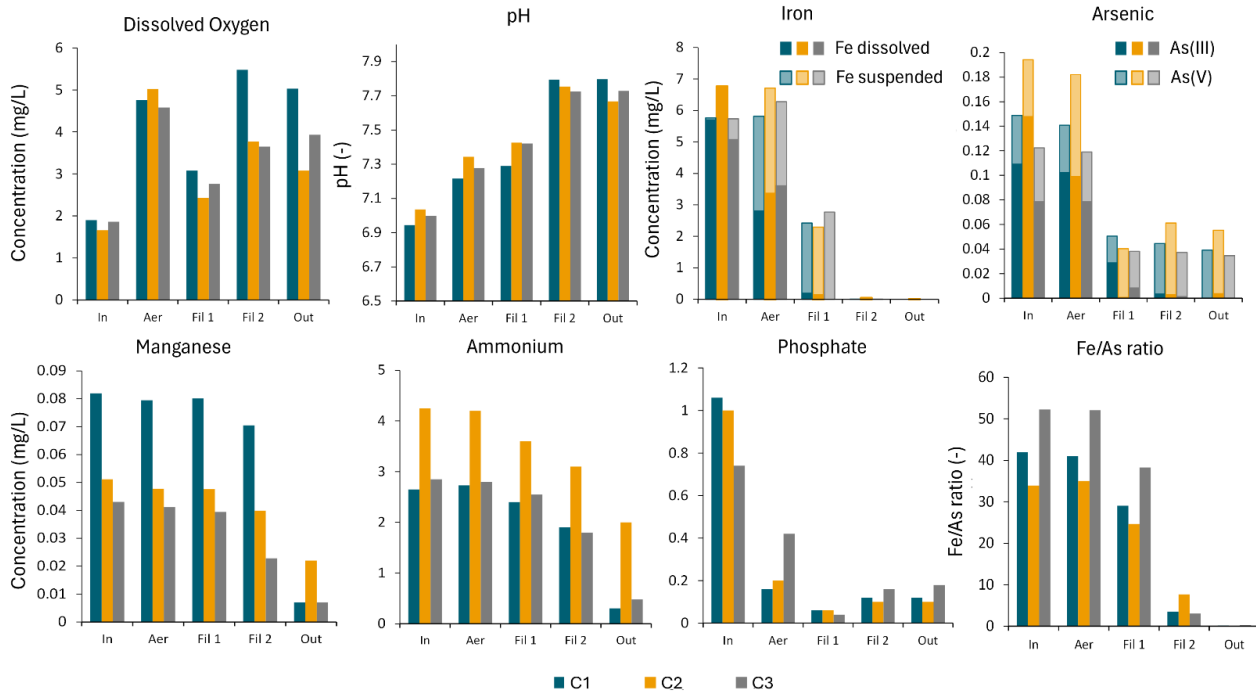

Figure 2: Community-scale treatment plants (C1-C3) profiles of DO, pH and Fe/As ratio and the removal efficiencies of Fe, As, Mn, NH_4, and P in the raw groundwater (In), after aeration (Aer), after filter 1 (Fil 1), after filter 2 (Fil 2) and in the effluent (Out).

2.3.2 Water quality performance of household-scale treatment plants

In contrast to the community-scale treatment plants, which operated triplo-like, the household-scale treatment plants showed substantial variability in both design and treatment performance. Figure 3 presents the concentrations of Fe, As, Mn, NH4 and PO_4, together with the profiles of DO, pH and Fe/As ratio throughout the individual treatment steps of H1-H3.

The large variability between household-scale systems is likely related to inconsistent operation, cleaning and maintenance. A previous study reported that the absence of trained operators and irregular maintence practices frequently result in non-ideal functional of As-treating groundwater plants (Sorensen and McBean (2015). One clear example was the absence of the aeration tray at H1 and H2. This appears to be a common issue for decentralized groundwater plants in Bangladesh. Hossain and Ahmed (2025) reported that approximately 38% of 310 evaluated plants lacked an aeration tray, Sorensen and McBean (2015) observed the same problem in 4 out of 14 investigated plants. The low DO concentrations measured at H1 and H2 (1.7 and 2.8 mg/L, respectively), compared to H3 (4.6 mg/L), clearly reflect the limited aeration in these systems.

Another inconsistency was observed in filter bed configuration. Especially the sand layer thickness varied greatly, ranging from max 2 cm at H1 to 10 cm at H2 and 20 cm at H3. All household-scale treatment plants showed the risk of Fe-floc breakthrough into the filtrate water. Visible Fe-flocs were observed in the supernatant water of all sytems (Figure S4), from which water is abstracted for usage. Insufficient retention of Fe is achieved in the filter bed. Since As is removed through adsorption onto Fe-(hydr)oxides, Fe-floc carryover

simultaneously increased the risk of elevated As concentrations in the produced water. Consumers at H1 and H2 did not drink the the treated water and reported issues with Fe staining during washing and cooking. Users at H3 did drink the water, but Table S1 demonstrates that effluent Fe and As concentrations varied strongly per sample moment. Effluent concentrations can vary tremendously at the same location, especially with the risk of Fe-floc carryover.

Hydraulic residence time further influenced treatment performance. Figure 3 presents concentration profiles obtained after 2.5 hours of stagnation, while different profiles were observed during continous operation (Figure S5). Longer hydraulic residence time substantially lowered pH and increased removal of Fe, As, Mn and NH_4 during filtration, although this removal was partly reversed in the last step, remobilizing the contaminants into the water.

The variability in effluent concentrations in Table S1 is likely partly explained by fluctuating residence times at time of sampling. Since the systems are operated intermittently, the exact residence time can greatly vary per use. In addition, previous studies report that cleaning frequency influences performance [10,30]. No regular cleaning schedule was in place for the household-scale treatment plants, which is another inconsistency among plants.

Together, these findings demonstrate that the household-scale treatment plants operated highly inconsistently, making it difficult to directly compare individual treatment steps or removal mechanisms between systems. Therefore, the detailed removal pathways are not further discussed for H1-H3. Nevertheless, the results show that users of these systems are exposed to As, Fe, Mn and NH_4 in the produced filtrate and at risk of detrimental health effects.

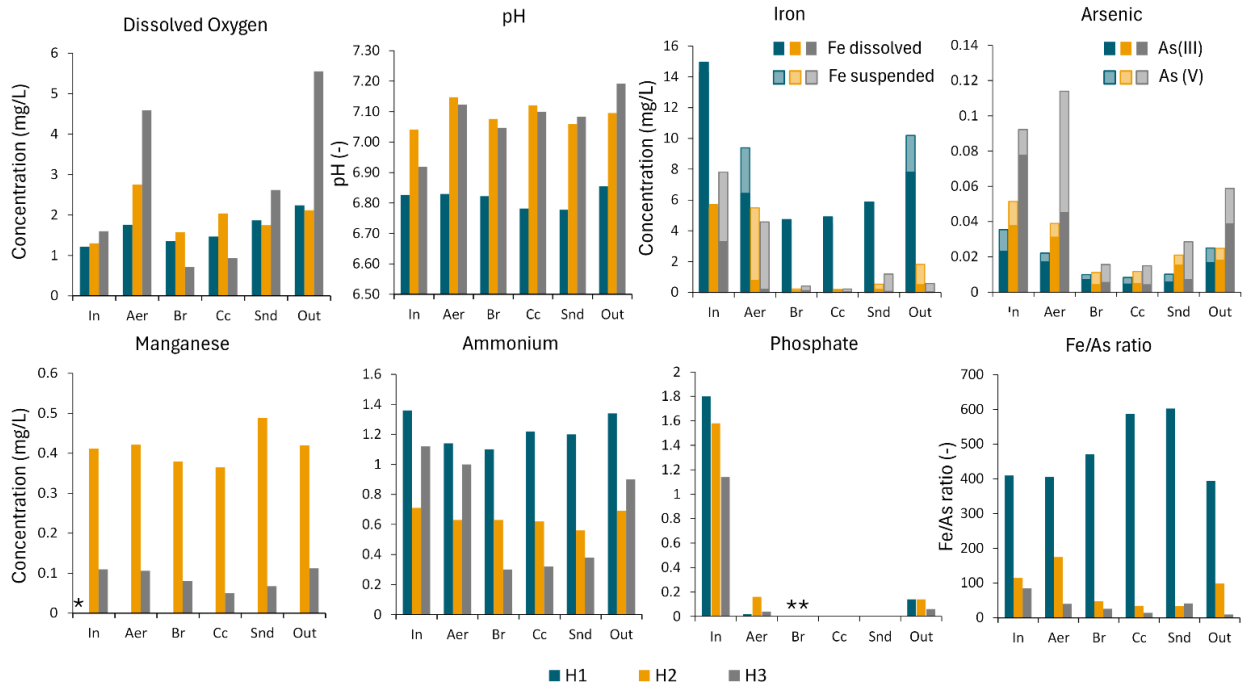

*Figure 3: Household-scale treatment plants (H1-H3) profiles of DO, pH and Fe/As ratio and the removal efficiencies of Fe, As, Mn, NH_4, and PO_4 in the raw groundwater (In), after aeration (Aer), in the brick chip filter (Br), in the charcoal filter (Cc), in the sand filter (Snd) and in the effluent (out). * Data Mn H1 missing, ** PO_4 for Br, Cc and Snd not measured*

2.3.3 Oxygen limitation in treatment plants

Sufficient DO availability is essential for the oxidation and subsequent removal of Fe, Mn and NH_4. Figure 4 presents the DO balance for plants H1-H3 and filter 3 of C1-C3. For C1-C3, a complete balance could not be made, due to the sequential aeration and filtration steps. In these systems, the most oxygen-consuming process, NH4 oxidation, occurred in filter 3, where DO was measured directly pre- and prior to filtration. Fe was almost completely removed prior to filter 3, and Mn requires much less oxygen compared to NH4. Therefore, Fe and Mn are not visible in C1-C3 of Figure 4. Oxygen demand was calculated based on the theoretical requirement for complete oxidation of influent Fe, Mn and NH4 concentrations (equations in section 2.4). Oxygen consumption was derived from the theoretical requirement corresponding to the observed removal of these constituents.

Of all investigated systems, H3 was the only treatment plant where aeration supplied sufficient DO to meet the calculated demand for complete oxidation of NH4, Fe and Mn. At H3, incoming Fe(II) indeed completely oxidized to Fe-(hydr)oxides. However, despite the oxygen availability, incomplete NH4 and Mn removal was observed. In all other plants, measured DO was lower than the calculated demand, consistent with the observed incomplete NH4 and Mn removal observed.

At C1 and C2, calculated oxygen consumption closely resembled the measured DO concentrations. At C3, calculated oxygen consumption slightly exceeded measured DO concentrations. Partial nitrification to NO_2 requires less oxygen than complete oxidation to NO3. The nitrite and nitrate concentrations were not measured, but this discrepancy

suggests the formation of nitrite in C3. In contrast, at H1-H3, calculated oxygen consumption was lower than the available DO, indicating that DO availability was not the primary limiting factor in these systems.

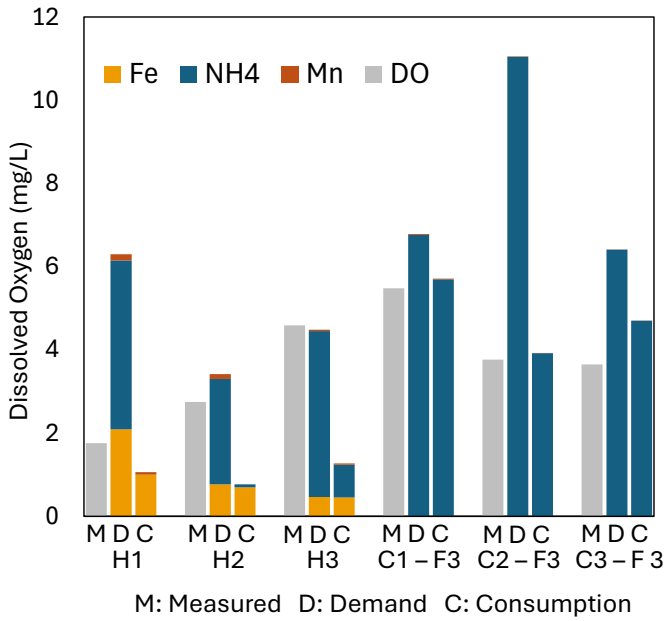

Figure 4: Oxygen balance for household-scale treatments plants H1-H3 and filter 3 (F3) of community-scale treatment plants C1-C3. Dissolved oxygen (DO) was measured (M) at the influent of the plant/filter during sampling. Oxygen demand (D) and consumed (C) was calculated based on NH_4 (blue), Fe (yellow) and Mn (red) concentrations in the influent and effluent of the plant/filter.

2.3.4 Microbial performance of treatment plants

The taxonomic composition of the microbial communities in the influent water (IN) and effluent water (OUT) of H3 and C1-C3 is presented in Figure 5. Communities are presented in relative abundance (RA), expressed as the percentage of Operational Taxonomic Units (OTUs) at the taxonomic ranks of class and family. The replicates showed relatively similar patterns, except for the influent of C2 and C3. Samples from H1 and H2 were excluded from sequencing, due to missing aeration step in these systems.

At class level, the communities were dominated by *Gammaproteobacteria* (8.9-85.9%), with the exception of one C1 influent replicate, which showed markedly lower RA (1.1%). Substantial contributions were additionally observed from *Bacteroidia* (1.3 – 26.3%), *Anaerolineae* (0.1 – 37.2%) and *Nanoarchaeia* (0.16 – 11.6 %).

At family level, dominant taxa included *Gallionellaceae* (0.0 – 49.9%), a family that includes Fe-oxidizing bacteria; *Methylophilaceae* (0.0-15.8%) and *Methylomonadaceae* (0.0-25.5%), which include methane (CH_4)-oxidizing taxa; and archaea *Woesearchaeales* (0.16-11.1%). These families have previously been identified in groundwater and drinking water treatment systems [48–52].

Surprisingly, ammonium-oxidizing bacteria were not among the ten most abundant classes or families. The RA of *Nitrospiria* ranged from 0.0 to 3.1%, while they are often found in much

higher abundance in groundwater filters [48,49]. In contrast *Nitrososphaeria,* a family including ammonium-oxidizing archaea, were more abundant, ranging from 0.01 to 12.6%.

Spatial variability in influent community composition was observed across the four locations. This variability is particularly notable for C1-C3, despite the close proximity of these locations and their groundwater sources (<1.5 km). Additionally, shifts in community composition were observed between influent and effluent samples at each location, indicating selective enrichment and/or removal of taxa during treatment.

2.3.5 PCR detection of 16S rRNA, arsenic- and iron-oxidizing bacteria

PCR results are provided in Table S2. Universal bacterial 16S rRNA genes were detected in nearly all water and filter media samples from both community- (C1-C3) and household- (H1-H3) scale treatment plants, confirming the presence of amplifiable bacterial DNA throughout the system. In C1, one of the two sand samples did not yield amplification; however, the duplicate sample and the overlying water sample were positive. Similarly, in H2, one sand sample was negative while its duplicate showed amplification. These isolated single-replicate negatives are most likely caused by amplification error rather than the absence of bacteria.

The arsenite oxidase gene was widely detected. In C1-C3, first-round amplification with AioAF/AioAR yielded positive signals in 39 out of 44 samples. Following semi-nested reamplification with aoxBM1-2F/aoxBM2-1R, detection increased to 41 out of 44 samples. In H1-H3, 23 out of 27 samples were positive for aioA, which increased to 24 after the second amplification round. In all but one case where a sample scored negative, the duplicate sample did show amplification. The sample of Filter 1 of H2, in which no aioA was detected, did not have a duplicate since removing too many bricks would disturb the filter. No amplification was observed in negative controls.

Nested amplification targeting *Gallionella*-like Fe-oxidizing bacteria also revealed widespread occurrence in both treatment systems. At C1-C3, 40 out of 44 samples showed a positive signal, and at H1-H3, 24 out of 27 gave a positive signal. No duplicate negatives were found. Fe-oxidizing bacteria were present in the influent samples and subsequent filter steps, even at treatment steps where no Fe(II) oxidation was observed (e.g. filter 2 of C1-C3). No amplification was observed in the negative controls.

Overall, genes encoding for arsenite-oxidizing and *Gallionella*-like Fe-oxidizing bacteria were detected throughout the different treatment stages, including influent water, filter material, and effluent samples.

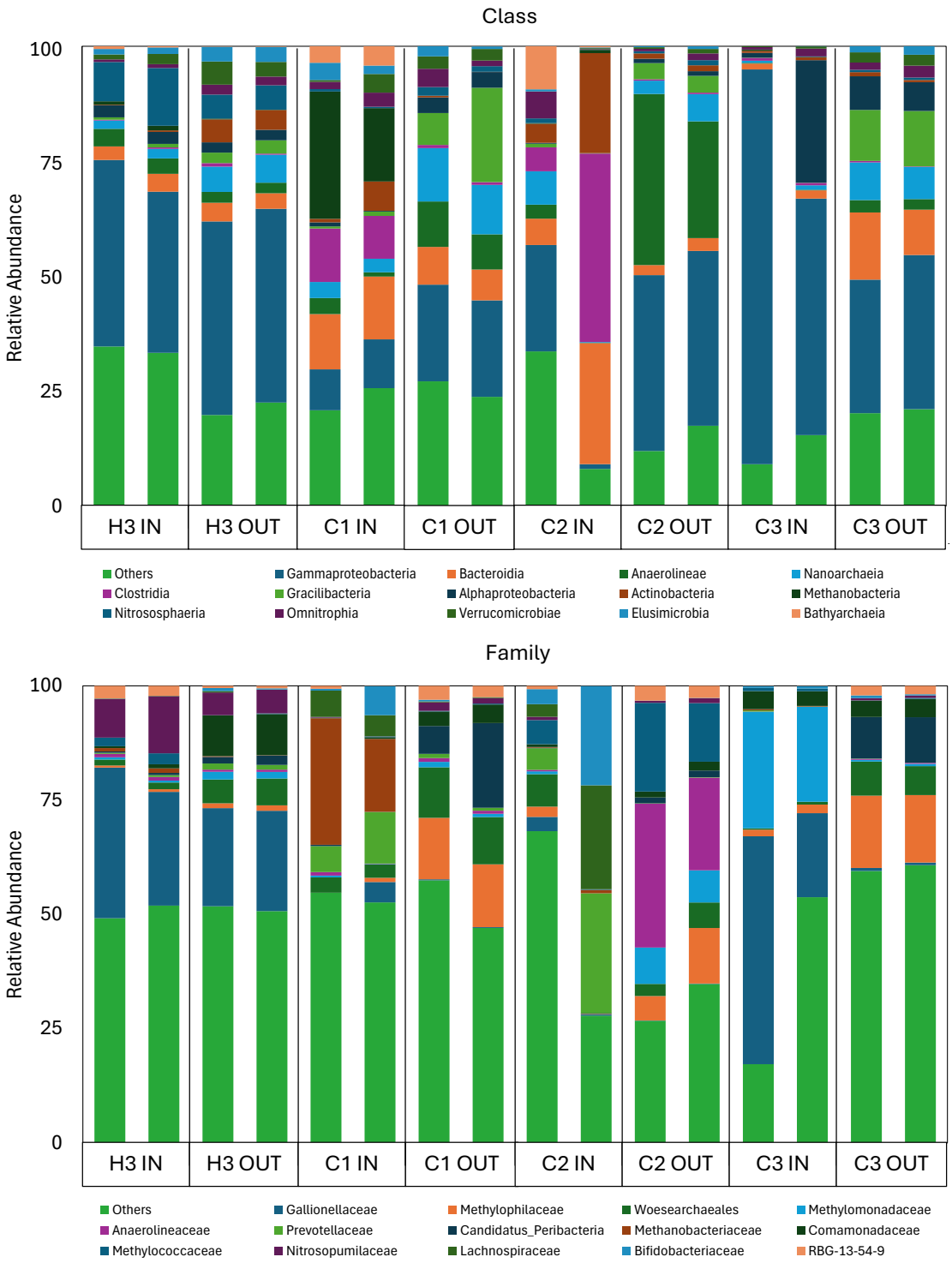

Figure 5: Distribution histogram of relative abundance of taxonomic rank Class (top) and Family (Bottom) of the microbial community in duplicates of the influent (IN) and effluent (OUT) water of household-scale treatment plant H3 and community-scale treatment plants C1-C3.

2.4 Discussion

2.4.1 Arsenic iron removal plants are biofilters

The results obtained suggest that biological processes play a key role in As, Fe, and NH_4 removal in both household- and community-scale treatment plants. NH_4 oxidation in groundwater treatment plants is inherently biological and, although incomplete, removal was observed in all plants, confirming the presence of active nitrifying communities. Notably, ammonium-oxidizing archaea (AOA) were detected in higher RA than ammonium-oxidizing bacteria (AOB). This is unexpected, as AOA are generally associated with low (<0.18 mg/L) NH_4 environments [53,54], whereas the groundwater in this study contained relatively high ammonium concentrations (0.5-4.5 mg/L). A possible explanation is their higher adaptability to low oxygen concentrations [55], which may provide a competitive advantage in these filters. Given that AOB have typically higher NH_4 oxidation rates than AOA [53], these findings further underline the importance of sufficient oxygen supply for optimal NH_4 removal.

Microorganisms associated with CH_4 oxidation, including *Methylococcaceae*, *Methylophilaceae* and *Methanobacteriaceae,* were detected throughout the systems. Although CH_4 concentrations were not measured in this study, their presence suggests that the microbial community was involved in converting CH_4 into CO_2.

There are also strong indications of biological Fe(II) oxidation in the filters. Low DO and pH are favorable conditions for Fe-oxidizing bacteria to grow [15] and PCR analysis detected *Gallionella*-related genes in all treatment plants. In H3 and C3, *Gallionellaceae* was the dominant family present in the influent, while lower RAs were observed in C1 and C2. These differences cannot be explained by influent Fe concentrations, which were comparable among C1-C3 (Figure 2). In all community-scale treatment plants, the RA of *Gallionellaceae* decreased at least fivefold from influent to effluent, consistent with Fe being removed predominantly in the early treatment stages. In contrast, *Gallionellaceae* remained abundant in the effluent of H3, in agreement with the high residual Fe flocs observed in the effluent of this plant (Figure S4). Other Fe-oxidizing bacteria, such as *Ferrovibrionales,* were also detected. Additionally, tube-like structures characteristic of *Leptothrix* were observed in sludge samples (Figure S6) [56], although they were not found with 16S rRNA sequencing. Together, these findings support active biological Fe(II) oxidation within the filters. Nevertheless, abiotic oxidation likely occurred simultaneously, as visible Fe flocs throughout the system (Figure S4) indicate homogeneous and heterogeneous Fe(II) oxidation.

In contrast to NH_4, CH_4 and Fe(II) oxidation – each associated with specific microbial taxa – As(III) oxidation is not restricted to a distinct phylogenetic cluster. The arsenite oxidase operon is widely distributed among bacterial taxa and may spread by horizontal gene transfer [57,58]. The aioA gene was detected by PCR throughout the treatment systems and was already present in influent groundwater, suggesting continuous inoculation from the source water and persistence within the treatment system. Although As speciation is difficult to track due to rapid adsorption onto Fe-(hydr)oxides, direct evidence of As(III) oxidation was observed in Filter 2 of C1 and C3, where increases in As(V) exceeded the amount of total As removed.

Furthermore, As(III) oxidation occurred in the absence of detectable Fe(II) oxidation in C3, and with only minimal Fe(II) oxidation (0.2 mg/L) in C1. These observations indicate that As(III) oxidation was unlikely to result from co-oxidation with Fe and suggests a contribution of As- oxidizing bacteria.

While microbial activity enhances contaminant removal, the presence of pathogens must also be considered. Bacteria associated with fecal contamination were detected in the treatment systems. The class *Clostridia* is linked to manure [59], and the families *Prevotellaceae* and *Bifidobacteriaceae* are associated with fecal pollution [60,61]. Potential contamination sources include nearby agricultural fields or septic systems. This might also explain the variability in influent microbial community among C1-C3, despite their close geographic proximity (<1.5 km). The most severely polluted plant, C2, exhibited 41% RA of the *Clostridia* and 26.2% and 21.7% of the families *Prevotellaceae* and *Bifidobacteriaceae,* respectively, in the influent. The strong variation between C2 replicates suggests that part of the observed signal may be attributable to incidental contamination during or after sampling. Nevertheless, members of these taxa were detected in all treatment plants, indicating that their presence is widespread. These taxa are anaerobic, and oxygenation reduced their RA to below 1%, providing an additional argument for adequate aeration to safeguard treatment performance.

Overall, these findings demonstrate that the treatment plants function as biologically active systems rather than purely physicochemical filters. Microbial communities contribute to the removal of NH_4, CH_4, Fe and As, and proper aeration is essential to suppress undesirable anaerobic pathogens. These biological pathways should be explicitly considered in plant design and maintenance. The community-scale treatment plants are monthly cleaned with bleach, which likely inactivates beneficial microbial processes. Further research is recommended to assess the impact of this practice on long-term treatment performance and to come up with possible alternative cleaning practices.

2.4.2 Process conditions to improve arsenic removal

In As-affected regions in Bangladesh such as Manikganj and Satkhira, decentralized groundwater treatment plants reduce exposure to As compared to direct consumption of untreated groundwater. Nevertheless, the treatment plants investigated in this study did not consistently achieve As removal below the WHO drinking water norm, meaning that health risks remain.

An additional concern was observed in the household-scale treatment plants, where Fe-floc breakthrough into the filtrate water increased the risk of elevated As concentrations in the produced drinking water. The operational variability between household-scale systems complicated robust interpretation of As removal pathways, because of differences in aeration, filter bed thickness, residence time and cleaning practices.

At C1-C3, three factors likely limited As removal. First, influent concentrations of PO_4 were several orders of magnitude higher than As, and PO_4 competes with As(V) for adsorption sites

on Fe-(hydr)oxides [45,62]. Second, the Fe/As ratio dropped below commonly reported thresholds of around 20-40 for effective As removal in the second filter (Leupin and Hug, 2005; Meng et al., 2002). Third, the gradual increase in pH from ~7 to ~8 likely reduced arsenate adsorption capacity, as higher pH is known to decrease both arsenate and phosphate binding to Fe-(hydr)oxides (Jain and Loeppert, 2000). This could also explain the release of PO_4 and As(V) in the second and third filter bed, respectively.

A practical strategy to overcome these limitations is to ensure rapid and complete As(III) oxidation in the first filter bed. Filter 1 at the community-scale treatment plants provides the most favorable conditions for As removal; freshly formed Fe-(hydr)oxides with unoccupied sorption sites, high Fe/As ratios and relatively low pH. Accelerating As(III) oxidation can be achieved by enhancing surface-catalyzed oxidation through increased reactive surface area [63,64] and/or by stimulating biological oxidation by AsOB [49,65].

Another possible solution to improve As removal is to slow down Fe(II) oxidation in the first filter bed. Lower pH and DO reduce the Fe(II) oxidation kinetics [14]. When Fe(II) and As(III) oxidation occur simultaneously, freshly formed Fe-(hydr)oxides remain available for adsorption of As(V). In the community-scale treatment plants, the DO entering filter 1 exceeds the oxygen demand for complete Fe(II) oxidation, while the remaining oxygen is not yet utilized for Mn or NH_4 oxidation. Reducing aeration prior to the first filter would lower both DO and pH, thereby slowing Fe(II) oxidation. Additionally, this shifts part of the Fe(II) oxidation to filter 2, where As(III) oxidation continues to occur, increasing the overlap between Fe-(hydr)oxides formation and As(III) oxidation. Therefore, lowering the DO in filter 1 would likely enhance the co-removal of As with Fe across the two filter beds. Such an approach would require stronger aeration after the first filter bed to provide sufficient oxygen for subsequent NH_4 and Mn oxidation. This strategy is not feasible with the current design of the household-scale treatment plants, where only a single aeration step is present.

For the household-scale treatment plants, it remains difficult to directly relate process conditions to As removal, due to the large operational variability among systems. A possible explanation for this variability is the lack of a maintenance and cleaning structure for the household-scale treatment plants, which has been shown to strongly affect treatment performance [30,47,66]. Community-based systems involve committees responsible for tariff collection, system monitoring, and maintenance scheduling, which has been shown to improve sustainability compared to standalone household systems [31]. Future research should therefore not only focus on optimizing physicochemical and biological removal processes, but also on identifying operational strategies that ensure stable long-term performance of decentralized treatment systems.

2.4.3 Process conditions to improve overall performance

Beyond As, incomplete removal of NH_4 and Mn is an additional concern for the plants monitored. NH_4 was detected in the effluent of all filters after treatment. The presence of residual NH_4 may promote microbial regrowth during transport and storage [67], thereby increasing the risk of recontamination with pathogenic bacteria such as *E.coli* [68]. In addition,

chronic exposure to elevated Mn concentrations in drinking water has been associated with neurotoxic effects. The WHO guideline value for Mn was exceeded in the household-scale treatment plants. Three operational conditions were identified with the potential to improve treatment performance.

First and foremost, DO concentration was a critical limitation. While all plants received sufficient oxygen to oxidize Fe(II), DO concentrations were insufficient to fully oxidize NH_4 and Mn (Figure 4). At household-scale treatment plants lacking the aeration tray, no NH_4 and Mn removal was observed. The absence of functional aeration trays was not incidental; a survey of 310 treatment plants in the same region showed that approximately 38% were equipped with a broken aeration tray [47]. Another disadvantage of anoxic conditions in the filter bed is the destabilization of As removal, as it can cause reduction of adsorbed As(V) to dissolved As(III). Reimplementing and optimization of the aeration step at the household-scale treatment plants is therefore essential. Similarly, despite multiple aeration steps at the community-scale treatment plants, oxygen supply remained insufficient to oxidize all NH_4 and Mn. Before filter 2 and filter 3 at the community-scale treatment plants, improved aeration is needed to meet the oxygen demand.

However, in some filters, oxygen consumption remained below the available DO concentration, suggesting that DO was not the sole limiting factor for removal. Hydraulic retention time and/or adsorption surface area, likely also contributed to the observed removal limitations.

The hydraulic retention time was indeed found to be a key controlling factor, influencing both physicochemical and biological removal processes. Longer residence times in H3 enhanced Fe(II) oxidation and subsequent As adsorption onto freshly formed Fe flocs (Figure S5), consistent with previous observations reported by Brennan and McBean, (2011). A higher hydraulic retention time also promoted biological processes; increasing the residence time from approximately 5 minutes to 2.5 hours resulted in a 2.5-fold increase in NH_4 removal (Figure S5).

Finally, increasing the surface area in the filter beds could improve both biological and physicochemical removal processes. Sand provides a large surface area for biofilm development and surface-catalytic reactions, supporting biological oxidation of NH_4, Mn and As [23,49], as well as surface-catalyzed Mn oxidation [69–71]. Additionally, it will reduce Fe floc breakthrough due to adsorption to surfaces and particle retention. The limited thickness of sand in the household-scale treatment plants (0-20 cm) and the use of stone beds with low surface area in the first two filters of the community-scale treatment plants likely constrained removal efficiency. Replacing stone beds with sand could enhance removal, although potential impacts on hydraulic conductivity and backwashing requirements should be evaluated.

2.5 Conclusion

The community- and household- scale groundwater treatment plants in Satkhira and Manikganj, installed to remove Fe and As, functioned as biologically active filtration systems rather than purely physicochemical treatment units. Genes associated with As- and Fe-oxidation were detected throughout the systems, and sequencing confirmed the presence of characteristic groundwater treatment microorganisms, including the Fe-oxidizing family *Gallionellaceae*.

The community-scale treatment plants achieved >99% Fe removal and 66-79% As removal. The household-scale treatment plants showed substantial variability in treatment performance due to inconsistent operation, with the risk of Fe-floc breakthroughs in the produced filtrate.

Optimization of these treatment plants requires explicit consideration of the biological removal pathways. Increasing oxygen availability, hydraulic retention time, and filter surface area could potentially stimulate biofilm development and improve removal performance. For As specifically, improved removal may be achieved by promoting rapid As(III) oxidation while delaying Fe(II) oxidation, thereby increasing the availability of adsorption sites for As(V). Overall, the findings show that biological processes are a central component of groundwater treatment plants in Bangladesh and should be actively considered in the design, operation and maintenance of the treatment plants to reduce health risks in As-effected regions.

References

1. Rahman MM, Ng JC, Naidu R. Chronic exposure of arsenic via drinking water and its adverse health impacts on humans. *Environmental Geochemistry and Health 2009 31:1*. 2009;31(1):189-200. doi:10.1007/S10653-008-9235-0

2. Ahmad A, van der Wens P, Baken K, de Waal L, Bhattacharya P, Stuyfzand P. Arsenic reduction to <1 µg/L in Dutch drinking water. *Environ Int*. 2020;134:105253. doi:10.1016/J.ENVINT.2019.105253

3. Podgorski J, Berg M. Global threat of arsenic in groundwater. *Science (1979)*. 2020;368(6493):845-850. doi:10.1126/science.aba1510

4. Fewtrell L, Fuge R, Kay D. An estimation of the global burden of disease due to skin lesions caused by arsenic in drinking water. *J Water Health*. 2005;3(2):101-107. doi:10.2166/WH.2005.0011

5. Van Halem D, Bakker SA, Amy GL, Van Dijk JC. Arsenic in drinking water: A worldwide water quality concern for water supply companies. *Drink Water Eng Sci*. 2009;2(1):29-34. doi:10.5194/DWES-2-29-2009

6. BGS and DPHE. *Arsenic Contamination of Groundwater in Bangladesh. 2, Final Report, BGS Technical Report*. 2001.

7. Huq ME, Fahad S, Shao Z, et al. Arsenic in a groundwater environment in Bangladesh: Occurrence and mobilization. *J Environ Manage*. 2020;262:110318. doi:10.1016/J.JENVMAN.2020.110318

8. Smith AH, Lingas EO, Rahman M. Contamination of drinking-water by arsenic in Bangladesh: a public health emergency. *Bull World Health Organ*. Published online 2000.

9. Rahman MA, Kumar S, Fazle Bari ASM, Sharma A, Rahman MM. Efficiency of arsenic and iron removal plants (AIRPs) for groundwater treatment in rural areas of southwest Bangladesh. *Water (Switzerland)*. 2021;13(3):1-18. doi:10.3390/w13030354

10. Brennan R, McBean E. A performance assessment of arsenic-iron removal plants in the Manikganj District of Bangladesh. *J Water Health*. 2011;9(2):317-329. doi:10.2166/wh.2011.107

11. Sorensen IM, McBean EA, Rahman M. Retrofitting arsenic-iron removal plants in rural Bangladesh for performance enhancement. *Journal of Water, Sanitation and Hygiene for Development*. 2014;4(3):400-409. doi:10.2166/WASHDEV.2014.122

12. Corbera-Rubio F, Goedhart R, Laureni M, van Loosdrecht MC, van Halem D. A biotechnological perspective on sand filtration for drinking water production. *Curr Opin Biotechnol*. 2024;90:103221. doi:10.1016/J.COPBIO.2024.103221

13. World Health Organization. *Guidelines for Drinking-Water Quality: Fourth Edition Incorporating the First and Second Addenda*. 2022.

14. Van Beek CGEM, Hiemstra T, Hofs B, Nederlof MM, Van Paassen JAM, Reijnen GK. Homogeneous, heterogeneous and biological oxidation of iron(II) in rapid sand filtration. Published online 2012. doi:10.2166/aqua.2012.033

15. Müller S, Corbera-Rubio F, Schoonenberg Kegel F, Laureni M, van Loosdrecht MCM, van Halem D. Shifting to biology promotes highly efficient iron removal in groundwater filters. *Water Res*. 2024;262:122135. doi:10.1016/j.watres.2024.122135

16. Corbera-Rubio F, Laureni M, Koudijs N, et al. Meta-omics profiling of full-scale groundwater rapid sand filters explains stratification of iron, ammonium and manganese removals. *Water Res*. 2023;233. doi:10.1016/J.WATRES.2023.119805

17. Ramsay L, Breda IL, Søborg DA. Comprehensive analysis of the start-up period of a full-scale drinking water biofilter provides guidance for optimization. *Drink Water Eng Sci*. 2018;11(2):87-100. doi:10.5194/DWES-11-87-2018

18. Kruisdijk E, van Breukelen BM, van Halem D. Simulation of rapid sand filters to understand and design sequential iron and manganese removal using reactive transport modelling. *Water Res*. 2024;267(September):122517. doi:10.1016/j.watres.2024.122517

19. Bruins JH, Petrusevski B, Slokar YM, et al. Biological and physico-chemical formation of Birnessite during the ripening of manganese removal filters. Published online 2014. doi:10.1016/j.watres.2014.11.019

20. Corbera-Rubio F, Kruisdijk E, Malheiro S, et al. A difficult coexistence: Resolving the iron-induced nitrification delay in groundwater filters. *Water Res*. 2024;260:121923. doi:10.1016/J.WATRES.2024.121923

21. Van Kessel MAHJ, Speth DR, Albertsen M, et al. Complete nitrification by a single microorganism. *Nature 2015 528:7583*. 2015;528(7583):555-559. doi:10.1038/nature16459

22. Chambers T, Willink R, Reynolds A, et al. Exposure to nitrate and nitrite in drinking water and cancers. *Cochrane Database of Systematic Reviews*. 2024;2024(3). doi:10.1002/14651858.CD015822

23. Gülay A, Tatari K, Musovic S, Mateiu R V., Albrechtsen HJ, Smets BF. Internal Porosity of Mineral Coating Supports Microbial Activity in Rapid Sand Filters for Groundwater Treatment. *Appl Environ Microbiol*. 2014;80(22):7010. doi:10.1128/AEM.01959-14

24. Cullen WR, Reimer KJ. Arsenic Speciation in the Environment. *Chem Rev*. 1989;89(4):713-764. doi:10.1021/cr00094a002

25. Kim MJ, Nriagu J. Oxidation of arsenite in groundwater using ozone and oxygen. *Science of The Total Environment*. 2000;247(1):71-79. doi:10.1016/S0048-9697(99)00470-2

26. Hug SJ, Leupin O. Iron-catalyzed oxidation of Arsenic(III) by oxygen and by hydrogen peroxide: pH-dependent formation of oxidants in the Fenton reaction. *Environ Sci Technol*. 2003;37(12):2734-2742. doi:10.1021/es026208x

27. Driehaus W, Seith R, Jekel M. Oxidation of arsenate(III) with manganese oxides in water treatment. *Water Res*. 1995;29(1):297-305. doi:10.1016/0043-1354(94)E0089-O

28. Crognale S, Casentini B, Amalfitano S, Fazi S, Petruccioli M, Rossetti S. Biological As(III) oxidation in biofilters by using native groundwater microorganisms. *Science of the Total Environment*. 2019;651:93-102. doi:10.1016/j.scitotenv.2018.09.176

29. Gude JCJ, Rietveld LC, van Halem D. Biological As(III) oxidation in rapid sand filters. *Journal of Water Process Engineering*. 2018;21:107-115. doi:10.1016/J.JWPE.2017.12.003

30. Sorensen IM, McBean EA. Beyond appropriate technology: Social considerations for the sustainable use of Arsenic-Iron Removal Plants in rural Bangladesh. *Technol Soc*. 2015;41:1-9. doi:10.1016/j.techsoc.2014.10.003

31. WaterAid. *Arsenic-Iron Removal Plants in a Local Context*. 2021. Accessed December 20, 2025. https://washmatters.wateraid.org/sites/g/files/jkxoof256/files/2021-07/Case%20Study%202%20Bangladesh%20DIGITAL.pdf

32. Voegelin A, Kaegi R, Frommer J, Vantelon D, Hug SJ. Effect of phosphate, silicate, and Ca on Fe(III)-precipitates formed in aerated Fe(II)- and As(III)-containing water studied by X-ray absorption spectroscopy. *Geochim Cosmochim Acta*. 2010;74(1):164-186. doi:10.1016/J.GCA.2009.09.020

33. Kaegi R, Voegelin A, Folini D, Hug SJ. Effect of phosphate, silicate, and Ca on the morphology, structure and elemental composition of Fe(III)-precipitates formed in aerated Fe(II) and As(III) containing water. *Geochim Cosmochim Acta*. 2010;74(20):5798-5816. doi:10.1016/J.GCA.2010.07.017

34. Wang J, Muyzer G, Le Bodelier P, Laanbroek HJ. Diversity of iron oxidizers in wetland soils revealed by novel 16S rRNA primers targeting Gallionella-related bacteria. *ISME J*. 2009;3:715-725. doi:10.1038/ismej.2009.7

35. Caporaso JG, Lauber CL, Walters WA, et al. Ultra-high-throughput microbial community analysis on the Illumina HiSeq and MiSeq platforms. *The ISME Journal 2012 6:8*. 2012;6(8):1621-1624. doi:10.1038/ismej.2012.8

36. Walters W, Hyde ER, Berg-Lyons D, et al. Improved Bacterial 16S rRNA Gene (V4 and V4-5) and Fungal Internal Transcribed Spacer Marker Gene Primers for Microbial Community Surveys. *mSystems*. 2015;1(1). doi:10.1128/MSYSTEMS.00009-15

37. Weisburg WG, Barns SM, Pelletier DA, Lane DJ. 16S ribosomal DNA amplification for phylogenetic study. *J Bacteriol*. 1991;173(2):697-703. doi:10.1128/jb.173.2.697-703.1991

38. Fierer N, Jackson JA, Vilgalys R, Jackson RB. Assessment of soil microbial community structure by use of taxon-specific quantitative PCR assays. *Appl Environ Microbiol*. 2005;71(7):4117-4120. doi:10.1128/AEM.71.7.4117-4120.2005

39. Ghosh D, Bhadury P, Routh J. Diversity of arsenite oxidizing bacterial communities in arsenic-rich deltaic aquifers in West Bengal, India. *Front Microbiol*. 2014;0(NOV):602. doi:10.3389/FMICB.2014.00602

40. Quéméneur M, Cébron A, Billard P, et al. Population structure and abundance of arsenite-oxidizing bacteria along an arsenic pollution gradient in waters of the upper isle river basin, France. *Appl Environ Microbiol*. 2010;76(13):4566-4570. doi:10.1128/AEM.03104-09

41. Bolyen E, Rideout JR, Dillon MR, et al. Reproducible, interactive, scalable and extensible microbiome data science using QIIME 2. *Nat Biotechnol*. 2019;37(8):852-857. doi:10.1038/S41587-019-0209-9

42. Callahan BJ, McMurdie PJ, Rosen MJ, Han AW, Johnson AJA, Holmes SP. DADA2: High-resolution sample inference from Illumina amplicon data. *Nat Methods*. 2016;13(7):581-583. doi:10.1038/NMETH.3869

43. Quast C, Pruesse E, Yilmaz P, et al. The SILVA ribosomal RNA gene database project: improved data processing and web-based tools. *Nucleic Acids Res*. 2013;41(Database issue). doi:10.1093/NAR/GKS1219

44. Meng X, Korfiatis GP, Bang S, Bang KW. Combined effects of anions on arsenic removal by iron hydroxides. *Toxicol Lett*. 2002;133(1):103-111. doi:10.1016/S0378-4274(02)00080-2

45. Jain A, Loeppert RH. Effect of Competing Anions on the Adsorption of Arsenate and Arsenite by Ferrihydrite. *J Environ Qual*. 2000;29(5):1422-1430. doi:10.2134/JEQ2000.00472425002900050008X;WEBSITE:WEBSITE:ACSESS.ONLINELIBRARY.WILEY.COM;ISSUE:ISSUE:DOI

46. Driehaus W, Dupont F. Arsenic removal - solutions for a world wide health problem using iron based adsorbents. *European journal of water quality*. 2005;36(2):119-132. doi:10.1051/water/20053602119

47. Hossain B, Ahmed T. Arsenic-Iron removal plants in water-challenged rural areas of Bangladesh: performance evaluation and user perception. *Journal of Water, Sanitation and Hygiene for Development*. 2025;15(12):1069-1083. doi:10.2166/washdev.2025.117

48. Boersma AS, Haukelidsaeter S, Kirwan L, et al. Influence of filter backwashing on iron, manganese, and ammonium removal in dual-media rapid sand filters used for drinking water production. *Water Res*. 2025;270:122809. doi:10.1016/J.WATRES.2024.122809

49. Goedhart R, Kruisdijk E, van Halem D. Biofilm Accelerates As(III) Oxidation on Reactive MnOx Coated Filter Sand in Groundwater Filters. *ACS ES&T Water*. 2025;5(12):7536-7547. doi:10.1021/ACSESTWATER.5C01031

50. Liu G, Zhang Y, van der Mark E, et al. Assessing the origin of bacteria in tap water and distribution system in an unchlorinated drinking water system by SourceTracker using microbial community fingerprints. *Water Res*. 2018;138(5):86-96. doi:10.1016/j.watres.2018.03.043

51. Poghosyan L, Koch H, Frank J, et al. Metagenomic profiling of ammonia- and methane-oxidizing microorganisms in two sequential rapid sand filters. *Water Res*. 2020;185:116288. doi:10.1016/j.watres.2020.116288

52. Villeneuve K, Violette M, Lazar CS. From Recharge, to Groundwater, to Discharge Areas in Aquifer Systems in Quebec (Canada): Shaping of Microbial Diversity and Community Structure by Environmental Factors. *Genes 2023, Vol 14,*. 2022;14(1). doi:10.3390/genes14010001

53. Di HJ, Cameron KC, Shen JP, et al. Ammonia-oxidizing bacteria and archaea grow under contrasting soil nitrogen conditions. *FEMS Microbiol Ecol*. 2010;72(3):386-394. doi:10.1111/j.1574-6941.2010.00861.x

54. Habteselassie MY, Stark JM, Miller BE, Thacker SG, Norton JM. Gross Nitrogen Transformations in an Agricultural Soil after Repeated Dairy-Waste Application. *Soil Science Society of America Journal*. 2006;70(4):1338-1348. doi:10.2136/sssaj2005.0190

55. Du J, Meng L, Qiu M, et al. Ammonia-oxidizing archaea and ammonia-oxidizing bacteria communities respond differently in oxy-gen-limited habitats. *Front Environ Sci*. 2022;10:976618. doi:10.3389/fenvs.2022.976618

56. Eggleton RA, Fitzpatrick RW. Characteristics of hollow microtubes consisting of amorphous iron oxide nanoparticles produced by iron oxidizing bacteria, Leptothrix ochracea. *J Magn Magn Mater*. 2007;310(2):2405-2407. doi:10.1346/CCMN.1988.0360203

57. Andres J, Bertin PN. The microbial genomics of arsenic. *FEMS Microbiol Rev*. 2016;40(2):299-322. doi:10.1093/FEMSRE/FUV050

58. Heinrich-Salmeron A, Cordi A, Brochier-Armanet C, et al. Unsuspected diversity of arsenite-oxidizing bacteria as revealed by widespread distribution of the aoxB Gene in prokaryotes. *Appl Environ Microbiol*. 2011;77(13):4685-4692. doi:10.1128/AEM.02884-10

59. Huysman F, Van Renterghem B, Verstraete W. Antibiotic resistant sulphite-reducing clostridia in soil and groundwater as indicator of manuring practices. *Water Air Soil Pollut*. 1993;69(3-4):243-255. doi:10.1007/BF00478161

60. Koskey AM, Fisher JC, Eren AM, et al. Blautia and Prevotella sequences distinguish human and animal fecal pollution in Brazil surface waters. *Environ Microbiol Rep*. 2014;6(6):696. doi:10.1111/1758-2229.12189

61. Rahman S, Kortman GAM, Boekhorst J, Lee P, Khan MR, Ahmed F. Effect of low-iron micronutrient powder (MNP) on the composition of gut microbiota of Bangladeshi children in a high-iron groundwater setting: a randomized controlled trial. *European Journal of Nutrition 2021 60:6*. 2021;60(6):3423-3436. doi:10.1007/s00394-021-02523-1

62. Leupin OX, Hug SJ. Oxidation and removal of arsenic (III) from aerated groundwater by filtration through sand and zero-valent iron. *Water Res*. 2005;39(9):1729-1740. doi:10.1016/J.WATRES.2005.02.012

63. Manning B, Fendorf S, Bostick B, Suarez D. Arsenic(III) Oxidation and Arsenic(V) Adsorption Reactions on Synthetic Birnessite. Published online 2002. doi:10.1021/es0110170

64. Gude JCJ, Rietveld LC, van Halem D. As(III) oxidation during full-scale aeration and rapid filtration. *Environmental Arsenic in a ChangingWorld - 7th International Congress and Exhibition Arsenic in the Environment, 2018*. Published online August 23, 2019:447-448. doi:10.1201/9781351046633-176

65. Kruisdijk E, Goedhart R, van Halem D. Biological arsenite oxidation on iron-based adsorbents in groundwater filters. *Water Res*. 2024;262:122128. doi:10.1016/J.WATRES.2024.122128

66. Jain CK, Singh RD. Technological options for the removal of arsenic with special reference to South East Asia. *J Environ Manage*. 2012;107:1-18. doi:10.1016/J.JENVMAN.2012.04.016

67. Miao X, Bai X. Characterization of the synergistic relationships between nitrification and microbial regrowth in the chloraminated drinking water supply system. *Environ Res*. 2021;199(7):111252. doi:10.1016/j.envres.2021.111252

68. Gärtner N, Germann L, Wanyama K, Ouma H, Meierhofer R. Keeping water from kiosks clean: Strategies for reducing recontamination during transport and storage in Eastern Uganda. *Water Res X*. 2021;10(4):100079. doi:10.1016/j.wroa.2020.100079

69. Katsoyiannis IA, Zouboulis AI. Biological treatment of Mn(II) and Fe(II) containing groundwater: kinetic considerations and product characterization. *Water Res*. 2004;38:1922-1932. doi:10.1016/j.watres.2004.01.014

70. Breda IL, Ramsay L, Roslev P. Manganese oxidation and bacterial diversity on different filter media coatings during the start-up of drinking water biofilters. *Journal of Water Supply: Research and Technology - AQUA*. 2017;66(8):641-650. doi:10.2166/AQUA.2017.084

71. Propolsky D, Romanovski V. Iron and manganese removal from groundwater: comprehensive review of filter media performance and pathways to polyfunctional applications. *Environ Sci (Camb)*. 2025;11(11):2499-2515. doi:10.1039/D5EW00751H

Supplementary Information

Figure S1: Pictures of sampled groundwater household-scale treatment plant in Manikganj. Left: missing aeration tray. Right: aeration tray present

Figure S2: Pictures of sampled community-scale treatment plant in Satkhira. Top: overview picture of the whole plant. Bottom left: Filter 2 (stones), bottom middle: Filter 3 (sand), bottom right: aeration plate

Figure S3: Pictures of the sampling setup of taking the vertical removal profile at household-scale treatment plants H1-H3. Left: the syringe and filter sock which was placed in each different filter layer (right top). Right bottom shows how the three tubes coming out of the bed after placing back the layers.

Figure S4: Pictures of Fe flocs present in the effluent of the tank at H1 (left two) H2 (middle two) and H3 (right). Both flocs floating in the water (top pictures), as flocs precipitated on the top of the filter bed (bottom and right pictures) are visible. Note: the filter is upflow, so the supernatant water is the treated effluent.

Table S1: Removal efficiencies in % of Fe(tot) and As(tot) for household-scale treatment plants H1-H3 at 4 different time points; during Flushing, after 2.5 hours of stagnation (as shown in Figure S5), and at 2 additional time points following variable periods of plant use stagnation. The variability in removal efficiencies between sampling events demonstrates the inconsistent performance of the household-scale treatment plants. At stagnant sample event 3 for H3, Fe flocs ended up in the filtrate water resulting in negative removal.

Location		Flush	Stagnant 1	Stagnant 2	Stagnant 3
H1	Fe (tot)	22.3	28.8	72.2	96.3
	As (tot)	22.9	26.0	82.4	90.7
H2	Fe (tot)	66.0	67.1	76.3	94.8
	As (tot)	36.1	41.8	57.3	81.4
H3	Fe(tot)	90.3	92.6	97.9	-103.7
	As(tot)	34.5	36.2	78.2	-174.5

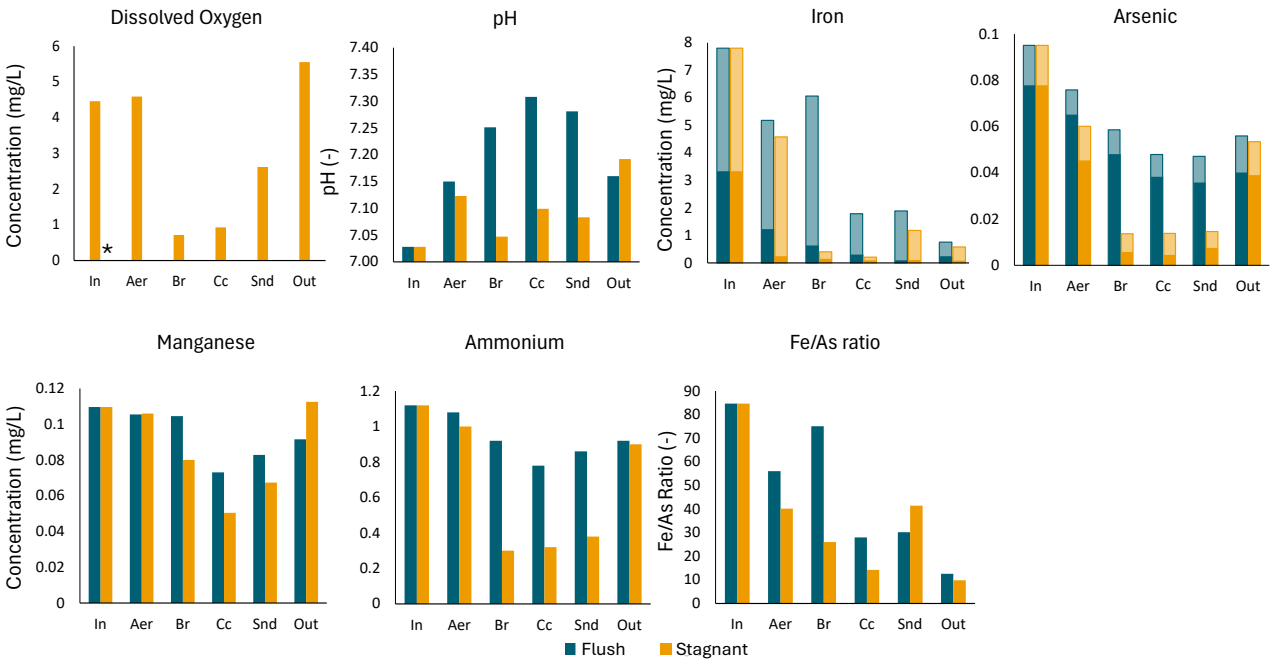

*Figure S5: H3 removal profiles during continuous flushing (left bars, blue) and after 2.5 hours of stagnation (right bars, yellow) of DO, pH and Fe/As ratio and the removal efficiencies of Fe, As, Mn and NH_4, in the raw groundwater (In), after aeration (Aer), in the brick chip filter (Br), in the charcoal filter (Cc), in the sand filter (snd) and in the effluent (out). *DO profile of flush is missing*

Table S2: PCR results for community- (C1-C3) and household- (H1-H3) scale treatment plants. "+" means a positive signal and "-" a negative signal. Sample refers to the sample points as identified in Figure 1. Type refers to sample form (water, stones, sand or Fe sludge). Conc DNA is is ng/uL. Details about the primers is given in Table 1.

C1

Sample	Type	Conc DNA	PCR Results				
			FC27/RC1492	Eub338F / Eub518R	aoxBM1-2F / aoxBM2-1R	aioAF / aioAR	628F / 998R
Influent	Water	7.5	"+"	"+"	"+"	"+"	"+"
Influent	Water	2.2	"+"	"+"	"+"	"+"	"+"
Aeration	Water	10.02	"+"	"+"	"+"	"+"	"+"
Aeration	Water	3.4	"+"	"+"	"+"	"+"	"+"
Filter 1	Water	41.3	"+"	"+"	"+"	"+"	"+"
Filter 1	Water	23.9	"+"	"+"	"+"	"+"	"+"
Filter 2	Stones	46.4	"+"	"+"	"+"	"+"	"+"
Filter 2	Stones	32.5	"+"	"+"	"+"	"+"	"+"
Filter 3	Sand	10.61	"+"	" - "	" - "	"+"	"+"
Filter 3	Sand	12.04	" - "	" - "	" - "	" - "	" - "
Filter 3	Water	13.6	"+"	"+"	"+"	"+"	"+"
Filter 3	Water	10.4	"+"	"+"	"+"	"+"	"+"
Effluent	Water	5.6	"+"	" - "	" - "	"+"	"+"
Effluent	Water	31.5	"+"	"+"	"+"	"+"	"+"

C2

Sample	Type	Conc DNA	PCR Results				
			FC27/RC1492	Eub338F / Eub518R	aoxBM1-2F / aoxBM2-1R	aioAF / aioAR	628F / 998R
Influent	Water	1.4	"+"	"+"	"+"	" - "	"+"
Influent	Water	10.1	"+"	"+"	"+"	" - "	"+"
Aeration	Water	5.4	"+"	"+"	"+"	"+"	"+"
Aeration	Water	20.9	"+"	"+"	"+"	"+"	"+"
Filter 1	Water	42.5	"+"	"+"	"+"	"+"	"+"
Filter 1	Water	50.9	"+"	"+"	"+"	"+"	"+"
Filter 2	Stones	45.2	"+"	"+"	"+"	"+"	"+"
Filter 2	Stones	14.5	"+"	"+"	"+"	"+"	"+"
Filter 3	Sand	9.75	"+"	" - "	" - "	"+"	" - "
Filter 3	Sand	6.56	"+"	" - "	" - "	"+"	"+"
Filter 3	Water	37.2	"+"	"+"	" - "	"+"	"+"

Filter 3	Water	34.6	"+"	"+"	"+"	"+"	"+"
Effluent	Water	4.6	"+"	" - "	" - "	"+"	"+"
Effluent	Water	15	" - "	"+"	" - "	"+"	"+"

C3

Sample	Type	Conc DNA	PCR Results				
			FC27/RC1492	Eub338F / Eub518R	aoxBM1-2F / aoxBM2-1R	aioAF / aioAR	628F / 998R
Influent	Water	1.8	"+"	"+"	"+"	"+"	"+"
Influent	Water	2	"+"	"+"	"+"	"+"	"+"
Aeration	Water	3.4	"+"	"+"	"+"	"+"	"+"
Aeration	Water	2.3	" - "	"+"	" - "	"+"	"+"
Filter 1	Stones	15.6	"+"	" - "	" - "	" - "	"+"
Filter 1	Stones	21.8	"+"	"+"	"+"	"+"	"+"
Filter 1	Water	14.3	"+"	"+"	"+"	"+"	" - "
Filter 1	Water	40.7	"+"	"+"	"+"	"+"	"+"
Filter 2	Stones	25.5	"+"	"+"	"+"	"+"	"+"
Filter 2	Stones	11.4	"+"	" - "	" - "	" - "	"+"
Filter 3	Sand	125.2	"+"	"+"	"+"	"+"	"+"
Filter 3	Sand	39.4	"+"	"+"	"+"	"+"	"+"
Filter 3	Water	13.9	"+"	"+"	"+"	"+"	"+"
Filter 3	Water	12.9	"+"	"+"	"+"	"+"	"+"
Effluent	Water	9.6	"+"	"+"	"+"	"+"	"+"
Effluent	Water	10.5	"+"	"+"	"+"	"+"	" - "

H1

Sample	Type	Conc DNA	PCR Results				
			FC27/RC1492	Eub338F / Eub518R	aoxBM1-2F / aoxBM2-1R	aioAF / aioAR	628F / 998R
Tank 1	Sludge	3.5	"+"	"+"	"+"	"+"	" - "
Tank 1	Sludge	195.3	"+"	"+"	"+"	"+"	"+"
Filter 1	Bricks	35.8	"+"	"+"	"+"	"+"	"+"
Filter 2	Charcoal	21.7	"+"	"+"	"+"	"+"	"+"
Filter 3	Sand	32.6	"+"	"+"	"+"	"+"	"+"

H2

Sample	Type	Conc DNA	PCR Results				
			FC27/RC1492	Eub338F / Eub518R	aoxBM1-2F / aoxBM2-1R	aioAF / aioAR	628F / 998R
Tank 1	Sludge	12.5	"+"	"+"	"+"	"+"	"+"

Filter 1	Bricks	109.3	" - "	"+"	" - "	" - "	" - "
Filter 2	Charcoal	89.4	"+"	"+"	"+"	"+"	"+"
Filter 3	Sand	13.9	"+"	"+"	"+"	" - "	"+"
Filter 3	Sand	7	" - "	"+"	" - "	"+"	"+"
Filter 3	Sand	11	" - "	" - "	" - "	" - "	" - "

H3

Sample	**Type**	**Conc DNA**	**PCR Results**				
			FC27/RC1492	**Eub338F / Eub518R**	**aoxBM1-2F / aoxBM2-1R**	**aioAF / aioAR**	**628F / 998R**
Influent	Water	4.3	"+"	"+"	"+"	"+"	"+"
Influent	Water	6.4	"+"	"+"	"+"	"+"	"+"
Influent	Water	4.2	"+"	"+"	"+"	"+"	"+"
Aeration	Water	11.1	"+"	"+"	"+"	"+"	"+"
Aeration	Water	10.6	"+"	"+"	"+"	"+"	"+"
Tank 1	Sludge	15	"+"	"+"	"+"	"+"	"+"
Tank 1	Sludge	11.7	"+"	"+"	"+"	"+"	"+"
Filter 1	Bricks	19.8	"+"	"+"	"+"	"+"	"+"
Filter 1	Bricks	11.3	"+"	"+"	"+"	"+"	"+"
Filter 2	Charcoal	6.2	"+"	"+"	"+"	"+"	"+"
Filter 2	Charcoal	2.3	"+"	"+"	"+"	"+"	"+"
Filter 3	Sand	2.9	"+"	"+"	"+"	" - "	"+"
Filter 3	Sand	2.7	"+"	"+"	"+"	"+"	"+"
Effluent	Water	2.4	"+"	"+"	"+"	"+"	"+"
Effluent	Water	15.5	"+"	"+"	"+"	"+"	"+"
Effluent	Water	29.6	"+"	"+"	"+"	"+"	"+"

Control

Sample	**Type**	**Conc DNA**	**PCR Results**				
			FC27/RC1492	**Eub338F / Eub518R**	**aoxBM1-2F / aoxBM2-1R**	**aioAF / aioAR**	**628F / 998R**
Control 1	Demi water	0.03	" - "	" - "	" - "	" - "	" - "
Control 2	Demi water	0.01	" - "	" - "	" - "	" - "	" - "

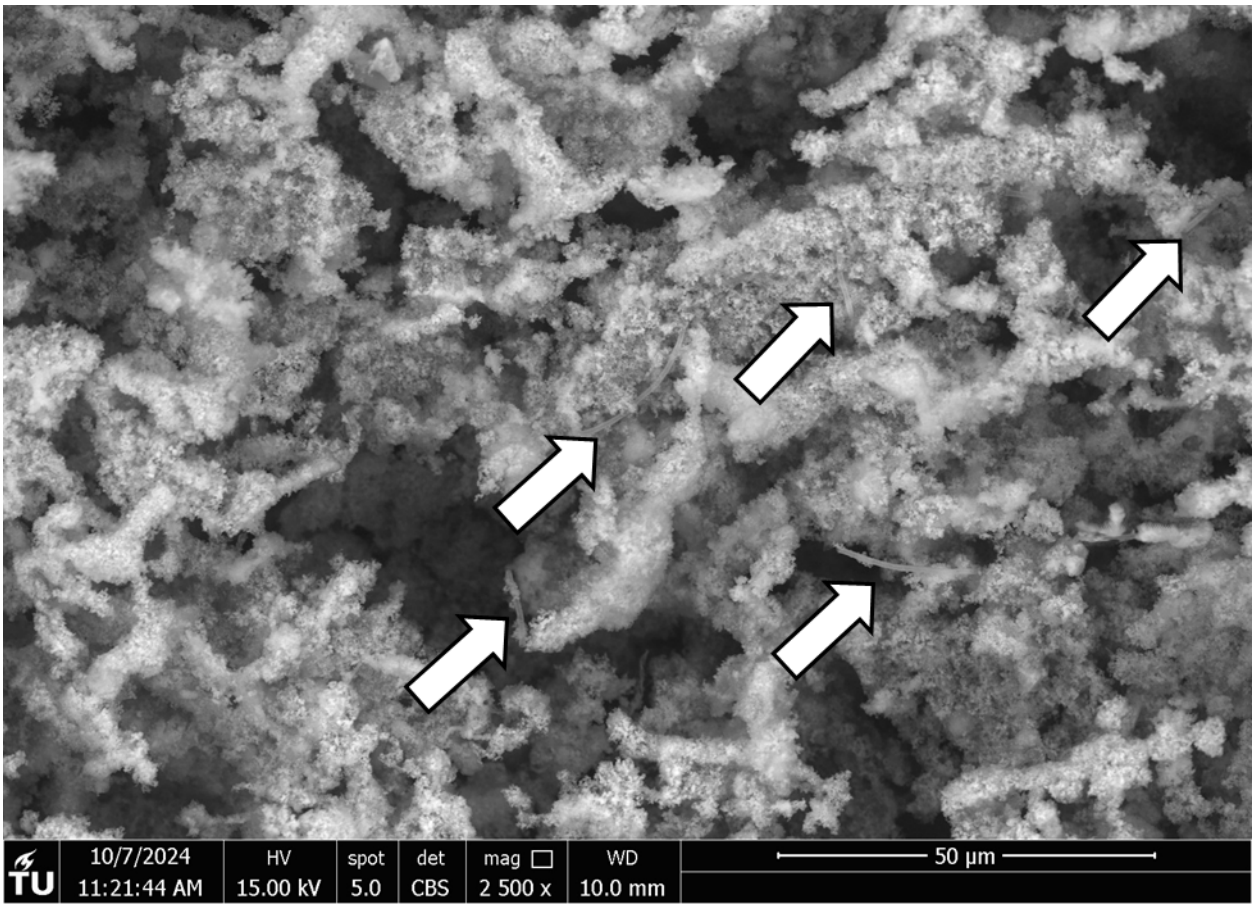

Figure S6: SEM Image of sludge sample from H2, taken from the bottom of the aeration tank. Filamentous deposits probably from lepthothrix are indicated by the arrows.

03

Biofilm Accelerates As(III) oxidation on Reactive MnOx Coated Filter Sand in Groundwater Filters

Published as:
Goedhart, R., Kruisdijk, E. & van Halem, D. (2025). Biofilm accelerates As(III) oxidation on reactive MnOx coated filter sand in groundwater filters. ACS ES&T | Water, 5, 7536-7547.

Abstract

Removal of carcinogenic arsenic (As) from groundwater is essential for safe drinking water. Arsenate (As(V)) is more effectively removed in groundwater filters than arsenite (As(III)), making the oxidation of As(III) to As(V) a key step in the treatment process. This study distinguishes between surface catalytic and biological As(III) oxidation on natural manganese oxides (MnO_x) coated filter sand, since it is unknown which pathway dominates in filters. The MnO_x coated sand was collected from a full-scale groundwater filter and consisted of a mixture of different abiotically and biologically formed Mn oxides, such as Birnessite and Todorokite. A lab-scale filter setup was operated with As(III)-containing water. Within three weeks, a shift from surface catalytic to biological As(III) oxidation was observed. Initially, surface catalytic As(III) oxidation (k_{CHEM}= 0.318 min^{-1}) was coupled to Mn(II) release at a ratio of 0.96, approximating the stoichiometric ratio of 1. This coupling disappeared over time, indicating the biological nature of the reaction as confirmed by microbial inhibition. An increase in relative abundance of the known As-oxidizing families *Comamonadaceae,* with the genus *Polaromonas* as the dominant species, and *Microscillaceae* were found post experiments. Except for these changes, the microbial community on the sand grains stayed relatively similar prior and post experiments. No significant changes in the physical-chemical properties of the MnO_x coating were found post experiments. A first-order biological As(III) oxidation rate constant k_{BIO} of 4.64 min^{-1} was found, yielding a half-life of 9 seconds. This represents a 14-fold acceleration compared to surface catalytic oxidation, revealing that kinetic limitations rather than surface passivation can be attributed to the loss of surface-catalytic oxidation. Our study demonstrates that biological oxidation of As(III) can outpace the acknowledged oxidizing power of MnO_x, offering a potential new pathway for the development of effective As removal systems.

3.1 Introduction

Elevated concentrations of arsenic (As) have been detected in groundwater in various countries, including Bangladesh, Vietnam, Argentina, the Unites States of America, and India [1]. An estimated 94 to 220 million people are potentially exposed to As concentrations above 10 µg/L in groundwater, from which the majority (94%) lives in Asia [2]. Groundwater serves as a common source for drinking water, and As, known for its carcinogenic properties, should be removed to provide safe drinking water. This remains a challenge due to lack of acceptable, affordable, robust, and sustainable arsenic-safe water alternatives and treatment methods [3].

The most common treatment method for groundwater is aeration followed by rapid sand filtration (RSF), primarily designed to target the removal of iron (as Fe^{2+}), manganese (as Mn^{2+}), and ammonium (NH_4^+). Removal of As in the treatment chain takes place through adsorption onto Fe oxides. The efficiencies of As removal vary strongly per location, caused by different Fe/As ratio's present and co-occurrence of competing anions (e.g., phosphate) [4]. Several field studies report levels of >50 µg As/L in the treated water [5–7], which can be toxic at lifelong consumption [1]. More modern technologies such as membrane filtration or anion exchange can also be ineffective in removing As [8,9]. In anaerobic groundwater, with typically near-neutral pH, As occurs predominantly as As(III) in the form of H_3AsO_3 (pK1 = 9.2). Under oxidizing conditions the pentavalent As(V) dominates in the form of $HAsO_4^{2-}$ or $H_2AsO_4^-$ (pKa = 2.2, pKb = 6.9 respectively) [10]. Fe oxides typically have a higher adsorption capacity for As(V), underlining the importance of oxidizing As(III) to As(V) in the treatment process [11].

Aeration alone is insufficient to oxidize As (half-life of 4-9 days [12]) within the time scale typical for RSF (residence time approx. 10 min). However, in aerobic full-scale filters, As(III) oxidation has been observed to occur within minutes, indicating the crucial role of the filter bed in this oxidation process [13]. The acceleration of As(III) oxidation has been attributed to three possible mechanisms: 1) generation of reactive oxygen species (ROS) during oxidation of Fe(II) [14] 2) surface catalytic oxidation by Mn oxides on the filter coating [15–18] or 3) biological oxidation by arsenic oxidizing bacteria (AsOB) [19–21]. The current research studies As(III) oxidation on Mn oxides coated filter sand, examining the contribution of the surface catalytic and biological mechanism. It is currently unknown which pathway dominates in filters.

The reactive Mn oxides coating on sand grains forms through oxidation of dissolved Mn(II) present in the influent water, facilitated by manganese oxidizing bacteria (MnOB) [22]. The formed amorphous biogenic Mn(III/IV)-oxides (called MnO_x hereafter) acts as strong oxidants that can further enhance surface catalytic Mn(II) oxidation [23,24] and As(III) oxidation [17]. The coating can also harbor a biofilm and thereby supporting biological oxidation. Figure 1 provides a schematic overview of the relevant As(III) oxidation processes on MnO_x coated sand.

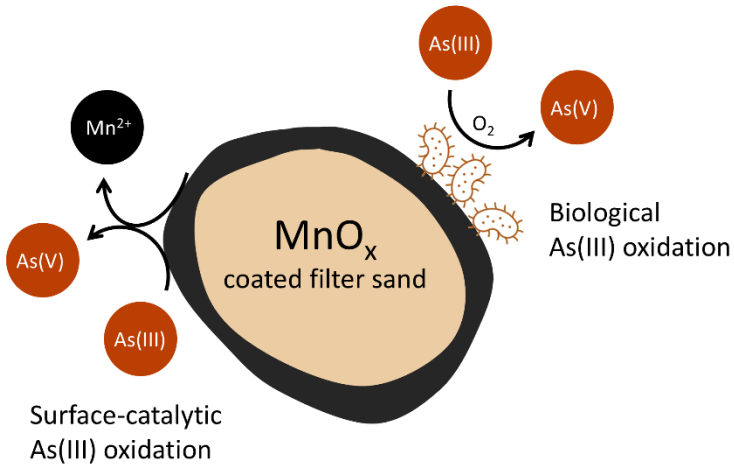

Figure 1: Schematic overview of surface catalytic and biological As(III) oxidation on MnO_x coated filter sand

During surface catalytic oxidation, the Mn(III/IV)-oxide coating serves as the elector acceptor, releasing Mn(II) while oxidizing As(III) at a stoichiometric ratio of 1 (equation 1). Scott and Morgan (1995) showed that synthetic MnO_2 is able to oxidize As(III) with a half-life of 10-20 minutes, which is also reported for MnO_x powder scraped from a mature filter sand coating [17]. A reduction in As(III) oxidation rates over time have been observed, caused by surface passivation of the reactive MnO_x coating [25–27]. Other constituents in the water such as Fe and Mn can hinder As(III) oxidation on the MnO_x surface in pH neutral water [17], so the availability of a MnO_x coated surface does not necessarily mean that As(III) gets oxidized, emphasizing the complex and currently unpredictable system.

Groundwater native bacteria are able to oxidize As(III) in biofilters [19,28], although only a few studies applied biological As(III) oxidation to treat groundwater [21,29,30]. Note that the aforementioned studies observed biological As(III) oxidation in laboratory or pilot setups only. The reaction equation of catalyzed As(III) oxidation by arsenic oxidizing bacteria (AsOB) is given in equation 2. Van Le et al. (2022) analyzed microbial communities within a functioning household sand filter[31]. While evidence of biological Fe and Mn oxidation was observed, AsOB were not found. Hence, although biological oxidation of As(III) might occur in filters, the question remains whether AsOB will thrive on a reactive and mature MnO_x filter coating.

Surface catalytic

$$H_3AsO_3 + MnO_2 + 2H^+ \longrightarrow Mn^{2+} + H_3AsO_4 + H_2O \quad \text{(equation 1)}$$

Biological

$$H_3AsO_3 + O_2 + 2H^+ \xrightarrow{AsOB} H_3AsO_4 + H_2O \quad \text{(equation 2)}$$

Achieving complete As(III) oxidation by the MnO_x coating eliminates the need for the addition of oxidative agents in the treatment chain. In rural areas where groundwater contains elevated concentrations of As, the addition of oxidative agents is often not an option because of high chemical costs, maintenance difficulties, and inadequate infrastructure. Complete As(III) oxidation by the filter bed itself can also contribute to the aim of the Dutch drinking water companies of lowering the As guideline to 1 ug/L, while maintaining a simple, robust and economically viable system [32].

The objective of this study is to distinguish between biological and chemical surface catalytic As(III) oxidation on MnO_x coated filter sand. Identifying the oxidation mechanisms can help to determine which pathway dominates in rapid sand filters. A lab-scale filter study was performed, using MnO_x coated sand ripened in a functioning full-scale treatment plant. The kinetics of both surface-catalytic and biological As(III) oxidation were determined, by collecting a time series of As speciated height profiles before and after the addition of a microbial inhibitor.

3.2 Materials & Methods

3.2.1 Lab-scale filter study

Figure 2 shows a schematic overview of the laboratory column setup. The unchlorinated tap water flowing through the column was spiked with 15 mg/L As stock solution, derived from a 0.05 M sodium arsenite solution (Merck). The pH of the stock solution was kept below 3 by the addition of 37% HCl (Fluka™). The column influent water had an average As concentration of 494.6 (STD +- 47.2) µg/L and a pH of 7.92 (STD +- 0.09). The As(III) concentration varied between 52% and 86% of the total arsenic concentration in the influent, the remainder was As(V). The columns, made from transparent PE, were wrapped in aluminum foil to avoid light intrusion. A second column was attached to the outflow of the column, filled with GEH 102 adsorption media to remove residual arsenic before discharging.

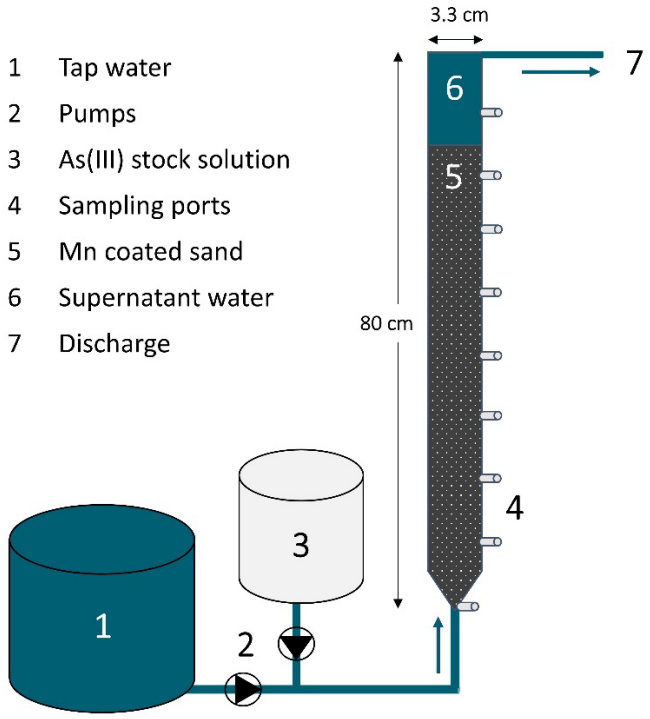

Figure 2: A schematic overview of the laboratory lab-scale filter set-up, consisting of an upflow column filled with MnOx-coated sand collected at a full-scale groundwater filter.

The design details and operational settings of the column are given in Table 1. Compared to groundwater filters (3-10 m/h), the column operated on a relatively high flow rate of 20 m/h. The high flow rate facilitated the replacement of many pore volumes within a short duration, saturating the adsorption sites and, consequently, establishing a sorption equilibrium. From that moment on, adsorption could no longer mask potential occurrence of As(III) oxidation, which enabled monitoring the oxidation state of arsenic. In total, the column remained operational for 66 days, corresponding to the treatment of 11.5 m^3 water and 41,000 pore volumes. Pore volumes is the number of times the pores are completely flushed with water. No clogging was observed during the experiment and therefore backwashing was not applied.

Table 1: Design details and flow settings of the lab-scale filter.

Column design		
Filter bed height	73	cm
Supernatant water level	7	cm
Column diameter	3.3	cm
Bed volume	624	cm^3
Porosity	0.45	-
HRT	2.2	min
Total flow rate	20	m/h

3.2.2 MnO_x coated sand

The MnO_x coated sand utilized in this study was collected from the secondary filter of a treatment plant treating anaerobic groundwater in Belgium (Pidpa). At the treatment location, the aim is to achieve biological iron removal in the primary filter bed by maintaining a relatively low pH (6.9) and O_2 concentration (3.4 mg/L). Manganese is subsequently removed in the secondary filter, resulting in a clear black coating on the sand, high in Mn content. Also arsenic was present in the groundwater at this location (40 µg/L) and removed to ±0.5 µg/L in the primary filter. The aeration step after the primary filter raised the O_2 concentration to 6.7 mg/L and the pH to 8.4. In the secondary filter, the Mn concentration of 34 µg/L lowered to <0.5 µg/L. For further details on the water quality data at this treatment location, see Supplementary Table 1.

The composition of the coating of the sand is determined using different methods. The coating was extracted as proposed by Claff et al. (2010)[33]. This extraction method allows for the determination of the Mn, Fe and As concentrations, by dissolving the coating and using inductively coupled plasma mass spectrometry (ICP-MS, Analytikal Jena PlasmaQuant MS). Additionally, the coating's properties were investigated using digital light microscope (VHX-5000, Keyence), Environmental SEM (Quanta FEG 650: FEI at 0.5 °C and 6 – 8 mbar H_2O atmosphere), X-ray diffraction (Bruker D8 Advance-ECO diffractometer with *Cu radiation* and Bragg-Brentano geometry), Raman spectroscopy (Renishaw Raman Invia Reflex: excitation wavelength, 514 nm; dwell time, 10 s; iterations, 10; grating, 3000 lines per mm) and EPR spectroscopy (Bruker EMX Bruker EMX plus X-band EPR spectrometer: microwave frequency, 9.797 GHz; Microwave power, 20 mW; modulation frequency, 100 kHz; modulation amplitude, 10 G; room temperature). The Brunauer-Emmett-Teller (BET) theory was used to determine the surface area of the sand grains in duplicate (Micromeritics Tristar II at 77K). Around two grams of sand was used for analysis, pretreated at 60 ^{0}C for 15h before measurement. The original biofilm on the sand grain prior to experiments was prepared for imaging using a Leica DM6 Stellaris 8 Confocal Scanning Laser Microscope using a 25x water immersion objective (0.95 NA, WD 2.5 mm) (RRID: SCR_026519). The biofilm was fixed by immersing the grain in a 4% paraformaldehyde solution for 90 minutes, followed by three washing steps in a phosphate-buffered saline (PBS) solution and a sequential 10-minute immersion in ethanol solutions of increasing concentration (20%, 50% and 80%). For staining, 5 µL of a 10,000 x SYBR® Green solution in DMSO (Sigma Aldirch) was dissolved to 1 x in PBS. The granule was submerged in the staining solution for 30 minutes before microscopic analysis.

3.2.3 Water quality analysis

To study the filter behaviour over time, height profiles were taken by sampling the influent, the effluent, and at different depths of the column (Figure 2). The samples were collected at a low velocity to minimize disturbing the system. The pH and Dissolved oxygen (DO) were measured using SenTix® 980 and FDO® 925 probe, respectively (WTW, Germany). As(III) was speciated immediately by an Amberlite® IRA-400 chlorite form anion ion-exchange resin

using a method similar to that described by Gude et al. (2016)[34]. Around 8 mL of resin was added to a 10 mL syringe. Initial preparation involved two washes of the resin with deionized water, followed by flushing the resin with one volume of the sample itself. When empty, 10 mL of the sample was dosed and collected. The resin was discarded after treating 4 samples. The gathered samples were preserved at 4^0C until analysis.

Concentrations of As and Mn were quantified using inductively coupled plasma mass spectrometry (ICP-MS, Analytikal Jena PlasmaQuant MS). Prior to analysis, the samples were acidified (ROTIPURAN® Ultra 69%, 1% v/v) and filtered through a 0.20 µm non-sterile Millex® Syringe filter with Durapore® membrane.

3.2.4 DNA extraction

DNA extraction is required to study the microbial composition of the biofilm on the sand grains. However, extracting DNA from metal-coated sand with Qiagen DNeasy Powersoil Pro Kit or Fast DNA Spin Kit for Soil, yielded DNA concentrations below 0.1 ng/µl, also after an additional sonication step. These low yields, as often reported in metal rich environments [35,36], hinder downstream processes such as sequencing.

A new method was therefore developed to release the DNA from MnO_x coated sand, by dissolving the coating in ammonium oxalate. A 0.5 M ammonium oxalate monohydrate (Sigma Aldrich, ≥99%) solution was brought to a pH of 3 by the addition of 37% HCl (Fluka™) and was subsequently sterilized by autoclaving. Five times one gram of sand was sonicated in 0.5 mL Tris+EDTA buffer solution (Sigma-Aldrich, BioUltra) with a VialTweeter (UP200St Hielscher) for two times 10 seconds (in pulses), followed by a vortex step of 2 seconds. A vacuum filter unit was used, holding a sterile 0.2 µm filter paper. The liquid (including detached coating) of the five vials was transferred together on the filter paper. Subsequently, 10 mL of the ammonium oxalate solution was added, which dissolved the black manganese coating. The filter paper was subsequently flushed with 5 mL of DNA-free water (VWR). The filter paper was transferred to the PowerBead Pro Tube of the QIAamp powerfecal pro DNA kit (Qiagen) and the manufacturer's instructions were followed further onwards. The concentration of extracted DNA was quantified using Qubit 4 Fluorometer and Qubit dsDNA HS assay kit (Invitrogen, Waltham, MA, USA) following the manufacturer's protocol. Sequencing of the extracted DNA was carried out by Novogene Europe. The methods are given in the Supplementary Information.

3.2.5 Sodium azide addition

After 36 days of operation (22,400 pore volumes), the microbial activity of the column was suppressed with sodium azide (NaN_3), since NaN_3 has no effect on the physico-chemical properties of the MnO_x coated filter material [37]. NaN_3 was added to the As-spiked tap water, with a final concentration of 25 mM NaN_3. The column was immersed in this solution for a duration of 12 hours. Subsequently, the column was flushed with 15 L of the NaN_3 - As solution at a flow rate 2.5 m/h. Just before and after the inhibition, 2 gr of grains were removed from the bottom of the column to determine the concentration of ATP (Luminultra®, DSA test

kit). After inhibition, the column was returned to its original operational settings. After two days, corresponding to 670 pore volumes, a height profile was taken again to assess the impact of the NaN_3 dosing on the system. The system remained operational for 30 more days.

3.2.6 Simulation As and Mn concentrations

Based on the As(III) concentrations measured, a first-order rate constant (k) was determined via:

$As(III) = As(III)_{in} \times e^{-kt}$ (equation 3.0)

The simulated As(V) and Mn(II) concentrations were calculated via the surface catalytic reaction equation as given in eq. 1.0, meaning that oxidizing 1 mole As(III) forms 1 mole of As(V) and releases 1 mole Mn(II). As(tot) was determined by summing the simulated As(V) and As(III) concentrations.

3.3. Results

3.3.1 As(III) oxidation on MnO_x coated sand

Figure 3 shows the As(III) and As(V) concentrations in the effluent of the column for the first 36 operational days, corresponding with 22,400 pore volumes. The mean As influent concentrations are indicated by the blue and yellow dashed lines, corresponding to 305.9 (STD +- 27.7) and 188.7 (STD +- 52.0) µg/L for As(III) and As(V), respectively. The system remained oxic (DO > 6.6 mg/L) over time. The average pH of the influent and effluent water was 7.92 (STD +-0.087) and 7.86 (STD +- 0.054) respectively.

On day 1, both As(III) and As(V) were found to adsorb in the column, resulting in a total As removal of 440.6 µg/L (75%). This loss of total As in the column due to adsorption may mask occurrence of oxidation mechanisms. On day 3, 16% of total As was removed, which further decreased to below 6% for subsequent data points. Production of As(V) by oxidation of As(III) was observed starting from day 3 (1,400 pore volumes), corresponding to an effluent As(V) concentration exceeding the As(V) influent concentration. The fraction of As(V) in the effluent further increased over time and on day 16 (9,600 pore volumes) As(III) was no longer detected in the effluent. In other words, a fully oxidizing system was reached in which all incoming As(III) was recovered in the effluent as As(V).

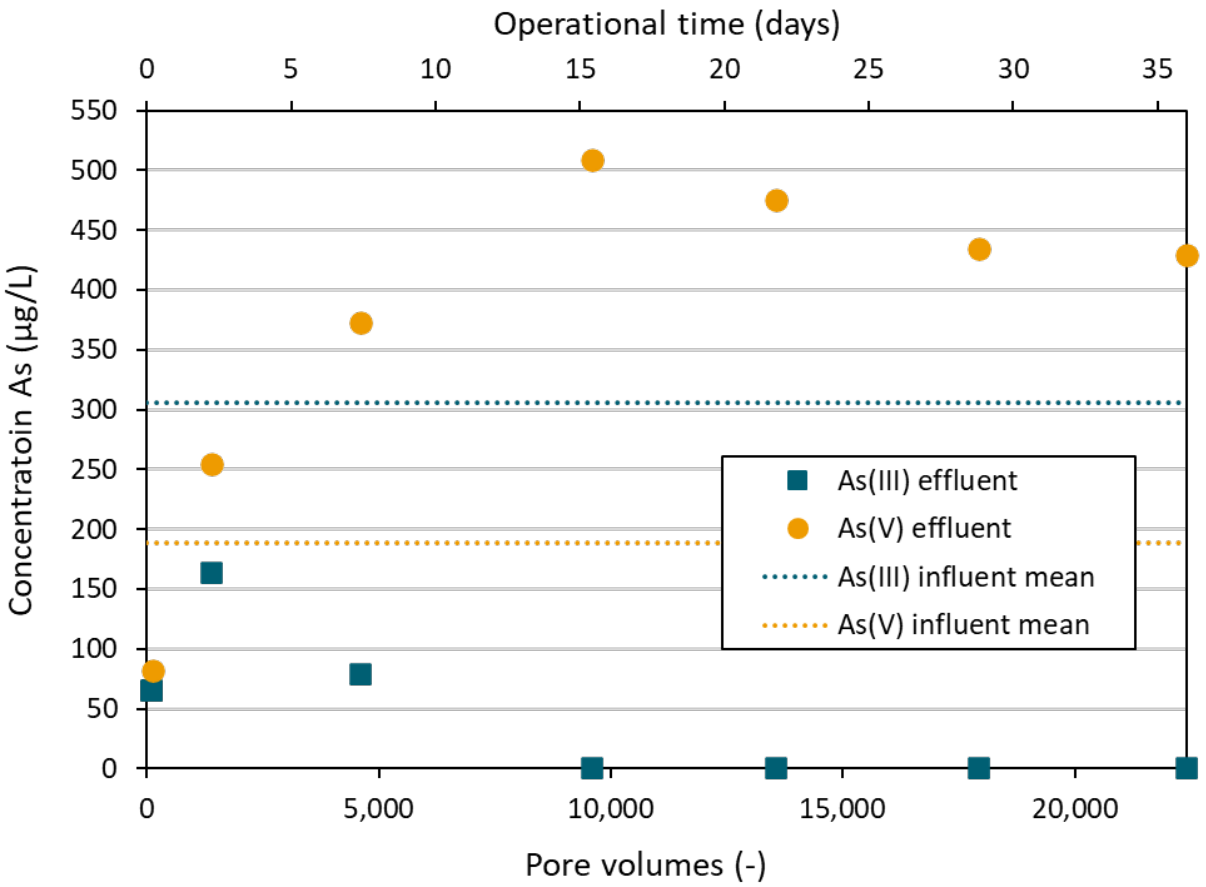

Figure 3: The As(III) and As(V) effluent concentrations of the columns over time (days) and over the corresponding replacement of pore volumes (-). The dotted lines are the mean As(III) (top) and As(V) (bottom) influent concentrations. Adsorption of arsenic was 75% on day 1, 16% on day 3 and <6% on the remaining days.

3.3.2 Oxidation over the height of the filter bed

Figure 4 shows the As(tot), As(III), As(V) and Mn(II) concentration profiles over the height of the column for day 3, marking the first day of observable As(III) oxidation (Figure 3), and for day 29, which is close to the end of the experiment. The height profiles of the other days can be found in Supplementary Figure 1. Total As removal was 82.1 µg/L (16%) and 4.8 µg/L (1.1%) on day 3 and day 29, respectively. This illustrates that although a fraction of As was still adsorbed in the column, the majority could be recovered in the effluent (84-99%).

On day 3, the As(III) concentration lowered over the height of the column from 342 to 163 µg/L, of which 95 µg/L was identified as As(V) in the effluent (Figure 4). The simulated concentrations for day 3 are also shown in Figure 4: a first-order As(III) oxidation rate was found (R^2 = 0.9291) with constant $k_{As(III)}$ of 0.318 min^{-1}. The As(tot) and As(V) concentration measured were slightly lower than predicted by the simulation based on the As(III) concentration, likely because of the 16% adsorption of As onto the column. Assuming this oxidation is surface-catalytic, the simulated Mn(II) released based on $k_{As(III)}$ and Mn:As(III) ratio of 1 predicted a Mn(III) concentration of 129 µg/L Mn. The Mn(II) concentration measured in the effluent was 110 µg/L.

On day 29, As(III) concentrations were below detection limit (6 µg/L) after the first 30 cm in the column. The first-order reaction constant increased to a $k_{As(III)}$ of 4.64 min^{-1} (R^2 = 0.9750). At this rate, the simulated surface-catalytic release of Mn(II) should reach 241 µg/L in the effluent; however the concentration of Mn(II) observed was below detection limit (6 µg/L).

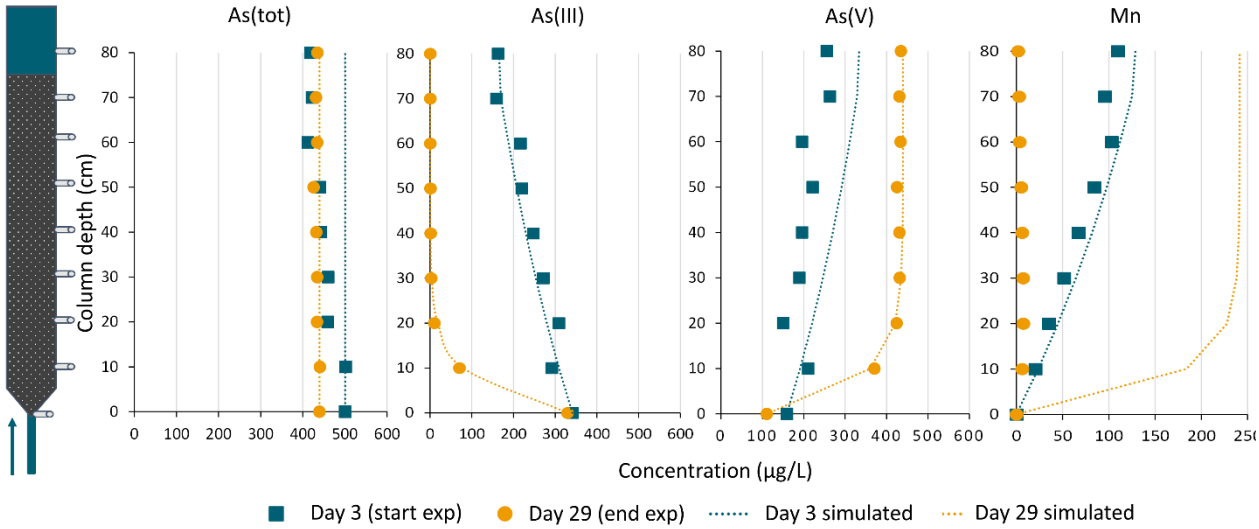

Figure 4: Height profiles of As(tot), As(III), As(V) and Mn(II) at the start (day 3, blue squares) and the end (day 29, yellow circles) of the experiment. The simulated concentrations with first-order kinetics are also depicted (dotted lines).

3.3.3 Characteristics of mineral-microbe coating

The MnO_x coating of the sand appears homogeneously black by eye and under the digital light microscope (Figure 5A). The confocal microscope and SEM images (Figure 5B and Supplementary Figure 2) reveal a more fractured morphology, with both rough and smoother patches. The surface area found using the BET theory was 1.51 (± 0.01) m^2/g, which is in a similar order of magnitude as found by Arora et al. (2025) [38]. Figure 5B shows the biofilm grows in patches on the MnO_x coated sand grain. The surface morphology of the sand directly collected from the sand filters is similar to that of the sand exposed to As in the columns (Supplementary Figure 2. Table 2 provides an overview of the contribution of Mn (15.3%), Fe (5.9%) and As (0.0032%) in the coating, measured by chemical extraction. The relatively high levels of Fe in the coating contrast with the initial homogenous impression of the coating. Additionally, the large deviation in Fe suggests that the amount of Fe precipitates varied greatly among grains. The presence of Fe in the coating was confirmed by point EDS measurements (Supplementary Table 2), which additionally showed presence of carbon and oxygen, as well as calcium and silica.

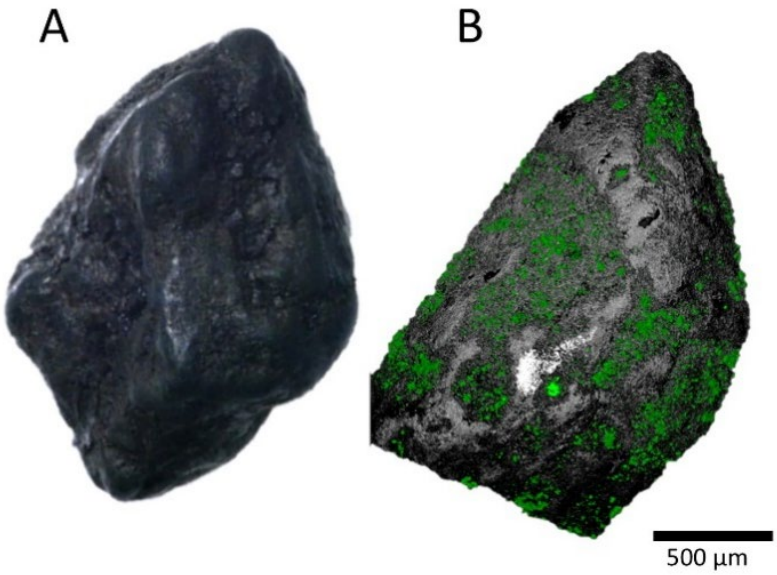

Figure 5: Representative digital light (A) and confocal (B) microscopy images of a sand grain prior to experiments. In (B): Green = SYBR Green stained microbes, grey = reflection of the sediment

Powder X-Ray Diffraction (XRD) was performed on the grain coatings prior to and post experiments. In both coatings the Mn mineral Todorokite was detected (Supplementary Figure 3). In the spectra of the coating post experiments slightly higher crystallinity was found, including crystallized Birnessite. Other typical Fe or Mn precipitates formed in groundwater filters, such as poorly ordered ferrihydrite or amorphous Birnessite, cannot be detected using XRD.

The Raman spectra of the sand prior and post experiments are shown in Figure 7A and 7B respectively. Different regions of the same samples were measured, at different angles. The spectra is dominated by the signal of the Quartz sand. All spectra show a peak around 625 cm^{-1}, which is likely a signal from the Mn oxides. Some spectra, both prior and post experiments, have an additional peak around 570 cm^{-1}. The variation in spectra among the different angles suggest that the coating is a mixture of different Mn oxides. The single peak around 625 cm^{-1} could be attributed to either Todorokite or Ranciéite [39]. Birnessite is known to have two Raman peaks between 575-585 cm^{-1} and 625-646 cm^{-1} [40], which could explain the second peak at 570 cm^{-1}. The slightly lower wavenumbers could be caused by strain effects.

Samples were measured by EPR to study the biotic or abiotic origin of the manganese oxides. The spectra are dominated by a very broad signal of circa Δ2000 Gauss and a sharp peak of Δ180 Gauss around 2400. In both spectra a small signal near 1600 Gauss was found, which is consistent with mononuclear Fe^{3+}.

Table 2: Mn, Fe & As content in the coating of the sand prior to experiments, measured by chemical extraction. n = 3, SD = standard deviation

Element	Average (mg/g)	SD (mg/g)	Average (%)
Mn	153.4	24.96	15.3
Fe	58.6	30.79	5.9
As	0.03254	0.01537	0.0032

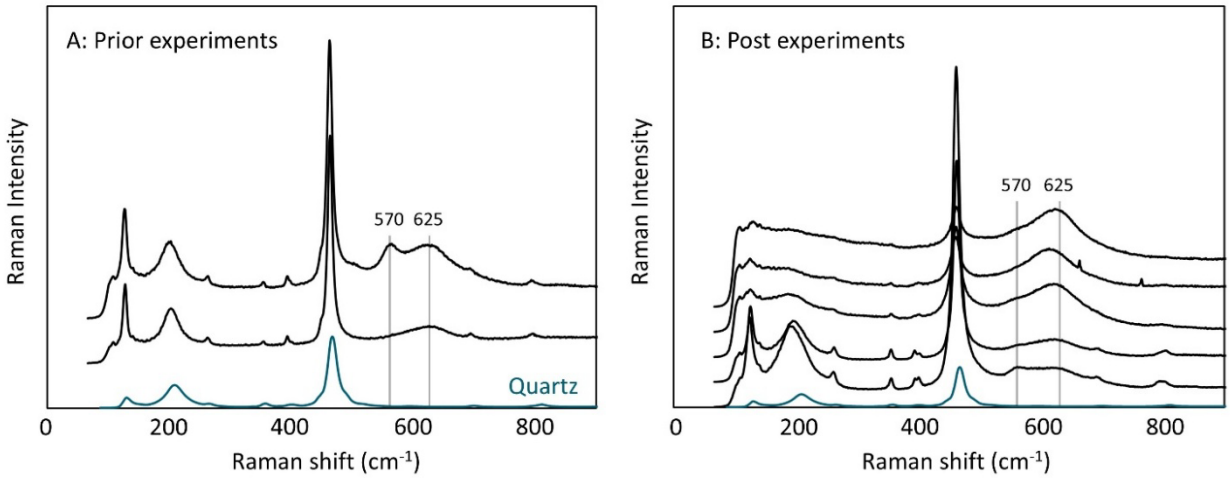

Figure 6: Raman spectra of Mn coated sand prior (A) and post (B) experiments. The different spectra represent different measurements of different regions and angles of the same sample. The bottom spectrum (blue) is a reference spectrum of Quartz. The peaks likely caused by the MnO_x coating are labelled (570 and 625 cm^{-1}).

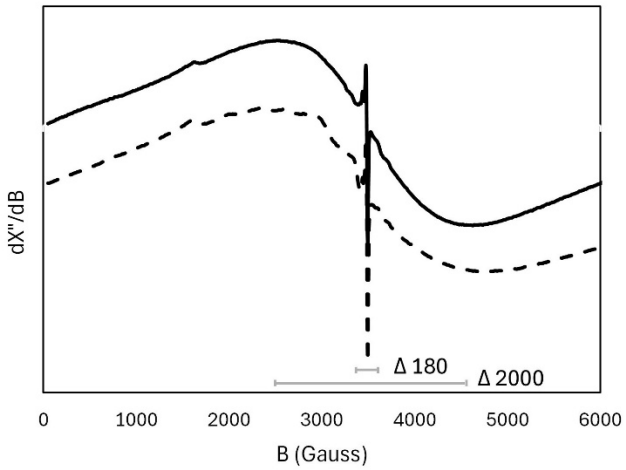

Figure 7: EPR Spectra of sand prior (top, solid) and post (bottom, dash) experiments. The differences in Gauss of the spectra are given.

3.3.4 Microbial community on mineral-microbe coating

The microbial community on MnO_x coated sand grains prior and post experiments are given in Figure 8. The communities are presented in relative abundance (RA) in percentage of OTUs at the taxonomic ranks of Class and Family. At class level, no major shift in the microbial community was observed when comparing prior and post experiment samples. Across all samples, *Gammaproteobacteria, Alphaproteobacteria,* and *Nitrospiria* were the most abundant classes with RAs ranging from 22-28%, 24-35%, and 22-27%, respectively. At family level, *Nitrospiraceae* dominated all samples, but shifts were observed from prior to post experiment. *Comamonadaceae* emerged post experiments, reaching a RA of 17% in both samples. Within the family *Comamonadaceae, Polaromonas* was the main detected genus, with a RA of 12% in both samples post experiment (data not shown). Additionally, the family *Microscillaceae* increased to 4% and 2% in the duplicate samples (data not shown). *Comamonadaceae, Polaromonas* and *Microscillaceae* are known arsenic oxidizing bacteria, as shown by e.g. Crognale et al., (2019); Huang et al., (2024); Osborne et al., (2013); Roy et al., (2021); Su et al., (2022)[45–49]. Post experiment, the growth of *Pseudonocardiaceae* was also observed till a RA of 5-6%, this family has previously been found in As-rich environments [50,51]. *Gallionellaceae* was no longer detected post experiments.

The addition of NaN_3 to the columns did not cause major shifts in the community composition compared to post-experiment (Supplementary Figure 4). It is important to note that the figures represent relative abundances, which do not reflect absolute microbial concentrations.

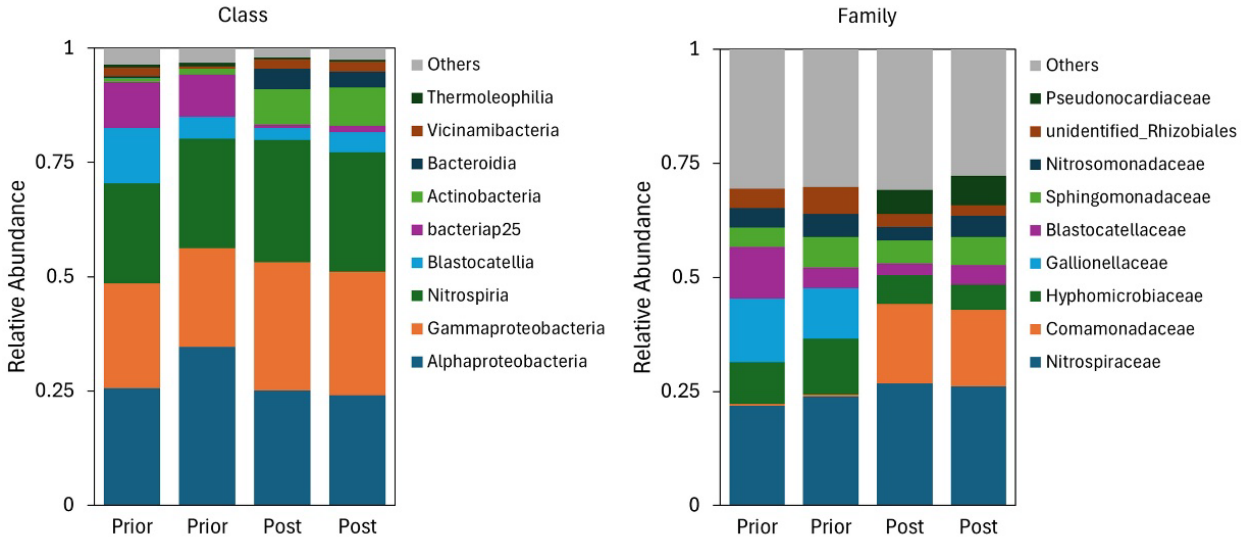

Figure 8: Distribution histogram of relative abundance of taxonomic rank Class (left) and Family (right) of the microbial community on the sand grains prior & post experiments. Both samples in duplo.

3.3.5 Ratio Mn(II) released over As(III) oxidized

Figure 9A presents the Mn(II) concentrations in the effluent of the column during the experiment. In addition, the molar Mn(II):As(III) ratio is shown for released Mn(II) over oxidized As(III). At the start, the released Mn(II) (110 µg/L) aligned with the stoichiometry of the surface

catalytic As(III) oxidation reaction by reduction of Mn oxides (equation 1). However, the molar ratio of 1 was temporary, because the ratio gradually decreased to 0.28 and 0.07 on day 8 and 16, respectively. By day 22, or 13,600 pore volumes, the Mn(II):As(III) ratio had reached 0, as Mn(II) effluent concentrations were below detection limit (6 µg/L). A ratio of 0 is expected during biological As(III) oxidation, as given in equation 2.

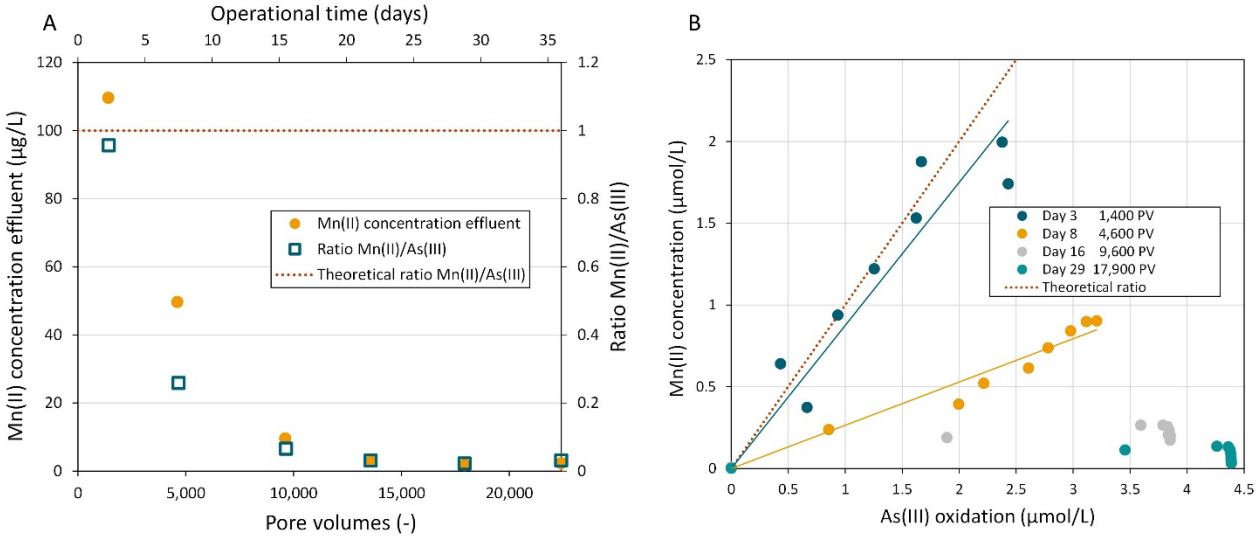

Figure 9: A) Mn(II) concentration in the effluent of the column and the ratio of Mn(II) released over As(III) oxidized for different days and) and the corresponding replacement of pore volumes (-). B) As(III) oxidized over the Mn(II) concentration released at the different tap heights on day 3, 8. 16 and 29 (PV = pore volumes). The theoretical line depicts 1 mole of Mn(II) release per mole of As(III) oxidized according to equation 1.

To investigate the Mn:As(III) ratio over the height of the filter column, the fraction of oxidized As(III) versus the Mn(II) concentration for the different taps in the column is depicted in Figure 9B. Particularly on day 3 and 8 a clear linear trend is visible (R^2 0.97, 0.99), with the ratio being closest to the stoichiometric value of 1 for day 3. For the later days of the experiment, the relationship between Mn(II) release and As(III) oxidation becomes less apparent. The As(III) oxidation increased over these days, while the amount of released Mn(II) decreased over time. The ratios found confirms that the pathway of As(III) oxidation is driven by Mn oxide reduction at the start of the experiment, but moves towards biological As(III) oxidation over time.

3.3.6 Inhibition of biological As(III) oxidation

Figure 10A shows the As(V) and As(III) concentrations in the effluent before and after microbial inhibition by NaN_3 on day 36. Prior to inhibition, a completely oxidizing system was obtained, as all incoming As(III) was converted to As(V) in the top 30 cm ($k_{As(III)}$= 4.64 min^{-1}). After exposure NaN_3, As(III) oxidation dropped by approximately 65%, with >200 µg/L As(III) in the effluent after inhibition ($k_{As(III)}$= 0.198 min^{-1}). The addition of NaN_3 decreased the ATP concentration by two orders of magnitude (16 x10^4 to 66 x10^2 pg ATP/g sand).

This inhibition demonstrate that the arsenic oxidizing bacteria found on the MnO_x coating were responsible for the observed acceleration of As(III) oxidation in the period prior to

inhibition. After exposure to NaN_3, these organisms could not oxidise As(III) for several days. On day 6 after inhibition, complete As(III) oxidation was again observed in the column, yet at a rate slower than prior to inhibition ($k_{As(III)}$= 1.55 min^{-1}).

The height profiles for As(III) oxidation, either before or after microbial inhibition, on similar operational days, show rather striking resemblance (Figure 10B). On day 3, $k_{As(III)}$ was 0.318 and 0.198 for before and after inhibition, respectively. At the end of the experiment, on day 29, $k_{As(III)}$ had reached 4.65 and 2.48 min^{-1}, before and after inhibition, respectively. This indicates that biological As(III) oxidation developed again in the days after inhibition. The rate constants for the other experimental days are presented in Supplementary Figure 5.

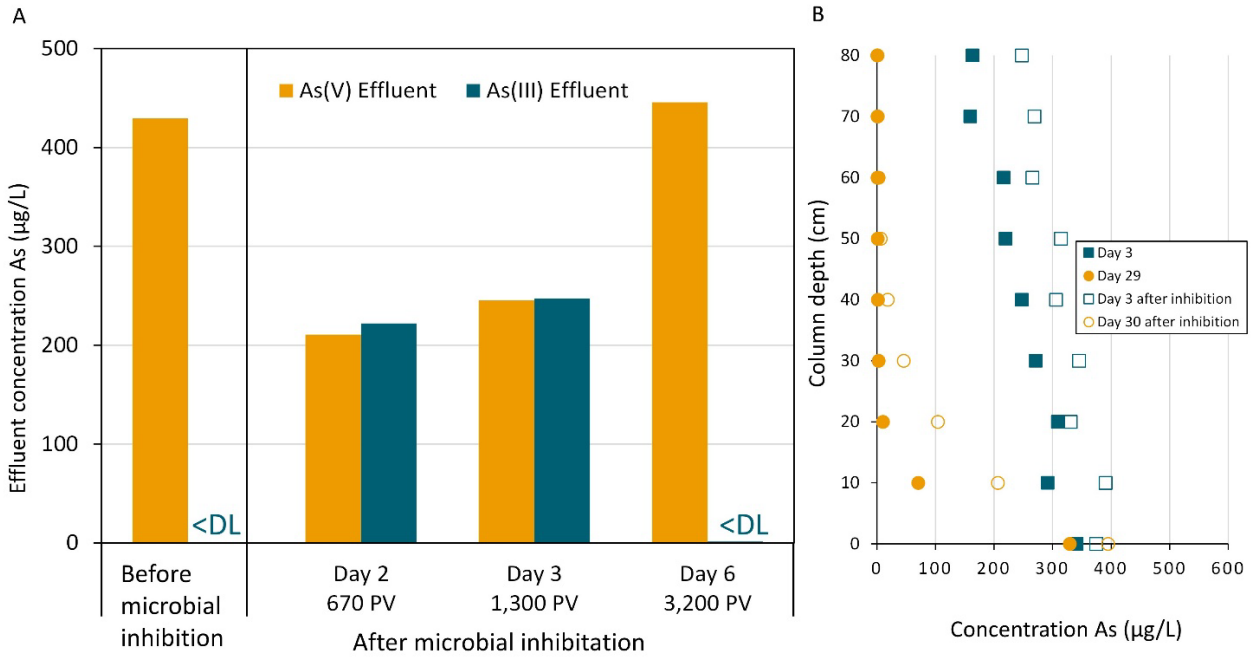

Figure 10: A) As(V) and As(III) effluent concentrations before and after microbial inhibition by NaN_3. <DL = below detection limit. PV = pore volumes B) Height profile of As(III) depletion on day 3 and day 29 before and after microbial inhibition by NaN_3.

3.4 Discussion

3.4.1 Shift from surface catalytic to biological As(III) oxidation on MnO_x coated sand

At the start of the experiment (day 3 or 1,400 pore volumes), As(III) oxidation was coupled to the reduction of Mn oxides, with an Mn(II):As(III) ratio of 0.96, closely resembling the stoichiometric ratio of 1. This shows that oxidation was chemical, according to the reaction formula for surface catalytic As(III) oxidation (equation 1). The column performed uniformly over the height of the filter bed, with similar ratios observed at every tap height (Figure 9B). By day 22 (13,600 pore volumes), Mn release dropped to below detection limit (6 µg/L), while a completely oxidizing As(III) system was obtained (Figure 9A). As(III) oxidation without Mn release indicates the reaction became biological, based on the reaction formula of equation 2. Additionally, known AsOB *Comamonadaceae*, *Polaromonas* and *Microscillaceae* emerged on the MnO_x coating during experiments. Introducing NaN_3, a microbial inhibitor,

resulted in a 65% decrease in the efficiency of the As oxidizing system. This further exhibits the biological nature of the oxidation at the end of the experiment.

Surface catalytic oxidation by Mn oxides was inadequate to completely oxidize all incoming As(III). The incomplete oxidation is likely attributed to kinetic limitations rather than surface passivation of the Mn oxides. Surface passivation of the reactive MnO_x coating would decrease the oxidation efficiency, yet in our system biological oxidation supplanted this process before passivation could occur. This is further supported by the return to surface-catalytic oxidation after microbial inhibition, demonstrating that passivation has not occurred. Additionally, surface passivation would cause the reaction to have two different kinetic regimes as described by Nielsen-Franco and Ginder-Vogel (2023)[52], yet such a two-phase pattern over the height of the filter column was not observed. A first-order model has shown to describe the kinetics well in our system (Figure 4).

3.4.2 Characteristics of the stable MnO_x coating

Exposing the MnO_x coated sand to arsenic and the growth of an arsenic oxidizing biofilm on the coating, had no major effects on the characteristics of the coating. The MnO_x coating on the sand grain is likely a mixture of different Mn oxides, in several oxidation states [Mn(II), Mn(III) and Mn(IV)]. The Raman spectra showed variability over different areas of the coating, detecting possibly Todorokite, Birnessite and Ranciéite both prior and post experiments (Figure 6). XRD also revealed the presence of Todorokite (Supplementary Figure 3) both prior and post experiments, but only detected Birnessite post experiments. However, the poor crystallinity of MnO_x and the presence of amorphous iron oxides make a proper characterization of manganese oxides by XRD challenging [39].

The manganese minerals have likely both a biotic and abiotic origin; Kim et al. (2011) concludes that in EPR a broad peak of $\Delta H>1200$ can be attributed to abiogenic Birnessite, while a sharp peak of $\Delta H<600$ is typical for biologically formed Birnessite [53]. The spectra of both coatings prior and post experiment show a clear broad and sharp peak (Figure 7). However, the theory of distinguishing the biological nature of manganese minerals on the linewidth of the narrow EPR spectra has been recently challenged [54]. Furthermore iron oxide minerals on sand have been shown to exhibit broad EPR spectra with some similarities of the manganese oxide signals [55]. In both spectra a small signal near 1600 Gauss was found, which is consistent with mononuclear Fe^{3+}.

3.4.3 Emerging AsOB in biofilm on MnOx coating

No major shifts in the microbial community were observed by exposing the drinking water biofilm to arsenic (Figure 8). At Family level, *Nitrospiraceae* dominated all samples post and prior experiments, despite the absence of nitrite and ammonium in the tap water supplied during the experiments (<0.01 mg/L NO_2 and <0.05 mg/L NH_4). *Comamonadaceae* emerged in the samples post experiment. *Comamonadaceae* contain known arsenite oxidizers and are frequently found in As rich environments (Crognale et al., 2019; Huang et al., 2024; Roy et al., 2021) [45,46,48]. The main genus found within *Comamonadaceae* was *Polaromonas*,

capable of oxidizing arsenite [43]. Similarly, an enrichment of *Microscillaceae* was found post experiments, aligning with findings by Su et al. (2022), who reported their enrichment in an arsenic contaminated rice terraces [49]. *Gallionellaceae*, known iron oxidizers, disappeared by exposure to As during the experiments. Apparently, *Gallionellaceae* cannot survive in the dosed water matrix, in which iron is absent and arsenic is present. The presence of *Gallionallaceae* on the sand grains prior experiments likely originates from flush out of the primary treatment filter, where biological iron removal takes place.

Both *Comamonadaceae* and *Microscillaceae* likely played a role in the accelerated As oxidation in the columns. However, it cannot be definitively concluded that they were the only As oxidizing bacteria present. The minimal shifts in community composition after As enrichment suggest that a typical sand filter microbial community can tolerate As concentrations of 500 µg/L. Besides As, there are very little nutrients present in the tap water. However, whether the abundant families such as *Nitrospiraceae* is passively present or actively contributing to As oxidation requires further investigation. It should be noted that 16s sequencing detects also dead bacteria, although dead cells are more likely to detach from the grains and end up in the water stream.

The addition of NaN_3 to the columns did not cause shifts in the community composition (Supplementary Figure 4). It is important to note that the figures represent relative abundances, which do not reflect absolute microbial concentrations. It can explain the faster establishment of a fully As-oxidizing system following microbial inhibition compared to the initial experimental stage. Although the activity was suppressed, the right community composition was present for the task.

Sequencing the microbial community was only possible due to the successful DNA extraction method as proposed in section 2.4. Dissolving the Mn mineral coating by ammonium oxalate resulted in DNA concentrations of 26 – 83 ng/µl, while without this additional step, the concentrations found were <0.1 ng/µL. This shows that standard DNA extraction kits are not suitable for Mn-coated sand. However, these kits are commonly used in drinking water research, which raises the question if certain colonies entangled in Mn oxides are often overseen. This highlights the necessity for a reliable and standardized method to extract DNA from filter sand.

3.4.4 Biological oxidation 14 times faster

The shift from a surface catalytic to a biological system enhanced the As(III) oxidation rate by 14-fold. At the start of the experiment, the determined rate constant k_{CHEM} (chemical) was 0.318 min^{-1}. By the end of the experiment, the constant increased to a k_{BIO} (biological) of 5.64 min^{-1} with a corresponding half-life of 9.0 seconds. The k values for the remaining days can be found in Supplementary Figure 5.

The rate constants of As(III) oxidation in manganese rich environments reported in literature are summarized in Table 3. The range for chemical oxidation rates varies greatly, influenced by factors such as pH, As:Mn ratio, other constituents present, and the type and crystallinity

of the Mn oxides [18,27,56,57]. The oxidation and mobility of As will therefore vary in different Mn rich environments, such as in soil, the deep sea or around mines. How other groundwater constituents, such as Fe or NH_4, influence As(III) oxidation on MnO_x coated filter sand should be considered for future studies. Both k_{CHEM} and k_{BIO} observed in this study notably exceed values reported in earlier studies. An explanation could be that different Mn oxides are known to have a wide range of surface properties [58], e.g., naturally formed Mn oxides have a much higher surface area compared to well-crystallized synthetic δ-MnO_2 [57].

The biological constant k_{BIO} is 8 times higher compared to the highest reported value thus far in a manganese rich environment [59]. One possible explanation for this disparity could be the presence of Mn in the influent in the study of Yang et al. (2015) as it has been found that the presence of Mn can hinder As(III) oxidation [17]. Another explanation might be the notably higher flow rate (20 m/h) in our study, although it has also been argued that a higher flow rate might limit As(III) oxidation kinetics [59,60]. Kruisdijk et al. (2024) found a similar kinetic constant for biological As(III) oxidation (2.94 min^{-1}) in an iron oxides coated sand filter [61], which indicates that the composition of the mineral coating might be of relatively little influence to the oxidation kinetics. However, the influence of the mineral coating on the oxidation efficiency would require further investigation.

Micro-organisms clearly played a vital role in the acceleration of As(III) oxidation in the experiment. This presents a potential new pathway for the development of effective As removal systems. Poor removal of As is often attributed to the slow oxidation of As(III) to As(V), subsequently hampering the removal on Fe hydroxides [62]. Practically promoting fast biological As(III) oxidation in existing water treatment plants could potentially overcome this problem; to trigger As removal, As(V) should form before all Fe(II) has been oxidized in the system. This finding marks a paradigm shift: in filters, Mn oxides have traditionally been demonstrated to be powerful oxidizers of As(III) [15,16,18], or oxidation was attributed to homogeneous oxidation by reactive oxygen species [14], but now it is demonstrated that biological oxidation might well dominate in filters.

Table 3: Kinetic constants for As(III) oxidation in Mn containing systems found in literature (for relevant conditions) and in this study

As(III) oxidation process	Description exp.	Kinetic constant (min^{-1})	Ref
Chemical			
Oxidation by dissolved oxygen	Batch exp. As: 46-62 µg/L pH 7.6-8.5 Fe: 100-1130 µg/L, Mn: 9-16 µg/L in groundwater.	2.2×10^{-4}	[12]
Synthetic Birnessite	Batch exp. As: 7.5 mg/L pH 6.8 Mn:As=12.4	0.035	[18]
Synthetic Birnessite	Batch exp. As: 100 mg/L pH 7.0 Mn:As=12.3	0.00445	[56]
k_{CHEM} day 3		0.318	This study
k_{CHEM} day 3 after inhibition		0.198	This study
Biological			
Mature biologically formed Mn oxides	Batch. As: 1.2 mg/L. Mn:As=64	0.068	[27]
As(III) oxidation during biological Mn(II) oxidation	Column study. flow 7 m/h As: 35-42 µg/L Mn: 400-500 µg/L	0.23	[57]
As(III) oxidation in a biological Mn(II) removal filter column	Column study. flow 7 m/h As: 1986 ug/L. Mn: 4.1 mg/L	0.56	[59]
k_{BIO} day 29		4.64	This study
k_{BIO} day 29 after inhibition		2.48	This study

3.5 Conclusion

The presented research distinguished the contribution of surface catalytic and biological As(III) oxidation on reactive MnO_x coated filter sand. Within three weeks, a shift from surface catalytic to biological As(III) oxidation was observed. Initially, surface catalytic As(III) oxidation (k_{chem}=0.318 min^{-1}) dominated, coupled to Mn release at a ratio of 0.96 (approximating the stoichiometric ratio of 1). This coupling disappeared over time, indicating the biological nature of the reaction as confirmed by microbial inhibition. Exposure to As during experiments led to an increase in RA of *Comamonadaceae,* with the genus *Polaromonas* as the dominant species, and *Microscillaceae*, which are known arsenic oxidizing bacteria. A first order As(III) oxidation rate constant k_{BIO} of 4.64 min^{-1} was found, yielding a half-life of 9 seconds. This represents a 14-fold acceleration, revealing that kinetic limitations rather than surface passivation can be attributed to the loss of surface-catalytic oxidation. Our study demonstrated that biological oxidation of As(III) can outpace the acknowledged oxidizing power of MnO_x, offering a potential new pathway to design effective biological As(III) oxidation and removal filters without the need for complex technologies or the addition of oxidative chemicals.

Supplementary information

The Supplementary Information is available at https://pubs.acs.org/doi/10.1021/acsestwater.5c01031.

References

1. WHO. Arsenic WHO Fact Sheet. Geneva, World Health Organization. 2018. https://www.who.int/en/news-room/fact-sheets/detail/arsenic

2. Podgorski J, Berg M. Global threat of arsenic in groundwater. *Science (1979)*. 2020;368(6493):845-850. doi:10.1126/science.aba1510

3. Ahmad SA, Khan MH. Groundwater arsenic contamination and its health effects in Bangladesh. Published online 2023. doi:10.1016/B978-0-323-89847-8.00007-9

4. Meng X, Korfiatis GP, Bang S, Bang KW. Combined effects of anions on arsenic removal by iron hydroxides. *Toxicol Lett*. 2002;133(1):103-111. doi:10.1016/S0378-4274(02)00080-2

5. Hossain MI, Bukhari A, Almujibah H, et al. Validation of the efficiency of arsenic mitigation strategies in southwestern region of Bangladesh and development of a cost-effective adsorbent to mitigate arsenic levels. *J Environ Manage*. 2023;348:119381. doi:10.1016/J.JENVMAN.2023.119381

6. Berg M, Luzi S, Trang PTK, Viet PH, Giger W, Stüben D. Arsenic removal from groundwater by household sand filters: comparative field study, model calculations, and health benefits. *Environ Sci Technol*. 2006;40(17):5567-5573. doi:10.1021/ES060144Z

7. Hug SJ, Leupin OX, Berg M. Bangladesh and Vietnam: Different groundwater compositions require different approaches to arsenic mitigation. *Environ Sci Technol*. *American Chemical Society*. 2008;42(17):6318-6323. doi:10.1021/es7028284

8. Thomas MA, Ekberg M. *The Effectiveness of Water-Treatment Systems for Arsenic Used in 11 Homes in Southwestern and Central Ohio, 2013*. 2016. doi:10.3133/SIR20155156

9. Moore KW, Huck PM, Siverns S. Arsenic removal using oxidative media and nanofiltration. *J Am Water Works Assoc*. 2008;100(12):74-83. doi:10.1002/J.1551-8833.2008.TB09800.X

10. Cullen WR, Reimer KJ. Arsenic Speciation in the Environment. *Chem Rev*. 1989;89(4):713-764. doi:10.1021/cr00094a002

11. Bissen M, Frimmel FH. Arsenic - a Review. Part II: Oxidation of Arsenic and its Removal in Water Treatment. *Acta hydrochim hydrobiol*. 2003;31:97-107. doi:10.1002/aheh.200300485

12. Kim MJ, Nriagu J. Oxidation of arsenite in groundwater using ozone and oxygen. *Science of The Total Environment*. 2000;247(1):71-79. doi:10.1016/S0048-9697(99)00470-2

13. Gude JCJ, Rietveld LC, van Halem D. Fate of low arsenic concentrations during full-scale aeration and rapid filtration. *Water Res*. 2016;88:566-574. doi:10.1016/J.WATRES.2015.10.034

14. Hug SJ, Leupin O. Iron-catalyzed oxidation of Arsenic(III) by oxygen and by hydrogen peroxide: pH-dependent formation of oxidants in the Fenton reaction. *Environ Sci Technol*. 2003;37(12):2734-2742. doi:10.1021/es026208x

15. Driehaus W, Seith R, Jekel M. Oxidation of arsenate(III) with manganese oxides in water treatment. *Water Res*. 1995;29(1):297-305. doi:10.1016/0043-1354(94)E0089-O

16. Manning BA, Fendorf SE, Bostick B, Suarez DL. Arsenic(III) oxidation and arsenic(V) adsorption reactions on synthetic birnessite. *Environ Sci Technol*. 2002;36(5):976-981. doi:10.1021/ES0110170/ASSET/IMAGES/LARGE/ES0110170F00008.JPEG

17. Gude JCJ, Rietveld LC, van Halem D. As(III) oxidation by MnO2 during groundwater treatment. *Water Res*. 2017;111:41-51. doi:10.1016/J.WATRES.2016.12.041

18. Scott MJ, Morgan JJ. Reactions at Oxide Surfaces. 1. Oxidation of As(lll) by Synthetic Bimessite. *Environ Sci Techno!*. 1995;29:1898-1905.

19. Crognale S, Casentini B, Amalfitano S, Fazi S, Petruccioli M, Rossetti S. Biological As(III) oxidation in biofilters by using native groundwater microorganisms. *Science of the Total Environment*. 2019;651:93-102. doi:10.1016/j.scitotenv.2018.09.176

20. Lytle DA, Williams D, Muhlen C, Riddick E, Pham M. Environmental Science Water Research & Technology The removal of ammonia, arsenic, iron and manganese by biological treatment from a small Iowa drinking water system †. *Cite this: Environ Sci: Water Res Technol*. 2020;6:3142. doi:10.1039/d0ew00361a

21. Gude JCJ, Rietveld LC, van Halem D. Biological As(III) oxidation in rapid sand filters. *Journal of Water Process Engineering*. 2018;21(September 2017):107-115. doi:10.1016/j.jwpe.2017.12.003

22. Katsoyiannis IA, Zouboulis AI. Biological treatment of Mn(II) and Fe(II) containing groundwater: kinetic considerations and product characterization. *Water Res*. 2004;38:1922-1932. doi:10.1016/j.watres.2004.01.014

23. Dangeti S, McBeth JM, Roshani B, Vyskocil JM, Rindall B, Chang W. Microbial communities and biogenic Mn-oxides in an on-site biofiltration system for cold Fe-(II)- and Mn(II)-rich groundwater treatment. *Science of the Total Environment*. 2020;710. doi:10.1016/j.scitotenv.2019.136386

24. Kruisdijk E, van Breukelen BM, van Halem D. Simulation of rapid sand filters to understand and design sequential iron and manganese removal using reactive transport modelling. *Water Res*. 2024;267(September):122517. doi:10.1016/j.watres.2024.122517

25. Ying C, Liu C, Zhang F, et al. Solutions for an efficient arsenite oxidation and removal from groundwater containing ferrous iron. *Water Res*. 2023;243:120345. doi:10.1016/J.WATRES.2023.120345

26. Owings SM, Luther GW, Taillefert M. Development of a rate law for arsenite oxidation by manganese oxides. *Geochim Cosmochim Acta*. 2019;250:251-267. doi:10.1016/j.gca.2019.02.003

27. Ichi Watanabe J', Tani Y, Chang J, Miyata N, Naitou H, Seyama H. As(III) oxidation kinetics of biogenic manganese oxides formed by Acremonium strictum strain KR21-2. *Chem Geol*. 2013;347:227-232. doi:10.1016/j.chemgeo.2013.03.012

28. Hambsch B, Raue B, Brauch H -J. Determination of arsenic(III) for the investigation of the microbial oxidation of arsenic(III) to arsenic(V). *Acta hydrochimica et hydrobiologica*. 1995;23(4):166-172. doi:10.1002/aheh.19950230404

29. Ike M, Miyazaki T, Yamamoto N, Sei K, Soda S. Removal of arsenic from groundwater by arsenite-oxidizing bacteria. *Water Science and Technology*. 2008;58(5):1095-1100. doi:10.2166/wst.2008.462

30. Battaglia-Brunet F, Dictor MC, Garrido F, et al. An arsenic(III)-oxidizing bacterial population: selection, characterization, and performance in reactors. *J Appl Microbiol*. 2002;93(4):656-667. doi:10.1046/J.1365-2672.2002.01726.X

31. Van Le A, Straub D, Planer-Friedrich B, Hug SJ, Kleindienst S, Kappler A. Microbial communities contribute to the elimination of As, Fe, Mn, and NH4+ from groundwater in household sand filters. *Science of the Total Environment*. 2022;838. doi:10.1016/j.scitotenv.2022.156496

32. van der Wens P, Baken K, Schriks M. Arsenic at low concentrations in dutch drinking water: Assessment of removal costs and health benefits. *Arsenic Research and Global Sustainability - Proceedings of the 6th International Congress on Arsenic in the Environment, AS 2016*. Published online 2016:563-564. doi:10.1201/B20466-262

33. Claff SR, Sullivan LA, Burton ED, Bush RT. A sequential extraction procedure for acid sulfate soils: Partitioning of iron. *Geoderma*. 2010;155(3-4):224-230. doi:10.1016/j.geoderma.2009.12.002

34. Gude JCJ, Rietveld LC, van Halem D. Fate of low arsenic concentrations during full-scale aeration and rapid filtration. *Water Res*. 2016;88:566-574. doi:10.1016/J.WATRES.2015.10.034

35. Bonsu DNO, Higgins D, Simon C, Henry JM, Austin JJ. Metal–DNA interactions: Exploring the impact of metal ions on key stages of forensic DNA analysis. *Electrophoresis*. 2024;45(9-10):779-793. doi:10.1002/elps.202300070

36. Foysal MJ, Salgar-Chaparro SJ. Improving the efficiency of DNA extraction from iron incrustations and oilfield-produced water. *Sci Rep*. 2024;14(1):1-10. doi:10.1038/s41598-024-53134-9

37. Breda IL, Ramsay L, Søborg DA, Dimitrova R, Roslev P. Manganese removal processes at 10 groundwater fed full-scale drinking water treatment plants. *Water Quality Research Journal*. 2019;54(4):326-337. doi:10.2166/WQRJ.2019.006

38. Arora H, Peldszus S, Lamba-Rautapuro N, Slawson R, Kendall B, Huck PM. Evaluating manganese removal in groundwater using pilot scale biofilters: The role of filter media characteristics during start-up. *Water Res*. 2025;268:122711. doi:10.1016/J.WATRES.2024.122711

39. Bernardini S, Bellatreccia F, Casanova Municchia A, Della Ventura G, Sodo A. Raman spectra of natural manganese oxides. *Journal of Raman Spectroscopy*. 2019;50(6):873-888. doi:10.1002/JRS.5583

40. Julien C, Massot M, Baddour-hadjean R, Franger S, Bach S, Pereira-ramos JP. Raman spectra of birnessite manganese dioxides. 2003;159:345-356. doi:10.1016/S0167-2738(03)00035-3

41. Huang D, Sun X, Usman M, et al. Bacteria associated with Comamonadaceae are key arsenite oxidizer associated with Pteris vittata root ☆. *Environmental Pollution*. 2024;349(December 2023):123909. doi:10.1016/j.envpol.2024.123909

42. Roy M, van Genuchten CM, Rietveld L, van Halem D. Integrating biological As(III) oxidation with Fe(0) electrocoagulation for arsenic removal from groundwater. *Water Res*. 2021;188. doi:10.1016/j.watres.2020.116531

43. Osborne TH, Heath MD, Martin ACR, Pankowski JA, Hudson-Edwards KA, Santini JM. Cold-adapted arsenite oxidase from a psychrotolerant Polaromonas species. *Metallomics*. 2013;5(4):318-324. doi:10.1039/c2mt20180a

44. Su P, Gao P, Sun W, et al. Keystone taxa and functional analysis in arsenic and antimony co - contaminated rice terraces. *Environmental Science and Pollution Research*. Published online 2022:61236-61246. doi:10.1007/s11356-022-20160-x

45. Crognale S, Casentini B, Amalfitano S, Fazi S, Petruccioli M, Rossetti S. Biological As(III) oxidation in biofilters by using native groundwater microorganisms. *Science of the Total Environment*. 2019;651:93-102. doi:10.1016/j.scitotenv.2018.09.176

46. Huang D, Sun X, Usman M, et al. Bacteria associated with Comamonadaceae are key arsenite oxidizer associated with Pteris vittata root ☆. *Environmental Pollution*. 2024;349(December 2023):123909. doi:10.1016/j.envpol.2024.123909

47. Osborne TH, Heath MD, Martin ACR, Pankowski JA, Hudson-Edwards KA, Santini JM. Cold-adapted arsenite oxidase from a psychrotolerant Polaromonas species. *Metallomics*. 2013;5(4):318-324. doi:10.1039/c2mt20180a

48. Roy M, van Genuchten CM, Rietveld L, van Halem D. Integrating biological As(III) oxidation with Fe(0) electrocoagulation for arsenic removal from groundwater. *Water Res*. 2021;188. doi:10.1016/j.watres.2020.116531

49. Su P, Gao P, Sun W, et al. Keystone taxa and functional analysis in arsenic and antimony co - contaminated rice terraces. *Environmental Science and Pollution Research*. Published online 2022:61236-61246. doi:10.1007/s11356-022-20160-x

50. Sun X, Kong T, Huang D, et al. Microbial Sulfur and Arsenic Oxidation Facilitate the Establishment of Biocrusts during Reclamation of Degraded Mine Tailings. *Environ Sci Technol*. 2024;58(28):12441-12453. doi:10.1021/ACS.EST.3C10945/ASSET/IMAGES/LARGE/ES3C10945_0005.JPEG

51. Arif S, Nacke H, Schliekmann E, Reimer A, Arp G, Hoppert M. Composition and niche-specific characteristics of microbial consortia colonizing Marsberg copper mine in the Rhenish Massif. *Biogeosciences*. 2022;19(20):4883-4902. doi:10.5194/BG-19-4883-2022

52. Nielsen-Franco D, Ginder-Vogel M. Kinetic Study of the Influence of Humic Acids on the Oxidation of As(III) by Acid Birnessite. *ACS ES&T Water*. 2023;3(4):1060-1070. doi:10.1021/acsestwater.2c00547

53. Kim SS, Bargar JR, Nealson KH, et al. Searching for biosignatures using electron paramagnetic resonance (EPR) analysis of manganese oxides. *Astrobiology*. 2011;11(8):775-786. doi:10.1089/AST.2011.0619/ASSET/IMAGES/LARGE/FIGURE6.JPEG

54. Huld S, McMahon S, Sjöberg S, Huang P, Neubeck A. Chemical Gardens Mimic Electron Paramagnetic Resonance Spectra and Morphology of Biogenic Mn Oxides. *Astrobiology*. 2023;23(1):24-32. doi:10.1089/ast.2021.0194

55. Wencka M, Jelen A, Jagodič M, Khare V, Ruby C, Dolinšek J. Magnetic and EPR study of ferric green rust- and ferrihydrite-coated sand prepared by different synthesis routes. *J Phys D Appl Phys*. 2009;42(24):245301. doi:10.1088/0022-3727/42/24/245301

56. Oscarson DW, Huang PM, Liaw WK, Hammer UT. Kinetics of Oxidation of Arsenite by Various Manganese Dioxides. *Soil Science Society of America Journal*. 1983;47(4):644-648. doi:10.2136/SSSAJ1983.03615995004700040007X

57. Katsoyiannis IA, Zouboulis AI, Jekel M. Kinetics of Bacterial As(III) Oxidation and Subsequent As(V) Removal by Sorption onto Biogenic Manganese Oxides during Groundwater Treatment. *Ind Eng Chem Res*. 2004;43(2):486-493. doi:10.1021/IE030525A

58. Min S, Kim Y. Physicochemical characteristics of the birnessite and todorokite synthesized using various methods. *Minerals*. 2020;10(10):1-17. doi:10.3390/min10100884

59. Yang H, Sun W, Ge H, Yao R. The oxidation of As(III) in groundwater using biological manganese removal filtration columns. *Environmental Technology (United Kingdom)*. 2015;36(21):2732-2739. doi:10.1080/09593330.2015.1045039

60. Katsoyiannis I, Zouboulis A, Althoff H, Bartel H. As(III) removal from groundwaters using fixed-bed upflow bioreactors. *Chemosphere*. 2002;47(3):325-332. doi:10.1016/S0045-6535(01)00306-X

61. Kruisdijk E, Goedhart R, van Halem D. Biological arsenite oxidation on iron-based adsorbents in groundwater filters. *Water Res*. 2024;262:122128. doi:10.1016/J.WATRES.2024.122128

62. Annaduzzaman M, Rietveld LC, Hoque BA, Bari MN, van Halem D. Arsenic removal from iron-containing groundwater by delayed aeration in dual-media sand filters. *J Hazard Mater*. 2021;411:124823. doi:10.1016/J.JHAZMAT.2020.124823

04

Biological Arsenite Oxidation on Iron-Based Adsorbents in Groundwater Filters

Published as:
Kruisdijk, E., Goedhart, R. & van Halem, D. (2024). Biological arsenite oxidation on iron-based adsorbents in groundwater filters. Water research, 262, 122128.

Abstract

Iron-based adsorbents are commonly used to remove arsenic (As) from water for drinking water purposes. Here, we study the role of biological As(III) oxidation on iron-based adsorbents in filters and its effect on overall As uptake. A lab-scale filter with iron oxide coated sand (IOCS), a commonly used adsorbent, was operated with water containing As(III) and As(V), while water samples were taken periodically over its height. As(III) oxidation initiated after approximately 10 days and increased to a first order rate constant of 0.09 s^{-1} after 57 days resulting in full oxidation of As(III) in <50 seconds. Consequently, the filter shifted from an As(III) to an As(V) adsorbing filter. Oxidation was not observed after inhibiting the microbial activity using sodium azide confirming its biogenic nature. This implies that As(III) oxidizing biomass can grow on iron-based adsorbents in water filters without requiring inoculation. As the experimental conditions were similar to full-scale As treatment plants, we believe that biological As(III) oxidation is widely overlooked in these systems. Occurrence of biological oxidation is, however, beneficial for removal, as at pH <8 the adsorption capacity for As(V) can be up to 10-fold higher than for As(III). With these new insights, arsenic treatment using iron-based adsorbents can be further optimized. We suggest a more robust new design with a biological active As(III) oxidizing top layer and an As(V) adsorbing bottom layer.

4.1 Introduction

Arsenic (As) is found in groundwaters around the world affecting the health of humans and wildlife. It is classified as a human carcinogenic substance [1], which increases the risk for skin lesions and cancers. Podgorski and Berg (2020) estimated that 94 to 220 million people drink or use groundwater with As concentrations exceeding the World Health Organization guideline of 10 µg/L [2,3]. It is generally observed in two redox states, as arsenite (As(III) and arsenate (As(V)). As(III) is the reduced form, and exists as oxyanion [H_3AsO_3] in natural waters at circumneutral pH, while arsenate is the oxidized form found as [$H_2AsO_4^-$ or $HAsO_4^{2-}$]. The reduced form, As(III), is most commonly found in anaerobic groundwaters.

Iron-based adsorbents represent a highly effective method to remove As from water [4–6]. They are environmentally friendly, highly abundant, and are, therefore, commonly used in wastewater and drinking water treatment [7]. Oxidation of As(III) to As(V) before treatment is often desired, as the negatively charged As(V) is more efficiently removed via adsorption [8]. Full oxidation with O_2 takes tens of days [9]. Therefore, to accelerate this process, chemical oxidants such as, ozone, chlorine, or permanganate are applied, but these oxidation pathways are more costly, need extra chemicals, and increase the risk of unwanted by-products [10]. Since the last decade, interest increased in another oxidation pathway: biological As(III) oxidation. Biological As(III) oxidation has already been studied and observed in lab-scale drinking water filters [11,12], and bioreactors [13–15]. The bioreactors were inoculated with As-oxidizing bacteria, while in rapid sand filters biological As(III) oxidation established without any inoculation. To our knowledge, biological As(III) oxidation on iron-based adsorbents has not yet been studied. The latest review articles on iron-based adsorbents highlight the importance of As(III) oxidation for efficient removal, but only focus on chemical oxidation [7,16–18].

Gude et al. (2018) showed that biological As(III) oxidation started after one week and really accelerated after two weeks without inoculation on virgin sand in a column study [12]. This and the common occurrence of As(III) oxidizing bacteria in aquatic environments [19], indicate that As(III) oxidizing bacteria are omnipresent. We therefore expect that As(III) oxidizing bacteria can also grow on iron-based adsorbents in water filters. Until now, research on iron-based adsorbents is mostly performed using batch or column experiments, which most often did not take longer than a couple of days [4–6,20–23]. This could be the reason that As(III) oxidation is never observed, as the duration of these experiments were likely too short for the growth of As-oxidizing bacteria. Driehaus (2002) and Petrusevski et al. (2007) studied full-scale treatment plants in which As was removed by granular ferric hydroxide and iron oxide coated sand, respectively [24,25]. The lifetime of the media was minimally a year, which we assume is more than enough for the growth of As-oxidizing bacteria, but their presence was never studied.

Based on this information, we hypothesize that biological As(III) oxidation (pH<6.94: $H_3AsO_3+H_2O \rightarrow H_2AsO_4^-+3H^++2e^-$, pH >6.94: $H_3AsO_3+H_2O \rightarrow HAsO_4^{2-}+4H^++2e^-$) is commonly occurring when treating water for As using iron-based adsorbents. This novel perspective

could be of great value for science and practice, as this would imply that treatment with iron-based adsorbents is working differently than understood until now. Based on this knowledge, treatment with iron-based adsorbents could be further optimised. To test this hypothesis, we performed an 80-day lab-scale filter experiment and studied As adsorption and oxidation on iron oxide coated sand with scenario modelling.

4.2 Methods

4.2.1 Adsorbent

In this research, iron oxide coated sand (IOCS) was used as adsorbent collected from a groundwater-fed rapid sand filter used for drinking water treatment. In this filter, the pH (6.9) and O_2 concentration (3.4 mg/L) are kept low to aim for biological Fe(II) oxidation and to prevent Mn(II)-oxidation. Similar IOCS from drinking water filters are commonly used in full-scale As treatment [24,26.]

4.2.2 Lab-scale filter design and operation

A PE column with a diameter of 3.3 cm and a height of 1 m was used during the experiment (Figure 1). IOCS grains were washed and used to fill the column, after which the column was wrapped in aluminium foil. The column was extensively backwashed before the start of the experiment. A salt tracer test was performed in the column to obtain the porosity (=0.28). During the experiment, unchlorinated tap water (for water quality parameter see appendix 1 (A.1)) was pumped, upflow, into the column (Watson Marlow 300 series, 314D pump head) without any nutrient additions. A small flow of a 15 mg/L As stock was added (Watson Marlow 300 series, 318MC pump head) resulting in a total flow of 146 mL/min, an influent concentration of ~400 µg/L As, a pH between 7.8-8.1, and an O_2 concentration between 9.2-10.0 mg/L. The As stock solution was prepared from a 0.05 M $NaAsO_2$ solution (Merck), and was acidified to about pH 3 by adding 37% HCl (Fluka) to prevent oxidation during storage, and was refreshed every three days.

4.2.3 Microbial inhibition procedure

When the As(III) oxidation rate stabilized, the IOCS in the column was flushed with a 25 mM sodium azide (NaN_3, Sigma Aldrich) solution, to inhibit microbial activity. We dosed 500 µg/L As (0.05 M $NaAsO_2$, Merck) to the solution to prevent desorption from the IOCS. The column was saturated with this solution and kept stagnant for 12 hours, after which the column was flushed with 15 L for 17 hours. ATP measurements were performed before and after microbial inhibition to analyse microbial activity using the Deposit & Surface Analysis kit (LuminUltra

Technologies Ltd.) following the protocol provided by the manufacturer. Afterwards, the column was operated identically as at the start of the experiment.

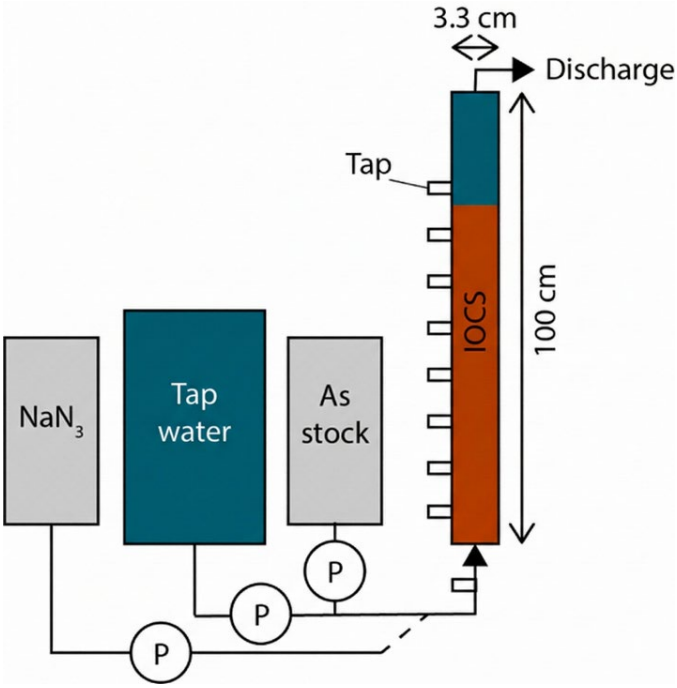

Figure 1: Schematic overview of the experimental setup, where the P within the circle depict the pumps. During the experiment the column was fed with tap water to which As was added. The tap water and As(III) stock pumps were stopped during microbial inhibition, and only a NaN_3 solution was fed to the column.

4.2.4 Water sampling and analysis

Water samples were taken periodically from the nine taps on the column (here referred to as height profiles) and more regularly from the influent and effluent water. They were acidified (ROTIPURAN® Ultra 69%, 1% v/v) and filtered (0.45 µm) before analysis. Inductively Coupled Plasma Mass Spectrometry (ICP-MS, Analytikal Jena PlasmaQuant MS) was used to determine As(III), As(tot), Fe, and Mn concentrations. The Clifford method was performed to separate As(III) and As(V) using a similar method as described by Gude et al. (2018) [12].

4.2.5 Characterisation of iron oxide coated sand

IOCS was analysed after collection from the groundwater-fed rapid sand filter. The IOCS coating was extracted following the method proposed by Claff et al. (2010)[27], after which, Fe, Mn and As was analysed using inductively coupled plasma mass spectrometry (ICP-MS, Analytikal Jena Plasma Quant MS). Furthermore, the untouched grain coatings were analysed using light microscopy (VHX-5000 series, Keyence) and Environmental SEM at 0.5 °C and 6 – 8 mbar H_2O atmosphere (Quanta FEG 650, FEI). After the experiments, IOCS grains were collected from close to the influent of the column and analysed using X-ray photoelectron spectroscopy (XPS, for more information see A.2).

4.2.6 Scenario modelling

The total mass of As adsorbed to the IOCS between two measurement dates was estimated based on the influent and effluent concentrations and summed for the total period using the following equation,

$$Mass\ adsorbed\ As = \sum \left(C_{in\_x} - C_{out\_x}\right) \times (t_x - t_{x-1}) \times q \quad (1)$$

where C_{in_x} is the influent concentration on day *x* (µg/L), C_{out_x} the effluent concentration on day *x* (µg/L), t_x is the day since the start of the experiment (days) and t_{x-1} the day since the start of the experiment from the previous measuring round (days), and q is the flow in (L/days).

The exact impact of oxidation and adsorption on the observed concentrations could not be disentangled, which made determining a precise rate of adsorption and oxidation impossible. Instead, two scenarios ("*prevalently As(III)*" or "*prevalently As(V)*", see Table 1) were simulated and compared to the height profiles obtained during the column experiments. We compared the scenarios and used the one that gave the best fit to estimate the rate of adsorption and oxidation in the columns. When no good fits were obtained, As(III) and As(V) concentrations were not simulated. This only occurred when both As(III) and As(V) were present in relatively high concentrations. We presented this data using a third scenario: "*As(III)+As(V)*" (Table 1).

Table 1: Scenarios used for fitting to height profiles to estimate oxidation and sorption kinetics.

Scenario name	How is the scenario simulated
Prevalently As(V)	As(V) is prevalently available, thus, we assume that: Only As(V) is sorbed – As(III) concentrations are only depending on oxidation
Prevalently As(III)	As(III) is prevalently available, thus, we assume that: Only As(III) is sorbed – As(V) concentrations are only depending on oxidation
As(III)+As(V)	Simulation is not possible, as both As(III) and As(V) are dominantly available. Therefore, sorption of both solutes is entangled.

For all scenarios except of *As(III)+As(V)*, sorption was fitted to the As(tot) concentrations, based on a first-order rate equation,

$$As(tot)_{sim} = As(tot)_{in} \times e^{-(k_{sorb} \times t)} \quad (2)$$

where $As(tot)_{sim}$ are the simulated concentrations (µg/L), $As(tot)_{in}$ the influent concentrations (µg/L), k_{sorb} the first order rate constant (s^{-1}), and t the travel time until each tap (s).

Next, biological As(III) oxidation was simulated. Depending on the scenario, we assumed that As(III) (Prevalently As(V); equation 3) or As(V) (Prevalently As(III); equation 4) concentrations were only relying on oxidation (and thus not on adsorption). Lastly, the residual As oxidation

state was determined by combining the sorption and oxidation reaction, as As(tot)=As(III)+As(V).

Scenario Prevalently As(V):

$$As(III)_{sim} = As(III)_{in} \times e^{-(k_{ox} \times t)} \quad (3)$$

Scenario Prevalently As(III):

$$As(V)_{sim} = As(V)_{in} + (As(III)_{in} \times ((1 - e^{-(k_{ox} \times t)}) + 1) - As(III)_{in}) \quad (4)$$

4.3 Results

4.3.1 Arsenic adsorption

Figure 2 shows the As concentration in effluent (C_{out}) divided by the influent (C_{in}) during the column experiment (black dots), where a C_{out}/C_{in}=1 means that all As in the influent is also observed in the effluent. The observed trend was similar as seen in prior research [5,6]. Initially almost all As was adsorbed to the IOCS (C_{out}/C_{in}=0), after which adsorption decreased. The 50% breakthrough occurred after approximately 15,000 pore volumes and the trend somewhat stabilised after 20,000 pore volumes. Note that still about 25% of the injected As was adsorbed after more than 70,000 pore volumes, which shows that tailing was still occurring [28]. The observed tailing is consistent with recent research into phosphorus adsorption to IOCS, where tailing was found to be caused by slower adsorption on sorption sites in the inner porosity of the iron coating [29]. Figure 2 also shows the cumulative weight of As sorbed to the IOCS (red triangles). Over the course of the experiment, approximately 2080 mg As was sorbed per kg of IOCS in the column (2.08 mgAs/gFe).

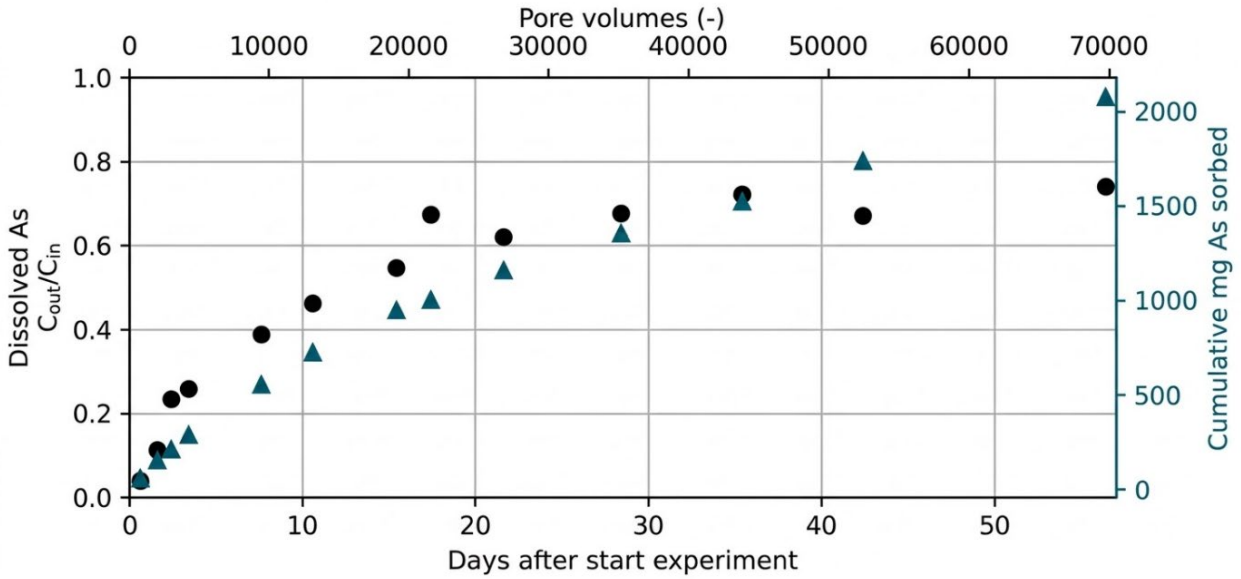

Figure 2: Fraction of As influent concentrations (C_{in}) divided by effluent concentration (C_{out}) (black dots) and the cumulative weight of As adsorbed to IOCS (blue triangles) during the experiment.

4.3.2. Arsenic speciation in produced water

Figure 3 shows the As(III) and As(V) concentrations in the effluent during the column experiment. The influent water contained between 211-346 µg/L As(III), and between 69-151 µg/L As(V). During the first ~5 days of the experiment, As(III) concentrations increased in the effluent water, but always stayed substantially lower than in the influent water. This increase in concentration corresponded to the simultaneous increase in total As concentrations shown in Figure 2, which was a result of a decrease in sorption capacity. Beyond these initial days, As(III) concentrations stabilised and subsequently decreased after ~12 days. Observed As(V) concentrations increased during this period, indicating a decreasing adsorption capacity of the IOCS. Beyond 12 days, the As(V) concentration in the effluent started to exceed the mean As(V) concentration in the influent. From approximately Day 22, the effluent water only contained As(V) (240 µg/L) and As(III) remained below the detection limit. Clearly, the IOCS column moved towards an almost stable condition where only As(V) was present in the effluent in the course of 20 days.

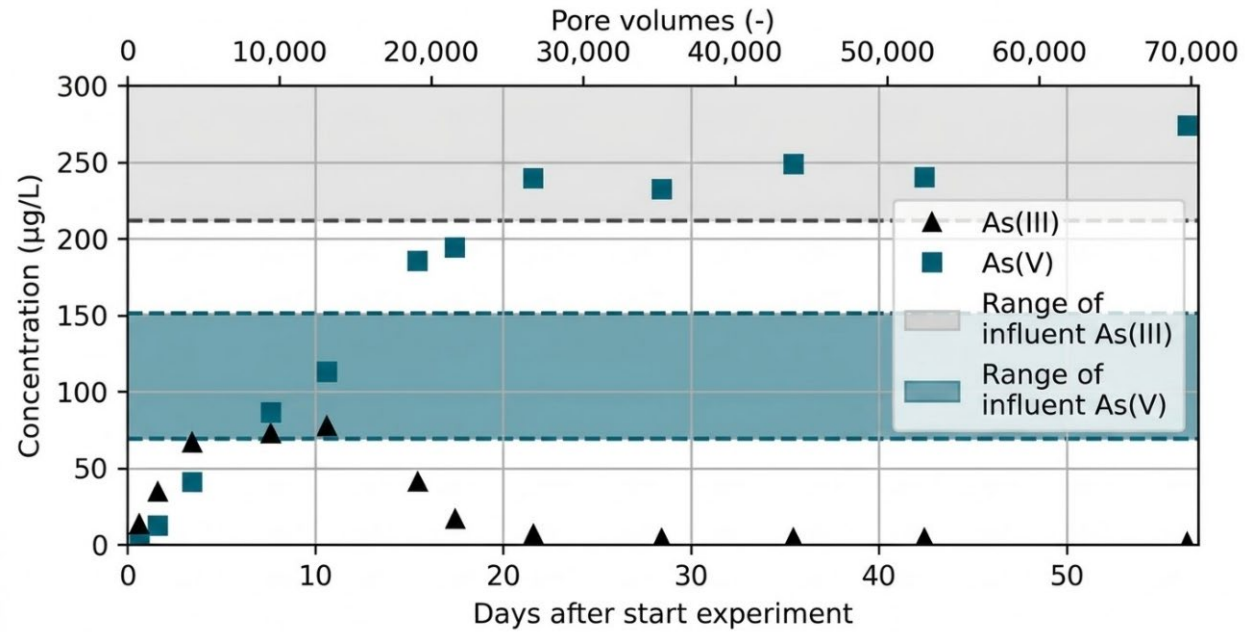

Figure 3: As(III) (black triangles) and As(V) (blue squares) concentrations in effluent water during the first 57 days of the experiment, where the grey and blue highlighted background depict the range of influent As(III) and As(V) concentrations, respectively.

4.3.3 Stratification of arsenic oxidation and adsorption

Figure 4 shows height profiles of the column taken at different days during the experiment. At the start of the experiment (Day 1), As adsorption resulted in a quick decrease of As(tot), As(III), and As(V) over the height of the column. On Day 8, neither As(V) adsorption or production was observed, and As(tot) removal followed the same trend as As(III). From Day 22, As(III) concentrations decreased faster than As(tot) concentrations. At the same time, As(V) concentrations were found to increase over the height of the column. This marks the

initiation of As(III) oxidation in the column. On Day 57, As(III) oxidation further accelerated, while As(tot) adsorption remained somewhat stable.

The height profiles were used to estimate the kinetics of As(III) oxidation and As(tot) adsorption using scenario modelling. The scenarios were fitted to the observed concentrations, and the best fitting scenario was used (and shown in Figure 4) to estimate first order oxidation and sorption rate constants. A good fit was not observed on Day 1; therefore, it was allocated to scenario *As(III)+As(V)*, as likely both As(III) and As(V) sorption occurred. Day 8 was simulated using scenario *Prevalently As(III)*, as oxidation and increasing As(V) concentrations was not observed yet. We assume that biological As(III) oxidation had not yet developed sufficiently this early in the experiment. Furthermore, As(V) adsorption has reached equilibrium, thus all observed removal was due to As(III) adsorption. For Day 22 and 57, As(III) is oxidizing, hence removal occurs primarily through As(V) adsorption, and therefore, scenario *Prevalently As(V)* started to fit best. As(V) sorption became dominant, due to faster As(III) oxidation resulting in higher As(V) concentrations, shifting its earlier adsorption equilibrium.

All days were simulated well using the different scenarios. The first order sorption rate constant (k_{sorb}) decreased over time from 0.012 s^{-1} on day 8 to 0.0035 s^{-1} on day 57. The first order oxidation rate constant (k_{ox}) increased over time from 0 s^{-1} on day 8 to 0.09 s^{-1} on day 57. On day 57, complete As(III) oxidation occurred within <50 seconds.

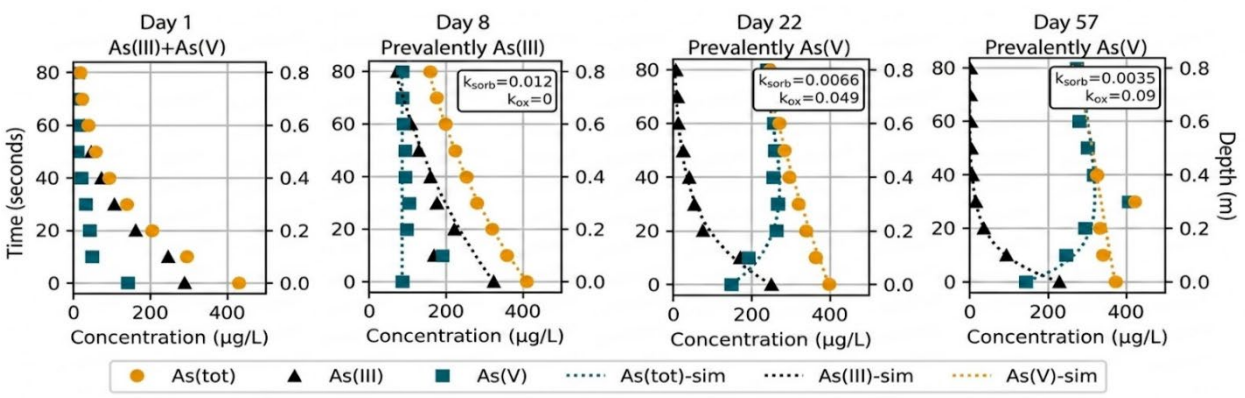

Figure 4: Height profiles of As(tot), As(III), and As(V) concentrations observed over depth in the IOCS column. The markers (yellow circle=As(tot), black triangle=As(III), blue square=As(V)) represent the observed concentrations, the dashed lines the simulated scenario fits.

4.3.4 As(V) and As(III) sorbed to IOCS

Figure 5A shows a light microscopy image of the IOCS prior to the experiments. The grain coating seemed to be equally distributed over the full surface of the quartz sand grain. The brownish/reddish colour is characteristic for a ferrihydrite coating [30]. Chemical extraction of the coating showed that it contained 440-620 mg/g Fe (n=3) and 0.09-0.12 mg/g Mn (n=3). Furthermore, the grain coating contained 0.16-0.17 (n=3) mg/g As, which corresponds with the relatively high influent As concentrations (~40 µg/L) at the rapid sand filter from which the IOCS were obtained. Figure 5B displays an ESEM image in which the grain coating is 20,000

times magnified. The image shows that the surface of the grain was relatively porous. Furthermore, twisted stalks were observed in the coating, which highlights the biogenic nature of (a part of) the Fe-(hydr)oxides [31,32].

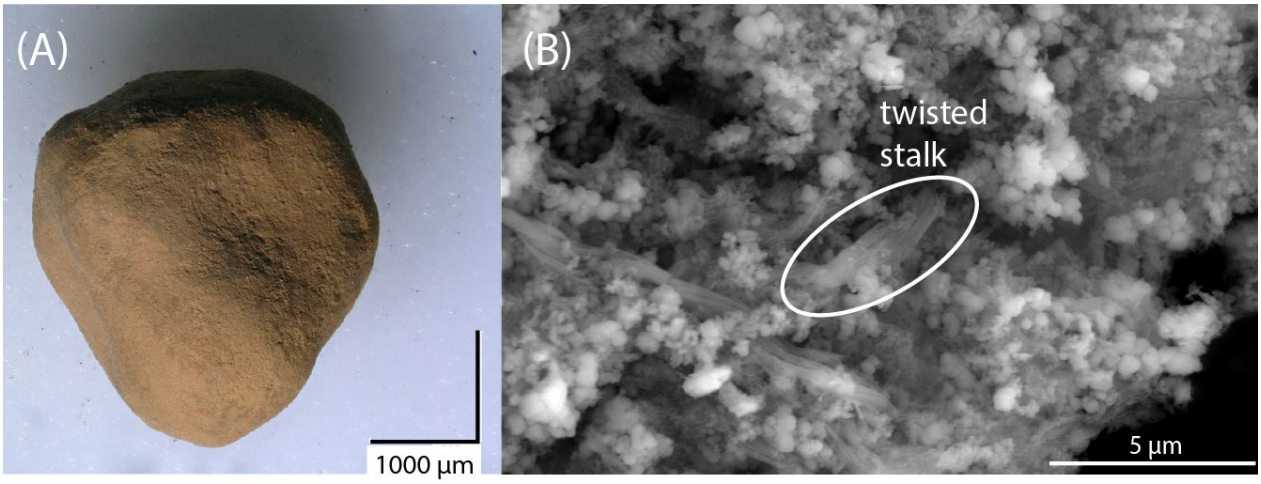

Figure 5: Images of surface of single IOCS grain taken using a light microscope (A) and ESEM (B).

Grains close to the influent of the column were analysed using XPS for the speciation of the adsorbed As after the experiment. About 53% As(III) and 47% As(V) was sorbed to the IOCS (Figure 6).

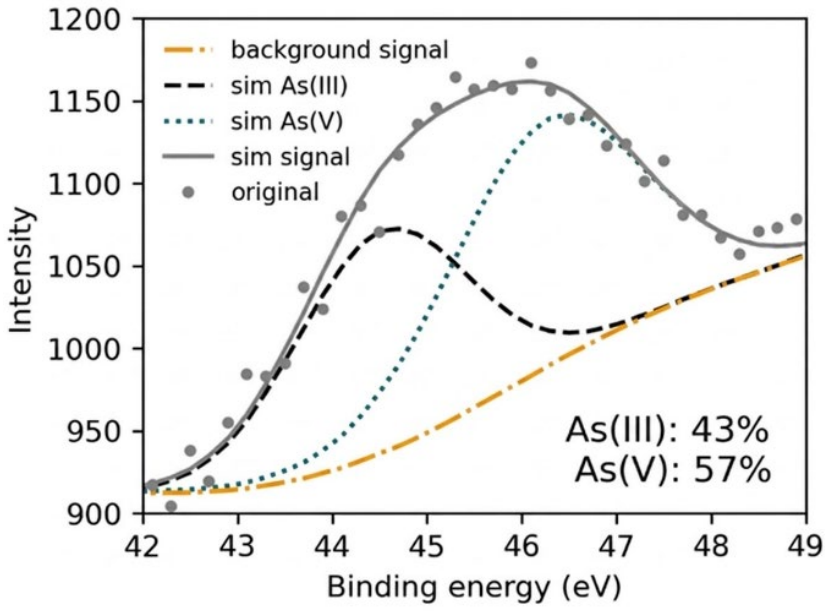

Figure 6: XPS analysis of As3d spectra of the coating of the grains collected close to the influent of the column.

4.3.5 Arsenic oxidation is of biological nature

Microbial activity was inhibited in the column after approximately 50,000 pore flushes, by dosing of NaN_3. A 30-fold reduction of the total ATP, from 29,500-35,100 pg ATP/g (n=2) to 1,160-1,300 pg ATP/g (n=2), was observed after inhibition. Figure 7 shows that the effluent water only contained As(V) before microbial inhibition, i.e., all As(III) was oxidized in the

column. After microbial inhibition, As(V) concentrations were lower in the effluent and As(III) was observed again. Therefore, oxidation was successfully inhibited, which confirms that oxidation was primarily biological. From Day 9, As(V) concentrations in the effluent water exceeded the mean influent As(V) concentrations. Simultaneously, As(III) concentrations decreased in the effluent, suggesting that biological As(III) oxidation was initiated again. After ~23 days, the effluent primarily contained As(V), which resembles the results prior to microbial inhibition (Figure 3).

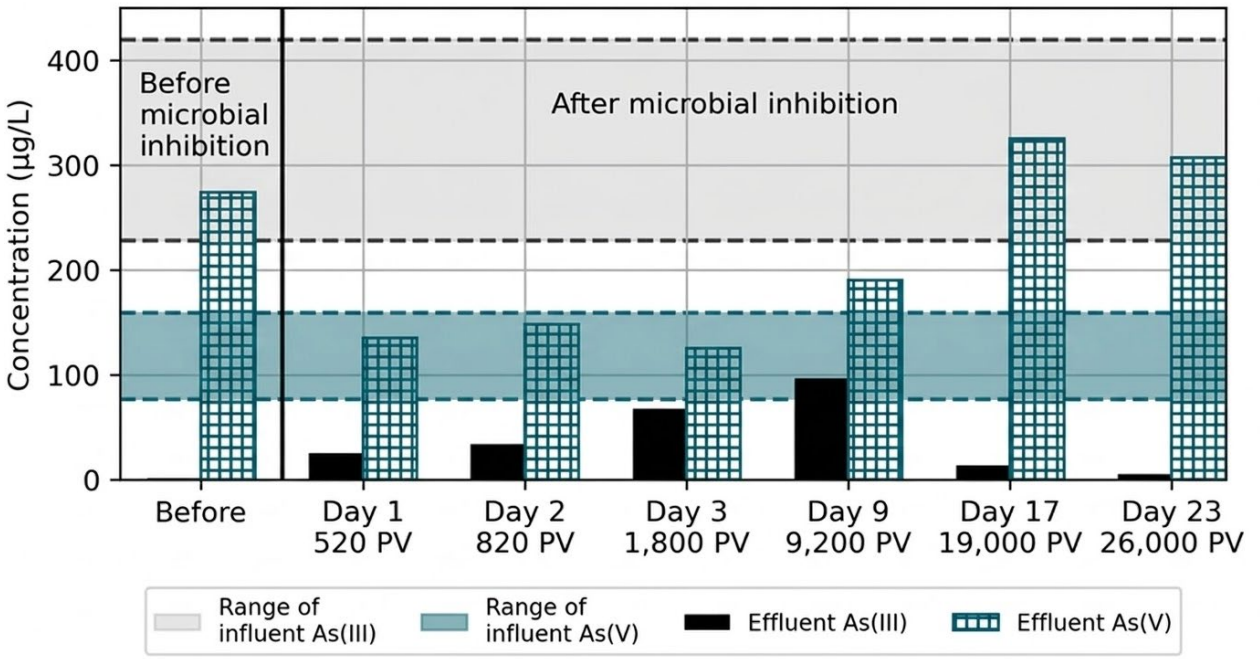

Figure 7: As(III) (black) and As(V) (blue hatched) concentrations in effluent of the column before and after microbial inhibition. The grey and blue highlighted background depict the range of influent As(III) and As(V) concentrations, respectively.

On Day 1 and Day 2 after microbial inhibition, the height profile was best simulated using scenario *Prevalently As(III),* as oxidation was only limited (k_{ox}=0 and 0.0047, respectively) (Figure 8). This corresponds to the results of Day 8 prior to inhibition, as no As(V) adsorption is being observed, while As(III) is. The absence of biological oxidation allows for adsorption of As(III), but the consequent lower concentrations of As(V) are not taken up. Once the column ran for a longer period (Day 8 and 16), scenario *Prevalently As(V)* started to fit best, as more As(III) oxidation occurred resulting in higher As(V) concentrations and thus As(V) sorption resumed. This sequence of scenarios is similar to the experiment before microbial inhibition.

The k_{ox} increased over time after microbial inhibition, and followed the same trend and order as before microbial inhibition. A maximum k_{ox} of 0.053 s^{-1} was reached on the last day of the experiment (Day 16), which is in the same order as observed on Day 22 (k_{ox}=0.049 s^{-1}) before microbial inhibition.

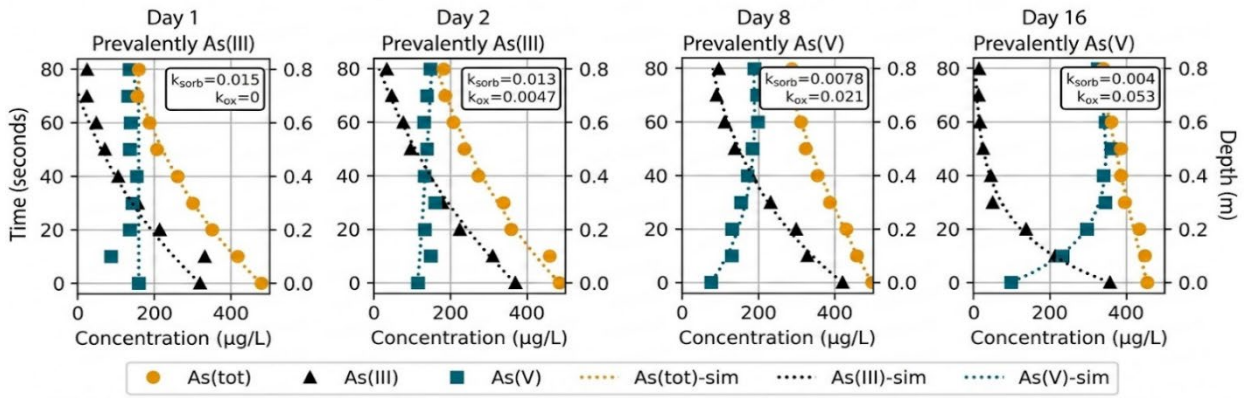

Figure 8: Height profiles of As concentrations of the IOCS column taken over time after microbial inhibition. The markers (yellow circle=As(tot), black triangle=As(III), blue square=As(V)) represent the observed concentrations, the dashed lines the simulated scenario fits.

4.4 Discussion

4.4.1 Biological As(III) oxidation results in higher adsorption capacity for adsorbent

At the end of the experiment (Day 57), biological As(III) oxidation was fast (k_{ox}= 0.09 s^{-1}). Merely <50 seconds were needed to fully convert As(III) and As(V) concentrations were higher than As(III) concentrations at almost all depths in the column (Figure 4). The XPS analysis showed that As(III) and As(V) was somewhat equally adsorbed close to the influent of the column. We expect that the fraction As(III) will only decrease with depth in the column, as (i) at the start almost all As(III) sorption occurred in the upper part of the filter and therefore not much As(III) was adsorbed deeper in the bed, and (ii) later a substantial fraction of As(III) was oxidized to As(V). Consequently, As is primarily adsorbed as As(V), because of its dominant presence and its higher affinity to sorb. This hypothesis is, furthermore, supported by the scenario modelling, and the observed sorption behaviour after microbial inhibition. We did not observe any evidence that As(III) oxidizing biomass masked available adsorption sites on the iron-coated sand. Casentini et al. (2019), similarly, found that arsenic adsorption remained rapid on iron oxide nanoparticles covered with bacterial exopolysaccharide [33].

Table 2 gives an overview of the operating conditions and performance of three types of full-scale As treatment filters using the Fe-based adsorbents; GEH and IOCS [24–26]. The life time of the media is considerably longer (0.14-2 years) than the ripening time needed (~weeks) to grow As-oxidizing bacteria observed in the current study and the study of Gude et al. (2018) [12]. Furthermore, the contact time (3-120 minutes) is substantially longer compared to the <50 seconds needed for complete oxidation observed in the current experiments. Therefore, we deem it likely that biological As(III) oxidation is occurring in these filters, and instead of adsorbing As(III) the filters are adsorbing As(V). We strongly recommend to study one of the existing As treatment plants based on GEH or IOCS over the height of the filter, in order to assess As(III) oxidation kinetics. When biological As(III) oxidation is observed, the next step for future research would be to identify which bacteria are executing this specific process, and to study the effects of pH, water matrix, and temperature.

Table 2: Overview of operational conditions of full-scale As treatment plants using iron-based adsorbents.

Operational conditions:	**GEH** [25]	**IHE-ADART** [24]	**IHE As removal family filter**[26]
As in influent water (µg/L)	10-40	20-295	180-480
Flow rates (m^3/h)	4-160	2.3	>0.004
Annual supply (m^3)	10,000-1,300,000	~20,000	>36,5
Life time media (years)	~2	>1	0.14 - >2.5
Contact time (min)	3-10 (mean= 4.2 minutes)	72	120
Treatment capacities (bed volumes)	50,000-200,000	unknown	unknown

Figure 9 depicts the adsorption capacity trends for a GEH filter where biological As(III) oxidation is occurring (=biotic filter) and not (=abiotic filter). For this analysis, we used the adsorption capacity of As(III) and As(V) on granular ferric hydroxide (GEH) as observed by Driehaus and Dupont (2005) [34]. The shown adsorption capacities are a rough estimate, as in the study of Driehaus and Dupont (2005) the influent concentrations are a tenfold lower and GEH is used instead of IOCS. However, note that similar trends for As(III) and As(V) adsorption capacity with pH are also observed for amorphous iron oxides and goethite [35], and IOCS [21,36]. The adsorption capacity in the biotic filter, loaded with As(V), is substantially higher than the abiotic filter loaded with As(III) at a pH below 8. The lower the pH the higher the adsorption capacity in the biotic filter. The adsorption capacity in the abiotic filter is relatively stable from pH 6-9. At pH 6, the adsorption capacity is about an order of magnitude higher for the biotic compared to the abiotic filter. This finding underlines the value of biological As(III) oxidation in Fe-based adsorbent reactors, as As-free water yields per filter lifetime, i.e., before media replacement, might be up to 10-fold.

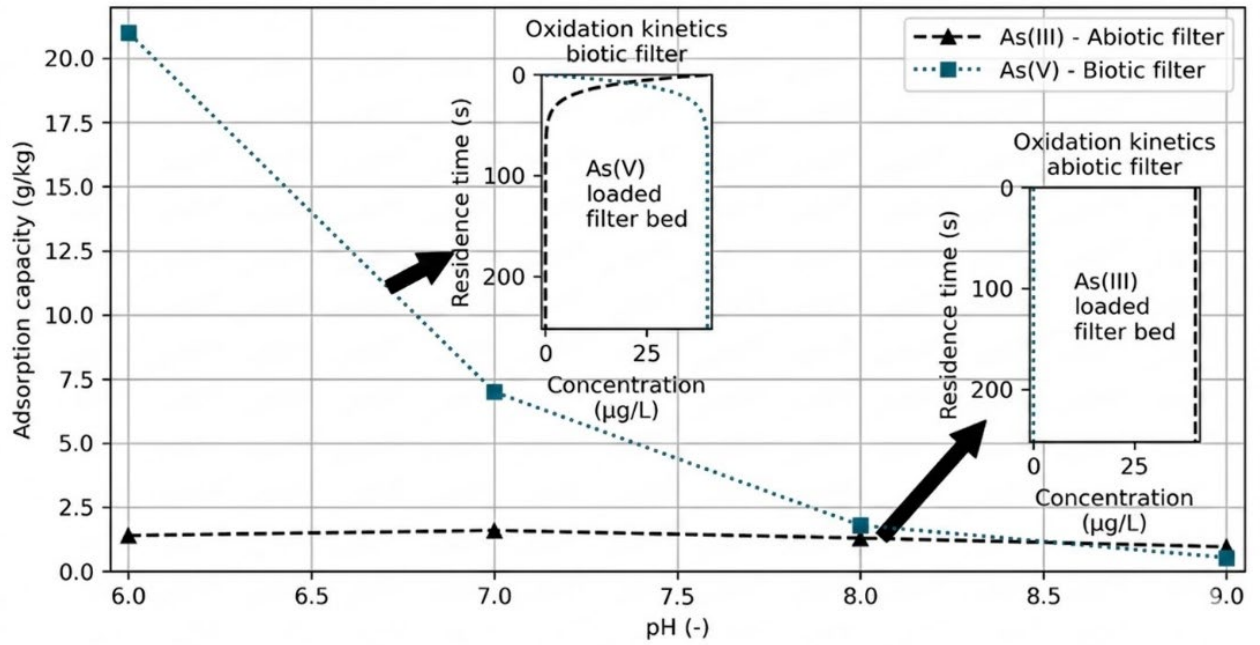

Figure 9: Adsorption capacity of As(III) as in an abiotic filter and As(V) as in a biotic filter under a range of pH. The oxidation kinetics in the biotic and abiotic filter which regulate As speciation, are appointed with a blue and black arrow, respectively. Adsorption capacity is estimated for GEH filters with a mean residence time of 4.2 minutes, an influent concentration of 40 µg/L, and a first-order oxidation rate constant of 0.09 s^{-1}. For the biotic GEH filter we assumed that only As(V) is present. Adsorption density is based and adapted from Figure 2 in Driehaus and Dupont (2005) [34].

4.4.2 Leveraging biological As(III) removal in new filter designs

The adsorbents in an As treatment plant need to be periodically exchanged, as the adsorbents become exhausted. After the media is exchanged, a ripening period is again needed for the microbiome in the new media to perform biological As(III) oxidation. This ripening period can be eliminated, when the upper layer of the filter, wherein all oxidation occurs, is kept in place. A double-filter system, i.e., two filter tanks in sequence, or a dual media filter, i.e., one tank with two layers of different density, could be suitable to achieve this. In these systems, compartmentalisation of processes can be achieved [37]. In the case of a dual media bed, this is due to density difference that allow for separation during backwashing. Note that the sorption capacity of the upper layer of the filter will decrease over time until sorption becomes negligible. Therefore, oxidation will occur in the upper layer and sorption in the lower layer. The advantage of the dual media filter is that it takes up a smaller area compared to a double-filter system. For the top layer suitable media should be chosen to host the As(III) oxidizing biofilm, which could be IOCS as in this study, but a lighter material might be more appropriate (e.g., plastic biocarriers, anthracite). The bottom layer has the function to adsorb As(V), so IOCS could be applied, but also activated alumina or ion exchange resins. Frank and Clifford (1986) showed a comparison of an As(III) and an As(V) breakthrough curve of a laboratory experiment using activated alumina [38]. The 50% breakthrough for As(III) already occurred after 300 pore volumes, while the 50% breakthrough for As(V) only occurred after 23,400 pore volumes. Similarly, anion exchange is not efficient to treat As(III) (H_3AsO_3), as it can only be applied to remove negatively charged ions. As(V)

($H_2AsO_4^-$ or $HAsO_4^{2-}$) is negatively charged and can be removed by anion exchange [8]. On top of this, exchange resin is interesting because it can easily be regenerated in-situ; maintaining its position below the biological layer. An additional advantage is that the As(V) can be recovered in the regeneration brine, which is of interest, as since 2023, As is on the Critical Raw Materials list of the EU [39]. This highlights the importance of As as a critical raw material for economic growth, as well as its vulnerability to supply disruptions.

4.5 Conclusion

This study aimed to investigate the role of biological As(III) oxidation in As removal technologies based on adsorption to iron, e.g., iron oxide coated sand (IOCS), for drinking water production. It was found that As(III) oxidation initiated after approximately 10 days of operating a lab-scale IOCS filter, eventually leading to a first order rate constant of 0.09 s^{-1} after 57 days. Consequently, the initial As(III) adsorbing filter moved towards an As(V) adsorbing filter in ~20 days. After microbial inhibition with NaN_3, As(III) oxidation became negligible, which confirms its biogenic nature. The naturally occurring biological As(III) oxidation, caused by omnipresent bacteria, largely improves the overall performance of filters, as As(V) adsorption capacities tend to be higher than for As(III). We expect that biological As(III) oxidation is also a prevalent process within full-scale As treatment facilities using iron-based adsorbents, as conditions are similar to the performed experiment. These new insights enable further optimization of As treatment using iron based adsorbents. We propose a new reactor design, with a biologically active top layer (i.e., biocarrier) and a bottom layer for the adsorbent. Alternatively, to fully utilise the charge advantage of As(V) at circumneutral pH, an anion exchange resin could be applied to recover As in the brine – since As is recently listed as critical raw material.

Supplementary information

The Supplementary Information is available at
https://www.sciencedirect.com/science/article/pii/S0043135424010285

References

1. IARC. *Some Drinking-Water Disinfectants and Contaminants, Including Arsenic*. Vol 84. IARC Monographs on the Evaluation of Carcinogenic Risks to Humans; 2004.

2. WHO. *Guidelines for Drinking-Water Quality*. 1993.

3. Podgorski J, Berg M. Global threat of arsenic in groundwater. *Science (1979)*. 2020;368(6493):845-850. doi:10.1126/science.aba1510

4. Banerjee K, Amy GL, Prevost M, et al. Kinetic and thermodynamic aspects of adsorption of arsenic onto granular ferric hydroxide (GFH). *Water Res*. 2008;42(13):3371-3378. doi:10.1016/J.WATRES.2008.04.019

5. Driehaus W, Jekel M, Hildebrandt U. Granular ferric hydroxide—a new adsorbent for the removal of arsenic from natural water. *Journal of Water Supply: Research and Technology—AQUA*. 1998;47(1):30-35. doi:10.2166/aqua.1998.0005

6. Sperlich A, Werner A, Genz A, Amy G, Worch E, Jekel M. Breakthrough behavior of granular ferric hydroxide (GFH) fixed-bed adsorption filters: modeling and experimental approaches. *Water Res*. 2005;39(6):1190-1198. doi:10.1016/j.watres.2004.12.032

7. Hao L, Liu M, Wang N, Li G. A critical review on arsenic removal from water using iron-based adsorbents. *RSC Adv*. 2018;8(69):39545-39560. doi:10.1039/C8RA08512A

8. Bissen M, Frimmel FH. Arsenic - a Review. Part II: Oxidation of Arsenic and its Removal in Water Treatment. *Acta hydrochim hydrobiol*. 2003;31:97-107. doi:10.1002/aheh.200300485

9. Kim MJ, Nriagu J. Oxidation of arsenite in groundwater using ozone and oxygen. *Science of The Total Environment*. 2000;247(1):71-79. doi:10.1016/S0048-9697(99)00470-2

10. Miklos DB, Remy C, Jekel M, Linden KG, Drewes JE, Hübner U. Evaluation of advanced oxidation processes for water and wastewater treatment – A critical review. *Water Res*. 2018;139:118-131. doi:10.1016/j.watres.2018.03.042

11. Crognale S, Casentini B, Amalfitano S, Fazi S, Petruccioli M, Rossetti S. Biological As(III) oxidation in biofilters by using native groundwater microorganisms. *Science of the Total Environment*. 2019;651:93-102. doi:10.1016/j.scitotenv.2018.09.176

12. Gude JCJ, Rietveld LC, van Halem D. Biological As(III) oxidation in rapid sand filters. *Journal of Water Process Engineering*. 2018;21:107-115. doi:10.1016/J.JWPE.2017.12.003

13. Kamei-Ishikawa N, Segawa N, Yamazaki D, Ito A, Umita T. Arsenic removal from arsenic-contaminated water by biological arsenite oxidation and chemical ferrous iron oxidation using a down-flow hanging sponge reactor. *Water Supply*. 2017;17(5):1249-1259. doi:10.2166/ws.2017.025

14. Li H, Zeng XC, He Z, et al. Long-term performance of rapid oxidation of arsenite in simulated groundwater using a population of arsenite-oxidizing microorganisms in a bioreactor. *Water Res*. 2016;101:393-401. doi:10.1016/J.WATRES.2016.05.058

15. Wan J, Klein J, Simon S, et al. AsIII oxidation by Thiomonas arsenivorans in up-flow fixed-bed reactors coupled to As sequestration onto zero-valent iron-coated sand. *Water Res*. 2010;44(17):5098-5108. doi:10.1016/J.WATRES.2010.08.044

16. Mohan D, Pittman CU. Arsenic removal from water/wastewater using adsorbents—A critical review. *J Hazard Mater*. 2007;142(1-2):1-53. doi:10.1016/J.JHAZMAT.2007.01.006

17. Siddiqui SI, Chaudhry SA. Iron oxide and its modified forms as an adsorbent for arsenic removal: A comprehensive recent advancement. *Process Safety and Environmental Protection*. 2017;111:592-626. doi:10.1016/j.psep.2017.08.009

18. Weerasundara L, Ok YS, Bundschuh J. Selective removal of arsenic in water: A critical review. *Environmental Pollution*. 2021;268:115668. doi:10.1016/j.envpol.2020.115668

19. Crognale S, Amalfitano S, Casentini B, Fazi S, Petruccioli M, Rossetti S. Arsenic-related microorganisms in groundwater: a review on distribution, metabolic activities and potential use in arsenic removal processes. *Rev Environ Sci Biotechnol*. 2017;16(4):647-665. doi:10.1007/s11157-017-9448-8

20. Gupta VK, Saini VK, Jain N. Adsorption of As(III) from aqueous solutions by iron oxide-coated sand. *J Colloid Interface Sci*. 2005;288(1):55-60. doi:10.1016/j.jcis.2005.02.054

21. Hsu JC, Lin CJ, Liao CH, Chen ST. Removal of As(V) and As(III) by reclaimed iron-oxide coated sands. *J Hazard Mater*. 2008;153(1-2):817-826. doi:10.1016/j.jhazmat.2007.09.031

22. Mähler J, Persson I. Rapid adsorption of arsenic from aqueous solution by ferrihydrite-coated sand and granular ferric hydroxide. *Applied Geochemistry*. 2013;37:179-189. doi:10.1016/j.apgeochem.2013.07.025

23. Thirunavukkarasu OS, Viraraghavan T, Subramanian KS. Arsenic Removal from Drinking Water using Iron Oxide-Coated Sand. *Water, Air, and Soil Pollution 2003 142:1*. 2003;142(1):95-111. doi:10.1023/A:1022073721853

24. Petrusevski B, van der Meer W, Baker J, Kruis F, Sharma SK, Schippers JC. Innovative approach for treatment of arsenic contaminated groundwater in Central Europe. *Water Supply*. 2007;7(3):131-138. doi:10.2166/ws.2007.075

25. Driehaus W. Arsenic removal - experience with the GEH® process in Germany. *Water Supply*. 2002;2(2):275-280. doi:10.2166/ws.2002.0073

26. Petrusevski B, Sharma S, van der Meer WG, et al. Four years of development and field-testing of IHE arsenic removal family filter in rural Bangladesh. *Water Science and Technology*. 2008;58(1):53-58. doi:10.2166/wst.2008.335

27. Claff SR, Sullivan LA, Burton ED, Bush RT. A sequential extraction procedure for acid sulfate soils: Partitioning of iron. *Geoderma*. 2010;155(3-4):224-230. doi:10.1016/j.geoderma.2009.12.002

28. Fetter CW, Boving TB, Kreamer DK. *Contaminant Hydrogeology*. 1999.

29. Barcala V, Zech A, Osté L, Behrends T. Transport-limited kinetics of phosphate retention on iron-coated sand and practical implications. *J Contam Hydrol*. 2023;255:104160. doi:10.1016/J.JCONHYD.2023.104160

30. Wielinski J, Jimenez-Martinez J, Göttlicher J, et al. Spatiotemporal Mineral Phase Evolution and Arsenic Retention in Microfluidic Models of Zerovalent Iron-Based Water Treatment. *Environ Sci Technol*. 2022;56(19):13696-13708. doi:10.1021/acs.est.2c02189

31. Chan CS, Fakra SC, Emerson D, Fleming EJ, Edwards KJ. Lithotrophic iron-oxidizing bacteria produce organic stalks to control mineral growth: implications for biosignature formation. *The ISME Journal 2011 5:4*. 2010;5(4):717-727. doi:10.1038/ismej.2010.173

32. Müller S, Corbera-Rubio F, Schoonenberg Kegel F, Laureni M, van Loosdrecht MCM, van Halem D. Shifting to biology promotes highly efficient iron removal in groundwater filters. *Water Res*. 2024;262:122135. doi:10.1016/j.watres.2024.122135

33. Casentini B, Gallo M, Baldi F. Arsenate and arsenite removal from contaminated water by iron oxides nanoparticles formed inside a bacterial exopolysaccharide. *J Environ Chem Eng*. 2019;7(1):102908. doi:10.1016/j.jece.2019.102908

34. Driehaus W, Dupont F. Arsenic removal - solutions for a world wide health problem using iron based adsorbents. *European journal of water quality*. 2005;36(2):119-132. doi:10.1051/water/20053602119

35. Dixit S, Hering JG. Comparison of Arsenic(V) and Arsenic(III) Sorption onto Iron Oxide Minerals: Implications for Arsenic Mobility. *Environ Sci Technol*. 2003;37(18):4182-4189. doi:10.1021/es030309t

36. Petrusevski B, Boere J, Shahidullah SM, Sharma SK, Schippers JC. Adsorbent-based point-of-use system for arsenic removal in rural areas. *Journal of Water Supply: Research and Technology-Aqua*. 2002;51(3):135-144. doi:10.2166/aqua.2002.0011

37. Corbera-Rubio F, Laureni M, Koudijs N, et al. Meta-omics profiling of full-scale groundwater rapid sand filters explains stratification of iron, ammonium and manganese removals. *Water Res*. 2023;233. doi:10.1016/J.WATRES.2023.119805

38. Frank P, Clifford DA. *Arsenic (III) Oxidation and Removal from Drinking Water*. Vol 86. Water Engineering Research Laboratory, Office of Research and Development, US Environmental Protection Agency; 1986.

39. Wang K, Holm PE, Trettenes UB, Bandaru SRS, van Halem D, van Genuchten CM. Molecular-scale characterization of groundwater treatment sludge from around the world: Implications for potential arsenic recovery. *Water Res*. 2023;245:120561. doi:10.1016/j.watres.2023.120561

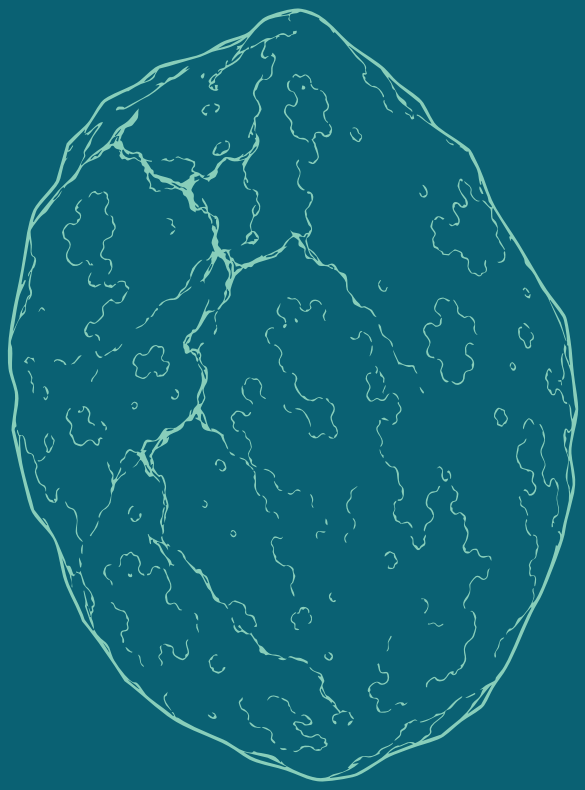

05

Biofilm Distribution on Metal-Coated Filter Sand and its Activity During Biological As(III) Oxidation Revealed by Bioorthogonal Non-Canonical Amino Acid Tagging (BONCAT)

In collaboration with:
Heidi Smith, Kristen Connolly and Al Parker (Montana State University); Merle de Kreuk and Doris van Halem (TU Delft).

Abstract

Poisonous arsenic (As) is sometimes still found in treated drinking water. In the groundwater treatment process, As gets removed by oxidation from As(III) to As(V) and subsequent adsorption to iron (hydr)oxides. Incomplete As removal is often attributed to faster iron (Fe^{2+}) versus As(III) oxidation, preventing effective uptake. Biological As(III) oxidation has the potential to increase the kinetics of oxidation compared to physicochemical oxidation; however, the factors governing the growth and activity of arsenic-oxidizing biofilms in sand filters remain insufficiently understood. This study investigated the composition and activity of drinking water biofilms on sand grains with predominantly iron oxide (FeOx), manganese oxide (MnOx) or mixed (FeMnOx) coating, prior and post As exposure. The mineral-microbe distribution over the surface and cross section of the coating was visualized using multimodal imaging, combining Confocal Laser Scanning Microscopy (CLSM) followed by Scanning Electron Microscopy with Energy Dispersive X-ray Spectroscopy (SEM-EDS). The activity and microbial composition prior- and post As exposure was assessed using bioorthogonal non-canonical amino acid tagging (BONCAT) and 16s rRNA gene sequencing, respectively. Biofilm development was found to depend more strongly on physical surface structure than coating chemistry, with rougher MnOx-coated sand supporting denser biofilms than smoother FeOx or FeMnOx-coated sand. Rapid coating growth in iron removal filters and frequent backwashing are likely limiting biofilm development. Despite effective As(III) oxidation, no major shifts in microbial community composition or overall activity were observed pre- and post- As exposure. These findings indicate that biological As(III) oxidation is an intrinsic function of drinking water biofilms, driven by a broad range of As-resilient bacteria present in the native filter biofilm.

5.1 Introduction

Groundwater provides drinking water to more than 50% of the global population [1], and is a preferred source because of its microbiological safety and stable temperature and quality. Anaerobic groundwater naturally contains iron (as Fe(II)), manganese (as Mn(II)) and ammonium (NH_4), which are removed via aeration and rapid sand filters (RSF) in treatment plants. The carcinogenic substance arsenic (in the form of As(III)) can be present in groundwater as well. For effective removal, As(III) should oxidize to the negatively charged As(V), which can adsorb to iron (hydr)oxides. Poisonous As is still often observed in treated drinking water, because of faster Fe(II) versus As(III) oxidation, preventing effective uptake. Podgorski and Berg (2020) estimated that 94 to 220 million people are exposed to As in groundwater above the World Health Organization guideline of 10 µg/L[2]. Increasing the As(III) oxidation kinetics would increase As uptake by iron (hydr)oxides.

Previous studies found that biological As(III) oxidation can increase the kinetics up to 14-fold compared to surface catalytic oxidation [3,4]. Bacteria oxidize As(III) as detoxification mechanism (heterotrophs) or for their energetic metabolism (chemolithoautotrophs) [5], carried out by the enzyme arsenite oxidase[6]. Genes encoding for the large and small subunit of arsenite oxidase were named *aioA* and *aioB*, respectively [7]. Arsenic oxidizing bacteria (AsOB) have been found in various environments, such as hot springs, mine sites, aquifers and biofilters [8,9].

Promoting biological As(III) oxidation in sand filters aligns with the changing perspective in the drinking water industry of switching from physicochemical towards biological removal processes [10]. The central role of biofilms growing on filter sand is gaining recognition - not only for As, but also for Fe and Mn: shifting to biological Fe removal yielded four times more water per run before backwashing [11] and biological Mn oxidation can reduce filter start up times by a third [12].

Microbes colonize more efficiently in the filter bed when the sand grains harbour a porous mineral coating [13]. Mineral coatings develop over time, by continuous oxidation and precipitation of Fe and Mn on the grains. In regular, aerated sand filters, removal of Fe always happens first in RSFs, followed by removal of Mn. In a treatment plant with a single RSF, grains harbour a coating of alternating layers of Fe and Mn caused by vertical grain movement during backwashing [14]. Another common treatment scheme is two RSFs in series; Fe removal takes place in the first filter and Mn removal in the second, forming more uniform coatings. The effect of different mineral coatings on biofilm distribution and activity and their morphology to harbour micro-organisms, remains unknown.

Our study aims to assess the composition and activity of drinking water biofilms on different mineral coatings before and after exposure to arsenic. Understanding and optimizing the growth of AsOB in drinking water biofilms has the potential to increase arsenic removal efficiencies while keeping regular, robust and low-cost sand filters and avoiding the need of chemicals or complex technical solutions. Three different sand types are used, harbouring a Fe-, Mn- or mixed mineral coating. The mineral-microbe distribution over the surface and

cross section of the coating is examined, by analysing the exact same grains with Confocal Laser Scanning Microscopy (CLSM) to visualize the biofilm, followed by Scanning Electron Microscopy (SEM) with Energy Dispersive X-ray Spectroscopy (EDS) to map the minerals. Subsequently, an As oxidizing biofilm is grown on the three different mineral coated grains in a column experiment. The activity of the microbial community on the grains pre and post exposure is determined using bioorthogonal non-canonical amino acid tagging (BONCAT), a next-generation physiology approach [15] that uses substrate analogue probing to visualize protein synthesis in active cells. The composition was assessed with 16s sequencing.

5.2 Methods

5.2.1 Metal coated sand from rapid sand filters

Three different sand types were collected from rapid sand filter beds at two separate treatment sites for use in this study. At the first location (Laren, the Netherlands), groundwater was treated by aeration and a single filter that removed both Fe and Mn. The silica sand harvested from this filter harbours a mixed metal coating of Fe- and Mn-oxides. At the second location (Mol, Belgium), groundwater was treated using two aeration-filtration set-ups in series. In the first filter, Fe was removed and partly precipitated as Fe-oxides onto the coating. In the second filter, Mn was removed, resulting in a Mn-oxide coating. These three sand types are hereafter referred to as FeMnOx, FeOx and MnOx, respectively. Images of the different sand types are shown in Figure 1.

5.2.2 Column study to expose biofilm to As

To assess the impact of As on drinking water biofilms, a laboratory column experiment was performed (Figure 1). Columns were constructed of disposable 60 mL syringes (BD Plastipak), with triplicate columns run for each sand type (FeMnOx, FeOx, MnOx). Prior to placing into columns, the sand was gently washed with tap water until the rinsing water ran clear. The empty bed volume of the columns was 55 cm^3 with a supernatant level of 5 cm^3. Columns were operated in up flow mode (pump flow 1.2 ml/min), with influent tubing connected at the bottom of the column and effluent outflow at the top of the column via tubing inserted through a rubber stopper. Each sand type had a porosity of approximately 0.45, resulting in a total flow rate of 0.24 m/h. The columns were wrapped in aluminium foil to avoid impacts from lights.

Columns were fed with an As solution (~500 µg/L), derived from a 0.05 M sodium As(III) solution (Merck) in unchlorinated tap water (composition in Table 1 in supplementary info). To compensate for partial oxidation of As (~30%), the stock solution was replenished twice a week. Controls were run in triplicate and consisted of FeMnOx sand, operated with only tap water as the influent.

From now on, sand directly harvested from the treatment plants is referred to as pre-experiment, while sand exposed to As-spiked tap water is referred to as post-experiment. In

total, seven conditions were studied: FeMnOx, FeOx and MnOx pre and post experiments, and the control.

Samples of the influent and effluent of the columns were taken weekly to determine As(III) and As(V) concentrations. Speciation of As was done in the same way as described in Goedhart et al. (2025) [3]. Concentrations of As(tot) and As(III) were measured using inductively coupled plasma mass spectrometry (ICP-MS, Analytikal Jena PlasmaQuant MS).

Following 45 days of continuous operation, sand from the columns were sampled. The bottom 50% of sand was collected for subsequent analysis, which included immediate freezing at -20°C or preparation for BONCAT incubations.

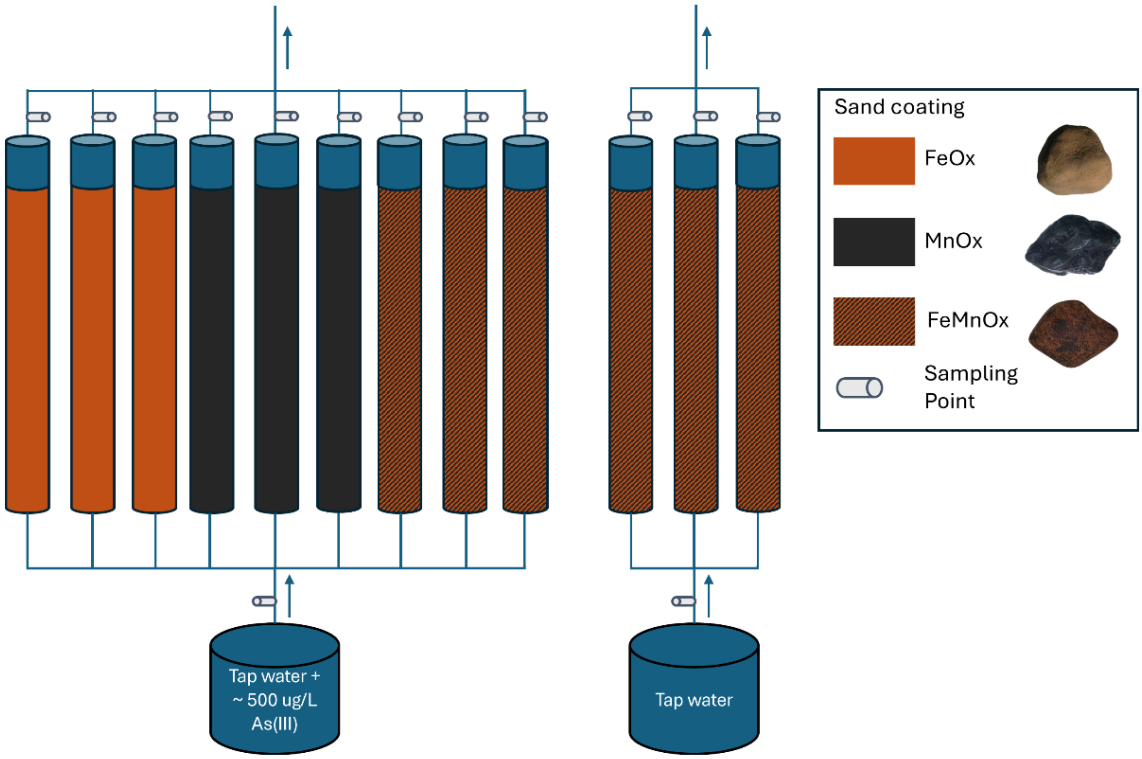

Figure 1: Schematic overview of the column experiment. Columns were 60 cm³ in total with 5 cm³ of supernatant water.. Triplicate columns filled with iron coated sand (FeOx), manganese coated sand (MnOx) and mixed coated sand (FeMnOx) were fed As-spiked tap water. A parallel control experiment consisted of triplicate FeMnOx columns receiving only tap water. Photographs of a single coated sand grain are included in the legend.

5.2.3 Sample incubation

Samples were incubated with the alkyne containing synthetic amino acid L-Homopropargylglycine (HPG), which enables subsequent azide-alkyne click-staining allowing fluorescent detection of newly synthesized proteins [16]. In duplicates, 30 grams of the seven sand types (FeMnOx, FeOx, MnOx (pre/post) and control) were transferred to individual sterile 100 mL glass bottles, containing either 50 mL of 500 µg/L As(III) in tap water (post experiments samples) or only tap water (pre-experiments and control samples). To one of the duplicate bottles, 50 µM of HPG (Vector Laboratories Click Chemistry Tools 1067) was

added. The other bottle served as control. Samples were incubated with HPG for 6, 12, 24, 48 and 72 hours. One hour before each respective sampling time, samples were spiked with 10 mL of 2500 µg/L As(III) to ensure sufficient substrate availability for microbial activity. Five grams of sand were collected at each incubation time and immediately fixed with 3% paraformaldehyde for 2 hours at room temperature, followed by three washes with 1x PBS. Post fixation samples were stored at -20°C in a 50% ethanol:PBS solution until further analysis. At the final sampling round, an additional 5 grams of sand was sampled and stored directly at -20°C for subsequent DNA extraction, to study the effect of HPG incubation on the microbial community.

5.2.4 Sample processing

Of each sand type, a few grains were embedded in epoxy. By slicing the epoxy-embedded grains, the mineral and biofilm distribution over the cross-section of the grains could be studied without breaking the grain. We used Buehler EpoxiCure® 2, hardened for 48 hours and sliced using a low speed saw (11-1180 Buehler) with a Medium Grit Smart Cut™ Diamond Blade and polished with CarbiMet PSA 600 [P1200], followed by MicroCut PSA 1200 [P2500].

BONCAT was only performed on the outer surface of the grains, since HPG does not penetrate the inner coating. To attach the azide-containing fluorophore to the alkyne group of HPG-labelled proteins, click staining is required. Prior to click staining, fixed samples were thawed and dehydrated by sequentially submerging samples for 3 min in a 50%, 80%, and 96% ethanol series followed by a 10 min drying step. A bulk click reaction solution was made following Hatzenpichler and Orphan (2015) [17]. Briefly, the solution consisted of 5mM amino guanidine hydrochloride (Sigma Aldrich), 5mM sodium L-ascorbate (Sigma Aldrich), 100 µM copper sulfate pentahydrate (Sigma Aldrich), 500µM THPTA (Click Chemistry Tools), and 6µM Cy5 picolyl-azide dye (Click Chemistry Tools) in 1× PBS. The grains were submerged in click solution and incubated for 45 minutes in the dark, followed by three washes with 1x PBS. Following click staining, all cells were stained with 100x SYBR® Green for ten minutes, after which samples were washed three times with 1X PBS. To ensure maximum fluorescent signals, click and SYBR® Green staining was done on the same day as the microscopic analyses. Experimental controls, i.e., sand grains not incubated with HPG, underwent the same click and SYBR® Green staining.

Given limitations with achieving a fluorescent click signal for Mn-coated sand grains, cells were detached form the surface of the sand particles prior to click staining. Briefly, detachment consisted of the sonication of 1.5 grams of sand grains in 1 mL of 1X PBS for 1 min (Qsonica LLC XL-2000 probe, power 20, continuously, ± 0.08 W). Post sonication samples were centrifuged at 500 x g for 5 min, and the cell containing supernatant was transferred to a clean Eppendorf and centrifuged again to precipitate any remaining minerals. Detached cells underwent the same click staining described above. To compare the results between staining planktonic cells and staining the whole biofilm, cells from FeMnOx were also detached and stained.

5.2.5 DNA Extractions and sequencing

To study the microbial composition of the drinking water biofilms pre and post experiments, DNA was extracted from the sand grains. DNA was also extracted from grains incubated with HPG to compare with non-incubated controls. Because standard extraction kits do not yield sufficient DNA from metal-coated sand, ammonium oxalate was used to dissolve the coatings prior to extraction [11]. The DNA extraction and sequencing procedures followed the method described in Goedhart et al. (2025) [3].

5.2.6. Fluorescence microscopy

Fluorescence imaging of fully hydrated sand grains was performed using an Upright Leica DM6 Stellaris 8 Confocal Scanning Laser Microscope (CLSM) equipped with an ELWD 25x water immersion objective (0.95 NA, WD 2.5mm). For each grain, 3D fluorescent images were acquired for three channels. Fluorophore excitation lasers and emissions bandwidths are as follow: SYBR® Green (ex 502/em 568) 492 nm excitation, Cy5 (ex 651/em 710) 641 nm; and reflection imaging 488 nm excitation. LAS X Stellaris Version 4.8.1 was used for imaging. Pixel frames of 1024 x 1024 or 2048 x 2048 were acquired, with two line-based scans averaged per image. Z-stacks were collected using a 0.8 µm step size in the Z-dimension, and a pixel size of 0.22 µm in both X and Y dimensions. Gain and intensity settings were manually adjusted to avoid saturation and minimize background and non-specific signals. To enable direct comparisons, image collection settings were kept constant for all grains within the same sample group. Between seven and eleven grains were imaged per sample group, with images collected for two different control conditions per sample type (*i.*) grains not incubated with HPG but subjected to the click reaction and SYBR staining, and (*ii.*) unstained grains.

Fluorescence imaging of cross section of the sand grains was performed using a DMI8 Inverted CSLM equipped with a HC PL APO CS2 63x oil immersion objective (1.4 NA, WD 0.14 mm). SYBR® Green excitation laser was 502 nm and emissions bandwidth 569 nm; and reflection imaging had a 488 nm excitation. Tilescan was used to image over the whole thickness of the coating, with a scan speed of 700 Hz and a LineAverage of 1. Z-stacks were collected using a 0.5 µm step size in the Z-dimension, and a pixel size of 0.07 µm in both X and Y dimensions. Gain and intensity settings were manually adjusted to avoid saturation and minimize background and non-specific signals.

5.2.7 Image processing and BONCAT active cells calculation

Fluorescence microscopy images were processed in IMARIS V10.2.0 (Zurich, Switzerland). Total and active biovolume were quantified by surface creation with absolute intensity thresholding on the SYBR® Green and Cy5 (BONCAT) channels, respectively. Images were smoothed with surface area detail level of 1.15 µm, and thresholds were manually adjusted to ensure accurate correspondence between the generated surfaces and the imaged cells. Percentage of active cells was calculated as: $\frac{active\ biovolume}{total\ biovolume} * 100\%$.

Cell coverage of the surface was quantified using object-to-object statistics. The reflective channel was used to generate the sand-grain surface volume, with a smoothing surface area detail level of 0.7 µm. The ratio of SYBR® Green volume versus total surface volume gave the percentage of overlap between cells and surface, used as a measure for cell coverage.

Differences in BONCAT activity among sample types were evaluated using linear mixed-effects models in R (R core Team, 2025), implemented with the package lme4 [18]. The model included condition (sand type and treatment) as a fixed effect and random intercepts for collection date at the treatment plants and imaging date at the microscope. Pairwise comparisons of estimated marginal means were performed with a family-wise confidence level of 95% using the single-step correction method in the R package multcomp [19].

5.2.8 Scanning electron microscopy

To study the spatial distribution of the biofilm compared to the metals on the sand grains, Field Emission Scanning Electron Microscope (FE-SEM) equipped with Energy Dispersion X-Ray Spectroscopy (EDS) was used (ZEISS SUPRA 66VP). Samples were coated with iridium before analyses. To analyze the biofilm and metal distribution over the surface of the grains, SEM stubs with carbon tape were used as a carrier. For both the whole grains and embedded grains, first CLSM images were made, after which the exact same grains were analyzed using SEM-EDS.

5.3 Results & Discussion

5.3.1 Biofilm distribution over metal coated sand grains

Figure 2 shows the biofilm distribution and mineral composition of the different sand types, both over the surface and the cross sections of the grains. FeOx has a homogeneous coating of iron oxides (Figure 2.iB), containing 30.7% Fe (±5.0%, n=4), 37.4% O (±7.2%), and 16.0% C (±4.7%). Bacteria grew scattered over the grain, covering 1.51% (±0.73%, n =18) of the surface (Figure 2.iC). Over the cross section of the grain, biofilm formed distinct rings (Figure 2.iE) and SEM-EDS detected less Fe within these rings (Figure 2.iD). Stratified Fe and NH_4 removal in the filter bed likely creates these rings. Grains vertically move in the bed because of backwashing; if the grain is located at the top of the filter bed, Fe removal takes place, while at the bottom (biological) NH_4 oxidation occurs, forming a dense biofilm. Additionally, at the top of the filter bed the biofilm might get continuously disturbed by the formation of Fe-flocs[20], preventing an established biofilm to form.

MnOx has a much thinner coating (Figure 2.iiD), with an Mn-content of 11.7% (±7.7%, n=4), 32.3% O (±6.6%) and 54.5% C (±1.1%). Biofilm formed in patches and covered 10.9% (±0.92%, n=9) of the surface (Figure 2.IIC). Areas of bare silica, where Mn oxides had not precipitated, did not host any biofilm (Figure 2.IIC&D. MnOx's surface appears visually less smooth compared to FeOx and the biofilm preferentially grows in the cavities of the grain, as also observed in the cross section (Figure 2.iiE).

FeMnOx outer coating is dominated by 28.1% Fe (±3.9%), compared to 7.3% Mn (±5.3%) and also contains 43.8% O (±3.9%), and 18.3 C (±1.3%, n = 29) (Figure 2.iiiB). The grains were harvested from the top of a filter bed, where Fe removal occurs. Backwashing moves grains through the bed, causing the alternating Fe and Mn rings (Figure 2.iiiD), consistent with observations by Haukelidsaeter et al. (2024) [14]. Over the surface of the grain, biofilm grows in a scattered pattern similar to FeOx, covering 3.6% (±0.65%, n = 7) of the surface (Figure 2.iiiC). Over the cross section of the grain, the biofilm also appeared scattered (Figure 2.iiiE). Unlike the metal distribution, no rings of biofilm were observed.

Our results show that drinking water biofilms grow on both Fe- and Mn-coated filter sand; the FeMnOx coating does not show a preference of the bacteria for either one of the metals. The coating's structure likely drives biofilm development: most cells grew in pores and biofilms formed inside cavities of the grain. The particularly dense biofilm on MnOx illustrates this effect well, as MnOx exhibits a more uneven surface than FeOx and FeMnOx.

Several factors may explain why biofilms grow more densely on MnOx. First, Fe-coatings build up faster because of higher Fe concentrations in the influent compared to Mn. The continuous precipitation of Fe reduces the chance for biofilms to establish. Second, Fe-removal filters are subjected to more intense backwashing than Mn-removal filters, which can wash away part of the biofilm [11,21]. Finally, the combination of fast FeOx growth and vigorous backwashing rounds Fe-coated grains, whereas Mn-coated grains retain cavities. As shown in Figure 2, FeOx and FeMnOx grains have smooth, almost marble-like surfaces, while MnOx grains contain more cavities. Rougher surfaces promote biofilm growth [22]

Kruisdijk et al. (2024) and Goedhart et al. (2025) demonstrated that biofilters with FeOx and MnOx oxidize As(III) at different rates [3,4]. MnOx showed a 1.6 times faster oxidation kinetics than FeOx (4.8 and 2.9 min^{-1} at ~20,000 pore volumes respectively). Our results indicate that MnOx supports a denser biofilm, which may explain the kinetic advantage.

Biological oxidation processes are increasingly applied in groundwater treatment, and sand is currently the most common filter material. However, our findings raise the question whether sand is the most efficient material for biofilters. No biofilm growth was found on bare silica (Figure 2.iiB), biofilms seem to only attach once a metal coating develops. Another disadvantage of silica is the smooth structure. Alternative starting materials, particularly with a porous structure, may enhance bioremediation efficiency. We therefore recommend investigating more porous media in future studies.

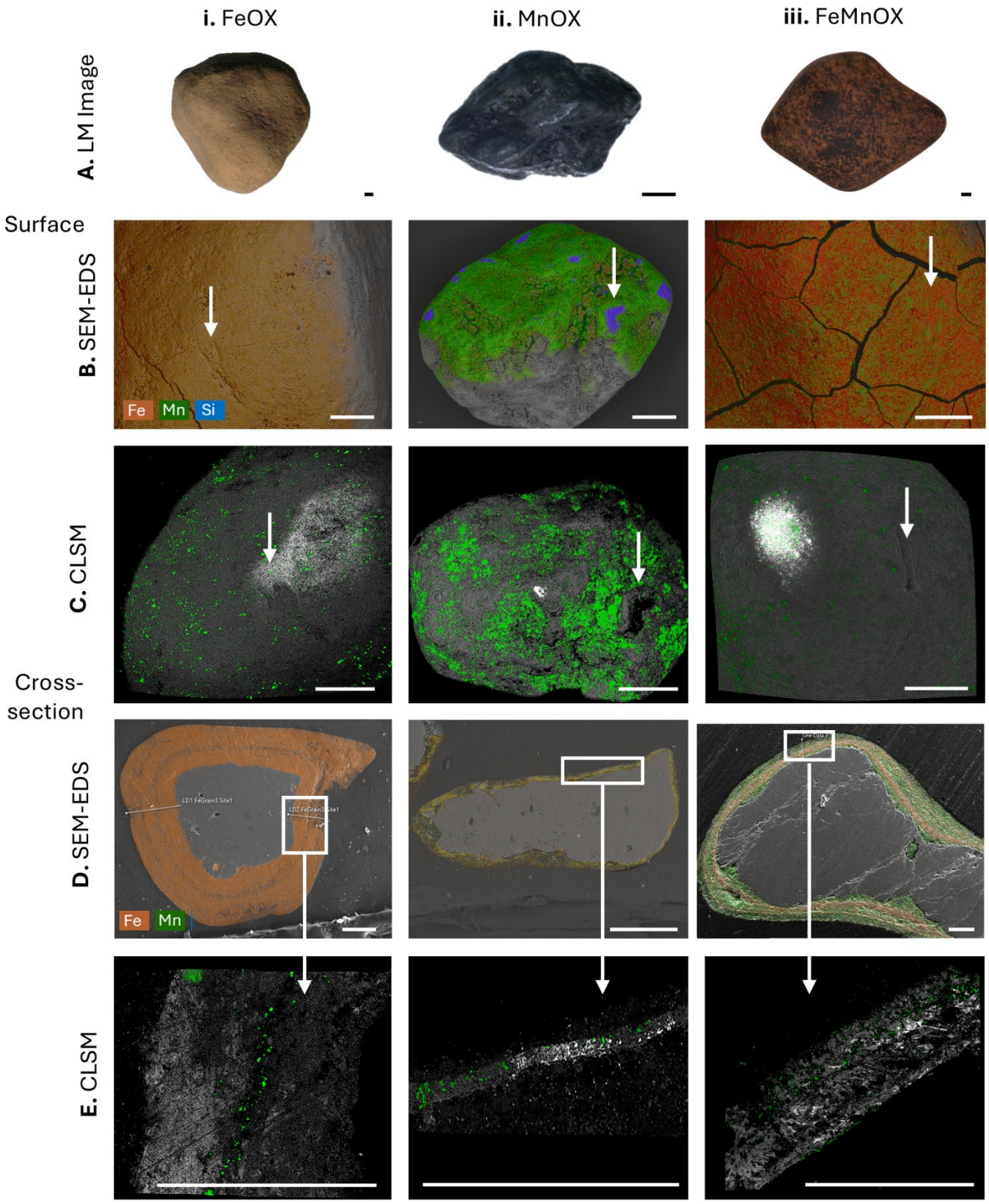

Figure 2: Mineral and microbe distribution on sand grains coated with i) FeOx, ii) MnOx, or mixed iii) FeMnOx. From top to bottom: A. Light microscopy (LM) image, B. SEM-EDS images and C. confocal laser scanning microscope (CLSM) images of the surface. D. SEM-EDS images and E. CLSM images over the cross section of the grains. The white arrows point to the same areas in the SEM-EDS and CLSM images. Scale bars in each picture represents 250 µm. In SEM-EDS Orange=Fe, Green=Mn, Blue=Si. In CLSM, green is total biofilm stained with SYBR® Green.

5.3.2 Biological arsenite oxidizing system

FeOx, MnOx and FeMnOx were exposed to As-spiked tap water to assess the effect on the drinking water biofilm activity and composition. Table 1 shows As(tot) and As(III) concentrations in the column effluent after 45 days. At least 97% of the effluent As was present as As(V). For MnOx and FeMnOx this confirms that As(III) oxidation occurs. For FeOx, the high As removal due to adsorption (97%) caused effluent levels to be too low to confirm As(III) oxidation in the column. However, Kruisdijk et al. (2024) showed that by using the same FeOx sand a biological As(III) oxidative system was obtained in a similar time span [4]. Additionally, FeOx was found to have a stronger binding preference for As(V), implying that As indeed got oxidized in our system.

Table 1¿Total arsenic (As(tot)) and As(III) concentration in the effluent on the last day of operation of the columns, and the total oxidation of As(III) and adsorption of As(tot) at that point.

Grain type	Exp condition	As(tot) Effluent	As(III) Effluent	Oxidation	Adsorption
FeMnOx	Post	394 ± 22.8	4.3 ± 1.8	99%	30%
FeOx	Post	19.0 ± 8.4	0.3 ± 0.27	97%	97%
MnOx	Post	449.2 ±7.5	3.2 ± 0.12	99%	25%
FeMnOx	Control	1.19 ± 0.40	x	x	x

5.3.3 Activity of biofilm under As rich conditions determined with BONCAT

The activity of the sand grains biofilm pre and post As exposure was tested using BONCAT, which enables fluorescent labelling of active proteins. This study is the first to use BONCAT on groundwater filter sand and we found that the method worked well when the outer coating consisted of mainly Fe (FeOx and FeMnOx), but failed when the outer coating consisted of mainly Mn (MnOx). The results of FeOx and FeMnOx are discussed first, followed by MnOx. Samples incubated with HPG for 24 hours were used for the analyses; it was found that an incubation of 12, 24 and 48 hours gave similar results, while 6 hours showed less activity and 72 hours incubation more activity.

Figure 3 shows the total and active biofilm on FeMnOx and FeOx pre and post experiments, as well as the control. Activity was detected on all samples. Cells were dispersed across the sand surface, and active cells showed a similar pattern, with no observable clustering or localized areas of increased or decreased activity.

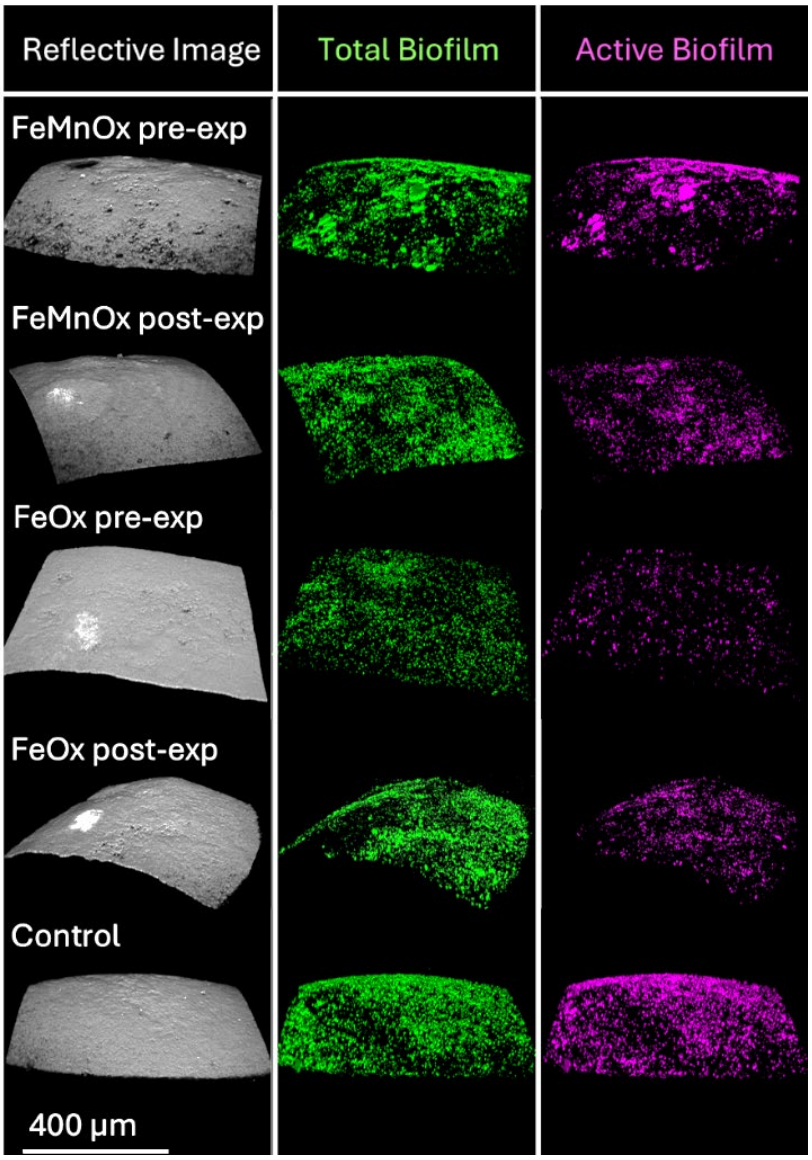

Figure 3: Confocal laser scanning microscopy images of Mixed coated sand grains for growth conditions Fresh, Tapwater and Arsenic. Left column; reflective images of the sand grain surface. Middle column: total biofilm stained with SYBR® Green. Right Column: active biofilm stained with Cy5 using BONCAT.

Table 2 reports the mean percentages of active cells for the five conditions, which ranged from 31.76% to 39.28%. No statistically significant differences were observed among conditions (p=0.343). Thus, biofilm activity did not differ between sand coatings (FeOx, FeMnOx) and was not affected by exposure to As-spiked tap water or tap water alone.

The linear mixed effect model indicated that most variation arose from actual differences of activity between individual grains, and only 4% of variability was attributed to collection date and none to imaging date. Experimental controls, grains not incubated with HPG but click stained, showed a maximum stained biovolume of 2% relative to SYBR® Green, indicating that unspecific clicking was limited.

Table 2: The percentage of active cells (mean activity), and the corresponding standard deviation (SD) and 95% Confidence Interval (CI), of sand types FeOx and FeMnOx pre- and post- experiments and the control. Activity = Biovolume BONCAT/Biovolume SYBR x 100%. The linear mixed effect model showed no significant difference between groups, p value = 0.343.

Grain type	Exp condition	Sample size	Mean Activity (%)	SD (%)	95% CI (%)
FeOx	Pre-exp	11	39.28	8.31	[28.17, 50.39]
FeOx	Post-exp	7	33.68	7.50	[24.22, 43.14]
FeMnOx	Pre-exp	7	38.36	8.49	[27.25, 49.47]
FeMnOx	Post-exp	12	31.76	7.10	[22.56, 40.95]
FeMnOx	Control	12	39.19	14.78	[30.00, 48.39]

MnOx grains were analyzed using detached cells instead of whole grains, because the non-HPG-incubated experimental controls produced a fluorescent click signal comparable to the HPG-incubated grains. Unstained MnOx grains showed no fluorescence; the background signal likely arose from interactions between the click reagents and the Mn coating, rather than the coating itself. FeMnOx samples were processed in the same way, to enable comparison between whole grain and detached cell analysis. No fluorescent click signal was found in the detached cells of the non-HPG-incubated samples.

Table 3 presents the mean percentages of active cells detached from the MnOx and FeMnOx grains. For MnOx, the mean activity pre and post experiments was 53.79% and 47.21%, respectively. Detached FeMnOx cells showed a mean activity of 42.84% post experiment. In comparison, whole grain FeMnOx samples showed 31.76% active cells post experiment (Table 1). No significant differences were observed among MnOx (pre/post) and FeMnOx (post) detached cell samples (p=0.335). However, activity in detached FeMnOx cells was significantly higher than in FeMnOx whole grain samples (p=0.0055). As a result, detached cells and whole grain data cannot be directly compared.

Table 3: The percentage of active cells (mean activity), and the corresponding standard deviation (SD) and 95% Confidence Interval (CI), from planktonic cells sonicated from sand types MnOx pre- and post- experiments and FeMnOx post experiments and the control. Activity = Biovolume BONCAT/Biovolume SYBR x 100%. The linear mixed effect model showed no significant difference between groups, p value = 0.335.

Grain type	Exp condition	Sample size	Mean Activity (%)	SD (%)	CI (%)
MnOx	Pre-exp	10	53.79	18.24	[40.96, 66.62]
MnOx	Post-exp	9	47.21	18.25	[29.31, 56.37]
FeMnOx	Post-exp	9	42.84	9.16	[33.68, 60.75]

5.3.4 Sequence results

Figure 3 presents the relative abundance of the 15 most abundant families across all samples. The communities were dominated by *Sphingomonadaceae, Methylomonadaceae, Nitrospiraceae* and *Hyphomicrobiaceae.* Differences in community composition among the different sand types FeMnOx-, FeOx-, MnOx-Pre reflect the function of the different filter beds. *Methylomonadaceae* was most abundant on FeMnOx and FeOx compared to MnOx, since aerobic methane oxidation takes place in the first filter bed alongside Fe removal. In contrast, *Nitrospiraceae* were more abundant on MnOx, since ammonium oxidation occurs alongside Mn removal in the second filter. The largest difference observed was *Gallionellaceae* on FeOx Pre. This family includes known Fe-oxidizing bacteria and are therefore expected in Fe removing sand filters (FeMnOx and FeOx). At the FeOx treatment location, oxygen and pH are kept low to promote biological Fe removal (alike Müller et al. (2024); Van Beek et al. (2016))[11,23]), which explains the higher abundance of the micro-aerophilic *Gallionellaceae* compared to the one step FeMnOx filter, where full aeration was applied prior to the filter.

Comparing sand pre and post arsenic exposure, and with the tap water control, shifts were associated with tap water addition rather than As addition. Only four genera increased more than two-fold in FeMnOx-post (fed with As-spiked tap water) compared to FeMnOx-control (fed with only tap water): *Acinetobacter* (3.2% f;*Moraxellaceae) Sphingobium* (3.5%), *Sphingopyxis* (2.4%, f; *sphingomonadaceae*) *and Polaromonas* (1.3%, f; *Comamonadaceae*). These genera were also enriched in As-fed samples FeOx-post (2.8, 2.8, 0.8, 2.4% respectively) and MnOx-post (2.9, 0.8 , 3.6 , 4.8% respectively), while their pre-experiment abundances were at least an order of magnitude lower. These four elevated genera are likely to be involved in arsenic cycling in the columns. Members of *Comamonadaceae*, particularly *Polaromonas,* include known As(III) oxidizing bacteria [24–26]. Both *Polaromonas sp. GM1* and *Acinetobacter* carry the arsenite oxidizing gene aioA [25,27,28] and have been found in As(III) rich environments [26,29–31]. In contrast, *Sphingobium* and *Sphingopyxis* are associated with arsenate reduction via arsC [30]. The biofilm in the column experiments was exposed to both As(III) and As(V), due to oxidation happening in the stock solution and in the column itself. The growth of these As(V) reducers suggests active As cycling in the columns. However, >97% of the effluent As was in the form of As(V), indicating that the system had a higher oxidation than reduction capacity.

While As cycling has been studied extensively in subsurface environments [31–36], it has not been examined in rapid sand filters. Assessing the As-concentrations and microbial community over the height of the filter bed and over time is recommended to better resolve As(III)/As(V) dynamics and associated microbial processes.

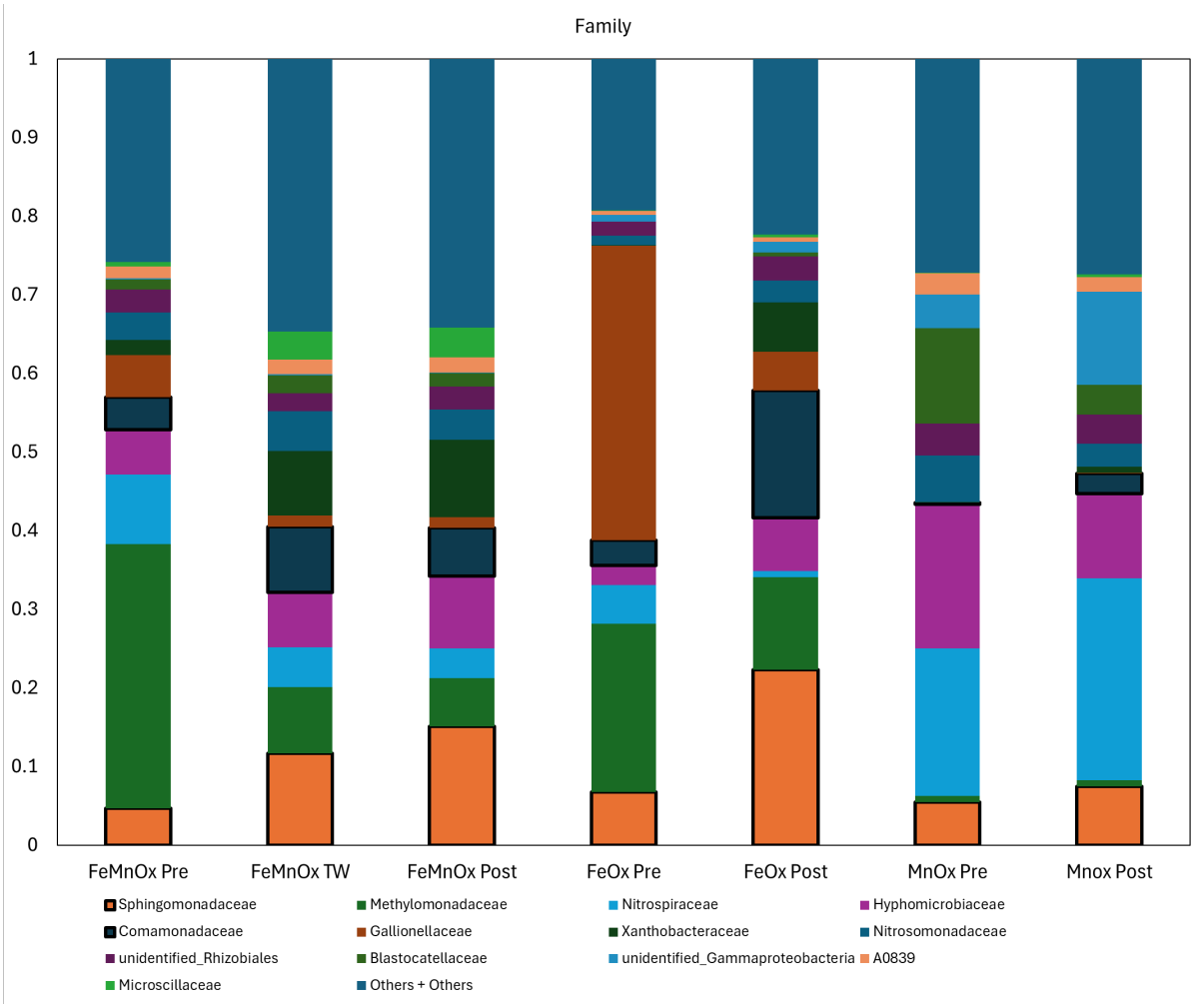

Figure 3: Distribution histogram of top 15 relative abundance of taxonomic rank family of the microbial community on FeMnOx, FeOx and MnOx sand pre- and post-experiment. The control fed with solely tap water is given as well (TW). The families containing known arsenic oxidizers, Sphingomonadaceae and Comamonadaceae, are framed.

5.3.5 Drinking water biofilm not altered by arsenic

Our results indicate that the drinking water biofilm was resilient to As exposure. Neither the microbial community composition nor the proportion of active cells differed significantly after 45 days of exposure to 500 µg/L As. The relative abundances of known As-oxidizing genera remained low (<5%), which aligns with previous findings where efficient biological As(III) oxidation was observed despite limited representation of known AsOB [3]. These observations suggest that additional but yet unrecognized community members may contribute to As(III) oxidation in drinking water biofilms. Future metagenomic and qPCR analyses targeting As transformation genes (e.g., aioA, arsC) could clarify which bacteria mediate As(III) oxidation and whether simultaneous As(V) reduction occurs.

The stable proportion of active cells determined by BONCAT pre and post experiments, demonstrates that the biofilm remained metabolically active throughout As exposure. Although 500 µg/L As exceeds concentrations considered safe for human consumption [37],

biofilm activity was unaffected, showing the robustness of drinking water filter communities under high As concentrations.

The unchanged community composition and activity support the feasibility of applying biological As(III) oxidation in rapid sand filters. AsOB can substantially accelerate overall As removal kinetics [3,4] without disrupting the biofilm composition, which suggests that it won't alter other biological processes. Nevertheless, the effect of biological As(III) oxidation on Fe, Mn, or NH_4 removal needs further investigation.

Our findings additionally highlight the role of filter media properties in shaping biofilms. Mn-coated sand carried a denser biofilm compared to the smoother Fe-coated grains, consistent with earlier findings showing that more porous surfaces enhance microbial colonization [13]. For optimal biofilters, smooth silica sand might not be the most efficient material.

Overall, this study fits the changing perspective of rapid sand filters as biologically driven systems rather than physicochemical. Understanding how microbial communities respond to contaminants such as arsenic will be essential for integrating biological As removal into drinking water treatment.

5.4 Conclusion

The potential of arsenic oxidizing bacteria to treat contaminated groundwater is getting more acknowledged nowadays, but the effect of As on the drinking water biofilm and how these biofilms grow related to the minerals present on the sand grains were unknown. This study aimed to assess the composition and activity of a drinking water biofilm before and after exposure to high concentrations of As (500 µg/L), using bioortogonal noncanonical amino acid tagging (BONCAT). Biofilms growing on Fe-, Mn- and Mixed-coated filter sand have been investigated, and the spatial distribution of the minerals and biofilm were visualized combining scanning electron microscopy and confocal laser scanning microscopy.

No major shifts were found in the community composition by exposing the biofilm to As. Additionally, no difference in metabolic activity was found when biofilm treated high As containing water. Although known arsenic oxidizing bacteria were detected, their relative abundance stayed low (<5%), suggesting that biological As(III) oxidation might be driven by a broader range of community members than currently known. Arsenic reducing bacteria were also found, suggesting that As(III)/(V) cycling might occur in the system. However, the system has a stronger oxidizing power and only As(V) is detected in the effluent.

The mineral-microbe distribution revealed that biofilm growth was independent of the metal content of the coating. Instead, physical surface structure seemed to play a more important role. Mn-coated sand, found to have a rougher, more irregular surface, colonized a denser biofilm compared to the smoother Fe- and mixed-coated sands. The faster growth of Fe-coatings and the vigorous backwashing necessary, makes it more difficult for bacteria to colonize.

This is the first application of BONCAT to drinking water biofilms. The combined imaging approach provides a more complete understanding of biofilm growth on different mineral coatings and their resilience under elevated As conditions. Our study highlights the potential of arsenic oxidizing bacteria to produce safe drinking water and calls for action to further optimize bioremediation by studying the effect of rougher, porous filter material as an alternative for smooth sand grains.

References

1. Connor R. *The United Nations World Water Development Report 2015: Water for a Sustainable World*. Vol 1. UNESCO publishing; 2015. Accessed November 21, 2025. https://books.google.nl/books?hl=nl&lr=&id=zQV1CQAAQBAJ&oi=fnd&pg=PR1&ots=9k0Kgb7nLj&sig=o7w29Nm5h80fcIMuElUG2I4h-a0&redir_esc=y#v=onepage&q&f=false

2. Podgorski J, Berg M. Global threat of arsenic in groundwater. *Science (1979)*. 2020;368(6493):845-850. doi:10.1126/science.aba1510

3. Goedhart R, Kruisdijk E, van Halem D. Biofilm Accelerates As(III) Oxidation on Reactive MnOx Coated Filter Sand in Groundwater Filters. *ACS ES&T Water*. 2025;5(12):7536-7547. doi:10.1021/ACSESTWATER.5C01031

4. Kruisdijk E, Goedhart R, van Halem D. Biological arsenite oxidation on iron-based adsorbents in groundwater filters. *Water Res*. 2024;262:122128. doi:10.1016/J.WATRES.2024.122128

5. Crognale S, Amalfitano S, Casentini B, Fazi S, Petruccioli M, Rossetti S. Arsenic-related microorganisms in groundwater: a review on distribution, metabolic activities and potential use in arsenic removal processes. *Rev Environ Sci Biotechnol*. 2017;16(4):647-665. doi:10.1007/s11157-017-9448-8

6. Anderson GL, Williams J, Hille R. The Purification and Characterization of Arsenite Oxidase from Alcaligenes faecalis , a Molybdenum-containing Hydroxylase *. 1992;267(33):23674-23682. doi:10.1016/S0021-9258(18)35891-5

7. Lett M claire, Muller D, Silver S, Santini J. Unified Nomenclature for Genes Involved in Prokaryotic Aerobic. 2012;(6). doi:10.1128/JB.06391-11

8. Cavalca L, Corsini A, Zaccheo P, Andreoni V, Muyzer G. Microbial transformations of arsenic: Perspectives for biological removal of arsenic from water. *Future Microbiol*. 2013;8(6):753-768. doi:10.2217/fmb.13.38

9. Crognale S, Casentini B, Amalfitano S, Fazi S, Petruccioli M, Rossetti S. Biological As(III) oxidation in biofilters by using native groundwater microorganisms. *Science of the Total Environment*. 2019;651:93-102. doi:10.1016/j.scitotenv.2018.09.176

10. Corbera-Rubio F, Goedhart R, Laureni M, van Loosdrecht MC, van Halem D. A biotechnological perspective on sand filtration for drinking water production. *Curr Opin Biotechnol*. 2024;90:103221. doi:10.1016/J.COPBIO.2024.103221

11. Müller S, Corbera-Rubio F, Schoonenberg Kegel F, Laureni M, van Loosdrecht MCM, van Halem D. Shifting to biology promotes highly efficient iron removal in groundwater filters. *Water Res*. 2024;262:122135. doi:10.1016/j.watres.2024.122135

12. Yang H, Bai L, Yu H, et al. Acceleration of sand filtration start-up for manganese-containing groundwater treatment: microbial-mediated autocatalytic oxidation of manganese oxides. *Environ Sci (Camb)*. 2023;9(10):2631-2642. doi:10.1039/d3ew00210a

13. Gülay A, Tatari K, Musovic S, Mateiu R V., Albrechtsen HJ, Smets BF. Internal Porosity of Mineral Coating Supports Microbial Activity in Rapid Sand Filters for Groundwater Treatment. *Appl Environ Microbiol*. 2014;80(22):7010. doi:10.1128/AEM.01959-14

14. Haukelidsaeter S, Boersma AS, Piso L, et al. Efficient chemical and microbial removal of iron and manganese in a rapid sand filter and impact of regular backwash. *Applied Geochemistry*. 2024;162(December 2023):105904. doi:10.1016/j.apgeochem.2024.105904

15. Hatzenpichler R, Krukenberg V, Spietz RL, Jay ZJ. Next-generation physiology approaches to study microbiome function at single cell level. *Nat Rev Microbiol*. 2020;18(4):241-256. doi:10.1038/s41579-020-0323-1

16. Sletten EM, Bertozzi CR. Bioorthogonal chemistry: Fishing for selectivity in a sea of functionality. *Angewandte Chemie - International Edition*. 2009;48(38):6974-6998. doi:10.1002/ANIE.200900942;PAGE:STRING:ARTICLE/CHAPTER

17. Hatzenpichler R, Orphan VJ. Detection of Protein-Synthesizing Microorganisms in the Environment via Bioorthogonal Noncanonical Amino Acid Tagging (BONCAT). Published online 2015:145-157. doi:10.1007/8623_2015_61

18. Bates D, Mächler M, Bolker BM, Walker SC. Fitting Linear Mixed-Effects Models Using lme4. *J Stat Softw*. 2015;67(1):1-48. doi:10.18637/jss.v067.i01

19. Hothorn T, Bretz F, Westfall P. Simultaneous Inference in General Parametric Models. *Biometrical Journal*. 2008;50(3):346-363. doi:10.1002/bimj.200810425

20. Corbera-Rubio F, Kruisdijk E, Malheiro S, et al. A difficult coexistence: Resolving the iron-induced nitrification delay in groundwater filters. *Water Res*. 2024;260:121923. doi:10.1016/J.WATRES.2024.121923

21. Boersma AS, Haukelidsaeter S, Kirwan L, et al. Influence of filter backwashing on iron, manganese, and ammonium removal in dual-media rapid sand filters used for drinking water production. *Water Res*. 2025;270:122809. doi:10.1016/J.WATRES.2024.122809

22. Braem A, Van Mellaert L, Mattheys T, et al. Staphylococcal biofilm growth on smooth and porous titanium coatings for biomedical applications. *J Biomed Mater Res A*. 2014;102(1):215-224. doi:10.1002/JBM.A.34688;CTYPE:STRING:JOURNAL

23. Van Beek CGEM, Dusseldorp J, Joris K, et al. Contributions of homogeneous, heterogeneous and biological iron(II) oxidation in aeration and rapid sand filtration (RSF) in field sites. *Journal of Water Supply: Research and Technology - AQUA*. 2016;65(3):195-207. doi:10.2166/aqua.2015.059

24. Huang D, Sun X, Usman M, et al. Bacteria associated with Comamonadaceae are key arsenite oxidizer associated with Pteris vittata root ☆. *Environmental Pollution*. 2024;349(December 2023):123909. doi:10.1016/j.envpol.2024.123909

25. Osborne TH, Heath MD, Martin ACR, Pankowski JA, Hudson-Edwards KA, Santini JM. Cold-adapted arsenite oxidase from a psychrotolerant Polaromonas species. *Metallomics*. 2013;5(4):318-324. doi:10.1039/c2mt20180a

26. Roy M, van Genuchten CM, Rietveld L, van Halem D. Integrating biological As(III) oxidation with Fe(0) electrocoagulation for arsenic removal from groundwater. *Water Res*. 2021;188. doi:10.1016/j.watres.2020.116531

27. Wang X, Rathinasabapathi B, Oliveira LM De, Guilherme LRG, Ma LQ. Bacteria-mediated arsenic oxidation and reduction in the growth media of arsenic hyperaccumulator Pteris vittata. *Environ Sci Technol*. 2012;46(20):11259-11266. doi:10.1021/ES300454B

28. Inskeep WP, Macur RE, Hamamura N, Warelow TP, Ward SA, Santini JM. Detection, diversity and expression of aerobic bacterial arsenite oxidase genes. *Environ Microbiol*. 2007;9(4):934-943. doi:10.1111/J.1462-2920.2006.01215.X

29. Ghosh D, Bhadury P, Routh J. Diversity of arsenite oxidizing bacterial communities in arsenic-rich deltaic aquifers in West Bengal, India. *Front Microbiol*. 2014;0(NOV):602. doi:10.3389/FMICB.2014.00602

30. Ke T, Zhang D, Guo H, Xiu W, Zhao Y. Geogenic arsenic and arsenotrophic microbiome in groundwater from the Hetao Basin. *Science of the Total Environment*. 2022;852. doi:10.1016/j.scitotenv.2022.158549

31. Yang J, Li Q, Chen T, Tao H, Jiang Y. Microbial regulatory mechanisms involved in groundwater arsenic enrichment: Synergistic interactions between key species and genes in C-N-S metabolism. *Geoscience Frontiers*. 2025;16(6):102132. doi:10.1016/J.GSF.2025.102132

32. Muehe EM, Scheer L, Daus B, Kappler A. Fate of arsenic during microbial reduction of biogenic versus abiogenic As-Fe(III)-mineral coprecipitates. *Environ Sci Technol*. 2013;47(15):8297-8307. doi:10.1021/ES400801Z

33. Masuda H. Arsenic cycling in the Earth's crust and hydrosphere: interaction between naturally occurring arsenic and human activities. *Progress in Earth and Planetary Science 2018 5:1*. 2018;5(1):68-. doi:10.1186/S40645-018-0224-3

34. Jiang Z, Li P, Wang Y, et al. Arsenic mobilization in a high arsenic groundwater revealed by metagenomic and Geochip analyses. *Scientific Reports 2019 9:1*. 2019;9(1):12972-. doi:10.1038/s41598-019-49365-w

35. Paul D, Kazy SK, Gupta AK, Pal T, Sar P. Diversity , Metabolic Properties and Arsenic Mobilization Potential of Indigenous Bacteria in Arsenic Contaminated Groundwater of. *Plos*. Published online 2015. doi:10.1371/journal.pone.0118735

36. Oremland RS, Stolz JF. Arsenic, microbes and contaminated aquifers. *Trends Microbiol*. 2005;13(2):45-49. doi:10.1016/J.TIM.2004.12.002

37. Smith AH, Lopipero PA, Bates MN, Steinmaus CM. Arsenic epidemiology and drinking water standards. *Science (1979)*. 2002;296(5576):2145-2146. doi:10.1126/SCIENCE.1072896;WEBSITE:WEBSITE:AAAS-SITE;ISSUE:ISSUE:DOI

Supplementary Information

Table S1: Water quality parameters of tap water used for column experiments

Parameter	Value	Unit
pH	7.99	-
EC	0.12	mS/m
HCO_3	120	mg/L
SO_4	56	mg/L
Na	45	mg/L
Turbidity	0.48	FTE
Fe	7.8	µg/L
O_2	9.1	mg/L
Hardness	1.45	mmol/L
DOC	2.0	mg/L C
F	0.16	mg/L
Br	0.12	mg/L
ClO_3	27	µg/L
ClO_2	37	µg/L
NH_4	<0.05	mg/L
NO_2	<0.01	mg/L
NO_3	6.9	mg/L
K	7.2	mg/L
Ca	45	mg/L
Mg	8.1	mg/L
Mn	<0.5	µg/L
Al	<3	µg/L
Sb	<0.5	µg/L
As	<0.5	µg/L
Ba	16	µg/L
B	47	µg/L
Cd	<0.05	µg/L
Cr	<0.2	µg/L
Ni	3.1	µg/L
Se	<0.5	µg/L
Sr	160	µg/L
U	0.20	µg/L

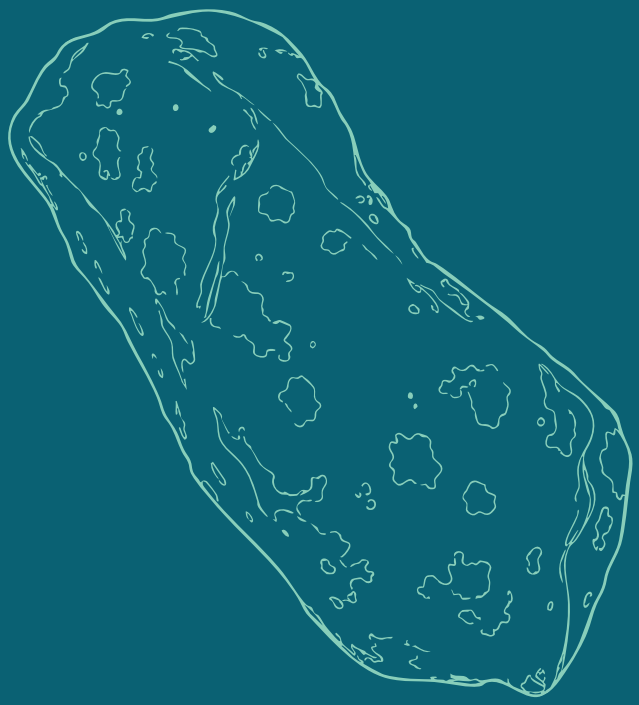

06

Outlook

The overall aim of this thesis was to unravel the removal pathways of arsenic in groundwater treatment systems, with a particular focus on the contribution of biological processes. We found that biology has a central role in oxidizing arsenic and can outcompete surface catalytic oxidation (Chapter 3). Arsenic oxidizing bacteria were widely detected in groundwater treatment filters in rural Bangladesh (Chapter 2), indicating that biological arsenic oxidation is widespread rather than incidental. Arsenic oxidizing bacteria did not appear to be a distinct or specialized microbial group: neither biofilm composition nor biological activity was affected by exposing the drinking water biofilm to arsenic, while efficient As oxidation was observed (Chapter 5). These findings show that biological arsenic oxidation is an important component of groundwater treatment and should be explicitly considered when designing arsenic removal plants. This aligns with the broader paradigm shift in which sand filters are increasingly recognized as biofilters.

Resolving questions inevitably raises new ones. In this final chapter, directions for future research are outlined, including considerations for applying these findings in practice and a reflection on the limitations of the work presented in this thesis. Ultimately, advancing this understanding is essential to further reduce arsenic concentrations in drinking water, here in the Netherlands, in Bangladesh and in every other affected region in the world.

6.1 Arsenic oxidation done by a standard drinking water biofilm

Both in literature and throughout this thesis, the term arsenic-oxidizing bacteria (AsOB) is commonly used. This terminology implicitly suggests that arsenic oxidation is carried out by a distinct and specialized microbial group, similar to ammonium being predominantly oxidized by *Nitrospira* or iron oxidation often associated with *Gallionella*. For these processes, clear shifts in microbial community composition are observed when filters are exposed to ammonium or iron [1,2].

In contrast, such clear shifts were not observed for arsenic. Although a modest increase in the relative abundance of the family *Comamonadaceae* – previously associated with arsenic oxidation – was detected, this group remained a minor fraction of the total community. The overall taxonomic composition of the biofilm remained remarkably stable, and BONCAT analyses showed no differences in microbial activity between biofilms exposed to arsenic and those that were not (Chapter 5).

These findings indicate that arsenic oxidation is not restricted to a single functional group of bacteria, but can be accommodated by a standard drinking water biofilm. Arsenic oxidation appears to be a broadly distributed metabolic capability. This hypothesis is supported by genomic surveys showing that the arsenite oxidase operon (aio) is found widespread across bacterial groups [3,4]. Although arsenic oxidation in heterotrophs has traditionally been regarded as a detoxification mechanism, it is also shown that energy conservation from As(III) oxidation in heterotrophs may occur [5].

Interestingly, an increased arsenic-oxidation capacity was observed in this study without a convincing shift in community composition. This suggests that the functional potential for

arsenic oxidation was already present within the biofilm and became upregulated upon As(III) exposure. Future studies should therefore prioritize *how* arsenic oxidation is regulated and stimulated, rather than focusing exclusively on *who* performs it. Functional adaptation could be quantified by targeting arsenite-oxidation genes using qPCR before and after As(III) exposure. Metatranscriptomics or metaproteomics approaches could directly demonstrate upregulations and expression of arsenic-oxidizing pathways.

6.2 Stimulate biological arsenic oxidation in sand filters

To fully utilize the potential of biological arsenic oxidation, treatment plants should be optimized to support biofilm development and activity. Currently, sand filters are mainly designed from a physicochemical perspective. Intense aeration introduces high dissolved oxygen concentrations, favoring homogeneous and heterogeneous iron oxidation. This has been shown to negatively affect biofilm activity [6]. Rather than requiring major design changes, relatively small adjustments in operational conditions may substantially influence biological performance. My recommendation would be to study the effect of milder aeration, hydraulic conditions and the choice of filter media on the efficiency of biological arsenic oxidation in sand filters.

Mild aeration

Aeration in groundwater treatment is often applied to reach oxygen saturation, yet lowering the oxygen concentration may create more favorable conditions for arsenic removal. First, milder aeration limits CO_2 degassing, thereby maintaining a lower pH. Since the adsorption capacity of iron-based adsorbents for As(V) increases substantially at lower pH – approximately an order of magnitude higher at pH 6 than at pH 8 – this directly enhances arsenic removal. Second, lower oxygen concentrations inhibit rapid homogeneous Fe(II) oxidation, while biological arsenic oxidation can proceed under anaerobic or low-oxygen conditions using alternative electron acceptors [7]. Müller et al. (2024) demonstrated that lowering dissolved oxygen from ~10 to ~5 mg/L shifted iron oxidation from predominantly chemical to biological pathways, thereby minimizing homogeneous iron-floc formation [8]. This may create more favorable conditions for biofilm development, as it is known that homogeneous Fe(II) oxidation can negatively affect biological NH_4^+ and Mn(II) oxidation [6,9]. Similar interference with biological arsenic oxidation is plausible and warrants further investigation. Another benefit of forming fewer iron-flocs is the reduced filter clogging, allowing substantially longer filter run times before backwashing is required [8]. This brings us to the second process condition recommended to study – hydraulic conditions.

Hydraulic conditions

Flow velocity and backwashing are two hydraulic parameters that are relatively easy to adjust and can influence biofilm stability. We found that filter media from a Mn-removing bed exhibited denser biofilms than from a Fe-removing bed. Lower backwash frequencies are typically applied to Mn-removing filters. Backwashing can detach the biofilm, through high shear forces caused by the water and air [10]. Li et al. (2012) also found that milder but more

frequent backwashing could better preserve biofilm growth [10]. It is suggested to study this effect on the efficiency of As(III) oxidation. The effect of additional parameters, such as water/air ratio during backwashing, should also be further investigated.

Filter media

Finally, the choice of filter media is an underexplored parameter, but can impact biological activity. Conventional materials such as sand and anthracite have relatively smooth surfaces, whereas biofilm development is favored in surface irregularities and cavities (Chapter 5). Alternative media with higher surface roughness or porosity may therefore stimulate biofilm growth and improve biological arsenic oxidation.

The parameters discussed above will not only affect arsenic oxidation, but a wide range of interconnected chemical and biological processes as depicted in Figure 2 in the introduction. The proposed adjustments may enhance biological pathways, and they will simultaneously affect iron, manganese and ammonium removal. Consequently, optimization strategies should be evaluated through pilot-scale studies using real groundwater with varying compositions, as currently system behavior cannot be reliably predicted from models or small-scale laboratory experiments alone.

6.3 Design optimization: Arsenic oxidation before Fe removal

Arsenic removal in groundwater treatment is intertwined with iron removal, as arsenic is predominantly removed by adsorption to iron hydroxides in the filter bed. Consequently, effective arsenic removal requires control of both processes. Sand filters should be designed to remove As(V) rather than As(III) for two reasons. First, biological arsenic oxidation is likely to occur in any mature sand filter, ensuring that As(V) is formed during filtration. Second, at pH <8 adsorption capacities of iron hydroxides for As(V) are higher than for As(III), making As(V) the preferred target species for removal (Chapter 4).

In practice, however, iron oxidation and removal often proceed faster than arsenic oxidation. As a result, iron is removed before arsenic has been fully oxidized, limiting the availability of sorption sites and allowing dissolved As(V) to break through into the effluent. The challenge is therefore to design systems in which arsenic oxidation occurs prior to, or simultaneously with iron removal. Figure 1 A+B shows a schematic overview of conceptual strategies to promote arsenic oxidation before or simultaneously with iron removal.

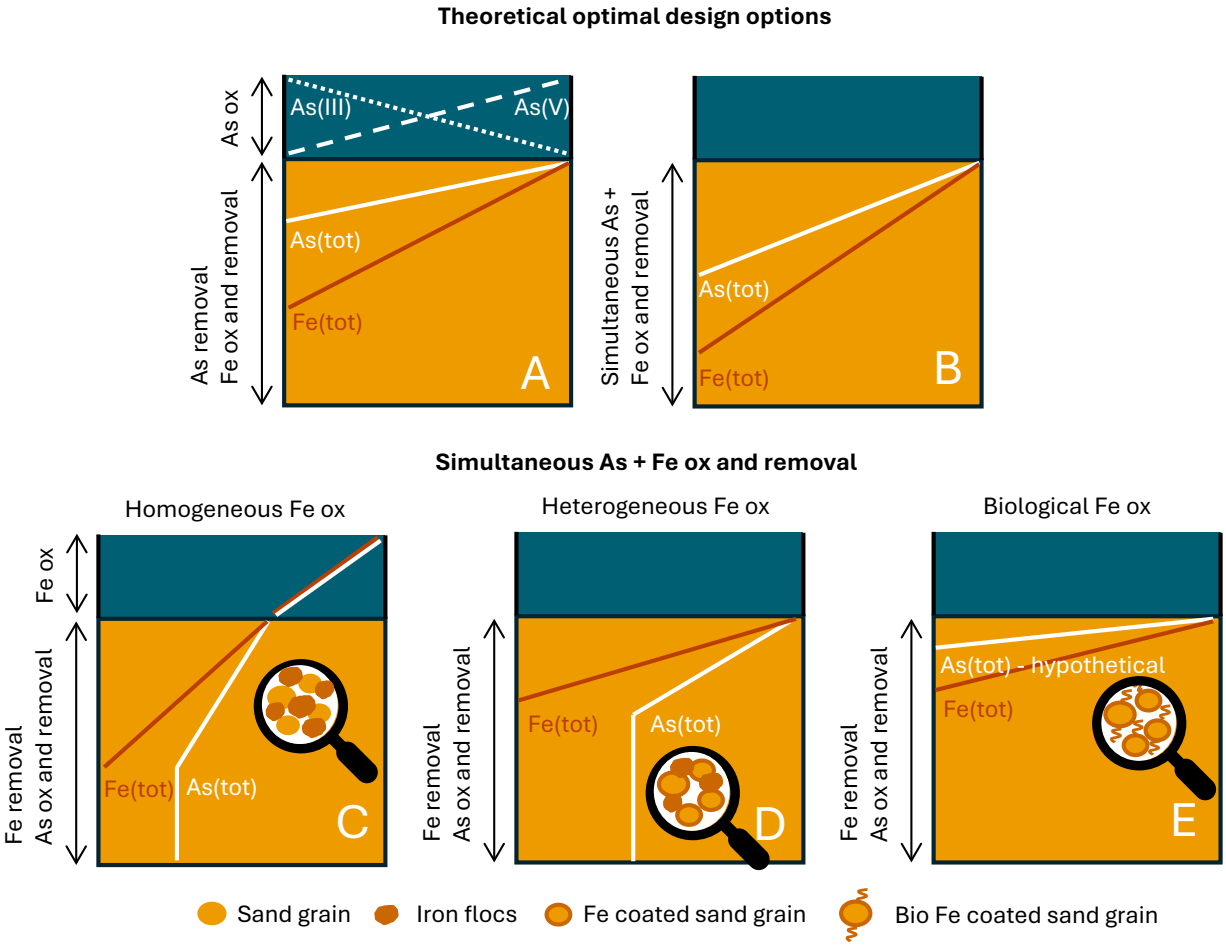

Figure 1: Schematic overview of possible optimization of iron-arsenic removing treatment plants (A+B) and iron-arsenic oxidation pathways in existing treatment plants (C-E). A: Stimulate arsenic oxidation prior to iron removal B: Simultaneous As and Fe oxidation and removal. C: As removal pathway in homogeneous iron oxidation plant. D: As removal pathway in heterogeneous iron oxidation plants. E: Hypothetical As removal pathway in biological iron oxidation plants.

Arsenic oxidation before iron removal (Figure 1A)

A first strategy to promote arsenic oxidation prior to iron removal is to utilize the difference in morphology between iron- and arsenic oxidizing bacteria. In a pre-treatment step, oxygen concentrations should be kept low to suppress homogeneous and heterogeneous Fe(II) oxidation. Under such conditions, biological iron oxidation will occur and is primarily performed by *Gallionella* and *Leptothrix,* excreting stalked or filamentous structures that extend away from the surface. These morphologies make them sensitive to hydraulic shear. By imposing high hydraulic shear, their growth could be reduced [11]. This is consistent with observations during backwashing, which has minimal impact on overall microbial community composition but selectively reduces the abundance of *Gallionella* [12] In contrast, arsenic oxidation is carried out by a phylogenetically diverse group of microorganisms and is therefore expected to be more resilient under high-shear conditions. Reactor designs that exploit this difference could selectively stimulate arsenic oxidation while preventing iron oxidation and therefore deserve further investigation.

A second option is to allow homogeneous iron oxidation under high oxidation conditions and biological arsenic oxidation to occur simultaneously, while actively preventing iron removal at this stage. This could be achieved by using bio-carriers that support the growth of arsenic-oxidizing biofilms, but with pore sizes large enough to limit iron floc retention. The subsequent carryover of iron flocs together with oxidized As(V) to the downstream sand filter would facilitate efficient arsenic removal. These bio-carriers could be placed in a separate reactor, or in the supernatant water above the sand filter bed.

Arsenic oxidation simultaneously with iron removal (Figure 1B and C-E)

Both approaches discussed above require the implementation of an additional treatment step. More readily applicable are optimizations in the existing treatment designs, stimulating simultaneous removal of iron and arsenic (Figure 1B). The expected arsenic removal pathways during the three dominant iron oxidation pathways – homogeneous, heterogeneous, and biological – are presented in Figure 1C-E respectively.

The effect of homogeneous versus heterogeneous iron oxidation on arsenic removal was evaluated by Gude et al. (2018), who demonstrated that homogeneous iron oxidation can enhance arsenic removal by allowing iron flocs to penetrate deeper into the filter bed (Figure 1C)[13]. Heterogenous iron oxidation proceeds rapidly on sand grain surfaces (Figure 1D), depleting dissolved iron at the top of the filter bed, limiting the capacity for subsequent As(V) adsorption. Even though both pathways are frequently applied in practice, they often show incomplete arsenic removal.

The third pathway to remove iron is via biological iron oxidation (Figure 1E), and the effect on arsenic removal is yet unexplored. Biological iron oxidation is favored at low oxygen concentrations, which limits CO_2 stripping and maintains a lower pH, suppressing homogeneous and heterogeneous iron oxidation. Lower pH values enhance arsenic adsorption; at pH 7 adsorption of As to iron (hydr)oxides can be around 3 times higher than at pH 8 (Chapter 4).

My recommendation is to study the effect of biological iron oxidation on the removal efficiencies of arsenic. At two drinking water treatment facilities operated by Pidpa (Belgium), biological iron removal is applied, resulting in good As removal efficiencies. Two fully aerated plants, stimulating homogeneous and heterogeneous oxidation, have a lower arsenic removal performance (Table 1). Likewise, a pilot study by Müller et al. (2024), comparing chemical and biological iron removal, found arsenic removal kinetics that were approximately twice as fast under biological iron oxidation conditions (BOX 1) [8]. Although the high influent iron concentrations in these systems undoubtedly contributed to the observed performance, the results do highlight the potential of biological iron oxidation to enhance arsenic removal. Exploring this synergy offers a promising option towards more reliable arsenic-removal filters.

Table 1: Four groundwater treatment locations of drinking water company Pidpa (Belgium). The top two operate at high O_2 and high pH conditions, stimulating chemical iron oxidation. The bottom two operate at low O_2 and low pH conditions, stimulating biological iron oxidation. The concentrations of Fe and As and the ratio Fe/As are given for the raw groundwater and the concentration of As and the As removal (rem) percentage of the treated water are given.

	Process conditions		Raw			Treated	
	O2 (mg/L)	pH	Fe (mg/L)	As (ug/L)	Fe/As	As (ug/L)	As rem (%)
Chemical							
Hoogstraten	7.5	7.61	2.2	11.6	190	2.7	77
Merksplas	10	7.48	2.8	6.8	412	1.8	74
Biological							
Oud-Turnhout	6	7.14	16.4	45.5	360	0.9	98
Mol	3	6.93	16.7	41.7	400	1.2	97

BOX 1: Arsenic removal efficiencies in chemical versus biological iron removal systems

Müller et al. (2024) operated two parallel full-scale rapid sand filters at different aeration intensities to compare chemical and biological iron removal [8]. One filter was operated under high aeration (>10 mg/L O_2, pH 7.4), stimulating homogeneous and heterogeneous iron oxidation (the *chemical filter*). The second filter was operated under low aeration (5 mg/L O_2, pH 6.9), conditions that favor biological iron oxidation (the *biological filter*). They found that biological iron removal caused less clogging. The biological filter could therefore be operated at twice the filtration velocity of the chemical column and required lower backwash frequencies, yielding four times more treated water per run.

In their study, arsenic was measured but not evaluated. Figure 2 shows the arsenic removal profiles in both filters based on samples taken at two different time points (March and November 2021, see Müller et al. (2024) for experimental details). Arsenic was removed approximately twice as fast in the biological filter compared to the chemical filter. In both systems, effluent arsenic concentrations decreased to below 1 µg/L, as can be expected with the high iron (26.7 mg/L) concentrations in the groundwater.

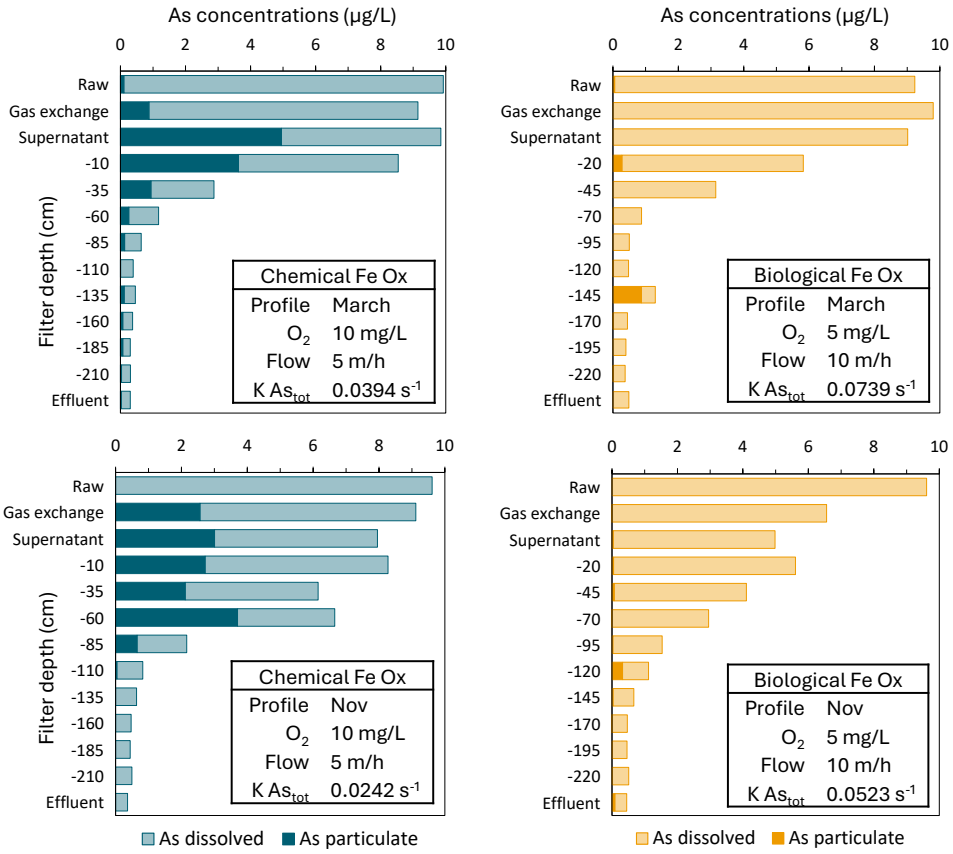

Figure 2: Data from Müller et al. (2024) with permission of the authors [8]. Arsenic concentrations along the depth of the chemical- (blue) and biological (yellow) iron-oxidation filter of the profiles taken in March (top) and November (bottom). Note; chemical filters operated at twice the flow rate (10 m/h) as biological filters (5 m/h).

6.4 Arsenic sludge handling

Throughout this thesis, the focus has been on removing arsenic from groundwater to produce safe, arsenic-free drinking water. This removal is essential, but it does not completely eliminate arsenic from the system. Instead, arsenic is transferred from the water phase to the solid phase through adsorption onto iron (hydr)oxides. During backwashing of the sand filters, part of this iron ends up in the backwash water, generating an iron-arsenic rich waste stream. Appropriate management of this stream is required to avoid secondary environmental contamination.

The handling of arsenic-containing waste streams is a major global challenge. In decentralized treatment systems such as those studied in Bangladesh (Chapter 1), backwash water is often discharged directly into the environment (Figure 3), resulting in uncontrolled arsenic release and substantially higher toxicity risks compared to managed disposal [14]. Also in large-scale centralized treatment plants, disposal of iron sludge remains problematic and is one of the highest operating costs [15]. At the same time, these waste streams contain valuable resources, and arsenic has been classified as a critical raw material by the European Commission since 2024, shifting arsenic removal from groundwater from a purely treatment necessity towards a potential opportunity for resource recovery.

Motivated by this recognition, a new research field is emerging focusing on arsenic recovery from water treatment residuals [16–18]. An important, yet unexplored, opportunity lies in the arsenic accumulated on iron-coated sand grains within filter beds. In systems dominated by heterogeneous and biological iron removal, a substantial fraction of iron precipitates onto grain surfaces rather than being washed out as flocs. Consequently, arsenic also accumulates in the filter coating rather than ending up in the diluted backwash water. The study of Wang et al. (2023) has shown that biological iron removal beds contain substantially less arsenic in the backwash waste stream compared to fully aerated systems, indicating enhanced retention within the filter bed [17]. The rapid growth of the iron coatings in biological filters requires periodic removal of the top filter layer, presenting a concentrated and accessible arsenic source. Targeting arsenic recovery from iron-coated filter media therefore offers a compelling and efficient pathway, which should be investigated in further research.

Figure 3: Backwashing procedure in Kolaroa, Bangladesh. Arsenic containing iron sludge is directly disposed into the environment.

References

1. Van Der Wielen PWJJ, Voost S, Van Der Kooij D. Ammonia-Oxidizing Bacteria and Archaea in Groundwater Treatment and Drinking Water Distribution Systems. *Appl Environ Microbiol*. 2009;75(14):4687-4695. doi:10.1128/AEM.00387-09

2. de Vet WWJM, Dinkla IJT, Rietveld LC, van Loosdrecht MCM. Biological iron oxidation by Gallionella spp. in drinking water production under fully aerated conditions. *Water Res*. 2011;45(17):5389-5398. doi:10.1016/j.watres.2011.07.028

3. Andres J, Bertin PN. The microbial genomics of arsenic. *FEMS Microbiol Rev*. 2016;40(2):299-322. doi:10.1093/FEMSRE/FUV050

4. Heinrich-Salmeron A, Cordi A, Brochier-Armanet C, et al. Unsuspected diversity of arsenite-oxidizing bacteria as revealed by widespread distribution of the aoxB Gene in prokaryotes. *Appl Environ Microbiol*. 2011;77(13):4685-4692. doi:10.1128/AEM.02884-10

5. Wang Q, Han Y, Shi K, et al. An Oxidoreductase AioE is Responsible for Bacterial Arsenite Oxidation and Resistance. *Sci Rep*. 2017;7(1):41536-. doi:10.1038/srep41536

6. Corbera-Rubio F, Kruisdijk E, Malheiro S, et al. A difficult coexistence: Resolving the iron-induced nitrification delay in groundwater filters. *Water Res*. 2024;260:121923. doi:10.1016/J.WATRES.2024.121923

7. Sun W, Sierra R, Field JA. Anoxic oxidation of arsenite linked to denitrification in sludges and sediments. *Water Res*. 2008;42(17):4569-4577. doi:10.1016/j.watres.2008.08.004

8. Müller S, Corbera-Rubio F, Schoonenberg Kegel F, Laureni M, van Loosdrecht MCM, van Halem D. Shifting to biology promotes highly efficient iron removal in groundwater filters. *Water Res*. 2024;262:122135. doi:10.1016/j.watres.2024.122135

9. Tong M, Zhao Y, Sun Q, Li P, Liu H, Yuan S. Fe(II) oxygenation inhibits bacterial Mn(II) oxidation by P. putida MnB1 in groundwater under O2-perturbed conditions. *J Hazard Mater*. 2022;435:128972. doi:10.1016/J.JHAZMAT.2022.128972

10. Li X, Yuen W, Morgenroth E, Raskin L. Backwash intensity and frequency impact the microbial community structure and function in a fixed-bed biofilm reactor. *Applied Microbiology and Biotechnology 2012 96:3*. 2012;96(3):815-827. doi:10.1007/S00253-011-3838-6

11. Ferris FG, James RE, Pedersen K. Fragmentation of Bacteriogenic Iron Oxides in Response to Hydrodynamic Shear Stress. *Geomicrobiol J*. 2015;32(7):564-569. doi:10.1080/01490451.2014.897775

12. Boersma AS, Haukelidsaeter S, Kirwan L, et al. Influence of filter backwashing on iron, manganese, and ammonium removal in dual-media rapid sand filters used for drinking water production. *Water Res*. 2025;270:122809. doi:10.1016/J.WATRES.2024.122809

13. Gude JCJ, Joris K, Huysman K, Rietveld LC, van Halem D. Effect of supernatant water level on As removal in biological rapid sand filters. *Water Res X*. 2018;1:100013. doi:10.1016/J.WROA.2018.100013

14. Van Genuchten CM, Etmannski TR, Jessen S, Breunig HM. LCA of Disposal Practices for Arsenic-Bearing Iron Oxides Reveals the Need for Advanced Arsenic Recovery. *Environ Sci Technol*. 2022;56(19):14109-14119. doi:10.1021/acs.est.2c05417

15. Turner T, Wheeler R, Stone A, Oliver I. Potential Alternative Reuse Pathways for Water Treatment Residuals: Remaining Barriers and Questions—a Review. *Water Air Soil Pollut*. 2019;230(9):227-. doi:10.1007/s11270-019-4272-0

16. Genuchten CM van, Etmannski TR, Reid MC, Breunig HM. Upcycling Metal(loid) Contaminants to Produce Critical Raw Materials: The Nexus of Water Treatment and Material Criticality. *Environ Sci Technol*. Published online November 30, 2025. doi:10.1021/ACS.EST.5C13163

17. Wang K, Holm PE, Trettenes UB, Bandaru SRS, van Halem D, van Genuchten CM. Molecular-scale characterization of groundwater treatment sludge from around the world: Implications for potential arsenic recovery. *Water Res*. 2023;245:120561. doi:10.1016/j.watres.2023.120561

18. Wang K, Liu J, Jiang M, Holm PE, van Genuchten CM. Crystal structure-dependent oxidation pathways of metallic arsenic(0): Implications for environmental risk and material handling. *J Hazard Mater*. 2026;504(4):141282. doi:10.1016/j.jhazmat.2026.141282

Acknowledgments

I often compare life to a river. Sometimes I feel like I am floating along a calm stream, carried gently by the current, while at other times the river becomes wild, exciting and a little scary. The river often splits, forcing us to choose a direction, but also offering a possible new path. The PhD path was certainly not the most peaceful one, but it was probably the most fun ride I will ever get. Part of that fun came from the work itself, but by far the largest part came from the amazing people that I got to share this path with.

Doris, I feel so incredibly lucky that I got to work on your VIDI project, thank you so much for your trust in me. I feel motivated and inspired by you in so many ways. You are truly an incredible example of a supervisor: every piece of feedback always starts with a cheer of encouragement, you create the perfect balance between being ambitious and taking time off, and you have always made me feel like a priority. You put your students in the spotlight and help them realize how brightly they can shine. This also helped my confidence grow over time, which is probably the most valuable outcome of a PhD. Slowly, the inflatable canoe I entered this river in turned into a pretty steady boat. I wish every PhD student a supervisor like you.

Another incredible example of a supervisor is **Merle**. Working at the Water Management Department has been such a pleasure, thanks to the welcoming and safe working environment you create. I have always appreciated how genuinely you check in on how I am doing, beyond just the work. And I cannot thank you enough for introducing me to your soul ground, Montana has my heart.

The most fun daily memories I have of my PhD journey were together with **Emiel**. I feel incredibly lucky that we got to navigate this project together. We spent countless hours in the lab, watching each other slowly become grumpy and laughing about it together. But the most unforgettable parts of our journey were far away from the Water lab; Bangladesh and India. Full of unexpected moments that still make me smile whenever I think about them, two of the most fun trips I have ever been on. We weren't allowed to swim together in Bangladesh, but during all the other moments, you have saved me from drowning many times. Watching Mount Everest together is a pretty good metaphor for the highlights I have experienced with you in my PhD.

Guus, your positivity and enthusiasm are contagious, and that energy can be felt throughout the entire Water Management Department. You are the backbone of Water for Impact, and I feel incredibly lucky that our paths crossed there. Pretty awesome that we made it to the UN Water Conference!! And at Water for Impact is also where my friendship with **Suzanne** took off. If you hadn't brought me into the team, I am not sure I would be where I am today. I am especially grateful for that week we spent together in Bozeman, filled with lab work, coffee, beers and bears. And let's just say that the FISH in this PhD river don't really bite... Thank you

for being my paranymph - on a stage surrounded by so many inspiring women, you certainly cannot be missed.

Nienke, what would I have done without you? The appendix is a tribute to you. I feel incredibly fortunate that you wanted to take on my Open Mind Project and it was awesome seeing you start your career in the beautiful water world. I hope our paths will continue to cross in the future. And somewhere along the way, another brilliant mind joined the project: **Tjark**, you are the MSc student every PhD student wishes for. Thank you for your hard work! But at the very beginning of this project stands **Simon**. A steady, calm rock in the water. You taught me so many valuable things that made the start of my scientific career a whole lot smoother. I truly wish I could water your river a little in return, but I have every confidence that you will get there too. And while every river needs its calm stretches, it also needs a few cascades. For those, there was **Francesc**. Thank you for keeping me sharp and for all the laughs.

I would like to thank **Frank, Gerard** and **Koen** for your support as the user committee of this project, and for the interesting discussions along the way. I am also very grateful to **Armand, Bright, Jane** and the rest of the Waterlab crew for all your help in the lab. **Mark,** your guidance in the vivianite project was invaluable. And during my research exchange in Montana, I was once again surrounded by amazing female scientists. **Heidi, Kristen** and **Cat,** thank you so much for having and helping me.

A special shout-out also goes to the students who have worked on my projects. **Alex** and **Nina**, our sample queens! Thank you for treating our columns with so much care. It was always a joy to walk into the lab and hear your giggles. **Harsh** took over the job very well, followed by **Zakaria.** It has been a pleasure working with you all.

In a PhD it does not always feel like the water is flowing in the right direction. Sometimes, it seems to flow everywhere except where it should. Luckily, even in those moments, I had plenty of reasons to enjoy coming into the office, thanks to my incredible colleagues: **Silvy, Carolina, Sander, Nikoletta, Akrivi, Andrea,** my 4.42 buddies, and **Adela, Akhilesh, Alex, Arash, Cole, Cynthia, Devanita, Emeka, Erik, Gladys, Ilya, Iosif, Joao, Mike, Mrinal, Omar, Roberto, Shreya, Simon, Timo, Tugba, Veerle, Yana,** and all the other incredible colleagues that have been part of our group. Thank you for all the chats, laughs, drinks at PSOR, Christmas parties and for patiently waiting while I brewed my own coffee during the breaks.

There is a famous saying from W.H. Auden: 'Thousands have lived without love, not one without water.' Although theoretically true, I could not have done this without the people around me that I love.

Eline, my partner in life. You have been there for every step of my academic career. The sunshine you brought into that dusty classroom at the start of the second year of Molecular Life Science has changed my life for the better. Thank you for your genuine attention, for all the questions, the life doubts, the endless conversations, and for always rooting for me and believing in me. You are a constant fountain of positive energy. Even when we live far away from each other, I have always felt heard and seen by you. I am excited to see where our rivers

will flow next, but of one thing I am certain: they will keep flowing side by side, because life is so much more fun with you.

Apparently, water has a way of attracting cool people, something I experienced firsthand during my MSc at the Water Management Department. **Ben, Floor, Stijn** and Eline – with you, conversations can move from deep questions to complete nonsense and back again within minutes, usually accompanied by plenty of jokes and laughs. The fact that you came all the way to my home in Montana is something I will never take for granted; my heart almost explodes whenever I think about it. Five adults squeezed into a camper van certainly produced some pretty good memories. I truly hope we keep going on these adventures, with our other buddy **Rob** too. And to the three other incredible women I met during my MSc, **Janieke, Jente** and **Juliette**: thank you for being such wonderful inspirations, and for always checking in, listening, and being there. Who run the world?

Sometimes, when you think your heart is already completely full, life reminds you that there is always room for more love. I spent half a year of my PhD in Montana, where I met some truly wonderful people. **Ana,** my sunshine, my research exchange wouldn't have been half as much fun without you. You are one of the most genuine people I have ever met, and I feel so incredibly lucky that we got to share such a special part of our lives in Bozeman. A shout-out as well to **Thomas, Kerem** and **Jenn**, for all the lunches and craft beers together and for making this half year unforgettable. **Jason**, you made me feel like I was floating, giving me the stability I needed during the final stretch of this PhD. Unfortunately, not every unexpected turn in life leads to positive outcomes only, but I am grateful for all the adventures we shared and thank you for showing me so many beautiful parts of your country.

Besides the people I have met through my work and studies, there are the friends that have been part of my life for a very long time. Amersfoort has brought me so much: **Eeke, Marijn, Marit, Mei, Mies, Yara**, **Xander** and **Pip** – spending time with you always recharges me with energy to keep going in my workweek. **Nicolaas,** thank you for widening my field of interest and for being one of my biggest cheerleaders. **Lilly**, you gave color to this thesis (thank you!!), but certainly also to my life. And I feel so lucky to call so many other wonderful people my friends: **Daphne, Eline, Jannah, Camilla, Jeffrey, Thiemo, Nicole, Amber, Anne, Aoife, Manouk, Rens, Tristan,** and **Sya.** Thank you for making my life so fun.

And then there are the people who have lived particularly close to me throughout this journey, those who have seen me in all my moods. Sometimes I feel people pity me when I tell them I (still) live with roommates in my late twenties, but those people simply have not experienced what it is to live with such awesome people.

Eva, I could have mentioned you several times already, because you are woven into so many parts of my life. Thank you for always being there: from cooking meals and drying tears to joining countless late-night dance parties. And then there is our (not so) little brother **Stijn**. The three of us created such a special place in Rotterdam. It truly became my safe harbor during my PhD, and I could not have wished for better people to share it with.

And then there is my second home in Amsterdam. **Jolijn**, I am so happy that you were always home during those last intense months. Having someone to dance through the living room with or to sit quietly together in the temple during my writing breaks made the whole experience so much better. And whenever I needed a chat, there was **Tessa.** Thank you both for bringing so much life into our home. I feel so incredibly lucky to live with you. Life has its challenges, but whenever the sky above the Entrepotdok turns pink, everything suddenly feels great again.

Every river has a source, and it is that spring that has shaped me into who I am today. **Mom, Dad** and **Hugo**, I am so grateful for all the support I have felt from you in my life. My river might run a little wild sometimes, but I know you are always there at the shore, cheering me on and ready to catch me whenever I need it. I realize more and more how incredibly valuable that is. Two of the main reasons I have been able to enjoy this PhD journey so much are that I am spending my days doing work that feels meaningful, while also being able to leave it behind when the working day is over. Mom and Dad, you have been the living example of that balance throughout my life. Thank you for showing Hugo and me how to live life with joy and how to care for the world around us. Love is the water of life, and you made sure my river never ran dry.

Roos Goedhart – Curriculum Vitae

Sanitary Engineer

My main goal in both my career and personal life, is to contribute to a healthier, sustainable and equal future. I am educated in waste- and drinking water treatment, with a specific focus on resource recovery and the chemical and microbiological reactions during treatment. I like to combine technical expertise with hands-on fieldwork to improve access to safe WASH services worldwide. I am a curious and responsible scientist with a positive mindset.

Work Experience

Postdoc – Sanitary Engineering Groundwater treatment design to optimize arsenic removal	TU Delft 2026 – 2027
PhD Candidate – Sanitary Engineering Unravelling microbial arsenic oxidation in rapid sand filtration	TU Delft 2021 – 2026
Coordinator Research Project NWO Open mind project. From waste to value: anoxic iron removal from groundwater	TU Delft 2022 – 2024
Research & Community Coordinator Strengthening the community of TU Delft | Global Initiative Water for Impact and organizing international events	Water for Impact 2020 - 2023

Education

Master Environmental Engineering, Technology Track Waste- and drinking water treatment, water & health, microbiology Thesis: Anaerobic Iron Removal from Groundwater via Vivianite	TU Delft 2018-2021
Bachelor Molecular Life Sciences Microbiology, (bio)chemistry, physics Minor AGH University, Krakow PL: Environmental Engineering Thesis: Analysing Biofilm from a Microbial Fuel Cell with NMR	Wageningen University & Research 2014-2017

Field Experience

Bangladesh – Fieldwork PhD Fieldwork PhD Assessing arsenic removal capacities of groundwater treatment plants | NGOs SPACE, WaterAID and Bangladesh University of Engineering and Technology	2023
South Africa – Engineering Consultancy Project MSc Stormwater harvesting in Capetown | NUFFIC and University of Cape Town	2019

List of Publications

Goedhart, R., Kruisdijk, E. & van Halem, D. (2025). Biofilm accelerates As(III) oxidation on reactive MnOx coated filter sand in groundwater filters. ACS ES&T | Water, 5, 7536-7547.

Goedhart, R., Koudijs, N., van Loosdrecht, M. & van Halem, D. (2025). Vivianite recovery from anaerobic groundwater reverse osmosis concentrate. Water Research, 285, 124101.

Holst, T., **Goedhart, R.**, van Loosdrecht, M. C. & van Halem, D. (2025). Anoxic iron sulfides formation for iron removal in groundwater treatment. Journal of Water Process Engineering, 76, 108234.

Corbera Rubio, F., **Goedhart, R.**, Laureni, M., van Loosdrecht, C. M. & van Halem, D. (2024) A biotechnological perspective on Sand filtration for drinking water production. Current opinion in Biotechnology, 90, 103221.

Kruisdijk, E., **Goedhart, R.** & van Halem, D. (2024). Biological arsenite oxidation on iron-based adsorbents in groundwater filters. Water research, 262, 122128.

Goedhart, R., Müller, S., van Loosdrecht, M. & van Halem, D. (2022). Vivianite precipitation for iron recovery from anaerobic groundwater. Water Research, 217, 118345.

Publications in preparation

Goedhart, R., Kruisdijk, E., Ahmed, T., Hasan, M., Hossain, B., Haider, A., Tuz Zohra Khan, F., de Kreuk, M.K. & van Halem, D. (2025). Biological performance of arsenic-treating decentralized groundwater plants in Bangladesh

Goedhart, R., Smith, H., Parker, A., de Kreuk, M.K. & van Halem, D. Biofilm distribution on metal-coated filter sand and its activity during biological As(III) oxidation revealed by bioorthogonal non-canonical amino acid tagging (BONCAT)

Conferences

International Water Association Biofilm Reactors Conference, Orange Beach, USA, 2026
Keynote speaker - Minerals meet microbes: Multimodal imaging of biofilms on metal coated sand from groundwater filters. 2nd presentation: Arsenic-free drinking water thanks to bacteria

International Congress & Exhibition on Arsenic in the Environment, Bhubaneswar, India, 2024
Keynote speaker - A biotechnological perspective on arsenic removal in groundwater filters

Young Water Professionals conference, Delft, Netherlands, 2022
Vivianite precipitation for iron recovery from anaerobic groundwater

United Nations Water Conference, New York, USA, 2023
Hosting 2 events and panel speaker: 'A trans-continental forum on setting the water action agenda for sustainable development' and 'Water Innovations for Sustainable Development'

Amsterdam International Water week, Netherlands, 2021
Vivianite precipitation for iron recovery from anaerobic groundwater

European Congress of Chemical Engineering and Applied Biotechnology, Online, 2021
Vivianite precipitation for iron recovery from anaerobic groundwater
Second price 'Science slam'


TU Delft
619


TEKNOWLOGY
Open Mind
2021
€50,000
Fifty thousand euros
Roos Goedhart

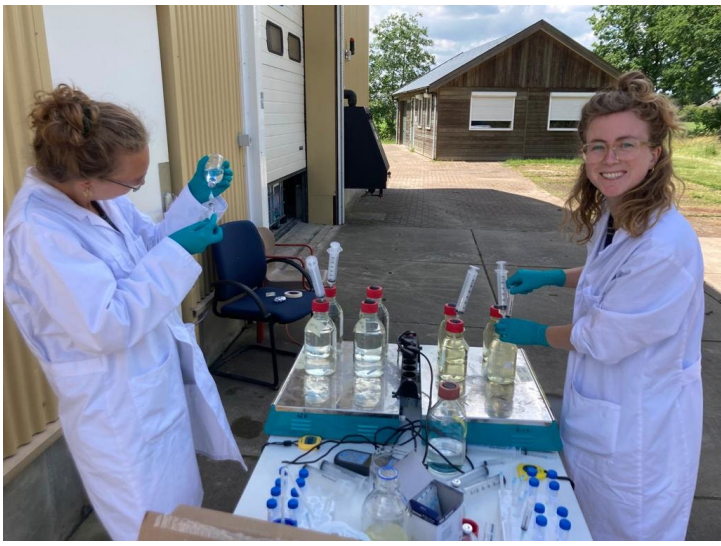

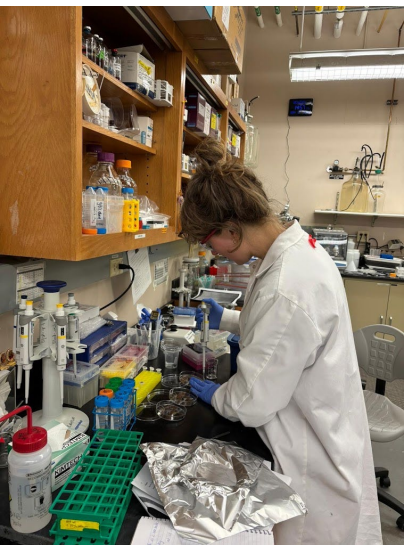


TU Delft
Water for Impact


Science for
people.
Worldwide











#WATERACTION


BIOLOGY

Four months into my PhD, I was awarded an Open Mind grant by the Dutch Research Council (NWO). The grant gave me the opportunity to set up my own research alongside my PhD project.

CHEMISTRY

The work resulted in three papers, which are included as an appendix to this thesis.

FROM WASTE TO VALUE

ANOXIC IRON RECOVERY FROM GROUNDWATER

APPENDIX

Ignorance was never bliss to me

Joe James & Loyle Carner

Introduction

Groundwater is a major source of drinking water worldwide and serves approximately half the world population [1]. Its use is expected to increase further in the coming decades due to population growth and rising water demand [2]. The deep aquifers used for drinking water production are typically anaerobic and contain elevated concentrations of reduced iron (Fe^{2+}). The World Health Organization sets a guideline of 0.3 mg/L for iron in drinking water, while the concentrations in raw groundwater can be as high as 100 mg/L [3].

Aeration followed by sand filtration has been the standard groundwater treatment method for centuries. This simple and robust technology is highly effective for the removal of iron, as well as for other common groundwater constituents such as manganese and ammonium. Iron is typically the first contaminant to be removed in the process: upon aeration, Fe^{2+} oxidizes to Fe^{3+} and precipitates as iron (hydr)oxides. Accumulation of iron precipitates delay the removal of other groundwater contaminants and clogs the filter bed [4], which causes the need of periodically backwashing the filter bed.

Backwashing disrupts the steady state of the filter bed, creating a dynamic and complex system [5]. Additionally, the treatment process must be temporarily stopped, decreasing the efficiency. A residual stream is created, referred to as 'iron sludge', which is the largest byproduct of groundwater treatment. In the Netherlands alone, the volume is around 100.000 ton per year [6]. The related disposal costs is a key driver behind the operational cost of water treatment [7].

This research deliberately breaks with this centuries-old method. Supported by the NWO Partnership program 'Dunea – Vitens: Sand Filtration' (project 17830) and an NWO Open Mind grant (project 19541), we explore the novel alternative of retaining iron in its reduced state and recover it anaerobically as a mineral. No longer considering iron as an inevitable byproduct but rather treating it as a valuable resource. This fits the growing trend in the drinking water industry, in which resource recovery and circularity are increasingly recognized as an important strategy.

The first strategy tested focuses on recovery of iron via vivianite ($Fe_3(PO_4)_2 \cdot 8\ H_2O$), an Fe(II)-phosphate mineral recognized in wastewater treatment for phosphorus recovery [8]. **Chapter 1** addresses:

Research Question 1: Can iron be recovered from anaerobic groundwater as vivianite, and how does this novel approach compare to conventional aeration-based removal in terms of efficiency, kinetics, and sludge volume?

Chapter 2 extends this concept to concentrate streams – an increasingly relevant residual stream in drinking water production. As membrane technologies are adopted to remove emerging contaminants, managing the iron-rich concentrate becomes a challenge. Here we investigate:

Research Question 2: How effectively can iron be recovered from anaerobic reverse osmosis (RO) concentrate streams through vivianite precipitation, and what is the impact of co-removal of divalent cations (Mn^{2+}, Mg^{2+}, and Ca^{2+}) on the removal efficiency and structure of the precipitated vivianite?

While vivianite recovery requires phosphate addition – a critical raw material – alternative Fe(II) minerals can offer a phosphate-free removal strategy. Therefore, **Chapter 3** explores anoxic iron sulfide formation as an alternative recover pathway:

Research Question 3: Can anoxic iron sulfides formation serve as an effective alternative to conventional aeration-filtration methods for iron removal in groundwater treatment, and what are the advantages compared to conventional iron removal?

References

1. United Nations. *The United Nations World Water Development Report 2024: Water for Prosperity and Peace*. UNESCO; 2024.

2. Loaiciga HA, Doh R. Groundwater for People and the Environment: A Globally Threatened Resource. *Ground Water*. 2023;62(3):332-340. doi:10.1111/gwat.13376

3. Pattnaik R, Adhya TK. Hydrologic fluxes of iron in groundwater ecosystems: Implications for global risks and challenges. *Inorganic Contaminants and Radionuclides*. 2024;15(1):215-238. doi:10.1016/B978-0-323-90400-1.00013-6

4. Van Beek CGEM, Hiemstra T, Hofs B, Nederlof MM, Van Paassen JAM, Reijnen GK. Homogeneous, heterogeneous and biological oxidation of iron(II) in rapid sand filtration. Published online 2012. doi:10.2166/aqua.2012.033

5. Corbera-Rubio F, Goedhart R, Laureni M, van Loosdrecht MC, van Halem D. A biotechnological perspective on sand filtration for drinking water production. *Curr Opin Biotechnol*. 2024;90:103221. doi:10.1016/J.COPBIO.2024.103221

6. AquaMinerals. *Annual Report AquaMinerals 2024*. 2024.

7. Turner T, Wheeler R, Stone A, Oliver I. Potential Alternative Reuse Pathways for Water Treatment Residuals: Remaining Barriers and Questions-a Review. *Water Air Soil Pollution*. 2019;230(227). doi:10.1007/s11270-019-4272-0

8. Prot T, Wijdeveld W, Eshun LE, et al. Full-scale increased iron dosage to stimulate the formation of vivianite and its recovery from digested sewage sludge. *Water Res*. 2020;182:115911. doi:10.1016/j.watres.2020.115911

A2

Vivianite Precipitation for Iron Recovery from Anaerobic Groundwater

Published as:
Goedhart, R., Müller, S., van Loosdrecht, M. & van Halem, D. (2022). Vivianite precipitation for iron recovery from anaerobic groundwater. Water Research, 217, 118345.

Abstract

Iron in anaerobic groundwater is commonly removed by oxidation followed by sand filtration. This produces large volumes of iron(III)(hydr)oxide sludge with little value. Our research investigates the novel concept of anaerobic iron(II) recovery from groundwater as the valuable mineral vivianite ($Fe_3(PO_4)_2 \cdot 8\ H_2O$) by the addition of phosphate to the water. We found that vivianite precipitated both in synthetic and natural groundwater when the saturation index (SI) was higher than 4. The SI can be increased by elevating the pH, which allows for iron removal at lower concentrations. Anaerobic iron removal reached 93.7% in natural groundwater, which increased further to 99.9% after a subsequent aeration step. Vivianite precipitation followed second order kinetics with a rate constant of 2.3 $M^{-1}s^{-1}$ and the sludge volume decreased by two third compared to iron oxidation. We therefore conclude that anaerobic iron removal is a promising new approach towards sustainable groundwater treatment.

A2.1 Introduction

The deep aquifers used for the production of drinking water are typically anaerobic and contain reduced iron (Fe^{2+}). The World Health Organization (WHO) recommends a maximum iron concentration of 0.3 mg/L in drinking water [1], while concentrations in raw groundwater of 15 mg/L are not exceptional [2,3]. Iron removal is one of the major challenges in drinking water production from anaerobic groundwater [4]. The conventional method of iron oxidation followed by granular filtration removes iron from the water, extensively discussed by Chaturvedi and Dave (2012), Van Beek et al. (2012) and others. This produces large volumes of watery iron(III)(hydr)oxide sludge with little value; currently an inescapable by-product of the groundwater treatment.

Backwashing the filter and disposing the sludge are cost-intensive steps in the production of potable water [7,8]. In water treatment plants around the globe, 10,000 tons of sludge are estimated to be produced per day [9]. The reuse of waterworks sludge has been reported a key step in increasing the economic and environmental sustainability of the industry [10,11]. Although some reuse opportunities of the currently produced sludge (e.g. as coagulant in wastewater treatment) are discussed by e.g. Ahmad et al. (2016), they come with several disadvantages and the pressure to find more sustainable solutions to avoid landfill disposal increases [8]. The stringent regulations for waste disposal together with an ever-increasing demand for clean and safe drinking water are the drivers to find a more efficient approach to handle the iron sludge.

This research proposes a novel concept to remove iron from groundwater: anaerobic precipitation with phosphate to form the mineral vivianite. Vivianite ($Fe_3(PO_4)_2 \cdot 8\ H_2O$) is an iron(II)-phosphate mineral commonly found in reducing environments rich in iron and phosphate, such as sediments of lakes, swamps, waterlogged soils, wastewater sludge etc. [13,14]. The colourless mineral turns blue upon gradual oxidation of Fe(II). Crystal growth can occur when the mineral saturation state is above the solubility equilibrium value, the solubility product constant (K_{sp}) of vivianite is reported to be 10^{-36} [15]. Al-Borno and Tomson (1994) found that the temperature has very little effect on the K_{sp} of vivianite.

Iron recovery from groundwater via vivianite crystallisation could create a compact end-product instead of the watery and voluminous iron sludge. The removal of iron in the reduced state contrasts the widely applied method of oxidation. Recently, the value of vivianite precipitation has been recognized in wastewater treatment to recover phosphate (PO_4) from the water by dosing iron [13,17]. The hypothesis of our study was that iron can be recovered from groundwater as vivianite when phosphate is dosed anaerobically. Vivianite can form from Fe^{2+} with either free [13] or protonated phosphate [18]:

$$3\ Fe^{2+} + 2\ PO_4^{3-} + 8\ H_2O \rightarrow Fe_3(PO_4)_2 \cdot 8\ H_2O \quad (1.1)$$

$$3\ Fe^{2+} + 2\ HPO_4^{2-} + 8\ H_2O \rightarrow Fe_3(PO_4)_2 \cdot 8\ H_2O + 2H^+ \quad (1.2)$$

$$3\ Fe^{2+} + 2\ H_2PO_4^{-} + 8\ H_2O \rightarrow Fe_3(PO_4)_2 \cdot 8\ H_2O + 4H^+ \quad (1.3)$$

The speciation of phosphate (Figure S.1. in Supplementary Information) depends on pH. At the pH of typical groundwater (pH 6.5-8.0), protonated phosphate dominates and the formation of vivianite will release protons. The pH dependent speciation of phosphate and iron and their total concentrations influence the saturation index (SI) of vivianite, which indicates if the mineral is supersaturated with respect to the solution. The expression of the SI is [19]:

$$SI = \log \frac{IAP}{K_{sp}} \tag{1.5}$$

With the formula of vivianite $Fe_3(PO_4)_2 \bullet 8\ H_2O$ the ion activity product (IAP) becomes:

$$IAP = (\gamma_{Fe^{2+}} \cdot C_{Fe^{2+}})^3 \left(\gamma_{PO_4^{3-}} \cdot C_{PO_4^{3-}}\right)^2 \tag{1.6}$$

In which γ is the activity coefficient of the corresponding ion in the solution (mol/L).

Studies so far have primarily focused on understanding vivianite formation pathways where microorganisms play a direct or indirect role, e.g., in sediments [14] or wastewater treatment [20,21]. However, the proposed iron removal strategy for groundwater is strictly abiotic, which makes the process conditions unique compared to previous research on vivianite formation. Consequently, known factors to influence vivianite formation such as co-occurring constituents or solution pH might be different. The main objective of this research was therefore to investigate abiotic precipitation of vivianite from anaerobic groundwater, with a particular focus on iron removal efficiencies, kinetics, and sludge volumes. To do so, experiments were conducted with natural and synthetic groundwater, under strictly anaerobic conditions. Produced solids were characterized by X-Ray Diffraction (XRD) to determine presence of vivianite.

A2.2 Materials and Methods

A2.2.1 Synthetic and natural groundwater

The experiments were conducted with two types of water: (i) a synthetic iron solution, where 50 mL of a 0.018 M $FeCl_2 \cdot 4\ H_2O$ (Sigma-Aldrich) stock solution was added to 400 mL demineralised deoxygenated water, flushed with N_2 (impurity <200 vpm) for at least 45 minutes in advance, and (ii) natural groundwater collected at a groundwater treatment plant in Loosdrecht, the Netherlands. In synthetic water, the iron removal efficiency was measured for initial concentrations of 1, 10, 25, 50 and 100 mg Fe/L. In groundwater, experiments were executed with the background iron concentration (around 3.8 mg Fe/L, see Table 1). To ensure enough precipitate would form for further analysis, groundwater was also spiked with $FeCl_2$ to reach an elevated concentration of 100 mg Fe/L. To prevent air contamination of the natural groundwater samples, 1L glass bottles (Schott DURAN®) were filled with a tube at the bottom and the water volume was replaced ten times before closing them with bromobutyl rubber stoppers secured with an open topped cap. After transportation, the bottles were stored in an anaerobic environment. Prior to the experiment, the natural groundwater was vacuum filtered with a 0.45 µm polyethersulfone membrane

(Pall Supor®) in the anaerobic environment. The average composition and pH of the natural groundwater are presented in Table 1.

Table 1: Composition of the natural groundwater, n=4. SD = Standard deviation

Parameter	Fe	P	Mn	Na	Mg	Si	S	Ca	pH
Conc. (mg/L)	3.81	0.18	0.12	7.78	2.16	8.26	3.39	36.18	7.39
SD	0.14	0.03	0.001	0.11	0.02	0.13	0.60	0.94	-

The phosphate and carbonate stock solutions used were prepared in the anaerobic environment by dissolving respectively Na_2HPO_4 and Na_2CO_3 to obtain a 0.018 M PO_4/CO_3 solution, in oxygen free water. All chemicals met or exceeded ACS reagent grade.

A2.2 Experimental setup

A vinyl (PVC) anaerobic chamber (Coy Laboratory Products, USA) filled with a gas mixture of 5% hydrogen and 95% argon gas (impurity <200 vpm) was used for the anaerobic experiments. The chamber had an airlock and weekly regenerated palladium catalysts to secure anaerobic conditions. Water vapor was entrapped by silica beads to keep the humidity < 70% (measured by a hygrometer). All experiments were performed at room temperature of approximately 21 °C.

The approach of the experiments is presented in Figure 1. A glass reactor with 450 mL of either the synthetic or natural groundwater was placed on a magnetic stirrer. While stirring continuously, 50 mL of the phosphate stock solution was added to achieve a 1:1 molar ratio (phosphate:iron) after which the solutions could react anaerobically. To track reaction kinetics, water samples were taken during the reaction and when no additional iron removal was observed, solids were collected for XRD. All water samples were immediately filtered through a 0.45 µm non-sterile Millex® Syringe filter with Durapore® membrane and acidified with HCl to bring the pH below 4 to prevent further reaction.

An aeration step was added (Figure 1, right) after the anaerobic reaction, the reactor was removed from the anaerobic chamber and flushed with compressed air for 10 minutes. After a 50 min period, the suspension was transferred to a plastic Imhoff cone of 1L. The volume of the liquid and sludge was measured after one day of settling and solids were collected for XRD. A set of reference experiment simulated the conventional treatment of oxidation and filtration, in which no phosphate was dosed for anaerobic iron precipitation. To compare sludge volumes, a set of experiments was conducted following the same procedure in which carbonate was anaerobically dosed instead of phosphate.

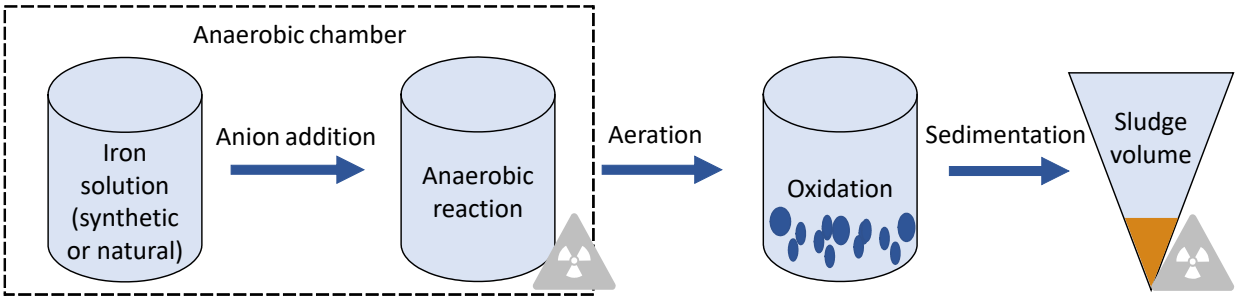

Figure 1: Graphical representation of the experimental setup, from anaerobic precipitation in the anaerobic chamber (left) to aeration and sedimentation under ambient conditions (right). The radiation icon indicates moments of solid sampling for analysis by XRD.

A2.3 Analysis

During the experiments, the pH, oxidation reduction potential (ORP), electrical conductivity (EC) and temperature were measured with a Multi-parameter electrode (Sension+ 5048 with MM150 multimeter, HACH) and the dissolved oxygen (DO) concentration with an optical DO sensor (WTW, FDO® 925). The concentration of DO stayed below 0.05 mg O_2/L during all experiments.

Iron concentrations and phosphate concentrations were measured with the standard phenantroline method (LCK 320 kits, HACH) for iron(II) and total iron and standard molybdenum blue method (LCK 348 kits, HACH) respectively. A HACH DR 3900 VIS spectrophotometer measured the absorbance and automatically calculated concentrations.

In the experiments in which natural groundwater was used, total iron and phosphorus concentrations were determined by inductively coupled plasma mass spectrometry (ICP-MS). The samples for ICP-MS analysis were acidified by adding 65% ultrapure HNO_3 to 1% vol.

XRD was applied to characterize the precipitates. The suspension was vacuum filtered with a 0.45 µm polyethersulfone membrane (Pall Supor®). For the anaerobic samples, the filter was covered in aluminium foil to prevent photo-oxidation and dried inside the anaerobic chamber for a day. Afterwards, the filter was covered with a layer of glycerol to minimise oxidation during XRD analysis open to the atmosphere. A Bruker D8 Advance diffractometer with Cu-Ka radiation was used for the XRD analysis, with coupled µ - 2µ scan 10°- 120°, step size 0.030 °2µ, counting time per step 2 s. Bruker software DiffracSuite.Eva vs 5.2 was used for the data evaluation.

A2.4 Geochemical Model

The saturation index of vivianite was calculated using the program Spec8 of the Geochemist's Workbench ® (GWB®) model and the standard database. The input was the measured iron and phosphate concentrations, pH and temperature.

A2.3 Results

A2.3.1 Vivianite precipitation in synthetic water

At initial iron concentrations above 25 mg/L, phosphate addition to the synthetic anaerobic solution removed iron from the water with a maximum recovery of approximately 79% (Figure 2a). XRD analysis of the generated solid phases showed that only vivianite crystallised in the samples (Figure 2b). At the lower initial concentration of 10 mg Fe/L, iron recovery remained below 35%, and for 1 mg Fe/L no iron removal was observed. The pH of the system depended on the concentration of iron and phosphate; for 1 mg Fe/L the pH was around 7.7 while it was 6.9 for an initial concentration of 100 mg Fe/L.

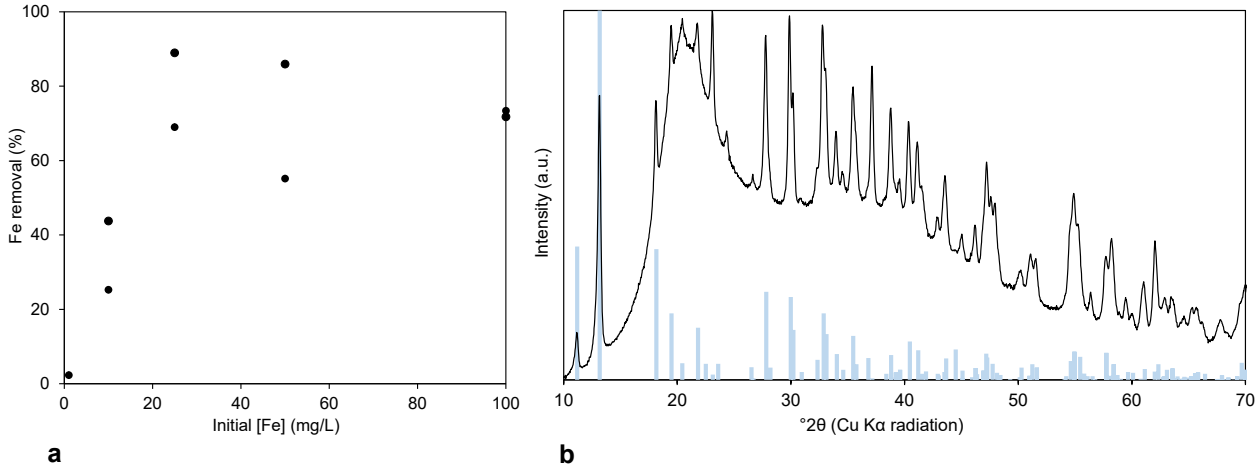

Figure 2 ***a)*** *Iron removal by vivianite crystallisation at different initial iron concentrations in synthetic groundwater. Reaction time 60 min, ratio PO_4:Fe 1:1. Data of duplo experiments given. Because of measurement error only one data point for 1 mg Fe/L.* ***b)*** *XRD pattern of the formed crystals (black line) on the filter at an initial iron concentration of 100 mg/L with the reference pattern of vivianite (blue bars).*

A2.3.2 Vivianite precipitation in natural groundwater

Anaerobic phosphate addition to natural groundwater also resulted in iron removal by vivianite crystallisation. With the background iron concentration of around 3.8 mg/L, the anaerobic removal was 16.9%. For the spiked groundwater with an elevated iron concentration of 100 mg/L, 93.7% of iron was recovered via vivianite crystallisation (Figure 3a). An additional oxidation step after the anaerobic reaction increased iron removal to 98.2% and 99.9% for the background and elevated iron concentrations, respectively. In both waters the efficiencies were approximately 3.5% higher than in the reference experiment of oxidation only; the addition of an anaerobic removal step improved the removal efficiencies. Vivianite was the only solid phase detected by XRD in this experiment, also after oxidation (Figure 3b). Pictures of the blue precipitate on the filter are presented in Figure 3c and 3d. The mass of anaerobic precipitate formed with the background iron concentration was too low to detect by XRD.

It is worth noting that to protect the samples from oxidation during XRD analysis, the anaerobic precipitates were covered with glycerol (see section 2.3). The background signal in Figure 2b and in the lower diffractogram of Figure 3b are probably caused by the glycerol. The glycerol was not added to the aerobic vivianite sample shown in the upper diffractogram of Figure 3b.

Rouzies and Millet (1993) specified that vivianite alters to metavivianite ($Fe^{2+}Fe_2^{3+}(PO_4)_2(OH)_2 \cdot 6H_2O$) at 50% iron oxidation in vivianite, which can be distinguished via its altered XRD spectrum [23]. No metavivianite is detected in the solids formed during the executed experiments of iron removal in groundwater. It is therefore concluded that the iron in the formed crystals were mainly present in its reduced Fe(II) form, even when an additional oxidation step was applied.

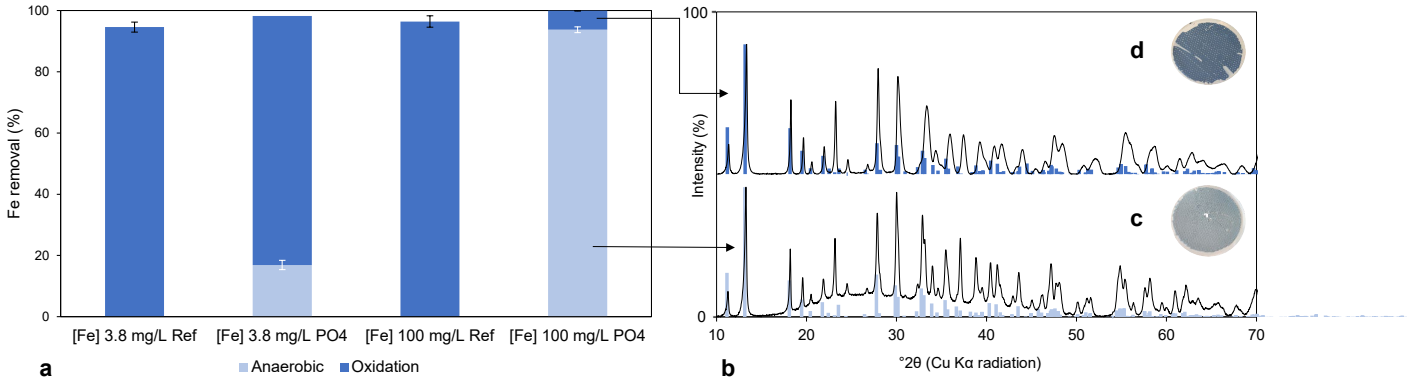

Figure 3 ***a)*** *Iron removal in the reference (Ref) experiment of iron oxidation and via anaerobic (AN) vivianite precipitation by phosphate (PO4) addition followed by an oxidation (OX) step in natural groundwater with the background iron concentration (3.8 mg Fe/L) and in spiked groundwater (100 mg Fe/L). AN and OX reaction time 60 min, ratio PO_4^-:Fe 1:1. Error bars are SD of n=2* ***b)*** *XRD patterns of the formed crystals during the anaerobic reaction in spiked natural groundwater to which phosphate was added (bottom diffractogram) and of the same crystals after the oxidation step (upper diffractogram) including the reference pattern of vivianite (blue bars).* ***c)*** *picture of formed anaerobic precipitate on filter and* ***d)*** *precipitate after oxidation*

A2.3.3 Kinetics and SI

In Figure 4, the removal kinetics (black circles) and calculated SI (blue circles) are depicted for the experiments with synthetic and natural groundwater containing an elevated initial iron concentration of 100 mg Fe/L. Iron removal stopped after 10 minutes in the synthetic solution, while in natural groundwater the removal continued for 60 minutes. A second order removal rate was found for both the iron removal in synthetic and natural groundwater (black lines). The rate constants were found to be 2.7 $M^{-1}s^{-1}$ (95% confidence interval [1.7, 3.6]) and 2.3 $M^{-1}s^{-1}$ (95% confidence interval [1.9, 2.7]) for synthetic and natural groundwater, respectively. The half-life of iron when removed via vivianite precipitation in both synthetic and natural groundwater is approximately 4 minutes for an initial concentration of 100 mg Fe/L.

From Figure 4 it is apparent that the vivianite precipitation reaction stopped after reaching the approximate SI of 4 (blue dotted line in Figure 4). In the synthetic solution, an SI < 4 is reached sooner (at minute 10) than in natural water (at minute 60), caused by stronger pH changes in the system. A pH drop from 6.9 to 5.8 occurred during the experiment with synthetic water, which was not observed in the natural groundwater due its higher alkalinity (graph in Supplementary Information, Figure S.2).

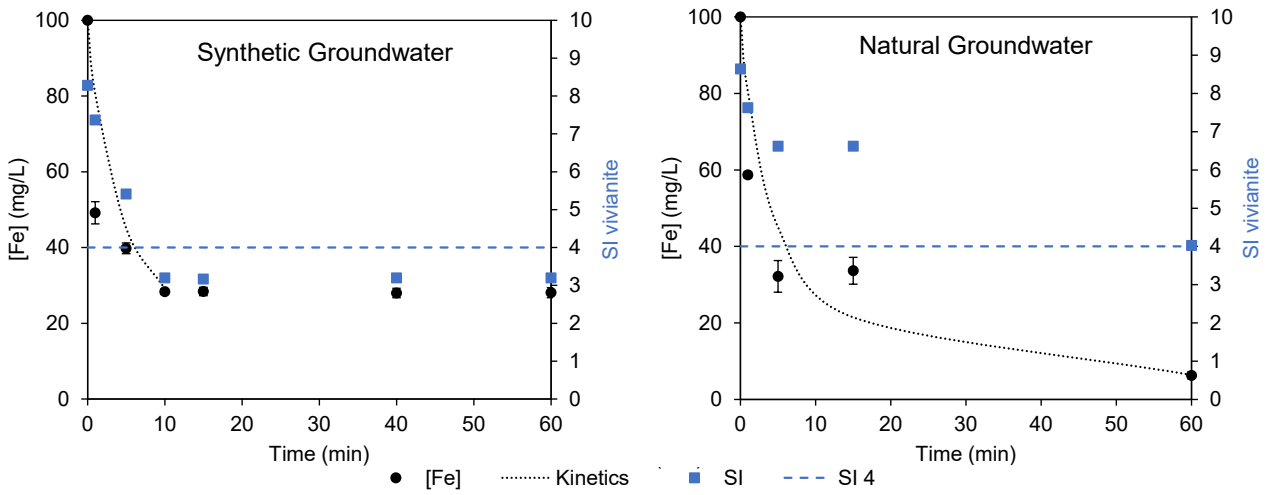

Figure 4: Dissolved iron concentration over time and the corresponding modelled SI of vivianite in synthetic (left) and natural groundwater (right) with an initial [Fe] of 100 mg/L. The kinetic relation is shown for points with a SI higher than 4. Kinetic relation synthetic water: $\frac{d[Fe]}{dt} = 2.7\ [Fe]^2$ *Kinetic relation natural groundwater:* $\frac{d[Fe]}{dt} = 2.3\ [Fe]^2$ *. Error bars are SD of n=2, most [Fe] error bars too small to see.*

The calculated kinetics of both (homogeneous) iron oxidation with oxygen and anaerobic removal via vivianite formation are plotted in Figure 5. The kinetics of homogeneous iron oxidation follows first-order removal with respect to Fe^{2+} at constant pH and DO. The rate law used in Figure 5 was determined by Sung and Morgan (1980) with a rate constant of $k = 2.1 \cdot 10^{13}\ M^{-2}\ min^{-1}$ as published by Schenk and Weber (1968). The rate of iron oxidation strongly depends on pH, Figure 5 provides the rate at groundwater-relevant pH's of 6.5, 7.0 and 7.5. The rate of vivianite precipitation is determined at pH 7, at which the half-life of iron is four times shorter than in iron oxidation at pH 7. This implies that iron recovery via vivianite precipitation has the potential to make the groundwater treatment system more efficient.

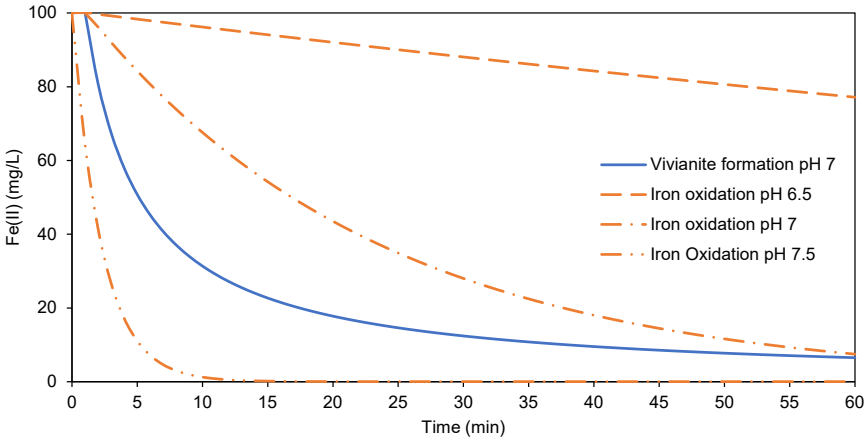

Figure 5: Kinetics of iron removal in natural groundwater by vivianite precipitation and by iron oxidation at pH 6.5, 7.0 and 7.5. Integrated rate law iron oxidation: $[Fe(II)]=[Fe(II)]e^{k1t}$, $k1 = k[OH^-]^2 \bullet p_{O2}$, $k = 2.1 \bullet 10^{13} M^{-2} atm^{-1} min^{-1}$ [25]. Integrated rate law vivianite precipitation: $[Fe(II)]= 1/kt + [Fe(II)]_0$ $k = 2.3\ M^{-1}s^{-1}$

A2.3.4 pH and iron concentration

The removal kinetics for the experiment with natural groundwater (background iron concentration of 3.8 mg Fe/L) are shown in Figure 6. As also seen in Figure 4, no additional removal is obtained when the SI dropped below the value of 4. The SI dropped below 4 in the first minute, while the pH of the system was around 7.7, which was higher than in the two experiments with elevated iron concentrations (see section 3.3). It demonstrates that both the pH and the initial iron concentration influence the SI of Vivianite.

Since the pH was not controlled during the experiments, the relation between SI and pH was modelled for different initial iron concentrations (Figure 7) in synthetic water. The boundary for vivianite crystallisation was found to be at a SI of 4. For a low iron concentration of 1 mg/L the model implies that vivianite crystallisation will only occur at a pH of 8.5. The higher iron removal in natural groundwater compared to the synthetic water can also be explained by this relationship. The alkalinity of the natural groundwater avoided a strong pH drop during vivianite formation, maintaining a higher SI.

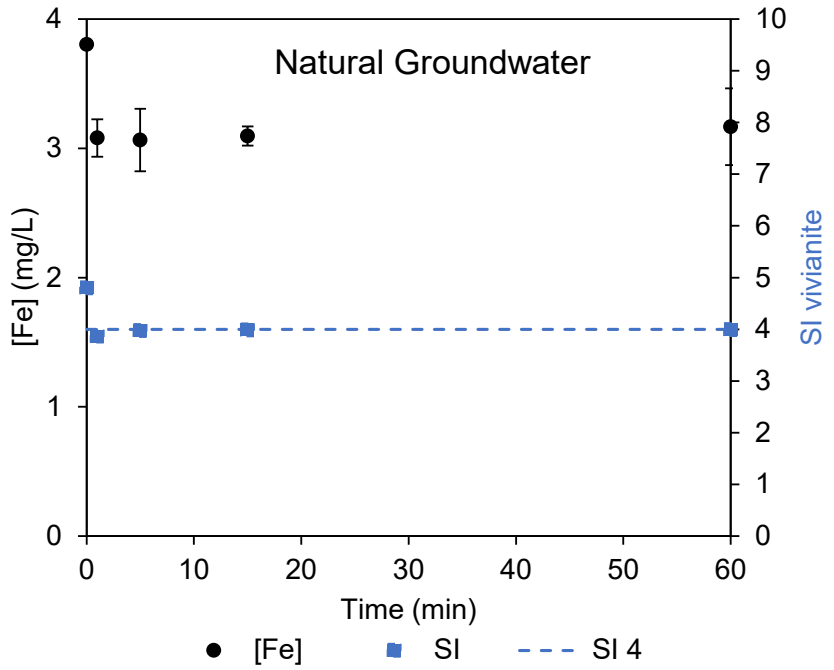

Figure 6: Dissolved iron concentration over time and the corresponding modelled SI of vivianite in natural groundwater with the background [Fe] of 3.8 mg/L. Error bars are SD of n=2, some [Fe] error bars too small to see.

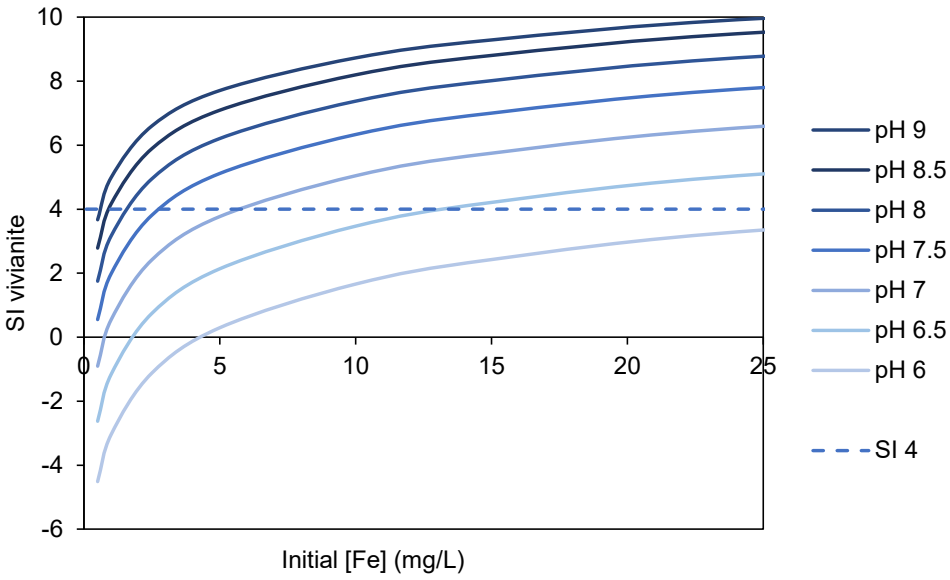

Figure 7: The modelled saturation index of vivianite at different initial iron concentration at different pH's. Modelled with GWB® spec8, ratio PO_4:Fe 1:1 at 21°C

A2.3.5 Sludge volume

Figure 8a shows that anaerobic precipitation of ferrous iron with phosphate reduces the sludge volume to a third compared to the conventional iron oxidation method. This considerable reduction was both obtained in the synthetic as in the spiked natural groundwater solution. The sludge volume formed in the groundwater without iron spiked was too small to measure. As a comparison, anaerobic carbonate addition was also tested, which increased the sludge volume approx. 6 times compared to the oxidation method. The difference in appearance and volume of the formed sludge is visible in Figure 8b, which also illustrates that vivianite settled better than the products of iron oxidation or carbonate addition.

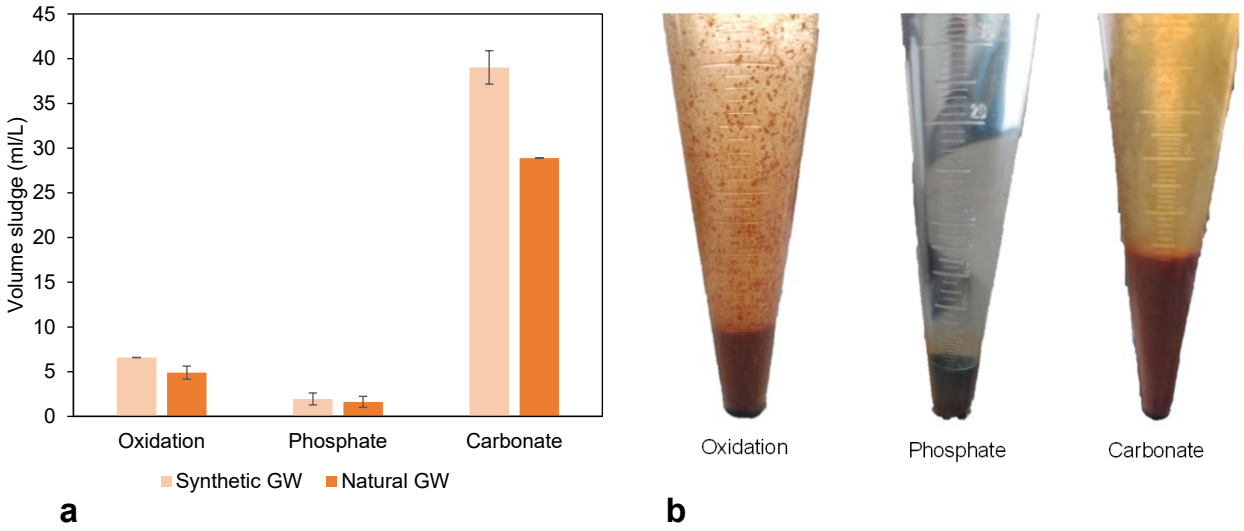

*Figure 8: **a)** Volume and **b)** appearance of sludge produced during iron oxidation (reference) and by anaerobic addition of phosphate or carbonate followed by oxidation in synthetic and natural groundwater. AN and OX reaction time 60 minutes, [Fe] initial 100 mg/L, ratio anion:Fe 1:1. Error bars are SD of n=2.*

A2.4 Discussion

A2.4.1 Conditions for abiotic vivianite crystallisation

The anaerobic groundwater conditions were shown to be feasible for abiotic vivianite crystallisation. The removal efficiencies of iron in the experiments with anaerobic treatment followed by oxidation were approximately 3.5% higher compared to iron oxidation only. The kinetics at neutral pH are faster, the half time of iron with anaerobic precipitation is 4 times shorter compared to iron oxidation. However, this is only applicable to conditions where the SI of vivianite crystallisation exceeds 4. This finding is in line with the outcome of Liu et al. (2018), who determined that the supersaturation level at which efficient crystallisation can take place is between 4 and 11. With the geochemical model it is shown that the SI values of vivianite in the executed experiments were within this range, in which heterogeneous crystallisation is expected to take place [26].

In groundwater with low to moderate iron concentrations (<25 mg/L) exceeding SI 4 might be particularly challenging. A possible solution to increase the SI of vivianite is to elevate the pH, which is a common procedure in groundwater treatment. A base can be dosed alongside the phosphate or the pH can be increased by stripping CO_2 with a vacuum degasser. OH^- ions can however trap the free Fe^{2+}, which makes the iron unavailable for vivianite precipitation [18]. A more attractive method might be to lower the supersaturation demand by the addition of a seeding material, such as quartz grains [18] or sponge iron [27]. Quartz is already a commonly used seeding material in groundwater treatment, e.g. in (anaerobic) pellet softening [28]. The addition of quartz in an anaerobic reactor before the oxidation step to offer a seeding material might therefore be a straightforward solution.

An alternative approach to increase the SI is to concentrate the iron in groundwater prior to the addition of phosphate. Anaerobic nano filtration and reverse osmosis are becoming competitive options to the conventional groundwater treatment technologies, since the quality of the produced water is high, the processes are easy to operate and a small footprint is required [29]. However, the disposal of the concentrate is an important issue regarding membrane processes (Van der Bruggen et al., 2003), which is expected to become more difficult in the future because of stricter European legislation [31]. Anti-scalants containing phosphate are often dosed during membrane filtration, which can cause eutrophication in the receiving waterbodies [32]. Controlled vivianite formation might be a suitable alternative to remove both the iron and phosphate in the anaerobic concentrate while the resources are recovered. The concentration of iron depends on the inlet concentration and the water recovery, but the concentrate typically contains 4 to 10 times higher concentrations than the feedwater [29], making it suitable for vivianite precipitation.

A2.4.2 Vivianite recovery: scope for application

Although vivianite is known to have a market value, its end use will depend on the grade of the vivianite obtained [33]. A knowledge gap in literature can be identified on the properties of the formed vivianite in (waste) water systems [13]. To investigate this will be a logical and valuable next step, which can give clarity about the value of the recovered vivianite versus the costs of the phosphate dosage and benefits of compact iron sludge. Recovery of vivianite from the water can be achieved by conventional granular filtration and periodically backwashing the filter bed. Vivianite is a paramagnetic mineral, which makes magnetic separation an alternative recovery option [33].

Important to acknowledge is that phosphate is a limited resource, making recovery of phosphate a key aspect of the approach. In the conducted experiments, phosphate was always slightly overdosed (P/Fe ratio of 1 while theoretical ratio is 0.67). In practice, residual phosphate in the produced drinking water is not desired. Identification of the optimal phosphate dosage for scaling up is therefore required, which depends on the pH (and SI) of the groundwater.

An alternative to phosphate dosage might be anaerobic iron precipitation by the addition of another anion. For example, Fe^{2+} can react with carbonate (log K 10.59 at 25°C) and sulphide

(log K 3.6 at 25 °C) [18], which can control Fe^{2+} concentrations in anaerobic aquifers [34]. We demonstrated that for anaerobic iron removal carbonate addition is possible, but this resulted in a significant increase in sludge volume. The iron-carbonate interaction might also impact iron recovery via vivianite precipitation in groundwater systems that contain high inorganic carbon concentrations. However, both Wu et al. (2019) and Liu et al. (2018) showed that iron precipitation with phosphate favours over carbonate for alkalinity up to 1000 mg/L. For sulphide, competition becomes significant at concentrations of 1.5 mM and the effect is neglectable up to 0.5 mM [18]. Concentrations of sulphide in groundwater are not common to transcend this value (thermal waters rich in H_2S have a concentrations of around 0.5 mM).

The production of vivianite and the corresponding reduction in sludge volume can reduce the costs of water treatment. The treatment of backwash water is currently a major contributor to the total cost of drinking water production [8]. Additionally, the production of compacter sludge reduces the transport and processing costs of the sludge. Vivianite also has an economic value in chemical and agricultural industries; it can be used as a pigment [35], in lithium ion batteries [36], as a slow P-release fertilizer [37] and to replenish Fe-poor soils [38].

The above discussed advantages and possibilities make iron removal and recovery via vivianite crystallisation an interesting approach for application in groundwater treatment plants to increase the environmental and economical sustainability of the industry. The concept is so far only tested in small batches. Given the promising results, scaling up this technology will be tested in continuous flow by the addition of an anaerobic reactor prior to the existing treatment system.

A2.5 Conclusion

The current research successfully demonstrated the recovery of iron from anaerobic groundwater via vivianite precipitation. No longer considering iron sludge a waste but rather a new resource, our study offers a new approach in the drinking water industry. A follow up question is how the vivianite can be recovered and reused from the stream, which can make groundwater treatment a more sustainable industry. Our novel technique reduces the volume of iron sludge produced to a third compared to the conventional technique of iron oxidation, while reaching similar or higher removal efficiencies. The 4 times shorter halftime found for anaerobic iron removal at pH 7 can lead to filters with a higher throughput rate and requires less backwashing. This can contribute to the design of efficient systems, while gaining economic savings.

Supplementary information

The Supplementary Information is available at
https://www.sciencedirect.com/science/article/pii/S0043135422003086

References

1. World Health Organization. *Guidelines for Drinking-Water Quality, 4th Edition, Incorporating the 1st Addendum*. WHO Library Cataloguing-in-Publication Data; 2017.

2. Ellis D, Bouchard C, Lantagne G. Removal of iron and manganese from groundwater by oxidation and microfiltration. *Desalination*. 2000;130(3):255-264. doi:10.1016/S0011-9164(00)00090-4

3. Kortatsi BK, Tay CK, Anornu G, Hayford E, Dartey GA. Hydrogeochemical evaluation of groundwater in the lower Offin basin, Ghana. *Environmental Geology 2007 53:8*. 2007;53(8):1651-1662. doi:10.1007/S00254-007-0772-0

4. Chaturvedi S, Dave PN. Removal of iron for safe drinking water. *DES*. 2012;303:1-11. doi:10.1016/j.desal.2012.07.003

5. Van Beek CGEM, Hiemstra T, Hofs B, Nederlof MM, Van Paassen JAM, Reijnen GK. Homogeneous, heterogeneous and biological oxidation of iron(II) in rapid sand filtration. Published online 2012. doi:10.2166/aqua.2012.033

6. Khatri N, Tyagi S, Rawtani D. Recent strategies for the removal of iron from water: A review. *Journal of Water Process Engineering*. 2017;19(13):291-304. doi:10.1016/j.jwpe.2017.08.015

7. Sharma SK, Kappelhof J, Groenendijk M, Schippers JC. Comparison of physicochemical iron removal mechanisms in filters. *Journal of Water Supply: Research and Technology-Aqua*. 2001;50(4):187-198. doi:10.2166/AQUA.2001.0017

8. Turner T, Wheeler R, Stone A, Oliver I. Potential Alternative Reuse Pathways for Water Treatment Residuals: Remaining Barriers and Questions-a Review. *Water Air Soil Pollution*. 2019;230(227). doi:10.1007/s11270-019-4272-0

9. Dharmappa HB, Hasia A, Hagare P. Water treatment plant residuals management. *Water Science and Technology*. 1997;35(8):45-56. doi:10.2166/wst.1997.0296

10. Albrektiene R, Karaliunas K, Baziene K. Sustainable reuse of groundwater treatment iron sludge for organic matter removal from river Neris water. *Sustainability (Switzerland)*. 2019;11(3):639. doi:10.3390/su11030639

11. Babatunde AO, Zhao YQ. Constructive approaches toward water treatment works sludge management: An international review of beneficial reuses. *Critical Reviews in Environmental Science and Technology*. *Taylor & Francis Group* . 2007;37(2):129-164. doi:10.1080/10643380600776239

12. Ahmad T, Ahmad K, Alam M. Sustainable management of water treatment sludge through 3'R' concept. *Journal of Cleaner Production*. *Elsevier Ltd*. 2016;124:1-13. doi:10.1016/j.jclepro.2016.02.073

13. Wu Y, Luo J, Zhang Q, et al. Potentials and challenges of phosphorus recovery as vivianite from wastewater: A review. *Chemosphere*. *Elsevier Ltd*. 2019;226:246-258. doi:10.1016/j.chemosphere.2019.03.138

14. Rothe M, Kleeberg A, Hupfer M. The occurrence, identification and environmental relevance of vivianite in waterlogged soils and aquatic sediments. *Earth Sci Rev*. 2016;158:51-64. doi:10.1016/J.EARSCIREV.2016.04.008

15. Nriagu JO. Stability of vivianite and ion-pair formation in the system fe3(PO4)2-H3PO4H3PO4-H2o. *Geochimica et Cosmochimica Acta*. 1972;36(4):459-470. doi:10.1016/0016-7037(72)90035-X

16. Al-Borno A, Tomson MB. The temperature dependence of the solubility product constant of vivianite. *Geochimica et Cosmochimica Acta*. 1994;58(24):5373-5378. doi:10.1016/0016-7037(94)90236-4

17. Wilfert P, Mandalidis A, Dugulan AI, et al. Vivianite as an important iron phosphate precipitate in sewage treatment plants. *Water Research*. 2016;104:449-460. doi:10.1016/j.watres.2016.08.032

18. Liu J, Cheng X, Qi X, et al. Recovery of phosphate from aqueous solutions via vivianite crystallization: Thermodynamics and influence of pH. *Chemical Engineering Journal*. 2018;349:37-46. doi:10.1016/j.cej.2018.05.064

19. Prot T, Wijdeveld W, Eshun LE, et al. Full-scale increased iron dosage to stimulate the formation of vivianite and its recovery from digested sewage sludge. *Water Research*. 2020;182:115911. doi:10.1016/j.watres.2020.115911

20. Wang S, An J, Wan Y, et al. Phosphorus Competition in Bioinduced Vivianite Recovery from Wastewater. *Environmental Science and Technology*. 2018;52(23):13863-13870. doi:10.1021/acs.est.8b03022

21. Cao J, Wu Y, Zhao J, et al. Phosphorus recovery as vivianite from waste activated sludge via optimizing iron source and pH value during anaerobic fermentation. *Bioresource Technology*. 2019;293. doi:10.1016/j.biortech.2019.122088

22. Rouzies D, Millet JMM. M6ssbauer study of synthetic oxidized vivianite at room temperature. *Hyperfine Interactions*. 1993;77:19-28.

23. Rothe M, Frederichs T, Eder M, Kleeberg A, Hupfer M. Evidence for vivianite formation and its contribution to long-term phosphorus retention in a recent lake sediment: A novel analytical approach. *Biogeosciences*. 2014;11(18):5169-5180. doi:10.5194/BG-11-5169-2014

24. Sung W, Morgan JJ. *Kinetics and Product of Ferrous Iron Oxygenation in Aqueous Systems*. Vol 12. 1980. doi:10.1021/ES60165A006

25. Schenk JE, Weber WJ. Chemical Interactions of Dissolved Silica With Iron (II) and (III). *Journal - American Water Works Association*. 1968;60(2):199-212. doi:10.1002/j.1551-8833.1968.tb03534.x

26. Li C, Sheng Y. Organic matter affects phosphorus recovery during vivianite crystallization. *Water Science and Technology*. 2021;83(8):2038-2050. doi:10.2166/WST.2021.112

27. Wu G, Zeng W, Li S, Jia Z, Peng Y. Phosphorus recovery from waste activated sludge by sponge iron seeded crystallization of vivianite and process optimization with response surface methodology. *Environmental Science and Pollution Research*. Published online 2021. doi:10.1007/s11356-021-14561-7

28. Harms WD, Bruce Robinson R. Softening by Fluidized Bed Crystallizers. *Journal of Environmental Engineering*. 1992;118(4):513-529. doi:https://doi.org/10.1061/(ASCE)0733-9372(1992)118:4(513)

29. Chelme-Ayala P, Smith DW, El-Din MG. Membrane concentrate management options: A comprehensive critical review. *Canadian Journal of Civil Engineering*. 2009;36(6):1107-1119. doi:10.1139/L09-042

30. Van der Bruggen B, Lejon L, Vandecasteele C. Reuse, Treatment, and Discharge of the Concentrate of Pressure-Driven Membrane Processes. *Environmental Science and Technology*. 2003;37(17):3733-3738. doi:10.1021/ES0201754

31. Nederlof MM, van Paassen JAM, Jong R. Nanofiltration concentrate disposal: Experiences in The Netherlands. *Desalination*. 2005;178(1-3 SPEC. ISS.):303-312. doi:10.1016/j.desal.2004.11.041

32. Jong RCM, Duiven J, Terhorst GG, Baas KJ. Implementation research of new phosphorus free antiscalant at an aerobic ground water RO plant. *New pub: Balaban*. 2013;51(25-27):5021-5025. doi:10.1080/19443994.2013.800342

33. Prot T, Nguyen VH, Wilfert P, et al. Magnetic separation and characterization of vivianite from digested sewage sludge. *Sep Purif Technol*. 2019;224:564-579. doi:10.1016/j.seppur.2019.05.057

34. van Beek CGEM, Cirkel DG, de Jonge MJ, Hartog N. Concentration of Iron(II) in Fresh Groundwater Controlled by Siderite, Field Evidence. *Aquatic Geochemistry*. 2021;27(1):49-61. doi:10.1007/S10498-020-09390-Y

35. Figueiredo MO, Silva TP, Veiga JP. The blue of iron in mineral pigments: A Fe K-edge XANES study of vivianite. *Applied Physics A: Materials Science and Processing*. 2010;99(2):357-361. doi:10.1007/s00339-010-5637-9

36. Raghupati Rao S, Varadaraju U V. Hydrothermal synthesis of LiFePO4 nanorods composed of nanoparticles from vivianite precursor and its electrochemical performance for lithium ion battery applications. *Bulletin of Materials Science*. 2015;38(5):1385-1388. doi:10.1007/s12034-015-1025-6

37. Yaya F, Nguetnkam JP, Tchameni R, Basga SD, Penaye J. Assessment of the Fertilizing effect of Vivianite on the Growth and yield of the Bean ‘“ phaseolus vulgaris ”’ on Oxisoils from Ngaoundere (Central North). *International Research Journal of Earth Sciences*. 2015;3(4):18-26.

38. Rombolà AD, Toselli M, Carpintero J, et al. Prevention of Iron-Deficiency Induced Chlorosis in Kiwifruit (Actinidia deliciosa) Through Soil Application of Synthetic Vivianite in a Calcareous Soil. *https://doi.org/101081/PLN-120024262*. 2007;26(10-11):2031-2041. doi:10.1081/PLN-120024262

39. Parkhurst DL, Appelo CAJ. Description of input and examples for PHREEQC version 3: a computer program for speciation, batch-reaction, one-dimensional transport, and inverse geochemical calculations. *Techniques and Methods*. Published online 2013. doi:10.3133/TM6A43

A3

Vivianite Recovery from Anaerobic Groundwater Reverse Osmosis Concentrate

Published as:
Goedhart, R., Koudijs, N., van Loosdrecht, M. & van Halem, D. (2025). Vivianite recovery from anaerobic groundwater reverse osmosis concentrate. Water Research, 285, 124101.

Abstract

To meet the increasing drinking water demand, membrane technologies are used to treat previously unavailable water sources. The waste stream of membrane technologies, called concentrate, contains concentrated valuable resources and must be treated before disposal. We studied the recovery of iron from different groundwater matrices and anaerobic reverse osmosis (RO) concentrates via precipitation of vivianite and the co-removal of other common groundwater divalent cations Mn^{2+}, Mg^{2+} and Ca^{2+} during vivianite precipitation. The formed precipitates were characterized using X-Ray Diffraction and Scanning Electron Microscope. Vivianite precipitation removed a maximum of 89% of Fe^{2+} in raw groundwater and 52% Fe^{2+} from RO concentrate. Substantial co-removal of Mn^{2+} (max 91%) and limited co-removal of Mg^{2+} (max 7%) were found, without hindering Fe removal efficiencies or altering morphological changes of the vivianite crystal. In contrast, co-removal of Ca^{2+} occurred at the expense of iron removal, forming amorphous calcium phosphate precipitates. This study shows the potential of vivianite precipitation for iron recovery across a wide range of groundwater matrices and highlights the need for further research to optimize this novel method to treat concentrate streams that are challenging to dispose of.

A3.1 Introduction

Groundwater in deep anaerobic aquifers is recognized for its excellent quality, making it a popular source for drinking water. A natural and common contaminant in anaerobic groundwater is iron (Fe^{2+}). Drinking water can contain a maximum concentration of 0.3 mg Fe/L [1]. The most common and ancient treatment method for groundwater is aeration followed by sand filtration. In this process, Fe^{2+} is oxidized to Fe^{3+}, which precipitates immediately as iron flocs ($FeOH_3$) [2]. The flocs are subsequently retained in the filter bed and thereby removed from the water stream [3]. Removal of iron comes with several challenges. The formed flocs clog the filter bed, requiring frequent backwashing [4]. The water needed for backwashing and the temporarily interruption of the treatment process decreases the overall efficiency of the plant, making it a cost-intensive step [5]. Moreover, backwashing generates a substantial waste stream of iron sludge. In the Netherlands alone, this waste stream accounts for ± 100,000 ton/year [6].

As an alternative to oxidation and filtration, Fe^{2+} can be recovered from anaerobic groundwater via vivianite ($Fe_3(PO_4)_2$) precipitation [7]. This is a novel approach in the industry: iron is no longer considered a waste but a new resource. The sludge volume can be reduced to a third, while the halftime for iron removal during vivianite precipitation was four times lower compared to iron oxidation and filtration. This approach can contribute to the design of more efficient filters, which results in fewer interruptions and water losses.

For groundwater-relevant iron concentrations (<25 mg/L), the saturation index (SI) for vivianite requires a relatively high pH [7]. Alternatively, elevating the iron concentration prior to vivianite precipitation also increases the SI. In reverse osmosis (RO) concentrate streams increased concentrations of Fe^{2+} are found. Therefore, we study vivianite precipitation to remove iron from RO concentrate from anaerobic groundwater. Membrane technologies, such as RO, are highly effective in removing iron, alongside other contaminants that are increasingly found in groundwater sources due to increasing pressure of human activities (e.g., pesticides [8]) and climate variabilities (e.g., salination [9]). However, membrane technologies produce a waste stream called ‘concentrate’. Currently, the concentrate is often discharged on surface waters or in wastewater treatment plants. With the increasing use of membrane technologies, it is expected that legislation around concentrate disposal will become stricter [10]. Additionally, the concentrate stream contains valuable resources [11]. Iron recovery via vivianite precipitation contributes to the growing implementation of resource recovery strategies in water treatment.

This research studies if Fe^{2+} can be recovered as vivianite from anaerobic groundwater RO concentrate streams. The concentrate, however, will also contain elevated levels of other cations. It is known that the iron in the vivianite crystal can be substituted by several other divalent cations [12,13]. Especially Mn^{2+} and Mg^{2+} are frequently present in the vivianite lattice in natural environments [12,14] and Ca^{2+} can compete with Fe^{2+} for phosphate and inhibit vivianite growth by covering its surface [15]. The divalent cations Mn^{2+}, Mg^{2+} and Ca^{2+} are common groundwater constituents. This study therefore also examines how Mn^{2+}, Mg^{2+} and Ca^{2+} are

removed from groundwater alongside Fe^{2+} during vivianite precipitation. To do so, Fe^{2+} removal via vivianite precipitation was tested in different water matrices containing groundwater and concentrate relevant concentrations of Mn^{2+}, Mg^{2+} and Ca^{2+}. The formed precipitates were analyzed by X-Ray Diffractions (XRD) and visualized by a Scanning Electron Microscope (SEM).

A3.2 Materials & Methods

A3.2.1 Groundwater and concentrate composition

Vivianite precipitation was tested in different water matrices and under different conditions. The composition of these different water matrices are given in Table 1. Experiments on site were performed at two different drinking water treatment plants of drinking water company Vitens (Netherlands): locations Witharen and Spannenburg. From now on we refer to these sites as TP1 and TP2. Experiments were performed using both natural groundwater and concentrate streams, produced by the anaerobic RO units. At TP1 the natural Fe^{2+} concentration was 8.4 mg/L and the pH 6.8, at TP2 Fe was present at 12.8 mg/L and the pH was 6.9.

At the third water treatment plant (Hammerflier), referred to as TP3 from now on, the natural concentration of Fe^{2+} in groundwater was the highest; 24.7 mg/L. The pH of the raw groundwater of TP3 was 7.1. This treatment plant does not have an RO step and therefore iron removal is solely tested in groundwater. The experiments with groundwater of TP3 were not performed on-site, but the water was transported to the lab and experiments were conducted in an anaerobic environment. The same was done with all experiments with groundwater obtained from Loosdrecht (TP4). With this water the individual effect of divalent ions Mn^{2+}, Mg^{2+} and Ca^{2+} on vivianite precipitation was tested by dosing desired concentrations of the required ions. This groundwater was chosen because it has relatively low concentrations of divalent cations, and previous experiments in Goedhart et al. (2022) have demonstrated that vivianite can indeed precipitate in this matrix [16]. The water obtained from TP4 was taken and handled in accordance with the description in Goedhart et al. (2022).

A3.2.2 On-site anaerobic groundwater and RO concentrate experiments

The recovery of Fe^{2+} through vivianite precipitation was studied in batch experiments at TP1 and TP2. Both anaerobic groundwater and anaerobic concentrate were used in these experiments. A bottle was filled from the bottom and overflown for 3 minutes before closing it with an airtight rubber cap, to maintain anaerobic conditions in the bottle. A closed, empty syringe was introduced as pressure release, such that the base and phosphate solutions could be added to the completely full bottles. The bottles were placed on a magnetic mixer plate. A picture of the setup is given in Figure 1. The pH was adjusted by dosing anaerobically prepared 0.1M NaOH (Sigma Aldrich). Afterwards, phosphate was dosed in a 1:1 molar ratio to Fe^{2+}, using an anaerobically prepared 0.1M Na_3PO_4 solution (Sigma Aldrich) of pH 8. Two samples of 5 mL were taken during the experiment: directly after base dosing, and 30 minutes after phosphate dosing. The samples were immediately filtered over a 0.2 µm filter and

acidified to 1-2% v/v HNO_3 (Carl Roth ROTIPURAN®Supra 69 %). The pH was measured at the end of the experiment, by opening the bottle and using a HACH Sension+ MM150 portable multimeter.

Table 1: Composition of raw groundwater and, if present, RO concentrate streams of Treatment plant (TP) 1 (Witharen), TP2 (Spannenburg), TP3 (Hammerflier) and TP4 (Loosdrecht).

		TP1		**TP2**		**TP3**	**TP4**
		Raw	**Conc**	**Raw**	**Conc**	**Raw**	**Raw**
Fe	mg/l	12.8	62.6	8.4	41.4	24.7	4.3
Mn	mg/l	0.5	2.4	0.3	1.6	0.3	0.2
Ca	mg/l	124	609	93	461	73	38.5
Mg	mg/l	10.5	48.0	6.5	30.0	4.3	2.2
Cond.	mS/m	68.5	214	53.0	182	41.1	23.3
pH	pH	6.9	7.3	6.8	7.3	7.1	7.3
HCO_3	mg/l	437	2130	335	1556	247	120
NH_4	NH_4/l mg	3.3	14.8	1.3	6.0	2.84	0.3
NO_3	NO_3/l	1.7	3.7	<0.2	<1.0	<0.2	<0.2
Na	mg/l	18.3	73.0	22.9	106	14.4	9.0
Cl	mg/l	36	171	31	143	23	15

A3.2.3 Anaerobic groundwater experiments in the laboratory

Water from TP3 and TP4 were transported anaerobically to the laboratory, in which experiments were performed in an anaerobic chamber (Coy Laboratory Products, USA), containing a gas mixture of 5% hydrogen and 95% argon gas (impurity <200 vpm). The chamber had an airlock and weekly regenerated palladium catalysts to secure anaerobic conditions. Water vapor was entrapped by silica beads to keep the humidity below 70%. The experiments using the water from TP3 were similar as described in 2.2, but then performed in the anaerobic chamber instead of in the field, obviating the need for the airtight rubber cap.

The interaction of divalent ions Mn^{2+}, Mg^{2+} and Ca^{2+} on vivianite precipitation was studied with water from TP4. Filtered anaerobic groundwater of TP4 was spiked with 2.5 mL of 0.179 M Fe/L $FeCl_2 \cdot 4\ H_2O$ (Sigma Aldrich), which makes the total Fe^{2+} concentration the sum of the spiked 1.79 mM (100 mg Fe/L), and the naturally present 0.077 mM of Fe^{2+} (see table 1). This equals 104.3 mg/L. Additionally, the water was spiked with either Mn^{2+} ($MnCl_2 \cdot 4H_2O$), Mg^{2+} ($MgCl_2 \cdot 6H_2O$) or Ca^{2+} ($CaCl_2 \cdot 2H_2O$) to obtain concentrations as listed in table 2. The concentrations spiked were chosen based on the concentrations present in natural groundwater and RO concentrate streams. Note that the background concentrations of Mg^{2+},

Mn^{2+} and Ca^{2+} in water from TP4 are 2.2, 0.2 and 38.5 mg/L respectively (table 1). The reactions were initialized by spiking the jar with 4.5 mL 0.1M Na_3PO_4 to obtain a 1:1 molar ratio of Fe:PO_4. Samples of 10 mL were taken just before, and 15 minutes after phosphate dosing. The samples were immediately filtered over a 0.2 µm nanopore filter and acidified using 1% v/v 65% HNO_3 upon removal from the anaerobic chamber. The pH was measured using the HACH Sension+ MM150 multimeter. After the experiment, the water was vacuum filtered over hydrophilic membrane filters (0.15-0.22 µm). These filters were covered in aluminum foil and stored in the anaerobic chamber until analysis.

Table 2: Concentrations of Ca^{2+}, Mg^{2+} and Mn^{2+} dosed in the different experiments. Only one of these three compounds was dosed in each experiment.

	Ca^{2+}		Mg^{2+}		Mn^{2+}	
	mg/l	mM	mg/l	mM	mg/l	mM
I	0	0	10	0.4	0.5	0.009
II	100	2.5	40	1.6	2	0.04
III	200	5	80	3.3	5	0.09
IV	400	10				
V	600	15				
VI	800	20				
VII	1000	25				

A3.2.4 Analysis

The concentrations of divalent ions and phosphorus in the water samples were measured using ICP-OES (Optima 8000, PerkinElmer). The samples were diluted beforehand in 3% HNO_3 to obtain concentrations in the range of 0.1 – 10 mg/L. A paired t-test was conducted to evaluate whether the removal percentage of the divalent cations significantly increased after adding either NaOH or Na_3PO_4. A significance level of 0.05 was used to determine statistical significance.

The precipitates formed were characterized by X-ray diffraction (XRD), using a Bruker D8 Advance with CuKα1 radiation (40 kV, 25 mA). A reference pattern from Morris et al. (1979) was used to verify the presence of vivianite in different samples [17]. From each experiment of TP4, at least one of the precipitates was analyzed by scanning electron microscope (SEM) (Novanano, FEI, Thermo Fischer) equipped with EDAX electron dispersive X-ray spectrometer (EDX) for chemical elements investigation at an acceleration voltage of 7.00 kV.

Figure 1: Picture of batch experiments using anaerobic concentrate (4 bottles left) and anaerobic groundwater (four bottles right) as performed on site TP1 & TP2.

A3.3 Results

A3.3.1 Co removal of divalent ions during vivianite precipitation in anaerobic groundwater

Vivianite precipitation to remove Fe^{2+} was investigated in different groundwater matrices. Figure 2 shows the Fe^{2+} removal and co-removal of divalent ions Mg^{2+}, Mn^{2+} and Ca^{2+} after addition of a base and phosphate at TP1, TP2 and TP3. Phosphate addition to anaerobic groundwater removed Fe^{2+} in all water matrices. The highest removal efficiency found was at TP3, with 89% Fe^{2+} removal at pH 9. The initial Fe^{2+} concentration at TP3 was 2-3 times higher compared to TP2 and TP1. An increase in pH enhanced Fe^{2+} removal, consistent with previous findings[16]. The experiments using TP3 water were performed in an anaerobic chamber, preventing oxidation of the formed solids. These solids were analyzed by XRD: at pH 7 and 8 only vivianite was detected, but an amorphous structure was found at pH 9 (Figure S1). Figure 2a shows that at pH 9, the addition of the base NaOH already resulted in Fe^{2+} removal up to 53%, which likely precipitated into amorphous structures as detected by XRD.

The removal efficiencies of Mn^{2+} were similar to Fe^{2+}, showing a maximum removal of 87% at pH 9 at TP3 (Figure 2b). The Mn^{2+} concentrations in the groundwater were, however, 100 times lower compared to Fe^{2+} (table 1). Ca^{2+} was present in higher concentrations and a maximum removal efficiency of 30% was found at pH 9, corresponding to 23 mg/L removed (Figure 2c). No significant (p 0.05) removal of Mg^{2+} by phosphate dosing was observed. Addition of NaOH removed a maximum of 7% of Mg^{2+}, at pH 9.

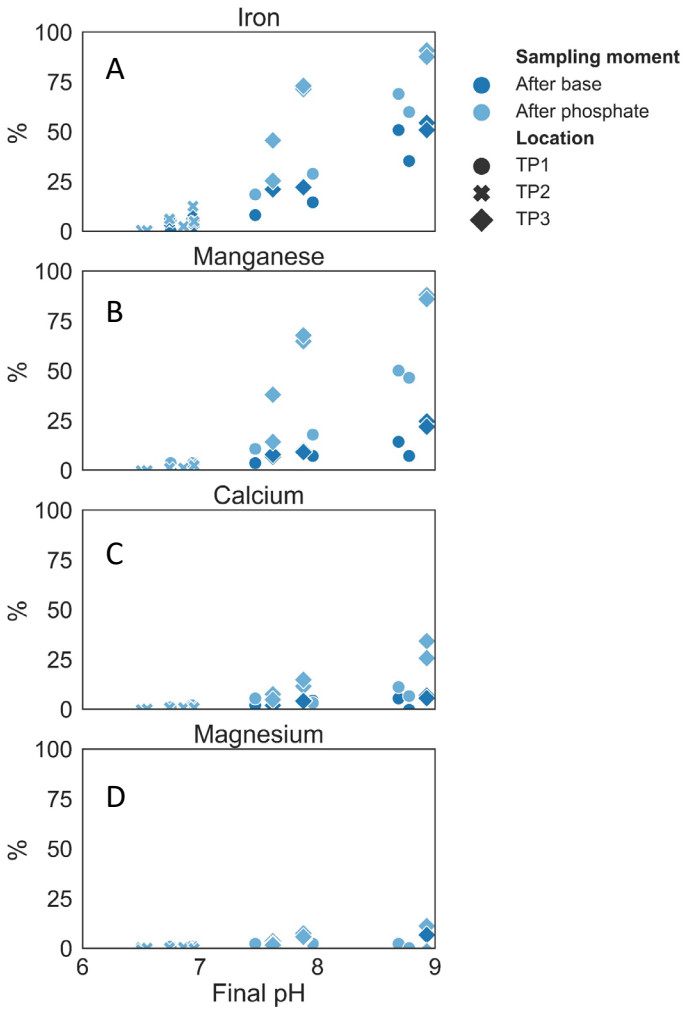

Figure 2: Removal efficiencies of A) Fe^{2+}, B) Mn^{2+}, C) Ca^{2+} & D) Mg^{2+} in anaerobic groundwater at TP1 (circles) TP2 (crosses) TP3 (diamonds) after dosing different amounts of NaOH (blue) and after dosing $Na_3(PO4)_2$ with Fe/PO_4 ratio of 1 (orange)

A3.3.2 Vivianite precipitation in reverse osmosis concentrate

The addition of phosphate resulted in removal of Fe^{2+}, Mn^{2+} and Ca^{2+} in anaerobic concentrate (Figure 3). No significant ($p > 0.05$) Mg^{2+} removal was obtained by phosphate addition (Figure 3d), aligning with our observations for groundwater (Figure 2). At elevated pH, higher removal efficiencies were found for all divalent cations. For Fe^{2+}, a maximum removal of 52% was found, corresponding to a removal of 19 mg Fe/L. Addition of the base prior to phosphate removal already removed 15% of Fe. For Mn^{2+}, a maximum removal of 49% was found, corresponding to 0.65 mg Mn/L. The maximum Ca^{2+} removal was 13%, corresponding to 58 mg Ca/L.

The highest removal efficiencies were found at TP1, since the pH of the concentrate was raised further compared to TP2. The initial concentrations of the divalent ions in the concentrates varied, as presented in Table 1. Around pH 7.3, the removal percentages of Fe^{2+}, Mn^{2+} and Ca^{2+} were higher at TP2 (24 mg Fe/L, 0.95 mg Mn/L, 48 mg Ca/L) compared to TP1 (12 mg Fe/L, 0.32 mg Mn/L, 28 mg Ca/L).

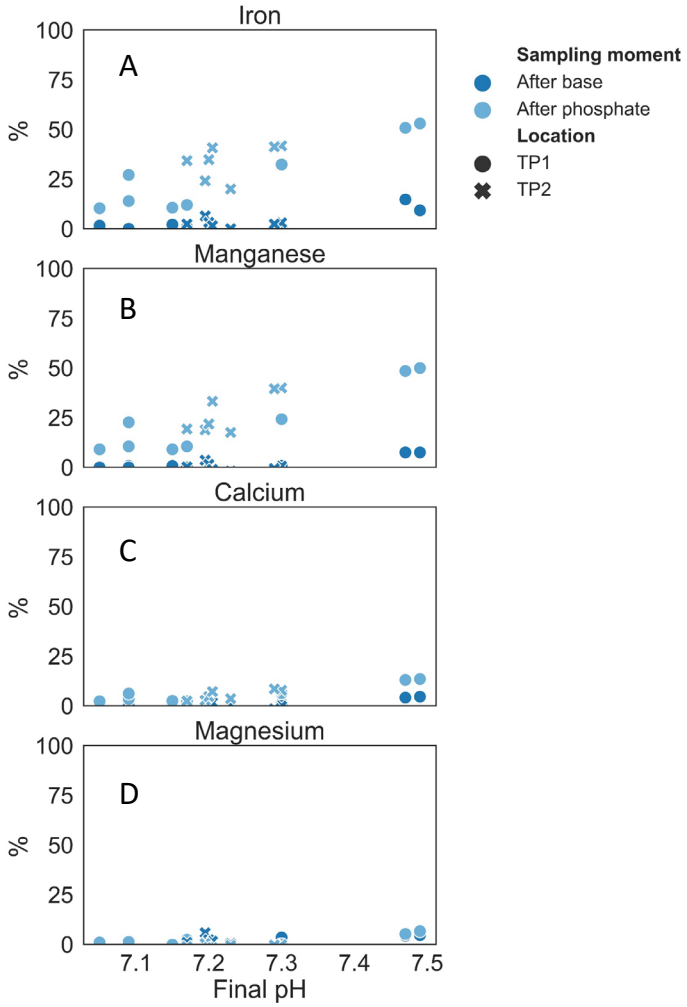

Figure 3: Removal efficiencies of A) Fe^{2+}, B) Mn^{2+}, C) Ca^{2+} & D) Mg^{2+} in anaerobic groundwater concentrate after dosing different amounts of NaOH (blue) and after dosing $Na_3(PO4)_2$ with Fe/PO_4 ratio of 1 (orange) at TP1 (circles) &TP2 (crosses).

A3.3.3 Manganese removal during vivianite precipitation

In the on-site experiments using anaerobic groundwater and RO concentrate, co-removal of Mn^{2+} was observed during vivianite precipitation. The influence of Mn^{2+} on vivianite precipitation was therefore further studied under controlled lab conditions. Figure 4 shows the removal of Mn^{2+} during vivianite precipitation at different concentrations, as presented in Table 2. In both Mn I and Mn II, 91% of Mn^{2+} and 90% of Fe^{2+} was removed. At Mn III, the highest Mn^{2+} concentration tested, 74% Mn^{2+} removal was obtained and 68% of Fe^{2+} (120 mg Fe/L). Under all investigated manganese concentrations partial Ca^{2+} co-removal was found (4.0-5.5 mg/L), but no significant Mg^{2+} removal was observed.

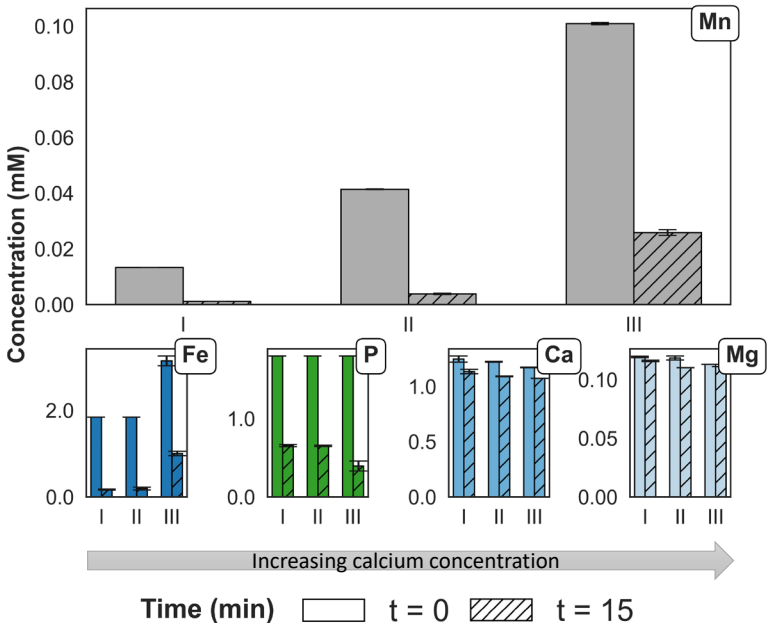

Figure 4: Concentration of Mn^{2+}, Fe^{2+}, P, Ca^{2+} & Mg^{2+} before and 15 min after the addition 0.1 M sodium phosphate to groundwater spiked with 0.179 mM Fe^{2+} and of I) 0.009 II) 0.04 or III) 0.09 mM of Mn^{2+}

A3.3.4 Calcium removal during vivianite precipitation

The removal of Ca^{2+} during vivianite precipitation was tested under seven different conditions (Figure 5). The average removal percentage was 10% and the maximum absolute removal was found at Ca VI (61.5 mg Ca/L). Note that although the removal efficiencies were lower compared to Mn^{2+}, the absolute concentrations removed were much higher, because the concentration of Ca^{2+} present in concentrate streams is around 250x higher compared to Mn^{2+}. The removal of Fe^{2+} decreased at increasing Ca^{2+} concentrations, while the phosphate removal was unaffected. The dilution needed to measure Ca^{2+} lowered the concentration of Mg^{2+} and Mn^{2+} below detection limit of the ICP-MS and are thus not included in these results.

A3.3.5 Magnesium removal during vivianite precipitation

Figure 6 shows the removal of magnesium during vivianite precipitation at different magnesium concentrations. The experiments Mg I and Mg II, containing 10 and 40 mg Mg/L, showed no significant removal of Mg^{2+}, while 88% and 77% of Fe^{2+} were removed respectively. A significant ($p > 0.05$) decrease of 7.2% was only found for the highest tested Mg^{2+} concentration of 80 mg Mg/L at which 84% of iron was removed. Partial Ca^{2+} co-removal was found (4.0-5.5 mg/L), which aligned with the removal found in the Mn^{2+} experiments.

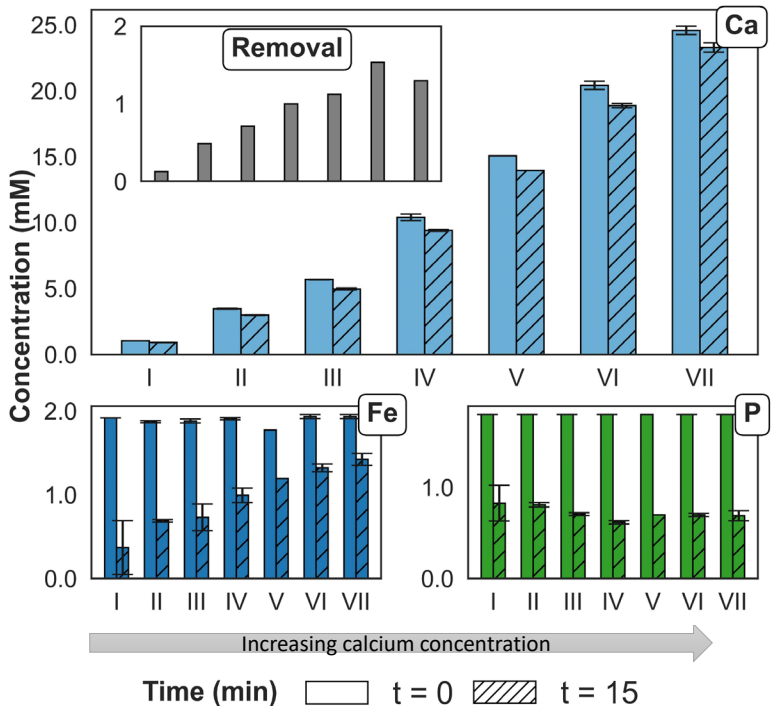

Figure 5: Concentration of Ca^{2+}, Fe^{2+} and P before and 15 min after the addition 0.1 M sodium phosphate to groundwater spiked with 0.179 mM Fe^{2+} and Ca^{2+} ranging between 0 (I) and 25 (VII) mM. Mg^{2+} and Mn^{2+} concentrations are below detection limit and therefore not shown.

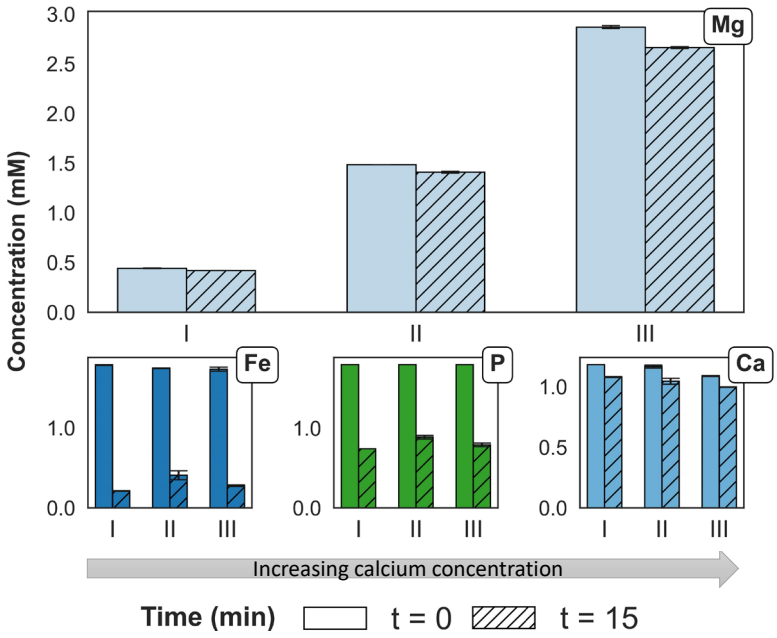

Figure 6: Concentration of Mg^{2+}, Fe^{2+}, P and Ca^{2+} before and 15 min after the addition 0.1 M sodium phosphate to groundwater spiked with 0.179 mM Fe^{2+} and of I) 0.4 II) 1.6 or III) 3.3 mM of Mg^{2+}. Mn^{2+} concentrations are below detection limit and therefore not shown.

A3.3.6 Co-removal of Mn^{2+} and Mg^{2+} does not affect mineral structure of vivianite

Figure 7 shows SEM-EDS photos of vivianite formed in the experiments Mn III and Mg III. The typical sheet-shape flowers of vivianite were observed in both environments. The addition of Mn^{2+} or Mg^{2+} did not lead to observable morphological changes. The XRD pattern of the precipitates formed in the presence of Mn^{2+} or Mg^{2+} all showed vivianite (Figure S2). However, the presence of magnesium phosphate hydrate ($Mg_3(PO_4)_2(H_2O)_8$) is difficult to exclude, because the main peaks appear at similar 2theta values. The XRD pattern of Mg III shows that amorphous structures were present in the sample alongside vivianite. An element map was made for the precipitated solids at Mn III and Mg I, which shows that the elements Fe, P and O were evenly distrubuted (Figure S3). Mg^{2+} and Mn^{2+} were not detected, because of the low concentration precipitated compared to Fe^{2+} and P.

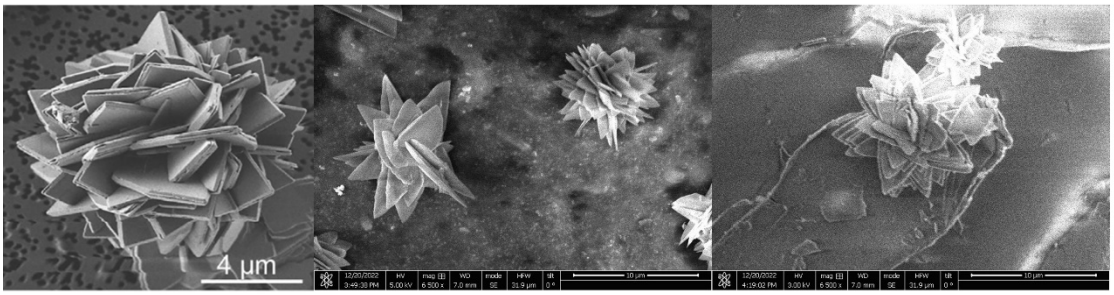

Figure 7: Scanning electron microscopy images of A) pure vivianite obtained from Joëlle Kubeneck et al., (2023) [18], B) experiment Mn III 0 and C) experiment Mg III

A3.3.7 Calcium outcompetes iron for phopshate

The XRD pattern of the precipitates formed in experiments Ca II, Ca III, Ca IV and Ca VII all show the presence of vivianite (Figure 8). At higher Ca^{2+} concentrations, the peaks were broadened, meaning that amorphous structures were present alongside the crystalline vivianite. Calcium-phosphate precipitates have likely precipitated; Figure 5 shows that phosphate removal was independent of the Ca^{2+} concentration present, while Fe^{2+} removal decreased at higher Ca^{2+} concentrations. Calcium outcompeted Fe^{2+} for precipitation with phosphate. The presence of Fe^{2+}, P, O and Ca^{2+} were evenly distributed over the precipitated solid (Fig S3); no seperate clusters of Ca-P and Fe-P were found.

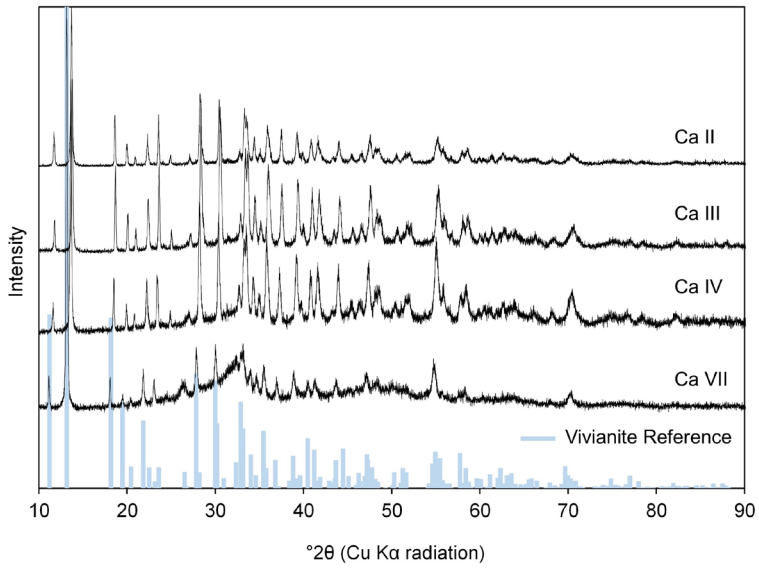

Figure 8: XRD pattern of the precipitates formed in experiments Ca II, Ca III, Ca IV and Ca VII and a reference pattern of vivianite (blue)

A3.4.0 Discussion

A3.4.1 Incorporation of manganese and magnesium in the vivianite structure

Iron recovery via vivianite precipitation was not found to be limited by the co-occurrence of divalent cations Mg^{2+} or Mn^{2+} in concentrations relevant to groundwater concentrates. Vivianite precipitation additionally removed Mn^{2+} up to 91%, while similar Fe^{2+} removal efficiencies were maintained. Removal of Mg^{2+} at 10 or 40 mg Mg/L was not significant ($p>0.05$) and only 7% was removed at an initial Mg concentration of 80 mg/L. Again, this Mg removal did not hinder the removal of Fe^{2+}. Note that this 7% Mg^{2+} removal corresponds to approx. 5.5 mg/L, which is higher than the total concentration of Mn^{2+} added in the Mn-experiments. In groundwater and many other aqueous environments, Mg^{2+} concentrations are generally higher than Mn^{2+}. Despite the higher concentrations of Mg^{2+} present, Mn^{2+} substitution in vivianite was more successful in groundwater and concentrate. This aligns with findings in literature, where favorable Mn^{2+} substitution even at large Mg/Mn ratio is also reported [14,19,20].

Substitution of Mn^{2+} in the vivianite crystal can result in pits and rosettes of a smaller size, and substitution by Mg^{2+} can lead to more platy globular structures and thicker crystals [14]. In our study, no structural changes of vivianite were identified in presence of Mn^{2+} or Mg^{2+} (Figure 7). The highest Mn/Fe ratio tested was 0.05, which is a 150 times lower ratio compared to the study of Joëlle Kubeneck et al., (2023)[18]. The concentrations relevant to groundwater or RO concentrate are probably too low to cause detectable morphological effects by the substitution of Mn^{2+} or Mg^{2+}.

Recovery of vivianite from the water stream can be achieved by magnetic separation [21]. For application purposes, it should be taken into account that impurities like manganese and

magnesium can decrease the extraction efficiency of iron and phosphate from the recovered vivianite [22].

A3.4.2 Calcium hinders iron recovery via vivianite precipitation

While Mn^{2+} and Mg^{2+} did not disturb Fe^{2+} removal during vivianite precipitation, the presence of Ca^{2+} did lower the Fe^{2+} removal efficiency. However, the concentrations of phosphate precipitated remained unaffected by the addition of Ca^{2+}. This indicates that Fe^{2+} and Ca^{2+} compete for phosphate, and Ca^{2+} competes with Fe^{2+} in the vivianite crystallization process, thereby decreasing the purity of vivianite [15]. At increasing Ca^{2+} concentrations, the Fe/P ratio removed became significantly ($p < 0.05$) lower, as previously reported [23]. In our study, at 1000 mg/L Ca^{2+}, the Fe/PO_4 ratio dropped from the theoretical molar ratio of 1.5 to 0.5. This ratio is much lower compared to the Fe/PO_4 ratio of 1.24 (at 1280 mg Ca^{2+} /L) as found by Chen et al. (2022) [23]. Two mechanisms can be responsible for the inhibition of Fe^{2+} removal when Ca^{2+} is present: i) Ca^{2+} replaces Fe^{2+} in the vivianite crystal and/or ii) Ca^{2+} precipitates with phosphate to form another mineral, most likely hydroxyapatite $Ca5(PO4)_3$ (HAP) or tricalcium phosphate $Ca_3(PO_4)_2$. Figure 9 shows the fractions of Fe, Ca and P removed in the experiments at different Ca concentrations and the theoretical ratios of HAP, vivianite and tricalcium phosphate. The ratio $PO_4/(Fe+PO_4)$ in vivianite and tricalcium phosphate is 0.4 and the ratio $PO_4/(Ca+PO_4)$ in HAP is 0.375. These nearly identical ratios make it difficult to distinguish which precipitate formed. Figure 9 shows that at different Ca^{2+} concentrations the ratios were indeed always around these values.

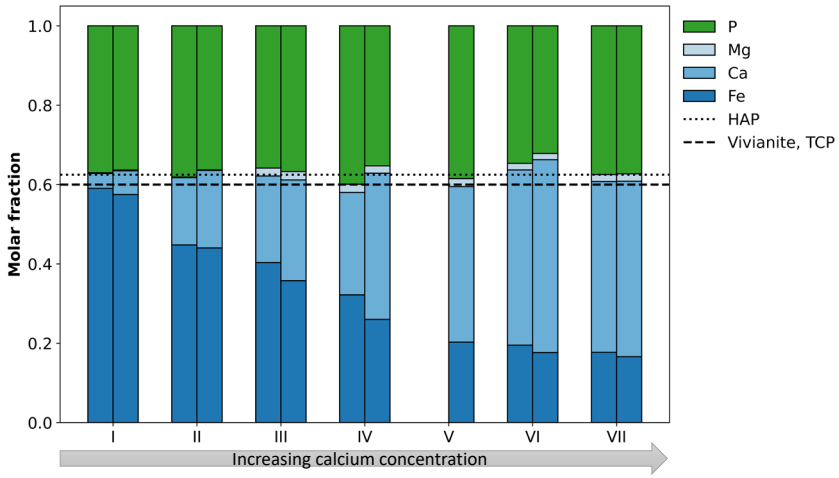

Figure 9: Molar fraction of removed Fe, Ca, Mg and P in experiments Ca I – Ca VII. The theoretical fraction of Phosphate in Vivianite, Tricalcium phosphate (TCP) and Hydroxyapatite HAP are also given.

XRD analysis showed the characteristic peaks of vivianite at all the different Ca^{2+} concentration measured (Figure 8), while Cao et al. (2023) lost the vivianite signal at 100 mg Ca/L and similar Fe^{2+} concentration [25]. At higher Ca^{2+} concentrations we did see a decrease of intensity of the main peaks and a broadened pattern, which indicates the presence of amorphous structures. Cao et al. (2023) showed that this decrease in crystallinity is caused by the formation of $Ca_3(PO_4)_2$ covering the surface of the vivianite crystals, which eventually inhibits vivianite crystallization. They report that inhibition starts from 50 mg/L, while we

detected crystalline vivianite even at concentration of 1000 mg/L of Ca^{2+}. Figure S3 shows that Ca^{2+} and Fe^{2+} are evenly distributed, suggesting that indeed Ca-PO_4 particles cover the vivianite surface. In practice, a pre-treatment step removing Ca^{2+} should be considered in order to achieve effective iron recovery via vivianite precipitation from RO concentrates. This will also result in better extraction efficiencies to eventually recover the iron and phosphate [22].

A3.5 Conclusion

This study shows evidence that vivianite can effectively precipitate across a wide range of groundwater matrices. Iron recovery via vivianite precipitation is a novel solution to manage streams such as membrane concentrate, that are currently difficult to treat due to high levels of iron and calcium. Our results indicate that divalent ions manganese and calcium are co-removed during the process, while magnesium removal was limited to only 7% removal at high concentrations (80 mg Mg/L). The presence of manganese and magnesium did not hinder the iron recovery or alter the crystalline structure of vivianite formed. The co-removal of calcium during vivianite precipitation occurred at the expense of iron removal, with the formation of amorphous calcium phosphate precipitates. Further investigation is required to determine if the divalent ions are incorporated into the vivianite structure itself, or if other precipitates form. This study underscores the potential of vivianite precipitation as a method for treating anaerobic concentrate streams and highlights the need for further research to optimize this novel treatment process.

Supplementary information

The Supplementary Information is available at
https://www.sciencedirect.com/science/article/pii/S0043135425010097

References

1. World Health Organization. *Guidelines for Drinking-Water Quality, 4th Edition, Incorporating the 1st Addendum*. WHO Library Cataloguing-in-Publication Data; 2017.

2. Van Beek CGEM, Hiemstra T, Hofs B, Nederlof MM, Van Paassen JAM, Reijnen GK. Homogeneous, heterogeneous and biological oxidation of iron(II) in rapid sand filtration. Published online 2012. doi:10.2166/aqua.2012.033

3. Müller S, Corbera-Rubio F, Schoonenberg Kegel F, Laureni M, van Loosdrecht MCM, van Halem D. Shifting to biology promotes highly efficient iron removal in groundwater filters. *Water Research*. 2024;262(March):122135. doi:10.1016/j.watres.2024.122135

4. Haukelidsaeter S, Boersma AS, Piso L, et al. Efficient chemical and microbial removal of iron and manganese in a rapid sand filter and impact of regular backwash. *Applied Geochemistry*. 2024;162(December 2023):105904. doi:10.1016/j.apgeochem.2024.105904

5. Turner T, Wheeler R, Stone A, Oliver I. Potential Alternative Reuse Pathways for Water Treatment Residuals: Remaining Barriers and Questions-a Review. *Water Air Soil Pollution*. 2019;230(227). doi:10.1007/s11270-019-4272-0

6. AquaMinerals. *Annual Report 2019*. 2020.

7. Goedhart R, Müller S, van Loosdrecht MCM, van Halem D. Vivianite precipitation for iron recovery from anaerobic groundwater. *Water Research*. 2022;217:118345. doi:10.1016/J.WATRES.2022.118345

8. Schipper PNM, Vissers MJM, van der Linden AMA. Pesticides in groundwater and drinking water wells: Overview of the situation in the Netherlands. *Water Science and Technology*. 2008;57(8):1277-1286. doi:10.2166/wst.2008.255

9. Zamrsky D, Oude Essink GHP, Bierkens MFP. Global Impact of Sea Level Rise on Coastal Fresh Groundwater Resources. *Earth's Future*. 2024;12(1). doi:10.1029/2023EF003581

10. Nederlof MM, van Paassen JAM, Jong R. Nanofiltration concentrate disposal: Experiences in The Netherlands. *Desalination*. 2005;178(1-3 SPEC. ISS.):303-312. doi:10.1016/j.desal.2004.11.041

11. Pérez-González A, Urtiaga AM, Ibáñez R, Ortiz I. State of the art and review on the treatment technologies of water reverse osmosis concentrates. *Water Research*. 2012;46(2):267-283. doi:10.1016/j.watres.2011.10.046

12. Rothe M, Kleeberg A, Hupfer M. The occurrence, identification and environmental relevance of vivianite in waterlogged soils and aquatic sediments. *Earth-Science Reviews*. 2016;158:51-64. doi:10.1016/J.EARSCIREV.2016.04.008

13. Kloprogge JT, Visser D, Martens WN, Duong L V., Frost RL. Identification by RAMAN microscopy of magnesian vivianite formed from Fe2+, Mg, Mn2+ and PO43- in a Roman camp near fort Vechten, Utrecht, the Netherlands. *Geologie en Mijnbouw/Netherlands Journal of Geosciences*. 2003;82(2):209-214. doi:10.1017/s0016774600020758

14. Kubeneck LJ, ThomasArrigo LK, Rothwell KA, Kaegi R, Kretzschmar R. Competitive incorporation of Mn and Mg in vivianite at varying salinity and effects on crystal structure and morphology. *Geochimica et Cosmochimica Acta*. 2023;346:231-244. doi:10.1016/j.gca.2023.01.029

15. Cao J, Zhao W, Wang S, Xu R, Hao L, Sun W. Effects of calcium on phosphorus recovery from wastewater by vivianite crystallization: Interaction and mechanism analysis. *Journal of Environmental Chemical Engineering*. 2023;11(5):2213-3437. doi:10.1016/j.jece.2023.110506

16. Goedhart R, Müller S, van Loosdrecht MCM, van Halem D. Vivianite precipitation for iron recovery from anaerobic groundwater. *Water Res*. 2022;217:118345. doi:10.1016/J.WATRES.2022.118345

17. Morris MC, McMurdie HF, Evans EH, et al. *Standard X-Ray Diffraction Powder Patterns: Section 16 - Data for 86 Substances*. 1979.

18. Kubeneck LJ, ThomasArrigo LK, Rothwell KA, Kaegi R, Kretzschmar R. Competitive incorporation of Mn and Mg in vivianite at varying salinity and effects on crystal structure and morphology. *Geochim Cosmochim Acta*. 2023;346:231-244. doi:10.1016/j.gca.2023.01.029

19. Egger M, Jilbert T, Behrends T, Rivard C, Slomp CP. Vivianite is a major sink for phosphorus in methanogenic coastal surface sediments. *Geochimica et Cosmochimica Acta*. 2015;169:217-235. doi:10.1016/J.GCA.2015.09.012

20. Kubeneck LJ, Lenstra WK, Malkin SY, Conley DJ, Slomp CP. Phosphorus burial in vivianite-type minerals in methane-rich coastal sediments. *Marine Chemistry*. 2021;231:103948. doi:10.1016/j.marchem.2021.103948

21. Prot T, Nguyen VH, Wilfert P, et al. Magnetic separation and characterization of vivianite from digested sewage sludge. *Separation and Purification Technology*. 2019;224:564-579. doi:10.1016/j.seppur.2019.05.057

22. Bec S, Prot T, Dugulan IA, Korving L, Mänttäri M. The challenges and limitations of vivianite quantification with 2,2'-bipyridine extraction. *Science of the Total Environment*. 2025;972(December 2024). doi:10.1016/j.scitotenv.2025.179112

23. Chen X, Zheng M, Cheng X, Wang C, Xu K. Resources , Conservation & Recycling Impact of impurities on vivianite crystallization for phosphate recovery from process water of hydrothermal carbonization of kitchen waste. *Resour Conserv Recycl*. 2022;185(June):106438. doi:10.1016/j.resconrec.2022.106438

24. Chen X, Zheng M, Cheng X, Wang C, Xu K. Resources , Conservation & Recycling Impact of impurities on vivianite crystallization for phosphate recovery from process water of hydrothermal carbonization of kitchen waste. *Resources, Conservation & Recycling*. 2022;185(June):106438. doi:10.1016/j.resconrec.2022.106438

25. Cao J, Zhao W, Wang S, Xu R, Hao L, Sun W. Effects of calcium on phosphorus recovery from wastewater by vivianite crystallization: Interaction and mechanism analysis. *J Environ Chem Eng*. 2023;11(5):2213-3437. doi:10.1016/j.jece.2023.110506

A4

Anoxic Iron Sulfides Formation for Iron Removal in Groundwater Treatment

Published as:
Holst, T., Goedhart, R., van Loosdrecht, M. C. & van Halem, D. (2025). Anoxic iron sulfides formation for iron removal in groundwater treatment. Journal of Water Process Engineering, 76, 108234.

Abstract

Groundwater is one of the major sources for drinking water supply worldwide. Conventional iron removal via aeration-filtration produces about 72,802 tonnes of iron sludge annually in the Netherlands alone. Iron sludge comprises low-density flocs of little to no commercial value. The current study explored a novel concept for iron removal, namely anoxic iron sulfides formation in a fixed bed continuous flow reactor. Iron sulfides usually form dense structures and offer a wider range of re-use applications. A packed bed up-flow column reactor filled with pyrite granules was fed iron and sulfide containing solutions. Produced solids were analyzed applying X-ray diffraction analysis, Raman spectroscopy, digital microscopy, scanning electron microscopy and energy dispersive X-ray spectroscopy. Rapid iron sulfides formation was observed after <10 minutes. The formed minerals were partially retained by the pyrite granules. The molar ratio of removed Fe(II) to removed S(-II) equaled up to 0.76 ± 0.16 mol $Fe(II)_{rem}$/(mol $S(-II)_{rem}$). Our results show that iron sulfides formation can present an interesting alternative to iron removal via aeration-filtration due to its compact particle sizes and fast formation rates.

A4.1 Introduction

Groundwater is one of the major sources of drinking water supply worldwide. One common groundwater constituent which needs to be removed is iron. Iron concentrations in groundwater can range from 0 to >50 mg/L. The limit set by the World Health Organization for drinking water is 0.3 mg/L [1], because elevated iron concentrations cause taste and staining issues and clogging of pipes. Conventionally, iron is removed via aeration followed by rapid sand filters. During this process Fe(II) is oxidized to Fe(III), which precipitates as $Fe(OH)_3$. Precipitated $Fe(OH)_3$ is subsequently retained by the rapid sand filter [2].

The conventional method produces strong water binding and bulky iron flocs. The formation of vast amounts of iron sludge leads to frequent energy intensive backwashing of the filters, and high energy use for the transport of iron sludge. Other disadvantages of conventional aeration-filtration are the water consumption required for backwashing and the temporary interruption of the filter operation. About 72,802 tonnes of iron sludge are produced annually in the Netherlands alone [3]. Iron sludge is typically of little to no commercial value and only has a few applications [4].

Precipitating Fe(II) anoxically before aeration has the potential to form a product that is denser than the iron sludge currently obtained, as previously demonstrated for the phosphate mineral vivianite [5]. The formation of valueless iron sludge and filter backwash frequencies could be reduced, and the overall amount of backwash water to be treated decreased. Sulfide might be an interesting alternative precipitant. Sulfide (S(-II)) is a groundwater-native compound known to readily precipitate Fe(II) forming a wide range of compact iron sulfides [6]. Additionally, sulfide as H_2S can participate in redox reactions, with protons acting as the oxidant reduced to H_2, and sulfide serving as the reductant [7]. One commonly found iron sulfide is pyrite (FeS_2), a dense crystal often formed in anoxic sediments [8]. Other prominent iron sulfides are greigite (Fe_3S_4), mackinawite (FeS_m) and marcasite (FeS_2) the polymorph of pyrite. FeS_m is usually the first precipitate to form in anoxic iron sulfide experiments at ambient temperatures [9].

Previous investigations into the formation of iron sulfides, such as pyrite, typically aimed to understand the fundamental formation pathways in natural systems such as marine sediments [8], to study iron sulfide scale formations in engineered systems [10,11], or to produce pyrite at high temperatures for technical applications [12]. To our knowledge, this study is the first to explore the concept of S(-II) dosing for iron removal using (i) a fixed bed continuous flow reactor, (ii) a hydraulic retention time comparable to drinking water treatment plant filters (19 min), and (iii) S(-II) dosing via a dissolved sulfide containing solution. There has been one previous study that explored S(-II) dosing by H_2S purging for six hours in groundwater batches, achieving iron removal efficiencies of 75 – 83 % [13]. In addition, iron sulfides are increasingly studied for their potential use in water treatment [14–20].This indicates that iron removal through formation of iron sulfides may be a promising alternative to conventional oxic removal, offering multiple benefits - not only removing iron but also potentially targeting other contaminants.

A4.2 Materials and methods

A4.2.1 Experimental set-up

Figure 1 shows a schematic overview of the lab-scale up-flow column reactor. The column reactor was filled with granular pyrite and fed with a sulfide and an Fe(II) containing solution which mixed just before entering the reactor. In- and effluent samples were analyzed for iron, sulfide and pH. Electrical conductivity was measured inline.

Inflatable aluminum-laminate bags (3 & 10L, Unibrew Nederland, Netherlands) were used for storing the influent media and collecting the effluent. One in- and effluent bag was operated at a time. The second bag allowed for uninterrupted operation of the reactor during replacement. The aluminum laminate provides an oxygen barrier to keep the liquid anoxic and deflates and inflates as liquid enters or leaves, respectively. A glass cylinder (117 mL) of 40.0 cm length with a diameter of 1.9 cm was selected as reactor. It has a stainless-steel mesh at the inlet and outlet. The reactor was operated in up-flow mode. Peristaltic pumps (120U, Watson-Marlow Fluid Technology Solutions, UK) were used to feed the system and Watson Marlow Marprene tubing was used for the pumps (902.0016.016, Watson Marlow, UK). All remaining tubing were made of polyurethane (PUN-H-6X1-SW, Festo, Germany). Experiments were performed in a fume hood.

The reactor was filled with granular pyrite (Mineraliengrosshandel Hausen GmbH, Austria) sieved for a diameter range of 1.4 to 2.8 mm. Additionally, two polished cubic pyrite granules (MIKON GmbH, Germany) were added for scanning electron microscopy analysis [20]. Pyrite was added since it is known to catalyze the formation of new pyrite crystals [11,20], can provide a surface area for pyrite crystal growth and, while other iron sulfides may also have catalytic effects, pyrite is the most stable iron sulfide mineral. The pyrite was thoroughly dried and rinsed using 0.5 M HCl and deionized water.

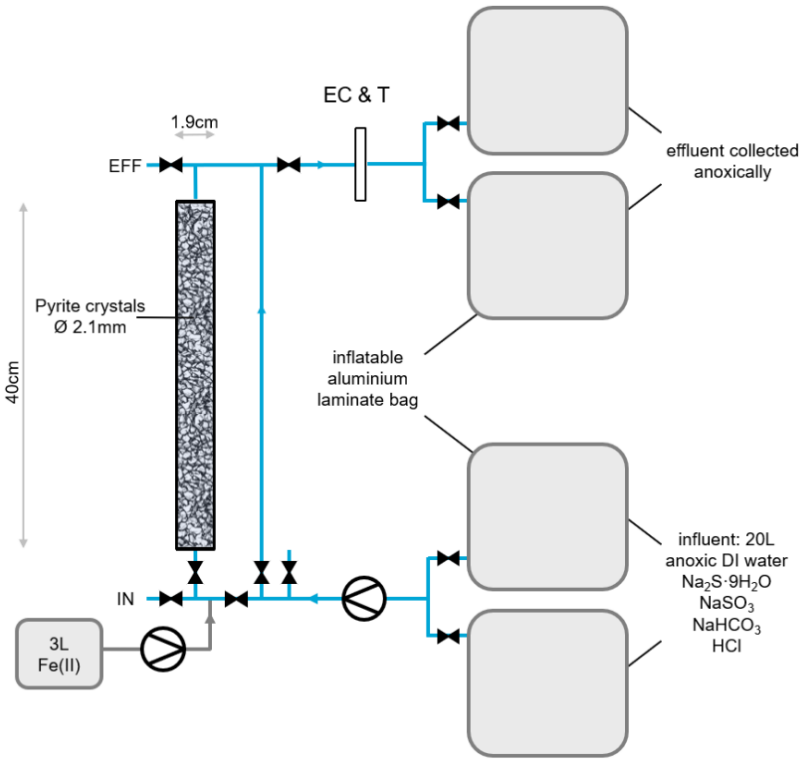

Figure 1: Scheme of the lab-scale packed bed up-flow column reactor for iron sulfide formation. The Rectangle labelled "EC & T" represents an electrical conductivity (EC) and temperature (T) probe. In- and effluent sampling ports are indicated with "IN" and "EFF", respectively.

A4.2.2 Operational conditions

Mohr's salt ((NH4)2Fe(SO4)2·6H2O) was used as Fe(II) source, as it is reported, that Fe(II) from this salt is more resistant to oxidation compared to other Fe(II) salts [6]. Na2S·9H2O was utilized as sulfide source [14]. There is little chemical difference between utilizing Na2S, NaHS or H2S+ NaOH, with respect to iron sulfide formation studies [6]. Sodium sulfite was utilized as oxygen scavenger (79 mg/L) and NaHCO3 was dosed as a pH buffer (235 mg/L). The pH was adjusted to 6.1 ± 0.1 using HCl (Honeywell, USA). Applied chemicals were of ACS Grade or higher and if not stated differently, purchased from Merck Sigma (Germany). All media were sparged using N2-gas until an oxygen concentration of <0.02 mg O2/L was reached. Subsequently, solutions were prepared in a vinyl (PVC) anoxic chamber (Coy Laboratory Products, USA). The anoxic chamber was filled with a gas mixture of 5% hydrogen and 95% argon gas (impurity <200 vpm). Anoxic conditions in the chamber were secured, by an airlock, weekly regenerated palladium catalysts and continuous O_2 measurements. The humidity was kept <70% using silica beads (confirmed by hygrometer measurements). Experiments were performed at room temperature of approximately 21°C.

For the experiment the reactor was fed Fe(II) and sulfide containing solutions that mixed just before entering the reactor. Two S(-II) dosing ratios were investigated, henceforth referred to as the low and high dosing ratio. These two ratios were used to derive a relationship between dosed sulfide concentrations and respective iron removals. After dosing the high sulfide

concentrations, the dose was decreased again to validate the relation between sulfide dose and iron removal. The low sulfide dosing ratio equaled 0.4 ± 0.1 mmol S(-II)/mmol Fe(II). The high dosing ratio equaled 1.1 ± 0.4 mmol S(-II)/mmol Fe(II). The incoming iron concentration was constant at 19.8 ± 1.8 mg Fe(II)/L, representing a typical level found in groundwater.

Phreeqc calculations indicate the principle feasibility of iron sulfide formation at the experimental conditions [15]. The calculated saturation indices were 2.1 and 17.3 for FeS_m and pyrite at the low dosing ratio and 2.2 and 17.5 for FeS_m and pyrite at the high dosing ratio, respectively.

Prior to starting the experiments, anoxic conditions were confirmed by dissolved oxygen measurements. The reactor inflow was adjusted to 185 mL/h leading to an average hydraulic retention time (HRT) of 19 minutes. The HRT was chosen to reflect typical values in drinking water treatment plant filters and because iron sulfide precipitation at the investigated concentrations typically completes within minutes [16]. The porosity used for calculating the HRT was 0.49 (57 ± 1 mL) and was estimated using a salt tracer and physical considerations (see SI 1).

A4.2.3 Analysis of dissolved constituents

Prior to use, sampling syringes were flushed using N_2 gas. Media was drained for two minutes through the sampling port before connecting the syringe to ensure anoxic conditions. The iron concentration was quantified using Hach method LCK 320 & LCK321 (Hach Lange GmbH, Germany). The pH was estimated using a sulfide resistant probe (InPro 3250i/SG/225, Mettler Toledo, Switzerland). An optical IDS sensor (FDO® 925, Xylem Analytics, USA) was used for dissolved oxygen measurements and the electrical conductivity was measured using a TetraCon® 925 (Xylem Analytics, USA).

S(-II) concentrations were determined using the methylene blue method applying Hach tests LCK653. S(-II) samples were analyzed immediately. However, a few sulfide samples were conserved by immediate addition of zinc acetate and NaOH for later analysis [19]. They were stored in the fridge prior to analysis. Conservation stabilizes the samples for at least seven days [17]. Successful conservation was confirmed by own measurements. If not otherwise specified, all uncertainty ranges indicate the standard deviation.

A4.2.4 Analysis of solid phases

Two kinds of solids were analyzed, namely, suspended solids in the effluent and the pyrite granules. Effluent suspended solids were analyzed applying X-ray diffraction (XRD), and Raman Spectroscopy. Pyrite granules were analyzed using a digital microscope, scanning electron microscope (SEM) and SEM-energy-dispersive X-ray spectroscopy (EDX).

Collection

The effluent was collected in the aluminum laminate bags. The bags were first flushed using N_2 gas and then evacuated before being connected to the system to ensure that the

collected effluent remained free from oxygen. Subsequently, the effluent was filtered to collect any formed solids on a filter paper disc. A Nalgene™ Reusable Filter Unit (Thermo Fisher Scientific Inc., USA) with three openings on top was used. After placing the 0.1µm filter paper discs (Cyclopore Track Etched Membrane, Whatman, USA) the headspace was flushed using N_2 gas for five minutes. The effluent bag was directly connected to the top part of the filter unit and the media was slowly added to the filter unit. The headspace of the filter unit was flushed using N_2 gas throughout the filtration process to keep the media anoxic. After filtration, the filter papers discs were immediately moved to the anoxic chamber where they were dried prior to analysis.

XRD

X-ray diffraction analysis was performed using a D8 Advance Eco (Bruker Corporation, USA) to identify any formed crystallographic structure that flushed out from the up-flow column reactor. Analysis was performed on the solids retained on the filter paper discs. XRD patterns were collected in the range of 5-90° 2θ using the following settings: 0.6mm receiving slit, 0.1s/0.0103° 2θ counting time.

Raman Spectroscopy

Raman spectroscopy was carried out using a Renishaw Invia Reflex (Renishaw, UK). Solids retained on the filter paper disc were analyzed under the following settings: 515 nm, 1% I of 50 mW, 20 acc, dwell time 2 s, center range 1050 cm^{-1}.

Digital microscope

A digital microscope (VHX-500, Keyence Corporation, Japan) was used to take pictures of the pyrite granules before and after the experiments. Pyrite granules were dried in an anoxic chamber containing silica desiccants.

SEM-EDX

Scanning electron microscopy and energy dispersive X-Ray spectroscopy were performed on two polished cubic pyrite granules to investigate whether any crystal growth, mineral depositing or surface transformation had occurred. The polished pyrite cubes were analyzed before and after the experiments. We used a NovaNano SEM (FEI, USA).

Before the experiments pyrite granules were immersed in 0.4 M HCl for ten minutes followed by polishing using a wool felt and subsequent cleaning with deionized (DI) water. After the experiments pyrite granules were taken from the reactor after draining the remaining anoxic water by flushing the column using N_2-gas. The column was then sealed and moved to the anoxic chamber to withdraw the polished cubic pyrite granules.

One face of each cubic pyrite crystal was analyzed. Half of the analyzed face was gently cleaned using a cosmetic tissue followed by rinsing with DI water. Afterwards the cubes were immediately freeze dried and Au-coated prior to analysis.

A4.3 Results

A4.3.1 Iron removal through sulfide dosage

A packed bed up-flow column reactor filled with pyrite granules was operated for the treatment of anoxic Fe(II) containing water (Figure 2). The average iron influent concentration equaled 19.8 ± 1.8 mg Fe(II)/L and the average influent sulfide concentration was 5.3 ± 1.6 mg S(-II)/L and 11.3 ± 2.5 mg S(-II)/L for the low and high dosing ratio, respectively. During the low dosing ratio, the effluent Fe(II) concentration was relatively high, 18.4 ± 0.5 mg Fe(II)/L (pore volume 0-240 and 900 onwards), removing an average of 2.4 ± 0.4 mg Fe(II)/L from the water. Increasing the sulfide dose led to a 4-fold increase in Fe(II) removal, reaching an average of 9.9 ± 1.5 mg Fe(II)/L in the effluent (between 500 and 730 pore volumes). The average effluent sulfide concentration equaled 1.2 ± 0.5 mg S(-II)/L and 4.6 ± 1.6 mg S(-II)/L for the low and high sulfide dosing, respectively. Effluent sulfide includes FeS bound sulfide; the methodology does not make it possible to distinguish free and bound sulfides. Thus, it remains unclear whether the dosed sulfide had entirely reacted with the iron in the column. A comparison between filtered (0.22µm nanopore filter) and unfiltered effluent samples indicated 55% lower sulfide concentrations for the filtered samples. Notably, part of the sulfide oxidized in the influent bag before entering the reactor.

The pH for the low Fe/S dosing ratio was 6.1 ± 0.1 for the in- and effluent. The pH for the high Fe/S dosing ratio was 6.0 and 5.9, for the in- and effluent respectively. The effluent electrical conductivity was 682 ± 19 µS/cm and 723 ± 49 µS/cm, for the low and high dosing ratio respectively.

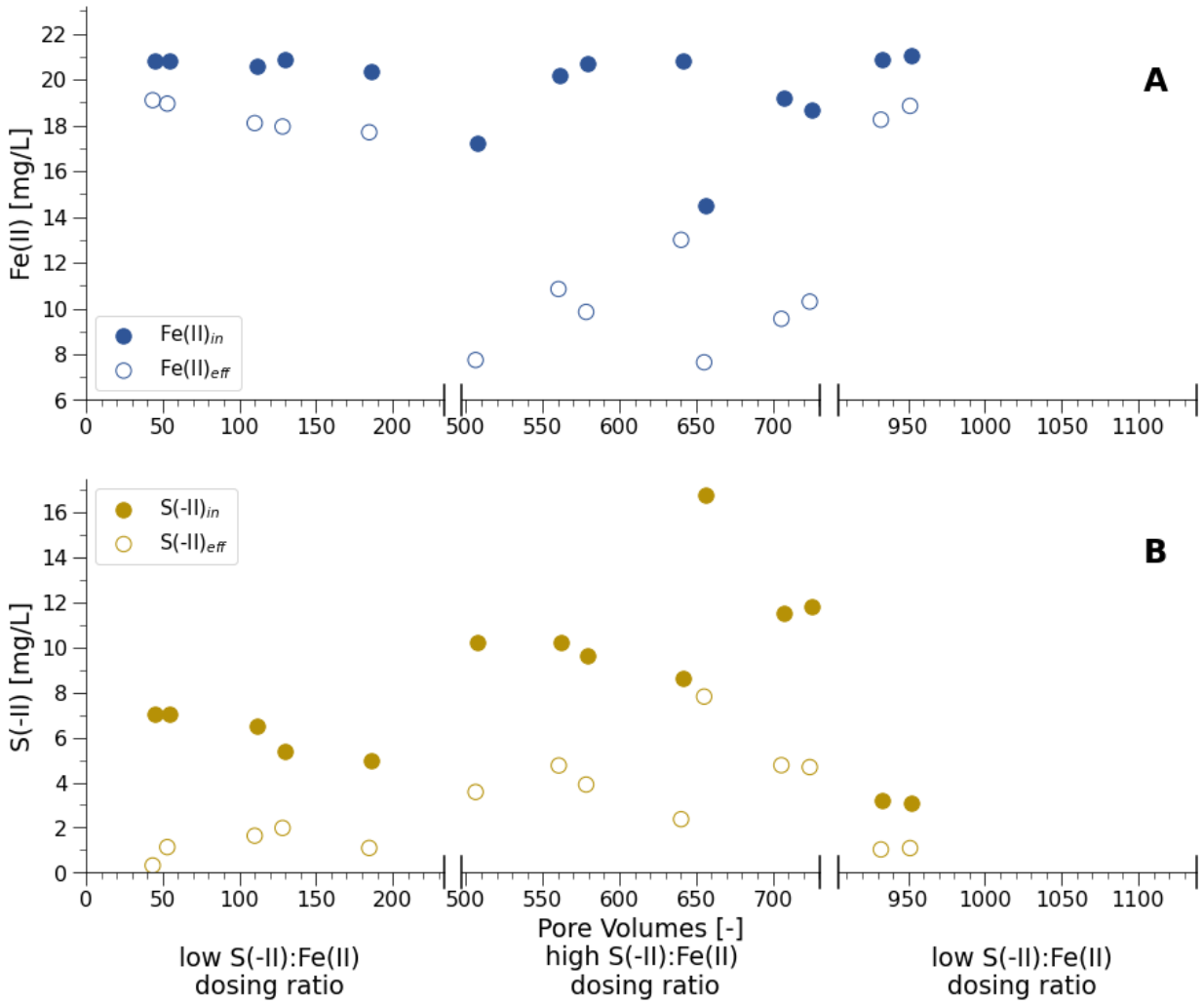

Figure 2: Iron (A) and sulfide (B) concentrations in the influent (closed circles) and effluent (open circles) in the up-flow packed bed reactor. Experiments were conducted at a low (0-240 and 900-960 pore volumes) and high (500 – 730 pore volumes) sulfide concentration in the influent. HRT = 19min.

A4.3.2 Iron to sulfide ratio

The ratio of removed Fe(II) over removed sulfide for the low and high dosing ratio is given in Figure 3. Higher levels of removed Fe(II) per removed sulfide were observed for the high dosing ratio. The removed Fe(II) and sulfide concentrations were calculated for each time point by subtracting the respective effluent from the influent concentration. The absolute standard deviation was approximately 0.15 for both dosing ratios. The dashed lines indicate the theoretical molar Fe:S ratios for iron sulfide minerals pyrite (0.5) and mackinawite (1.0).

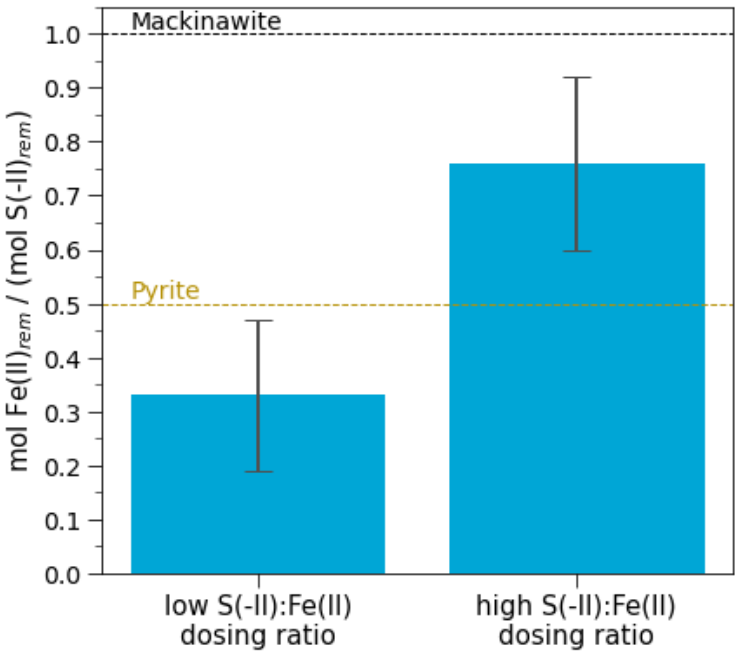

Figure 3: Molar ratios of removed Fe(II) to removed sulfide. Error bars indicate the standard deviation. For reference, dashed lines are added indicating molar ratios of Fe:S for mackinawite (FeS_m) and pyrite (FeS_2).

A4.3.3 Deposits on pyrite granules

Figure 4 shows digital microscopy pictures of pristine and recovered pyrite granules after reactor operation. Clear black deposits can be seen on the pyrite granule recovered after the experiment (Figure 4 B) compared to the pristine one (Figure 4 A). The formed deposits could easily be wiped off from the pyrite granule, which is illustrated in Figure 4 (C). Following a gentle cleaning, the shiny area marked with the red frame regained its pre-experiment appearance.

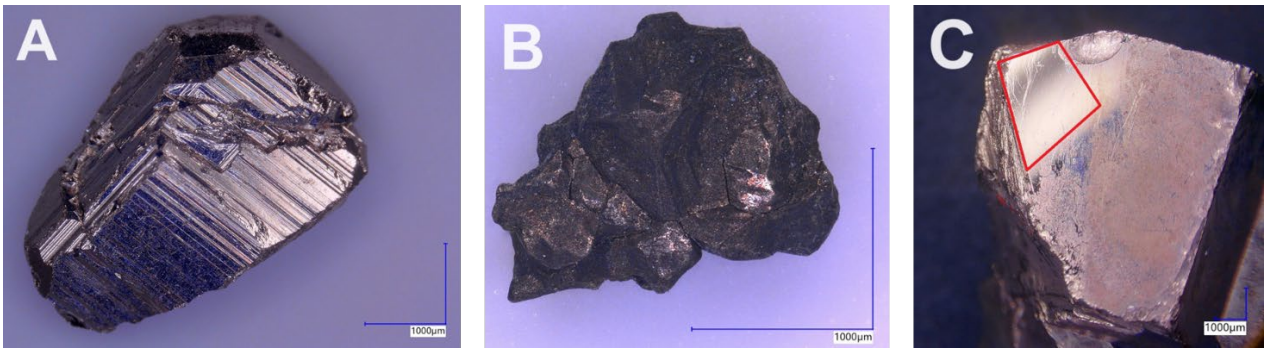

Figure 4: Digital microscope images of pyrite granules. Pristine pyrite granule (A). Pyrite granule recovered at the end of reactor operation (B). Polished pyrite cube recovered at the end of reactor operation; a part of the surface was gently wiped off using a cosmetic tissue and rinsed with anoxic DI-water (red framed area) (C).

To examine potential occurrences of crystal growth, mineral deposition, and surface transformation, and to determine the elemental composition of the surface SEM and SEM-EDX analyses were performed. Figure 5 shows the polished pyrite surface before and after the experiment. SEM-EDX analysis revealed the presence of sulfur and iron minerals on the pyrite cubes. No evidence of pyrite crystal growth was found. The white leaf-like shape in the center of Figure 5-B is most likely an irregularity of the crystal itself, rather than a structure which formed during the experiments.

The average ratio of Fe:S detected at the pyrite surface equaled 1.0:4.5 ± 0.6 (n=4) and was estimated using SEM-EDX.

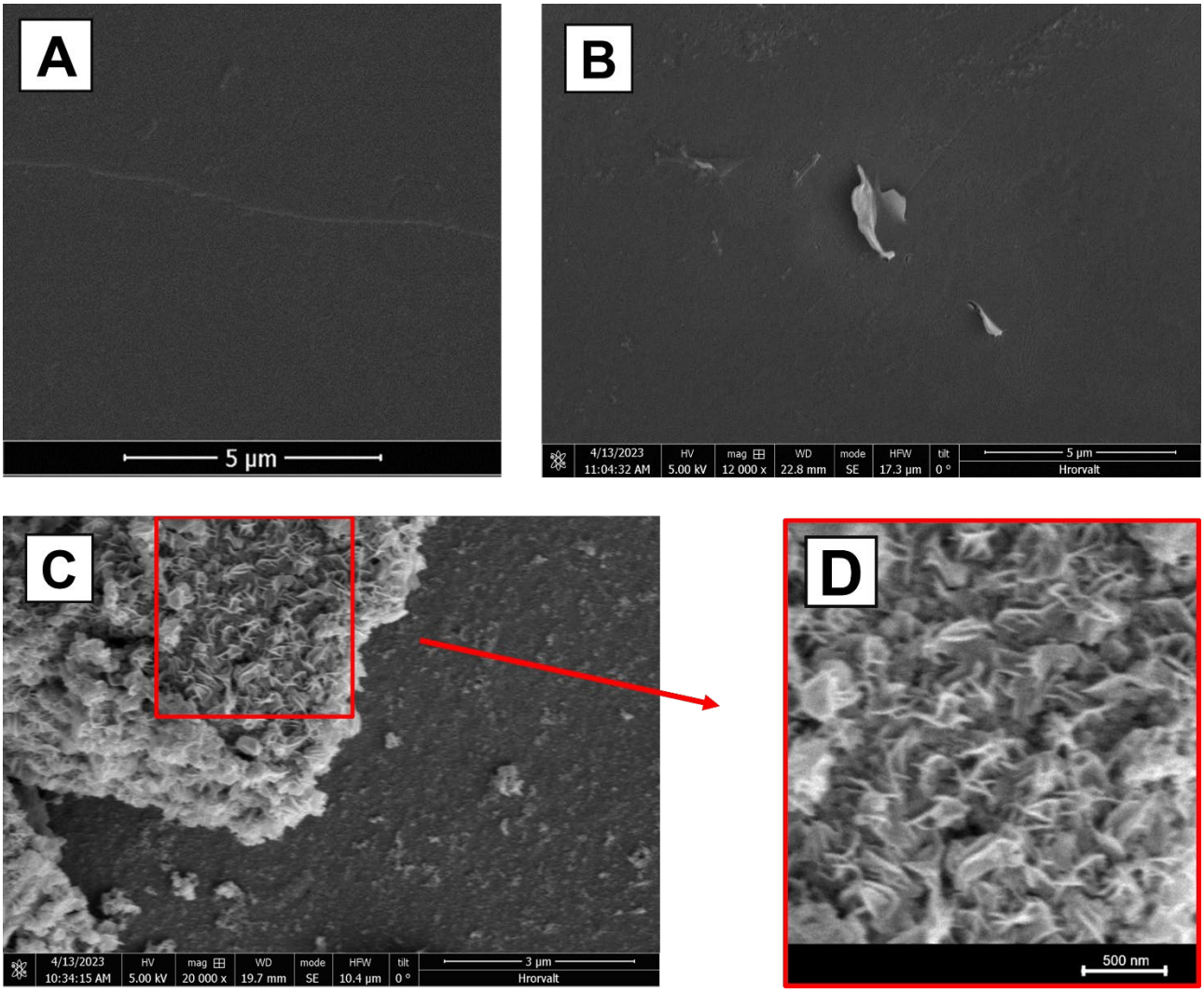

Figure 5: SEM images of polished pyrite surface before the experiment (A). Images after the experiment of gently wiped and rinsed surface (B) and solely rinsed surface (C). D shows an amplification of C.

A4.3.4 Suspended solids in water

Both influent and effluent visually contained black suspended solids (Figure 6). Raman spectroscopy indicated the presence of rhombic sulfur (Figure 7 A and B) and pyrite (Figure 7 C) in the effluent filter residues collected during the high sulfide dosing [18]. Note that most analyzed samples did not result in any identifiable Raman spectra. No samples delivered an interpretable Raman spectrum for the lower sulfide dose. XRD analysis could not identify any crystalline structures on the anoxic filter residues. Oxidized filter samples indicated the presence of the iron oxyhydroxide lepidocrocite.

Figure 6: Syringe filled with an influent sample taken during the high sulfide dosing.

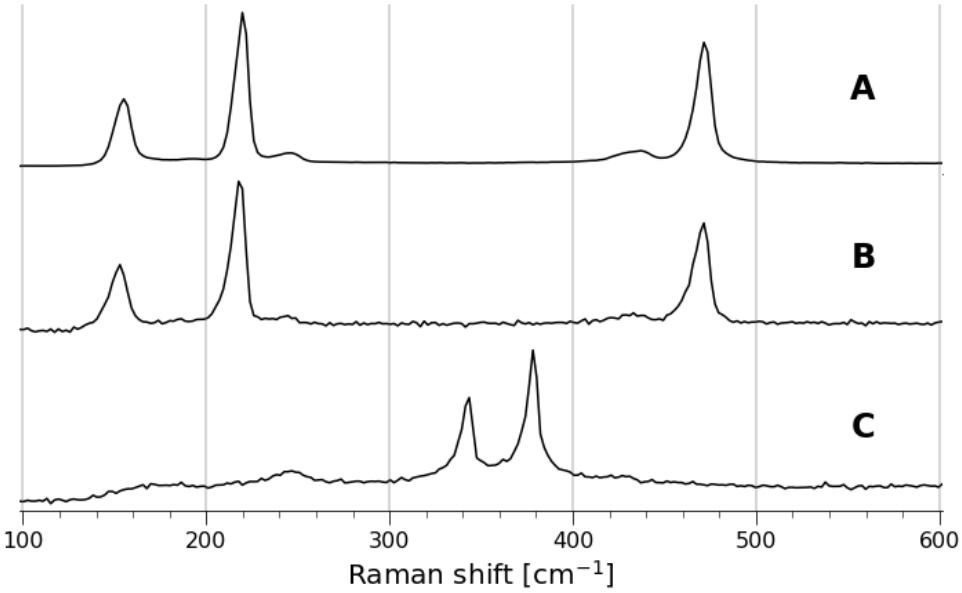

Figure 7: Raman pattern of effluent suspended solids. A-C were retrieved from solids retained during the high sulfide dose. A and B show peaks at 152, 218 and 472 cm^{-1} indicating the presence of rhombic sulfur. C shows peaks at 342 and 378 cm^{-1} indicating the presence of pyrite.

A4.4 Discussion

A4.4.1 Particulate iron sulfides formation

The current investigation successfully demonstrated iron removal via sulfide dosing. One possible mechanism for iron removal was the formation of mackinawite. FeS_m forms from the reaction of HS^-, H_2S and polysulfides with Fe(II), becomes visible in solutions as black

discoloration and usually is nanocrystalline [21]. In this study, the sampled influent clearly showed a black discoloration (Figure 6).

Applying the rate equation for FeS_m formation to the investigated conditions of about 19.8 mg Fe(II)/L and 11.3 mg S(-II)/L yields in initial formation rates that suggest a depletion of reactants in approximately 6.6 minutes [8]. This is a third of the applied HRT and matched well with the observation that most of the black precipitates retained in the bottom half of the up-flow-column reactor.

Several studies observed mackinawite formation under similar conditions. It is generally mentioned as the first precipitate to form in anoxic iron sulfide formation experiments at ambient temperatures [8,9]. Especially, in studies towards pyrite formation it has been observed [6] due to its rapid formation kinetics and low solubility [22]. In the current investigation the SEM image in Figure 5 D shows similarities to images of mackinawite [23]. Additionally, lepidocrocite, an oxidation product of FeS_m [24], was identified.

Mackinawite is difficult to detect applying XRD and Raman analysis. Firstly, the nanocrystalline FeS_m is sensitive to oxidation[6,25,26]. Even though handled carefully, it cannot be excluded that FeS_m oxidized before analysis. Secondly, the nanocrystalline size is too small to be detected by XRD [6]. XRD therefore indicates it is an amorphous state, although it is not [27]. Future investigation could utilize Mössbauer spectroscopy. Mössbauer spectroscopy seems to overcome the issue of nano crystallinity, since it does not require long-range ordering of the crystal structure [25]. The clear black discoloration of the influent samples and comparison to similar studies suggest that mackinawite was the main iron sulfide formed in this investigation. The molar ratios of removed Fe(II) to S(-II) do not equal the mackinawite ratio (1:1) (Figure 3), suggesting that other reactions took place leading to the removed Fe(II) to S(-II) ratios.

Minor amounts of pyrite were detected in the suspended solids in the effluent. There are three mechanisms that can explain pyrite formation in this investigation. These can be categorized in nucleation and crystal growth [8]. Nucleation can occur via the polysulfide [8,28–30] and H_2S pathway [8,28,31,32], crystal growth via the congruent dissolution reaction [8]. All these pathways are thermodynamically favorable at investigated conditions [6].

In this study, pyrite formed most likely via the H_2S-paythway. H_2S and Fe(II) were present in sufficient concentrations for the SI to exceed 11 and pyrite granules were present to catalyze the reaction [8]. Pyrite formation via the polysulfide pathway is unlikely, because polysulfides only make up a minor fraction at the investigated pH of 6.0 ± 0.2 [33]. Also, the polysulfide pathway is about two magnitudes slower than the H_2S-pathway [28]. Lastly, crystal growth likely did not occur, since FeS_m would form more rapidly than pyrite under the studied experimental conditions [8]. Thus, FeS_m would have depleted the reactants for crystal growth.

A4.4.2 Iron sulfides retention in column and competing formation pathways

It is assumed that rhombic sulfur accounts for the relatively low Fe:S ratio of 1.0:4.5 ± 0.6 on the pyrite cubes surface, measured by SEM-EDX. Therefore, also leading to the relatively low

$Fe(II)_{rem}$:$S(-II)_{rem}$ ratios (Figure 3). Note that, a ratio of 1:1 would be expected if pyrite formation does not occur and S(-II) would only be consumed by FeS_m formation. Rhombic sulfur likely formed through the oxidation of sulfide by oxygen since millimolar sulfide solutions are sensitive to oxidation [8]. Part of the sulfide appears to have oxidized to rhombic sulfur prior to entering the reactor. Moreover, Fe(III) impurities could have caused S(-II) oxidation [16] and the dosed sulfite could have oxidized part of the S(-II) leading to rhombic sulfur formation [34]. To provide direct evidence of rhombic sulfur on the pyrite granules, a follow-up study could employ X-ray photoelectron spectroscopy (XPS) or sulfur isotope analysis.

Impurities of Fe(III) and the dosed sulfite likely also contributed to the differences in removed Fe(II) to removed S(-II) ratios shown in Figure 3. For the low and high sulfide dosing the ratios were 0.33 ± 0.14 and 0.76 ± 0.16 $Fe(II)_{rem}$:$S(-II)_{rem}$, respectively. Assuming the offset from impurities is consistent across both conditions and that FeS_m is the primary iron sulfide formed, this suggests that a greater fraction of sulfide at the low dosing level reacts with sulfite and Fe(III), leaving less available for Fe(II) removal. As a result, the removed Fe(II) to removed S(-II) ratio is lower at the lower sulfide dose. Note that the removed Fe(II) to removed S(-II) ratios in Figure 3 do not directly represent the stoichiometry of formed solids. This is due to the consumption of sulfide by Fe(III) impurities and sulfite and because some solids might have flushed out. Moreover, the applied analytical method did not allow differentiation between bound and free sulfides in the effluent.

The pyrite granules led to the retention of iron sulfides in the reactor. This retention likely occurred through two mechanisms: (i) filtration, where particulate iron sulfide aggregated and got trapped based on size, and (ii) electrostatic interactions. The mechanism of electrostatic interaction is illustrated by comparing the point of zero charges (PZC) for the iron sulfide FeS_m and pyrite with the pH during the experiments. The PZC of FeS_m equals pH = 7.5 [21]. Meaning the FeS_m surface is charged positively at a pH < 7.5 and negatively at a pH > 7.5. The PZC of pyrite is pH 2 in the absence of potential-determining ions and pH 5 in the presence of potential-determining ions, specifically around 28 mg Fe(II)/L [35]. This implies that, at the measured pH of approximately 6.0 ± 0.1, the pyrite surface is negatively charged, while the FeS_m surface is positively charged. The opposite surface charges probably led to the retention of FeS_m on the pyrite granules surface. The pyrite granule bed did not catalyze pyrite formation nor served as a base for pyrite crystal growth, as reported elsewhere [11]. One possible explanation is that rhombic sulfur and iron sulfide deposits coated the surface of the pyrite crystals, significantly reducing the available catalytic surface area.

A4.4.3 Prospects on iron sulfides formation for groundwater treatment

This study has shown rapid anoxic iron sulfides formation in solution upon sulfide dose and achieved a molar Fe(II)rem:S(-II)rem of up to 0.76 ± 0.16 (Figure 3). Experimentally observed iron sulfides formation characteristics indicated general applicability for typical groundwater treatment settings for two reasons. Firstly, iron sulfides formed rapidly within a timeframe of <10 minutes which allows for small reactor design. Secondly, iron sulfildes could be retained. The design and operational parameters need to be optimized for the

formation and retention of iron sulfides. Moreover, interactions with other ions commonly found in groundwater, such as Mn^{2+} and Ca^{2+}, need to be investigated.

In a typical groundwater treatment scheme for drinking water production this technique could be placed after groundwater extraction and before aeration and filtration. Therefore, the number of backwashes is drastically reduced, while compact iron sulfides are produced instead of low-value bulky iron sludge. Formed particulate iron sulfide would need to be separated prior to aeration. A potential method to separate formed particles is filtration. Additionally, the hypothesized electrostatic removal of FeSm particles could be further investigated. FeS_m could potentially be removed via an oppositely charged surface. For instance, an electrically charged surface, which allows for charge dependent adhesion and detachment.

In-situ electrochemical sulfate reduction producing S(-II) could provide a viable solution for iron sulfide formation. This approach would make chemical sulfide dosage redundant since groundwater native sulfate could be reduced electrochemically to S(-II) [36,37]. Fortunately, sulfate concentrations often exceed iron concentrations to such an extent that in-situ electrochemical S(-II) formation could provide sufficient reactants even for pyrite (FeS_2) formation (groundwater data in [38]). Aeration facilities can remove excess sulfide that might escape from an iron-sulfide formation reactor. It is estimated that aeration removes H_2S concentrations up to 2 ppm [39].

The estimated costs for electrochemical generation of sulfide to treat a groundwater containing 10 mg Fe(II)/L equal 0.012 €/m^3, for the formation of the iron sulfide mackinawite (see SI 3 for details). These additional costs might be balanced by the sale of produced iron sulfides, and lower transport and disposal costs. Additionally, filter backwash frequencies and backwash water treatment can be reduced. The principle feasibility of in-situ electrochemical sulfate reduction producing S(-II) has been demonstrated [36,37,40]. A previous investigation showed in-situ electrochemical generation of H2S for a fluidized bed reactor reporting a precision of ± 0.25% in concentration ranges of 0.06 and 1900 µmol L^{-1} [40].

The rapidly formed iron sulfides do not only remove iron, but have several properties that allow to be employed for further treatment of water. For instance, FeS_m could be used for the simultaneous treatment of As(III). Although, As(III) sorps better to ferrihydrites, also FeS_m can be used as As(III) adsorbent [41].The adsorption capacity of As(III) to FeS_m was estimated to equal 0.012 mol As(III) per mol FeS_m [42]. Converting this to Fe(II) equals a capacity of 16 µg As(III)/mg Fe(II). Next to adsorption, also formation of minerals such as orpiment (As_2S_3), realgar (AsS) and arsenopyrite (FeAsS) are proposed for arsenic immobilization [43]. Yet, it should be noted that As speciation in the presence of sulfide is complex and requires applied investigations. Other literature suggests iron sulfides have potential for co-removal of metals, organic contaminants and nutrients, such as nitrogen and phosphate [26,44,45]. More recently also removal of chromium [46], PFOA [47] and pharmaceuticals [48] are linked to iron sulfide formation, illustrating their potential wide range of interest.

A4.5 Conclusion

This study has provided a novel perspective on anoxic groundwater treatment for drinking water production. It demonstrated the principal feasibility of iron removal via sulfide dosing in a fixed bed continuous flow reactor. We have revealed that iron sulfides formation can present an interesting alternative to conventional aerobic iron removal, due to its fast formation rates (<10 minutes) and relatively compact particle sizes. The molar ratio of removed Fe(II) to removed S(-II) equaled up to 0.76 ± 0.16 mol $Fe(II)_{rem}$/(mol $S(-II)_{rem}$). Further investigations are needed to optimize the design and operational parameters for the formation and retention of iron sulfides in groundwater treatment.

References

1. World Health Organization. *Guidelines for Drinking-Water Quality: Fourth Edition Incorporating the First and Second Addenda*. 2022.
2. Van Beek CGEM, Hiemstra T, Hofs B, Nederlof MM, Van Paassen JAM, Reijnen GK. Homogeneous, heterogeneous and biological oxidation of iron(II) in rapid sand filtration. Published online 2012. doi:10.2166/aqua.2012.033
3. AquaMinerals. *Annual Report AquaMinerals 2024*. 2024.
4. Ahmad T, Ahmad K, Alam M. Sustainable management of water treatment sludge through 3'R' concept. *J Clean Prod*. *Elsevier Ltd*. 2016;124:1-13. doi:10.1016/j.jclepro.2016.02.073
5. Goedhart R, Müller S, van Loosdrecht MCM, van Halem D. Vivianite precipitation for iron recovery from anaerobic groundwater. *Water Res*. 2022;217:118345. doi:10.1016/J.WATRES.2022.118345
6. Rickard D, Luther GW. Chemistry of Iron Sulfides. *Chem Rev*. 2007;107(2):514-562. doi:10.1021/cr0503658
7. Butler IB, Rickard D. Framboidal pyrite formation via the oxidation of iron (II) monosulfide by hydrogen sulphide. *Geochim Cosmochim Acta*. 2000;64(15):2665-2672. doi:10.1016/S0016-7037(00)00387-2
8. Rickard D. Sulfidic Sediments and Sedimentary Rocks. *Developments in Sedimentology*. 2012;65:685-766. Accessed March 9, 2026. http://www.scopus.com/inward/record.url?eid=2-s2.0-84869048910&partnerID=tZOtx3y1
9. Rickard D, Griffith A, Oldroyd A, et al. The composition of nanoparticulate mackinawite, tetragonal iron(II) monosulfide. *Chem Geol*. 2006;235(3-4):286-298. doi:10.1016/j.chemgeo.2006.07.004
10. Alduailej YK, Sorbie KS. Iron Sulfide Scale Formation: A New Anaerobic Setup and New Insights. In: *SPE International Oilfield Scale Conference and Exhibition*. SPE; 2020. doi:10.2118/200660-MS
11. Harmandas NG, Navarro Fernandez E, Koutsoukos PG. Crystal Growth of Pyrite in Aqueous Solutions. Inhibition by Organophosphorus Compounds. *Langmuir*. 1998;14(5):1250-1255. doi:10.1021/la970354c
12. Xian H, Zhu J, Liang X, He H. Morphology controllable syntheses of micro- and nano-iron pyrite mono- and poly-crystals: a review. *RSC Adv*. 2016;6(38):31988-31999. doi:10.1039/C6RA04874A
13. Jusoh H, Sapari N, Azie RZR. Removal of Iron from Groundwater by Sulfide Precipitation. *World Academy of Science, Engineering and Technology, International Journal of Environmental, Chemical, Ecological, Geological and Geophysical Engineering*. Published online 2011:652-658.
14. Rickard D, Grimes S, Butler I, Oldroyd A, Davies KL. Botanical constraints on pyrite formation. *Chem Geol*. 2007;236(3-4):228-246. doi:10.1016/j.chemgeo.2006.09.011
15. Parkhurst DL, Appelo CAJ. *Description of Input and Examples for PHREEQC Version 3: A Computer Program for Speciation, Batch-Reaction, One-Dimensional Transport, and Inverse Geochemical Calculations*. 2013. doi:10.3133/tm6A43
16. Kiilerich B, Nielsen AH, Vollertsen J. Kinetics of sulfide precipitation with ferrous and ferric iron in wastewater. *Water Science and Technology*. 2018;78(5):1071-1081. doi:10.2166/wst.2018.382
17. Cassella1 RJ, de Oliveira1 LG, Santelli RE. On Line Dissolution of ZnS For Sulfide Determination in Stabilized Water Samples with Zinc Acetate, Using Spectrophotometry by Methylene Blue Method. *Spectroscopy Letters*. 1999;32(3):469-484. doi:10.1080/00387019909349999

18. Monachon M, Albelda-Berenguer M, Lombardo T, et al. Evaluation of Bio-Based Extraction Methods by Spectroscopic Methods. *Minerals*. 2020;10(2):203. doi:10.3390/min10020203

19. Eaton AD, Clesceri LS, Greenberg AE, et al. *Standard Methods for the Examination of Water and Wastewater*. 20th ed. 1998. American Public Health Association; 1998. Accessed April 6, 2019. https://www.worldcat.org/title/standard-methods-for-the-examination-of-water-and-wastewater/oclc/40733179

20. Butler IB, Rickard D. An anoxic chemostat for controlled sulphide mineral synthesis. *TRANSACTIONS-INSTITUTION OF MINING AND METALLURGY* . 2003;112(B).

21. Wolthers M, Van der Gaast SJ, Rickard D. The structure of disordered mackinawite. *American Mineralogist*. 2003;88(11-12):2007-2015. doi:10.2138/am-2003-11-1245

22. Rickard D. Kinetics of FeS precipitation: Part 1. Competing reaction mechanisms. *Geochim Cosmochim Acta*. 1995;59(21):4367-4379. doi:10.1016/0016-7037(95)00251-T

23. Bolney R, Grosch M, Winkler M, van Slageren J, Weigand W, Robl C. Mackinawite formation from elemental iron and sulfur. *RSC Adv*. 2021;11(51):32464-32475. doi:10.1039/D1RA03705F

24. He J, Miller CJ, Collins R, Wang D, Waite TD. Production of a Surface-Localized Oxidant during Oxygenation of Mackinawite (FeS). *Environ Sci Technol*. 2020;54(2):1167-1176. doi:10.1021/acs.est.9b03975

25. Schröder C, Wan M, Butler IB, Tait A, Peiffer S, McCammon CA. Identification of Mackinawite and Constraints on Its Electronic Configuration Using Mössbauer Spectroscopy. *Minerals*. 2020;10(12):1090. doi:10.3390/min10121090

26. Morse JW, Arakaki T. Adsorption and coprecipitation of divalent metals with mackinawite (FeS). *Geochim Cosmochim Acta*. 1993;57(15):3635-3640. doi:10.1016/0016-7037(93)90145-M

27. Butler IB, Archer C, Vance D, Oldroyd A, Rickard D. Fe isotope fractionation on FeS formation in ambient aqueous solution. *Earth Planet Sci Lett*. 2005;236(1-2):430-442. doi:10.1016/j.epsl.2005.05.022

28. Butler IB, Böttcher ME, Rickard D, Oldroyd A. Sulfur isotope partitioning during experimental formation of pyrite via the polysulfide and hydrogen sulfide pathways: implications for the interpretation of sedimentary and hydrothermal pyrite isotope records. *Earth Planet Sci Lett*. 2004;228(3-4):495-509. doi:10.1016/j.epsl.2004.10.005

29. Rickard DT. Kinetics and mechanism of pyrite formation at low temperatures. *Am J Sci*. 1975;275(6):636-652. doi:10.2475/ajs.275.6.636

30. Luther GW. Pyrite synthesis via polysulfide compounds. *Geochim Cosmochim Acta*. 1991;55(10):2839-2849. doi:10.1016/0016-7037(91)90449-F

31. Rickard D. Kinetics of pyrite formation by the H2S oxidation of iron (II) monosulfide in aqueous solutions between 25 and 125°C: The rate equation. *Geochim Cosmochim Acta*. 1997;61(1):115-134. doi:10.1016/S0016-7037(96)00321-3

32. Rickard D, Luther GW. Kinetics of pyrite formation by the H2S oxidation of iron (II) monosulfide in aqueous solutions between 25 and 125°C: The mechanism. *Geochim Cosmochim Acta*. 1997;61(1):135-147. doi:10.1016/S0016-7037(96)00322-5

33. Kamyshny A, Goifman A, Gun J, Rizkov D, Lev O. Equilibrium Distribution of Polysulfide Ions in Aqueous Solutions at 25 °C: A New Approach for the Study of Polysulfides' Equilibria. *Environ Sci Technol*. 2004;38(24):6633-6644. doi:10.1021/es049514e

34. Siu T, Jia CQ. Kinetic and Mechanistic Study of Reaction between Sulfide and Sulfite in Aqueous Solution. *Ind Eng Chem Res*. 1999;38(10):3812-3816. doi:10.1021/ie990254x

35. Bebié J, Schoonen MAA. Pyrite surface interaction with selected organic aqueous species under anoxic conditions. *Geochem Trans*. 2000;1(1):47. doi:10.1186/1467-4866-1-47

36. Bilal BA, Tributsch H. Thermo-electrochemical reduction of sulfate to sulfide using a graphite cathode. *J Appl Electrochem*. 1998;28(10):1073-1081. doi:10.1023/A:1003455219932

37. Su W, Zhang L, Tao Y, Zhan G, Li D, Li D. Sulfate reduction with electrons directly derived from electrodes in bioelectrochemical systems. *Electrochem commun*. 2012;22:37-40. doi:10.1016/j.elecom.2012.04.030

38. Mendizabal I. Public supply well fields as a valuable groundwater quality monitoring network. Published online 2011. Accessed March 9, 2026. https://research.vu.nl/en/publications/public-supply-well-fields-as-a-valuable-groundwater-quality-monit/

39. McFarland ML, Provin TL. Hydrogen Sulfide in Drinking Water - Causes and Treatment Alternatives.

40. Peiffer S, Gade W. Reactivity of Ferric Oxides toward H_2S at Low pH. *Environ Sci Technol*. 2007;41(9):3159-3164. doi:10.1021/es062228d

41. Couture RM, Rose J, Kumar N, Mitchell K, Wallschläger D, Van Cappellen P. Sorption of Arsenite, Arsenate, and Thioarsenates to Iron Oxides and Iron Sulfides: A Kinetic and Spectroscopic Investigation. *Environ Sci Technol*. 2013;47(11):5652-5659. doi:10.1021/es3049724

42. Wolthers M, Charlet L, van Der Weijden CH, van der Linde PR, Rickard D. Arsenic mobility in the ambient sulfidic environment: Sorption of arsenic(V) and arsenic(III) onto disordered mackinawite. *Geochim Cosmochim Acta*. 2005;69(14):3483-3492. doi:10.1016/j.gca.2005.03.003

43. Zhang X, Fan H, Yuan J, et al. The application and mechanism of iron sulfides in arsenic removal from water and wastewater: A critical review. *J Environ Chem Eng*. 2022;10(6):108856. doi:10.1016/j.jece.2022.108856

44. Li R, Niu J, Zhan X, Liu B. Simultaneous removal of nitrogen and phosphorus from wastewater by means of FeS-based autotrophic denitrification. *Water Science and Technology*. 2013;67(12):2761-2767. doi:10.2166/wst.2013.200

45. Yang Y, Chen T, Sumona M, et al. Utilization of iron sulfides for wastewater treatment: a critical review. *Rev Environ Sci Biotechnol*. 2017;16(2):289-308. doi:10.1007/s11157-017-9432-3

46. Pan J, Liu L, Pan H, Yang L, Su M, Wei C. A feasibility study of metal sulfide (FeS and MnS) on simultaneous denitrification and chromate reduction. *J Hazard Mater*. 2022;424:127491. doi:10.1016/j.jhazmat.2021.127491

47. Sühnholz S, Gawel A, Kopinke FD, Mackenzie K. Evidence of heterogeneous degradation of PFOA by activated persulfate – FeS as adsorber and activator. *Chemical Engineering Journal*. 2021;423:130102. doi:10.1016/j.cej.2021.130102

48. Yang SR, He CS, Xie ZH, et al. Efficient activation of PAA by FeS for fast removal of pharmaceuticals: The dual role of sulfur species in regulating the reactive oxidized species. *Water Res*. 2022;217:118402. doi:10.1016/j.watres.2022.118402

Outlook

This study redefines iron removal from groundwater and concentrate streams by enabling the recovery of Fe(II) minerals under anoxic conditions. This novel finding marks a paradigm shift: rather than relying on aeration followed by filtration, where iron is oxidized to poorly crystalline iron (hydr)oxides, iron can be selectively converted into dense, crystalline minerals. Across different water matrices and process conditions, the results consistently show that deliberate control of redox chemistry enables efficient iron removal, both via phosphate- and sulfide- induced precipitation. The overarching innovation of this work lies in reframing iron removal from contaminant removal to resource recovery, thereby reducing the volume of by-products, improving process efficiency, and creating opportunities for secondary use of Fe(II) minerals.

Two potential design options for anoxic iron removal proposed in this outlook. First, phosphate, sulfide, or an alternative anion could be dosed directly into the anaerobic stream or mixed in an anoxic reactor to induce mineral precipitation. The resulting solids could subsequently be separated using common filtration. Although periodic backwashing would remain necessary, the denser mineral product is expected to reduce backwash frequency. Additionally, the paramagnetic properties of Fe(II) minerals may offer alternative separation strategies.

Second, installation of a pellet reactor upstream of filtration could facilitate controlled precipitation. Seeding with pellets of the desired Fe(II) mineral may promote rapid crystallization and yield a concentrated, high purity product. Pellet reactors are already widely applied in drinking water treatment for softening (e.g. lime dosing), and formed pellets can be harvested from the reactor bottom while treated water exits at the top, simplifying product separation.

The implementation of anoxic iron removal may be particularly attractive for membrane concentrate streams, which currently lack robust and sustainable treatment solutions. With increasingly stringent discharge regulations, solutions for these streams are urgently necessary. In contrast, direct implementation in conventional groundwater treatment would require a fundamental redesign of the established infrastructure, making short-term adaptation less likely.

This study represents a first exploration of anoxic Fe(II) removal from groundwater matrices. Prior to implementation, pilot-scale validation and cost-benefit analyses are required to assess technical feasibility and economic viability. Ultimately, by demonstrating that iron removal does not require oxidation, this work challenges the oxygen-dependent dogma of groundwater treatment and lays foundation for circular, redox-controlled process design.